

RCA Engineer

Vol. 31 No. 3 May/June 1986



RCA-developed
sensors for
meteorological
observation
page 53

electro-optics

RCA Engineer

A technical journal published by the
RCA Technical Excellence Center □ 13 Roszel Road □ P. O. Box 432 □ Princeton, NJ 08543-0432 □ Tacnet: 226-3090

RCA Engineer Staff

Tom King Editor

Mike Lynch Associate Editor

Louise Carr Art Editor

Rosemarie Cruz Editorial Assistant/Composition Specialist

Maria Pragliola Secretary

Operations, RCA Americom □ **Jim Feller** Division Vice-President, Technology, Aerospace and Defense □ **Mahlon Fisher** Division Vice-President, Engineering, Video Component & Display Division □ **Larry Gallace** Division Vice-President, Product Assurance, MIS and Materials, Solid State Division □ **Arch Luther** Senior Staff Scientist, RCA Laboratories □ **Bill Webster** Vice-President and Senior Technical Advisor, Electronic Products and Technology

Editorial Advisory Board

Tony Bianculli Manager, Engineering Information, Technical Excellence Center □ **Jay Brandinger** Staff Vice-President, Engineering, Electronic Products and Technology □ **Frank Burris** Director, Technical Excellence Center □ **Jim Carnes** Division Vice-President, Engineering, Consumer Electronics □ **John Christopher** Vice-President, Technical

Consulting Editors

Ed Burke Administrator, Marketing Information and Communications, Aerospace and Defense □ **Walt Dennen** Manager, Naval Systems Department Communications and Information, Missile and Surface Radar □ **John Phillips** Director, Business Development and Services, RCA Service Company



Our front cover shows an artist's rendition of the Windsat Free Flyer for the global measurement of tropospheric winds on an operational basis. The satellite design is the result of a study carried out by RCA Astro-Electronics Division for NOAA and the Air Force Space Division. A laser-based wind sensor is carried on a modified Advanced TIROS-N spacecraft, designed and built by Astro-Electronics for NOAA.

Cover illustration by Al Vergari and Sal Asaro, RCA Astro-Electronics Division

□ To serve as a medium of interchange of technical information among various groups at RCA □ To create a community of engineering interest within the company by stressing the interrelated nature of all contributions □ To disseminate to RCA engineers technical information of professional value □ To publish in an appropriate manner important technical developments at RCA, and the role of the engineer □ To help publicize engineering achievements in a manner that will promote the interests and reputation of RCA in the engineering field □ To provide a convenient means by which the RCA engineer may review professional work before associates and engineering management □ To announce outstanding and unusual achievements of RCA engineers in a manner most likely to enhance their prestige and professional status.

Laser diodes: We have the technology and the market is ripe.

The explosive growth of fiber-optic communications is often referred to as the "communications revolution." Perhaps a more apt description would be the "diode laser revolution." These diode chips, each the size of a salt grain and with semiconductor reliability, efficiently emit spectrally narrow light beams that can be directly modulated by controlling the injected diode current. Furthermore, the modulation capability extends from dc to at least several gigahertz.

Laser diodes revolutionized the audio optical memory market by making possible the introduction of the compact disc digital audio player. This cost-effective, reliable machine is becoming the fastest growing consumer electronics product ever produced.

There are also revolutionary changes occurring in the telecommunications industry. All long-distance installations underway, or being planned, are now cabled, or will be cabled, by optical fibers, not copper wire—all because of these small, reliable, and efficient diode lasers.

In 1985, diode lasers were the fastest growing segment of worldwide laser market sales. Diode sales in optical communications grew 42 percent, and optical memory diode laser sales grew by 44 percent. Sales of all lasers increased by 23 percent, but without diode lasers sales the increase would have been only 15 percent.

While this is outstanding growth, the laser diode revolution is far from over. It is just beginning, and in fact is spilling over into new applications areas. For instance, in this issue on laser technology there are two articles dealing with solid-state lasers for communications and remote sensing. In both, the authors discuss the current major thrust to develop diode laser arrays to replace the flash lamps used to "pump" solid-state lasers. In the area of high-performance optical disc recording, another article

describes the work underway to replace high-power gas lasers with monolithic diode laser arrays.

RCA is in the forefront of this technology revolution with new device and subsystem programs at RCA Laboratories, strong manufacturing capability at New Products Division for the commercial and military arenas, and high-level electro-optic-system skills for both satellite and terrestrial applications in the Aerospace & Defense Divisions.

New developments underway include internally and externally stabilized (single-wavelength) diode lasers; new structures and/or optical-combining techniques directed at higher power, two-dimensional surface-emitting stabilized diode lasers; photoconducting optical detectors; and new longer wavelength diode laser and detector devices.

These developments will affect satellite communications, repeaterless transoceanic fiber-optic communications, local-area networks (including high-speed computer links), printing, optical memories and data storage (compact-disc read-only memories—CD-ROMs—and erasable optical discs), fibered and fiberless circuit-board interconnects, and so forth. Current microwave capabilities in communications and radar—electronically steerable phased-array antennas, heterodyne receivers, signal processing—will be duplicated in the optical spectrum with these tiny diode laser chips.

Diode lasers offer prospects for exciting new technical and business opportunities, and happily, our company is not only well positioned but has seized the initiative.



Bernard Hershenov
Director, Optoelectronics Research Laboratory
RCA Laboratories

RCA Engineer

Vol. 31 | No. 3 May | June 1986

introduction & tutorial

- 4** Laser diode systems and devices
M. Ettenberg
- 9** Fiber-optic light sources
I. Ladany | J.T. O'Brien

applications

- 20** Multichannel diode laser arrays for high-data-rate optical recording
D.B. Carlin
- 26** Solid-state and semiconductor lasers
D.A. Wille | J.P. Kurmer
- 36** Optical disk recording
R.W. Johnson | S.M. Ravner
- 43** Local-area networks employing fiber optics at very high data rates
D.R. Patterson | J.B. Sergi
- 50** Lightweight target designator
W.S. Radcliffe
- 59** Laser remote sensors for space applications
A.R. Bogdan | R.H. Kagann | J.C. Petheram | A. Rosenberg | J.T. Sroga | S.E. Taylor

departments

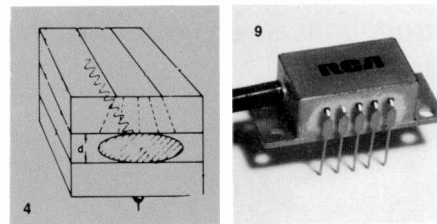
Pen and Podium, **72** | News and Highlights, **75**

Copyright © 1986 RCA Corporation
All rights reserved

in this issue . . .
electro-optics

■ **Ettenberg:** "Optical signals are playing an increasingly important role in communications and sensing in our electronic world. To this end, the laser diode is analogous to the transistor in making the transition from electronic to optical sensing, communications, and computing."

■ **Ladany/O'Brien:** "There is no doubt whatsoever that fiber optics will continue to take over communication channels . . ."



■ **Carlin:** "A monolithic linear array of individually addressed diode lasers, each falling within the field of view of imaging optics, is an obviously appropriate configuration . . ."

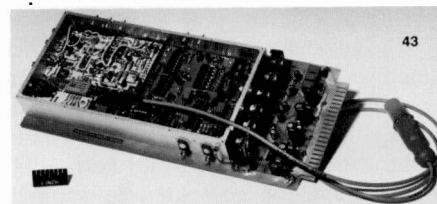
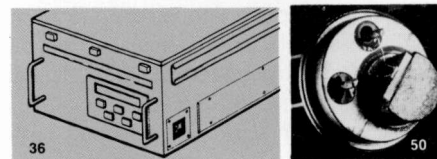
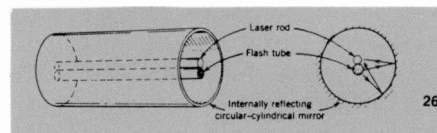
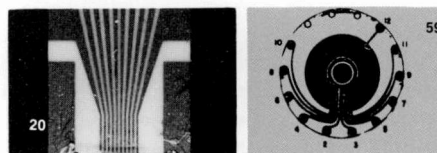
■ **Wille/Kurmer:** "RCA's interest in lasers has been continuous and has been directed toward a small number of applications, with the emphasis on two types of lasers—solid-state and semiconductor."

■ **Johnston/Ravner:** "Higher bit packing densities can be achieved by utilizing encoding schemes in which one recorded feature represents more than one digital bit."

■ **Patterson/Sergi:** "The star bus configuration allows the distribution of the signal from any one node to all of the receivers on the network in a broadcast fashion over a totally passive medium."

■ **Radcliffe:** "Size and weight are of top priority, as the forward observer is already carrying about 75 lb of survival gear."

■ **Bogdan/Kagann/Petheram/Rosenberg/Sroga/Taylor:** "Lidar measurements are based on the fact that naturally occurring aerosol particles can effect laser light from which inferences can be made regarding the properties of the atmosphere."



in future issues . . .

- manufacturing
- quality
- surface mount technology

Laser diode systems and devices

Solid-state laser systems are being put to work in everything from optical recording to satellite communications and weather tracking.

Our society is becoming more and more dependent on information that we need to transmit, store, and display. The eye, a visible-light sensor, is one of our main conduits of information to the brain. Optical signals in the visible and near infrared thus play an increasingly important role in communications in our electronic world. The articles in this issue of the *RCA Engineer* demonstrate the broad fronts of applications for lasers and electro-optics. These applications include earth-bound ranging and target designation by small Nd:YAG lasers, spaceborne weather sensors, fiber-optic communications, and optical recording and playback.

The advantage of optical radiation over microwaves for free-space sensing, communications, and ranging is derived primarily from the smaller wavelength of light, $\sim 1.0 \mu\text{m}$ (10^{-4} cm) for near-visible optical radiation compared to approximately 1.0 cm for microwave radiation. Since the beam divergence from any antenna varies as λ/D (the wavelength λ over the antenna diameter D), the collection efficiency of the return signal in a sensing application or the transmitted signal in a communication application will simply

Abstract: *This paper describes the fundamental operating characteristics of laser diodes as well as their applications to various systems. The advantages of optical systems compared to their electronic and microwave counterparts are reviewed. Possible future laser diode sources are also discussed.*

©1986 RCA Corporation.
Final manuscript received May 7, 1986
Reprint RE-31-3-1

be proportional to $D^2/(\lambda/D)^2$ as illustrated in Fig. 1. To maintain a constant collection efficiency and thus, to first order, constant information rate (data rate for communications, sensitivity or accuracy for sensing) the required antenna diameter varies as $\lambda^{1/2}$. An optical communications system, therefore, requires antennas 1/100 the diameter of their microwave counterpart.

There are obvious advantages to reduced antenna size when light waves are used for mobile terrestrial ranging and target designation applications. For space applications, where scattering and attenuation are not an issue, and size and weight are critical, optical sensing, ranging, and intersatellite communications have obvious advantages over microwave systems. Besides, the frequency of optical electromagnetic radiation exceeds that of microwaves by the inverse of the wavelength ($\sim 10^4$) and the information bandwidth capacity is commensurately increased, resulting in substantially improved sensing precision or increased data rate for intersatellite communications.

Also, while the electron is a charged particle, the photon is not. Thus, in conventional electrical communications networks, interactions between the electric field and electrons in the wire or cable limit the speed at which information can be modulated. Optical signals, however, can be modulated at rates approaching the frequency of light, 10^{14} Hz (100 terahertz, or 100 mega-megahertz), without any increased loss in glass fibers. For the same reason, optical-fiber communications are immune to interference by electromagnetic (EMI) or radio-frequency (RFI) radiation. This is important for secure communications and will become even more important as

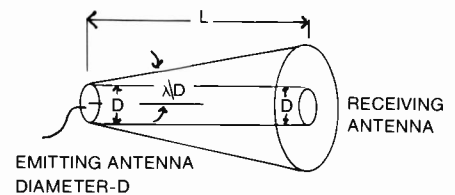


Fig. 1. *Schematic illustration of an emitting and receiving antenna communicating by electromagnetic radiation. Beam divergence is proportional to λ/D so that for a fixed spacing L the collection efficiency of the receiving antenna will be proportional to the area of the receiving antenna D^2 divided by the area of the beam $(\lambda/D)^2$.*

information bandwidths are increased. We will be forced, because of interwire and interconnection interference on circuit boards, to move to the optical domain for interboard and interchip connections. A significant increase in resistance to electromagnetic pulse (EMP) destruction may also be realized by connecting electronic circuits with nonconducting glass wires.

The first commercial impact of optical communications has been in the area of long-distance telecommunications. This stems from the very low loss achieved in pure glass fibers, about 0.2 dB/km at a wavelength of about $1.5 \mu\text{m}$. At this attenuation rate the signal level diminishes by only a factor of two every 15 km; repeaterless links in excess of 100 km are practical, making remote repeaters in most terrestrial applications unnecessary. Since the loss in optical fibers varies as λ^{-4} , it is theoretically possible to make fibers with losses of 10^{-2} to 10^{-3} dB/km at wavelengths of 3 to $5 \mu\text{m}$, allowing transcontinental and undersea

intercontinental transmission without repeaters. Research to develop such fibers is now underway.

Magnetic data sensing requires the detection magnet to be closer to the medium than the size of the information spot. High-density magnetic disc recorders require the magnetic heads be so close to the disc that dust mechanically interferes with the operation of the system. The head and disc, therefore, are hermetically sealed in magnetic Winchester hard disc drives. Magnetic tapes are held so close to the heads that the tape erodes. This contact problem is solved by the use of optical-disc data memory systems, in which lenses are used to focus laser light to a spot on the recording medium. The spot formed is on the order of a single wavelength of light ($<1 \mu\text{m}$), allowing information densities on the order of 10^9 bits/sq. inch in removable wearless media. In fact, a read-only optical memory system, the digital audio disc, represents the first consumer application of lasers. The increased information storage density of optical discs allows music to be read out digitally, yielding signal-to-noise ratios and dynamic ranges of 90 dB, a value far exceeding those obtained with the best new LP records and magnetic tapes.

While there have been numerous advances in various aspects of optical technology, including optical fibers and optical disc media, the one technical advance that has made many of the various systems practical has been the development of laser diodes.

Laser diodes

An analogy may be drawn between laser diodes and transistors. Whereas the transistor is the solid-state counterpart of the vacuum-tube amplifier, the laser diode is the solid-state counterpart of the gas laser (i.e., HeNe, argon, CO_2). The laser diode, compared with its tube counterpart, has significantly lower cost, higher reliability, and higher efficiency; it also is much smaller.

As development continues, the power, efficiency, and reliability of laser diodes are increasing, while the cost keeps decreasing. Devices capable of a 5-mW output, manufactured for digital audio discs, are now priced below \$10. Single-laser diodes have been made to emit more than 200 mW cw (continuously) at room temperature, while monolithic arrays of closely spaced lasers can emit many watts cw. Specially designed devices can be directly modulated at speeds in excess of 10 GHz. A conversion efficiency of optical light

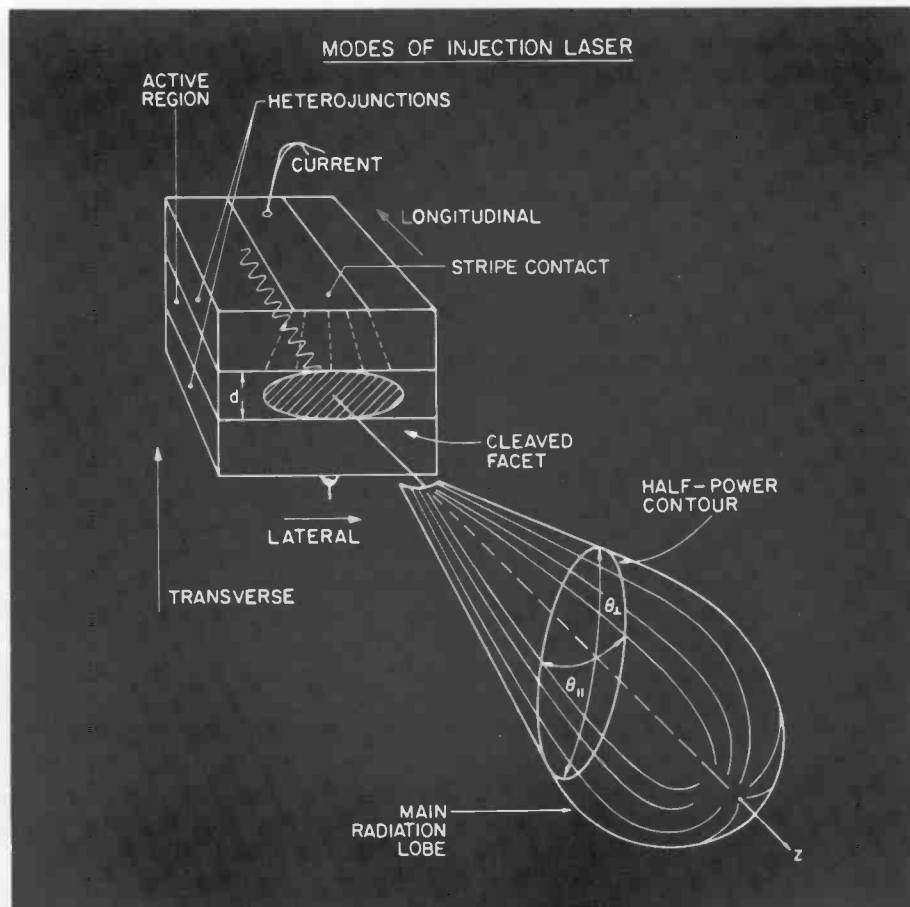


Fig. 2. General schematic of a laser diode illustrating many of its important features.

output power to electric input power of $>40\%$ has been achieved in the laboratory, and $>10\%$ is typical. At low power (<10 mW), the operating life at room temperature of laser diodes is 10^5 to 10^6 hours (10 to 100 years).

Laser diode construction and characteristics

Laser diodes, sometimes called injection lasers, resemble light-emitting diodes (LEDs). In forward bias (p-side+), electrons are injected across a p-n junction into the semiconductor to create light. These photons are emitted in all directions from the plane of the p-n junction. To achieve lasing, however, we must provide mirrors for feedback and a waveguide to confine the light distribution. As illustrated in Fig. 2, the mirrors of a laser diode are cleaved facets of the III-V semiconductor from which laser diodes are made, and the waveguide is formed by a stripe current contact in one plane and multiple semiconductor layers (called heterojunctions) in the other plane. The stripe and the heterojunction layers confine both the light

and injected electrons to a small volume between the cleaved facet mirrors. In a laser diode the applied current level is increased until the injected electron and/or hole density is at a level high enough for the population to be inverted. This inversion typically takes place at an injected carrier density of $\sim 10^{18} \text{ cm}^{-3}$ (corresponding to about 1000 A/cm^2). When the electron and hole populations are inverted, the next electron injected creates a photon that traverses the cavity between the mirrors, is substantially amplified, and emits a directed light beam at a single energy (single wavelength) corresponding approximately to the bandgap energy of the semiconductor. In the case of the LED, the photons emit independently at energies approximately corresponding to the bandgap but smeared by the ambient thermal energy. For an $8000\text{-}\text{\AA}$ ($0.8\text{-}\mu\text{m}$) emission from AlGaAs LEDs the thermal broadening corresponds to a spectral width of $\sim 300 \text{ \AA}$; for $13,000 \text{ \AA}$ ($1.3 \mu\text{m}$) from InGaAsP LEDs it corresponds to a spectral width of $\sim 800 \text{ \AA}$. The laser emission, however, corresponds to a single photon being amplified so that the emission is at a discrete wavelength (much

less than $0.1\text{-}\text{\AA}$ spectral width). However, several simultaneous wavelengths (separated by a few angstroms) may be emitted at a time.

The waveguide within the laser directs

the light toward the mirror facet. The laser diode, however, does not emit the light as a pencil beam, as does a gas laser, but as a diverging beam. To make the power input low so as to be able to adequately remove

the heat and operate the laser cw at room temperature and above, the pumped volume is made very small. Even though the laser chip is a few hundred micrometers on a side (about the size of a grain of salt), the emission source size or waveguide is only a few micrometers on a side, which is on the order of the wavelength of the emitted light. This produces a diffracted light emission pattern in the form of a diverging, elliptical output beam, typically 8° in the plane of the p-n junction and 35° in the plane perpendicular to the p-n junction, as illustrated in Fig. 2.

The type of early semiconductor laser that could operate cw at room temperature is illustrated in Fig. 3. The current stripe may be defined by several methods, including the use of an insulating oxide or a reverse-biased p-n junction, as illustrated for lasers made of InGaAsP. These lasers can be made to emit light at wavelengths between 1.1 and $1.6\ \mu\text{m}$, depending on the composition of the InGaAsP alloy. AlGaAs lasers can be made to emit between 0.72 and $0.88\ \mu\text{m}$, again depending on composition. The AlGaAs laser is shown in Fig. 3b in a phase-locked configuration, a type of device that will be discussed below. These lasers are called gain-guided structures because the light distribution between the mirror facets is defined by the injected carriers or the presence of gain along the stripe. Because this distribution is not stable with current level, temperature,

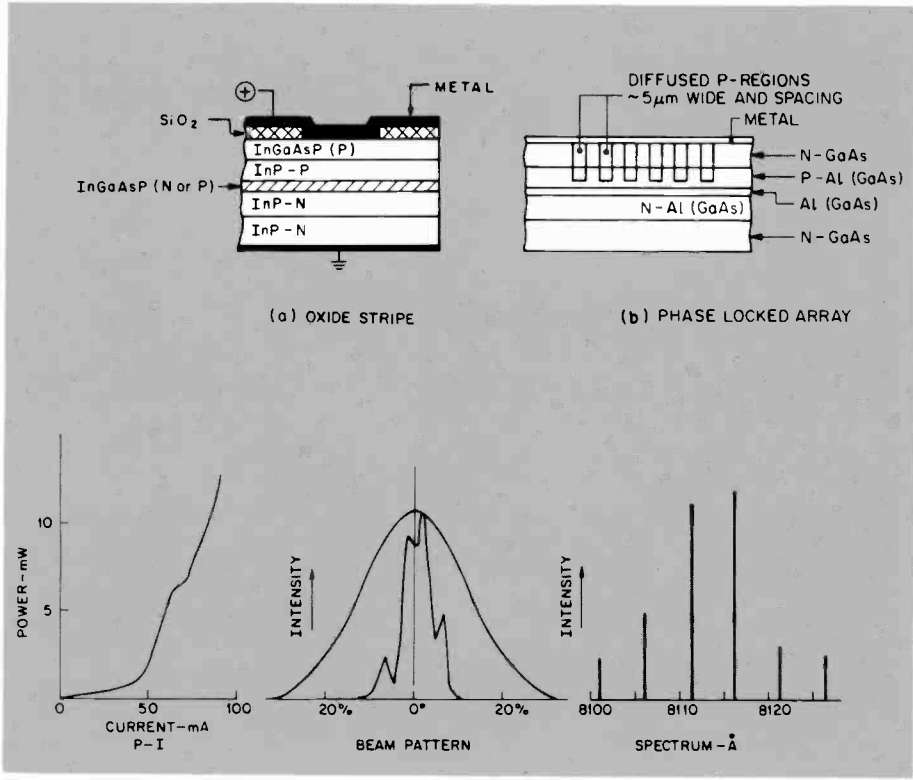


Fig. 3. Cross sections of two gain-guided structures and typical operating characteristics. Phased arrays can have outputs exceeding 200 mW.

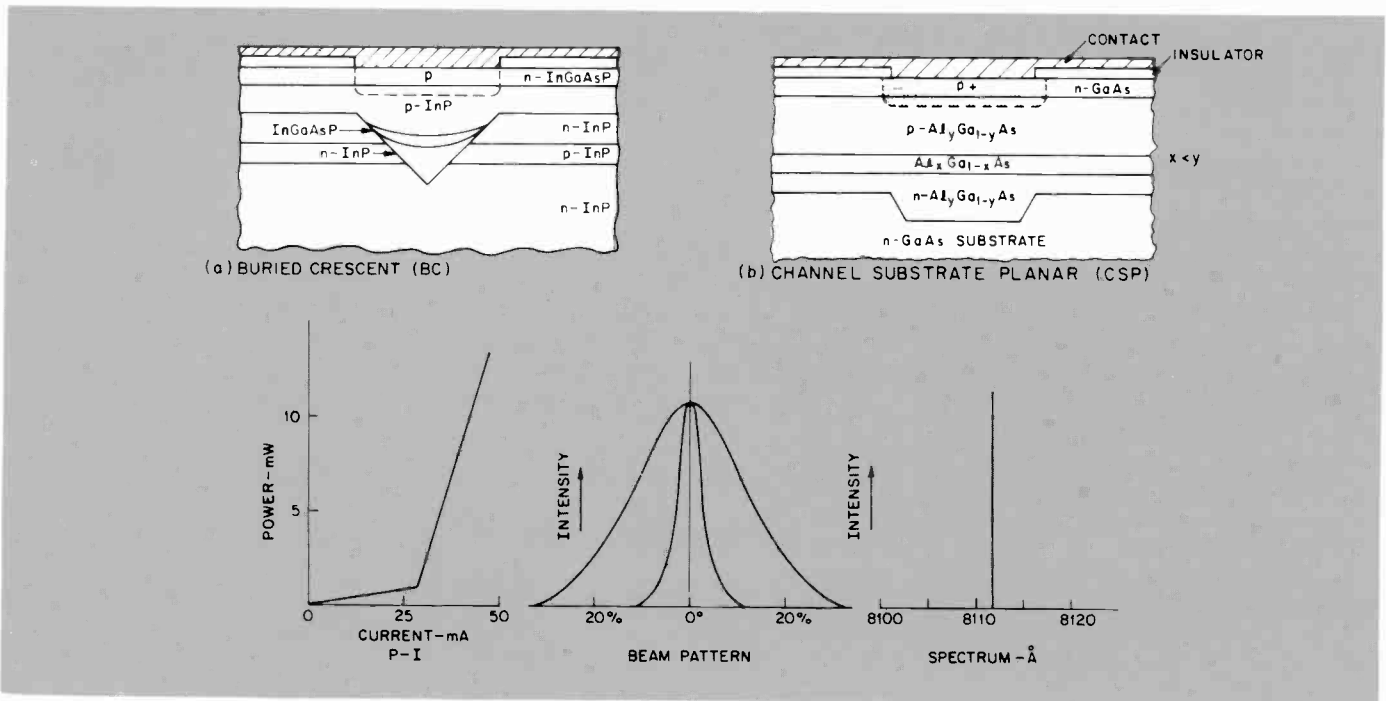


Fig. 4. Cross sections of two index-guided structures and typical operating characteristics.

or time, these lasers are somewhat unstable with respect to their output characteristics.

As illustrated in the bottom part of Fig. 3, the power output/current input of such devices is generally nonlinear, exhibiting a kink in what should ideally be a linear output with current past the threshold current. This kink is usually associated with a change in the laser beam pattern (also called far-field pattern or spatial mode of the laser) caused by a current (and, thus, waveguide) redistribution. In addition, these lasers emit in a number of spectral lines simultaneously. Because these devices may operate in a multilobed beam pattern (spatial mode) and multispectral line (spectral mode), they are called multimode devices. Such devices are useful as optical pumps for solid-state lasers,¹ sources for optical switches, and fiber-optic communications of short lengths (< 1 km), such as local-area networks or electronic interconnects. Narrow-stripe (<10 μm) devices have outputs of about 5 to 20 mW; wider-stripe ($\sim 100 \mu\text{m}$) and phase-locked arrays of multiple, closely spaced narrow stripes can achieve powers of $\sim 1 \text{ W}$. Two-dimensional arrays of laser diodes can be assembled with outputs of up to 10^3 W/cm^2 . These devices are useful for replacing flashlamps as pumps for solid-state lasers, such as Nd:YAG.

For critical optical applications, such as optical-disc reading and recording, as well as intersatellite communications and long-distance optical communications, stable single-lobed beam patterns are required. Such patterns are achieved by introducing a carefully designed perturbation in the plane of the p-n junction, as illustrated in Fig. 4. This creates a fixed internal waveguide that is independent of current drive. Since this type of guiding is formed by a real index step rather than the gain, these lasers are called index-guided lasers. Of the large variety of available structural alternatives, two are illustrated in Fig. 4. The power-current characteristic of index-guided lasers is linear, the far-field pattern is stable and single-lobed (single spatial mode), and, in general, these devices have single-line spectral output under cw operating conditions. For this reason they are sometimes called single-mode lasers. These lasers have been produced both in AlGaAs, with wavelengths around $0.8 \mu\text{m}$, and in InGaAsP, with emissions between 1.3 and $1.55 \mu\text{m}$. Outputs of more than 100 mW cw have been achieved, as shown in Fig. 5 for an experimental channeled substrate planar (CSP) laser developed at RCA Laboratories. Research is now going on to make phase-

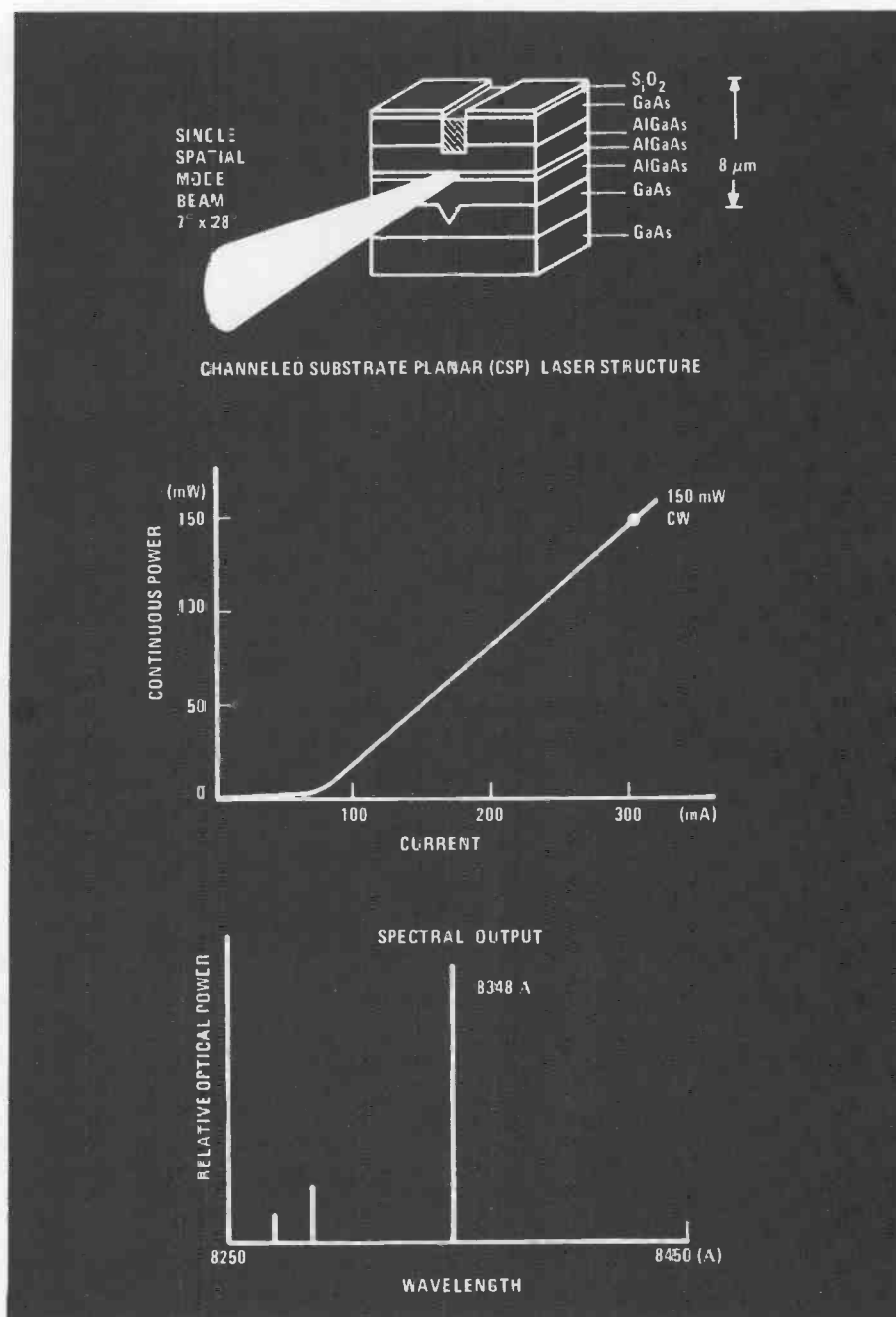


Fig. 5. Room-temperature cw operating characteristics of a high-power AlGaAs CSP laser diode.

locked arrays of such index-guided devices so that stable, single-spatial-mode coherent beams of up to 1-W cw power can be realized.

While the spatial mode is stable in index-guided laser diodes, the spectral line is not and changes with input current, temperature, and time; under modulation, multispectral line behavior is observed. To maintain a stable single spectral line, a grating may be incorporated into the laser. Such lasers are called distributed-feedback (DFB) lasers. The grating that selects the chosen wavelength also provides the feed-

back for lasing (instead of the cleaved mirrors, which are not wavelength selective). Such devices, at $1.3 \mu\text{m}$, are about to become commercially available. Because of the shorter wavelengths and smaller required grating spacing ($< 0.25 \mu\text{m}$), as well as more difficult materials problems, progress on DFB lasers at $\sim 0.8 \mu\text{m}$ has lagged behind that at the longer wavelengths.

The availability of stabilized single-mode lasers and low-loss single-mode fibers has made it possible to demonstrate very long repeaterless ($> 100 \text{ km}$) high-bandwidth

links (>1 GHz), unencumbered by the limitations imposed by wavelength dispersion effects from laser diodes not spectrally stabilized. In addition, spectrally stabilized lasers permit the use of coherent heterodyne detection in communications systems. This feature not only significantly increases the sensitivity of the receiver, but opens up the bandwidth of the system by allowing frequency or phase modulation of the laser, a faster and more efficient modulation format than on/off direct amplitude modulation.

The future

Laser diodes, as transistors have done before them, are starting to become *integrated*. Phase-locked arrays of closely spaced lasers on a chip will allow the formation of not only higher-power (1 W or more), narrow ($<1^\circ$ at least in one plane), coherent beams, but electronically steerable beams. Current research is intended to integrate lasers with switches and modulators as well as driving electronics. Recent results show that good-quality GaAs—and, thus, eventually lasers—can be grown on Si substrates, allowing the chip integration of Si integrated circuits and optoelectronics. Laser diodes with threshold currents of <5 mA at <2 -V bias are now possible, and 1 mA is in sight, making the laser's thermal dissipation and power requirements compatible with those of integrated circuits.

Finally, to make laser diodes highly integrated and cost effective, access to the light output and electrical leads from the top surface is under development. Such access permits wafer-level processing and testing; it also lowers package cost by



providing easier light output coupling. To this end, several laboratories, including our own, have been working on surface-emitting individual lasers and arrays, with good initial success. A false-color photograph of such a device appears on the back cover of this issue. It consists of a diode laser, optical waveguide, and grating, all operating in combination to produce a surface-

Michael Ettenberg received his BS degree in Metallurgy from the Polytechnic Institute of Brooklyn in 1964, and the MS and PhD degrees from New York University in 1967 and 1969, respectively.

Dr. Ettenberg joined RCA Laboratories, Princeton, N.J., in 1969, and has made major contributions in the area of III-V compounds and devices. In 1979 he was appointed Head of the Optoelectronic Devices and Systems Research group at RCA Laboratories. In 1984 Dr. Ettenberg received a David Sarnoff Award for Outstanding Technical Achievement, RCA's highest honor, for leadership in the understanding, development, and manufacture of solid-state optoelectronic devices.

He has authored or coauthored more than 95 papers and several book chapters. He holds 26 U.S. patents, all dealing with the properties of III-V compounds and with laser diodes and LEDs. Dr. Ettenberg is a Fellow of the IEEE and a member of the Optical Society of America, American Physical Society, and Alpha Sigma Mu Metallurgical Honor Society.

Contact him at:
RCA Laboratories
Princeton, N.J.
Tacnet: 226-3149

emitting diode laser. This development is comparable with the earlier progress of transistors from bipolar to planar types.

References

1. D. Wille, A. Rosen, "Laser development and applications," *RCA Engineer*, Vol. 31, No.1 (Jan./Feb. 1986).

Fiber-optic light sources

As the prime light source for fiber optics, InGaAsP has surpassed AlGaAs in importance. Here is a discussion of what it is and of how it is used.

The enormous expansion of the field of fiber optics in recent years has been due to new developments in fibers, detectors, and emitters. In this article, some of the developments in emitters (i.e., lasers and LEDs) will be reviewed, with emphasis on devices of current interest. Wherever appropriate, structures fabricated at New Products Division or RCA Laboratories will be described in some detail.

Initially, light sources used in fiber optics were based on AlGaAs (aluminum gallium arsenide), but currently, because of the much lower attenuation of fibers at longer wavelengths¹ (Fig. 1), there has been a change to the quaternary material InGaAsP (indium gallium arsenide phosphide).

Both of these materials exhibit the phenomenon of injection luminescence, which is the generation of light by the radiative recombination of minority carriers injected across a p-n junction. This mechanism is essential for fiber-optic communi-

Abstract: *The intensive development of fiber-optic communications in recent years is based on advances in both fibers and light sources, with one often stimulating further development in the other. The currently favored light source material is InGaAsP. This paper deals with the design, fabrication, and properties of lasers and LEDs based on this material. The objective is to give the reader an idea of the current state of development in the field of long-wavelength devices used in fiber optics.*

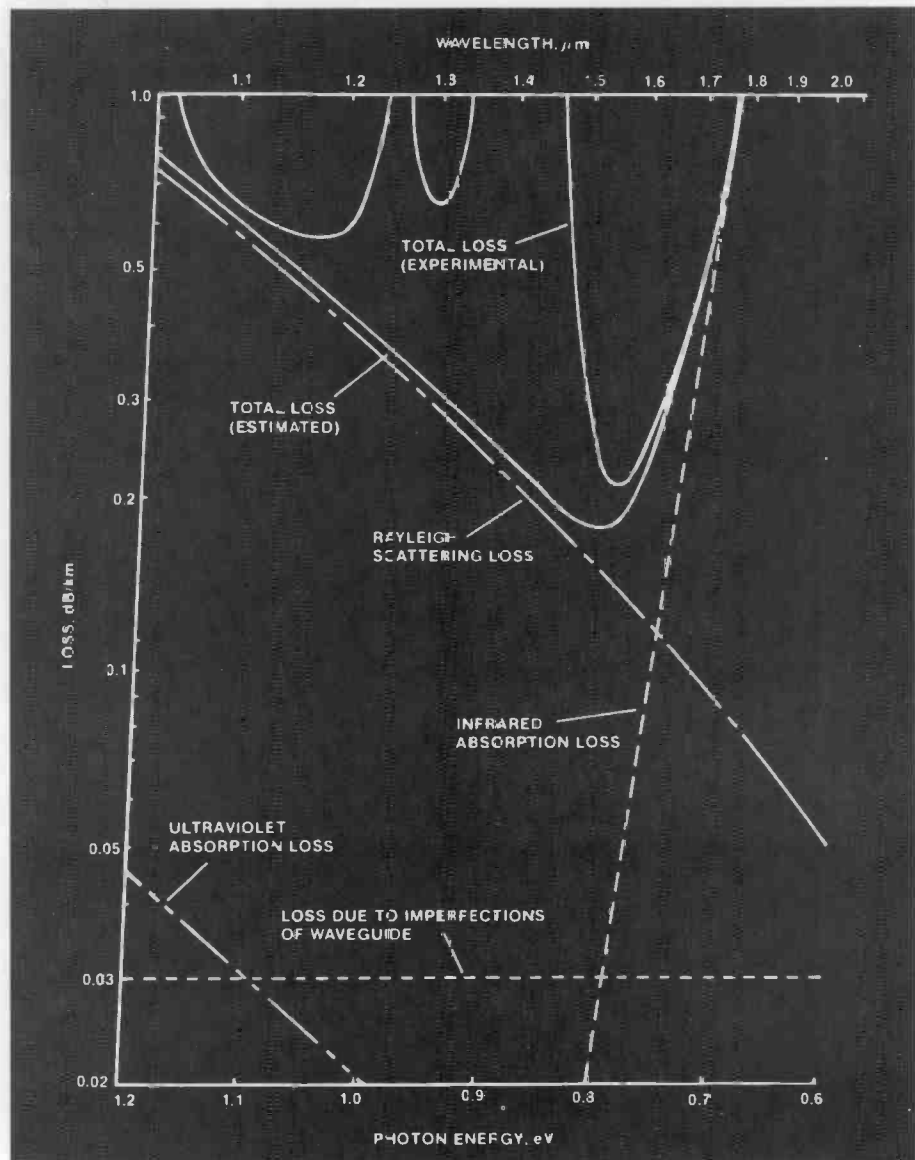


Fig. 1. Fiber attenuation vs. wavelength.

©1986 RCA Corporation.
Final manuscript received April 28, 1986
Reprint RE-31-3-2

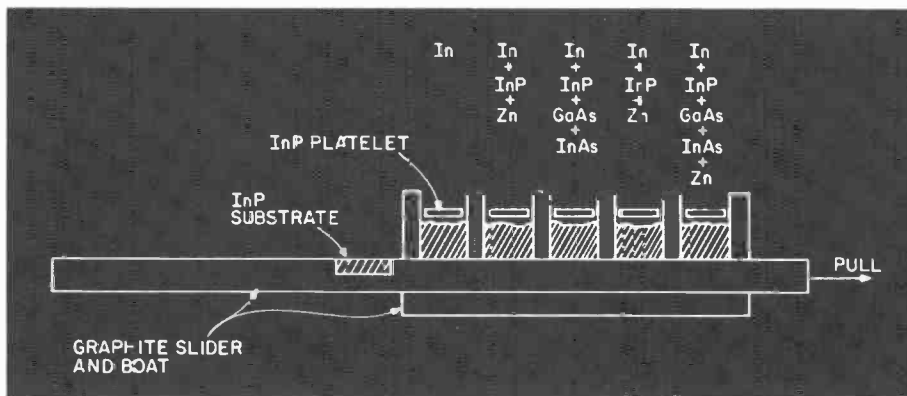


Fig. 2. Typical graphite boat showing melts used in growing InGaAsP material by LPE.

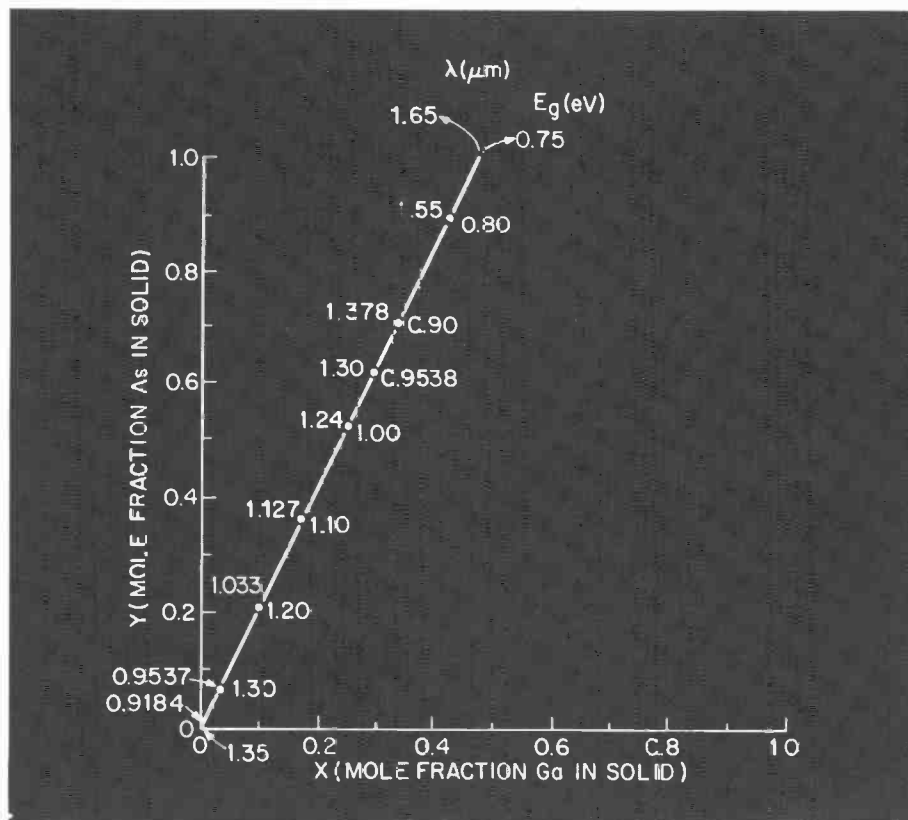


Fig. 3. InGaAsP material lattice matched to InP. The bandgap and the corresponding wavelength for a few compositions are indicated along the curve.

tions since it alone provides the radiance, the efficiency, the wavelength, and the speed needed to replace conventional copper coaxial cables in telecommunications applications.

Growth of InGaAsP materials

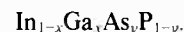
InGaAsP is grown by liquid phase epitaxy (LPE), by vapor phase epitaxy (VPE), by organometallic vapor phase epitaxy (OMVPE), or by molecular beam epitaxy (MBE). All of these methods are in use, but the oldest and still the most popular is

LPE, first developed by H. Nelson at RCA.² As adapted to the quaternary material, it is based on forming a solution of the required elements in liquid indium, bringing this solution into contact with an InP substrate wafer at an elevated temperature, and allowing the furnace where this process takes place to cool at a fixed rate. During the cooling period, an epitaxial layer of single-crystal material grows onto the surface of the substrate. In practice, this process is carried out several times during a single furnace cycle, by placing a number of different solutions in separate

bins of a graphite boat, and advancing the substrate stepwise from bin to bin (Fig. 2). Thus a multilayer structure can be built up, consisting of as many as eight or more different layers. The purpose served by these layers will be discussed further below.

In order to successfully grow the materials required, it is necessary to make sure the substrate and the grown layers have the same lattice constant. Violation of this requirement leads to outright epitaxial growth failure, or to the introduction of faults that manifest themselves in reduced light output and shortened operating life. It was a fortunate coincidence of nature as far as early work in this field was concerned that AlAs and GaAs have a virtually identical lattice constant. Thus the alloy in this system can be grown in almost any composition and a lattice-matched, strain-free layer may be grown on the single-crystal gallium arsenide substrate wafer. Therefore, in growing layers of GaAlAs on GaAs substrates, no special precautions need be taken to obtain lattice-matched epitaxial layers. However, in the quaternary InGaAsP system, the value of the lattice constant varies considerably with alloy composition and great care must be taken to ensure that lattice-matching is achieved in order to obtain strain-free, metallurgically perfect layers.

The solid composition is specified by the parameters x and y occurring in the compound formula:



Note that because of stoichiometry, In and Ga together (and As and P) form exactly 50 percent of the molecule. Although this alloy exists for all values of x and y between 0 and 1, one desires only certain values dictated by the device structure. These values are specified by means of two equations originally derived by Moon et al³ and subsequently modified by a number of authors,⁴ which give the bandgap E_g and the lattice constant a as a function of x and y :

$$E_g \text{ (in eV)} = 1.35 + 0.668x - 1.068y \quad (1)$$

$$+ 0.758x^2 + 0.078y^2 - 0.069xy - 0.332x^2y + 0.03xy^2$$

$$a \text{ (in } \text{\AA}) = 5.8696 + 0.1894y \quad (2)$$

$$- 0.4184x + 0.0130xy$$

Equation 2 can be used to obtain the compositions for which the lattice constant equals 5.8696 Å, the value for InP:

$$y = x / (0.4527 + 0.0311x) \quad (3)$$

Furthermore, the equation for the bandgap of those compositions lattice matched to InP becomes (expressed in terms of y)

$$E_g \text{ (in eV)} = 1.35 - 0.738y + 0.138y^2 \quad (4)$$

Figure 3 gives a plot of compositions of InGaAsP lattice matched to InP, showing the values of E_g and λ_g , the corresponding photon emission wavelengths, along the curve. It can be seen that materials with a certain range of bandgap values can be grown epitaxially onto InP without lattice mismatch.

The control of bandgap and refractive index in the grown layers is of critical importance in determining the final device performance. The bandgap of the material in the active layer of an emitter, i.e. the recombination region, determines the output wavelength of the device according to the relationship $E_g \text{ (in eV)} = 1.2399/\lambda \text{ (in } \mu\text{m)}$. The layers grown on adjacent sides of the recombination region are designed to have a lower index of refraction and a higher bandgap energy than the recombination layer. The larger bandgap on both sides of the recombination region confines the carriers injected into the recombination region, thus promoting a higher carrier density and increasing the probability of obtaining radiative recombination. The step in refractive index helps to contain the generated photons in the active region by converting it into a plane waveguide. This process again leads to higher efficiency and increased radiance in the finished device.

We have seen how the bandgap steps can be introduced by varying the layer composition. In regard to the refractive index step, the situation is more difficult, mainly because of the problems encountered in both measurements and calculations of the index. However, there are many materials, examples being AlGaAs and InGaAsP, in which the refractive index is inversely related to the bandgap; in other words, where the index decreases as the bandgap increases. In the present case, therefore, the index step is obtained simultaneously with the bandgap step.

Figure 4 shows the refractive index for several InGaAsP compositions, and for InP with two different impurity levels. While some of the values in this chart must be taken as approximate, it nevertheless seems to be consistent with other observations. Thus, taking the case of a laser emitting at $1.3 \mu\text{m}$, a layer of $\text{In}_{0.72}\text{Ga}_{0.28}\text{As}_{0.60}\text{P}_{0.40}$ surrounded by two layers of InP will result in a structure having an index step of 0.3, and a bandgap

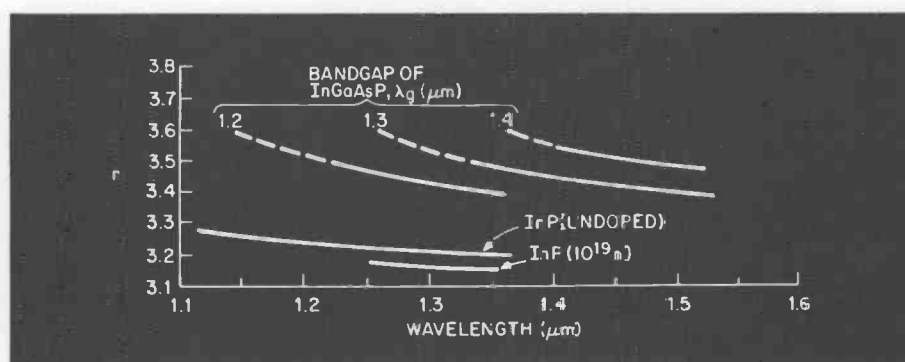


Fig. 4. Refractive index for several InGaAsP compositions defined by the bandgap wavelength, and for InP at two impurity levels.

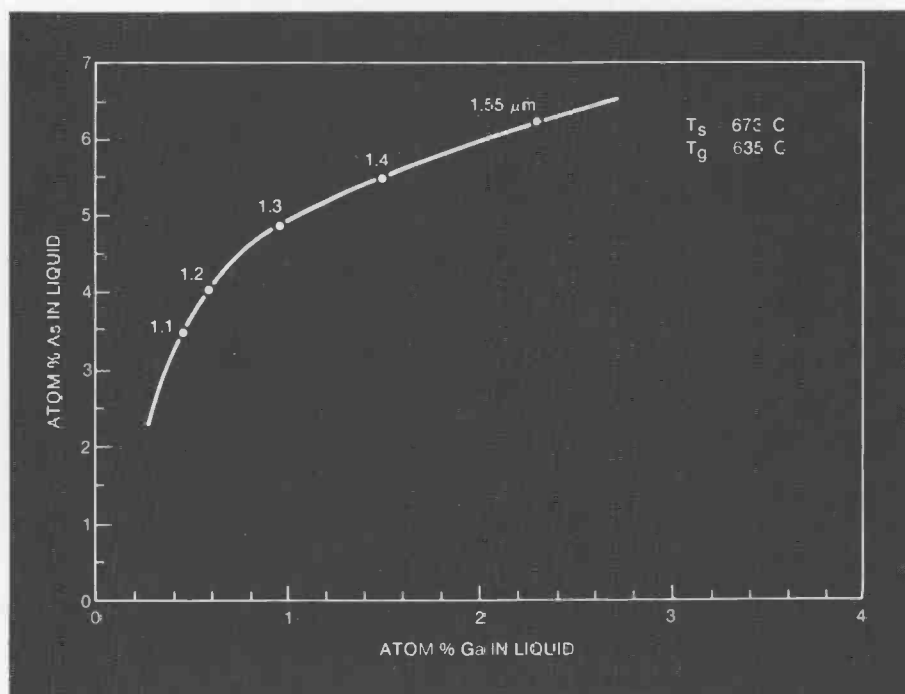


Fig. 5. Melt compositions for two-phase growth of lattice-matched InGaAsP. T_s is the melt saturation temperature, and T_g is the growth temperature.

step of 0.4 eV surrounding the emitting layer. These steps are typical of what is needed for injection lasers in order to obtain strong carrier and optical confinement and therefore low threshold current.

A more complicated situation arises in determining the melt needed to grow material with a particular composition. It has been found that this depends on the following:

1. Desired solid composition
2. Growth temperature
3. Previous melt history
4. Furnace atmosphere
5. Presence of solid InP in the melt
6. Degree of supercooling

It should not be surprising that published compositions obtained in one laboratory

seldom apply to the growth carried out in another laboratory. Figure 5 shows melt compositions and corresponding bandgap values obtained at RCA for a "two-phase" growth process, i.e. a process where platelets of InP are maintained in contact with the melt at all times.

LEDs

The C86013E, a typical edge-emitting LED available from NPD, is shown in Fig. 6. The device emits at a wavelength of approximately $1.3 \mu\text{m}$ and is fabricated by growing a sequence of layers, including the InP cladding layers and the InGaAsP active layer, and evaporating the metallic contacts. Individual devices are made by cleaving bars and sawing or breaking them

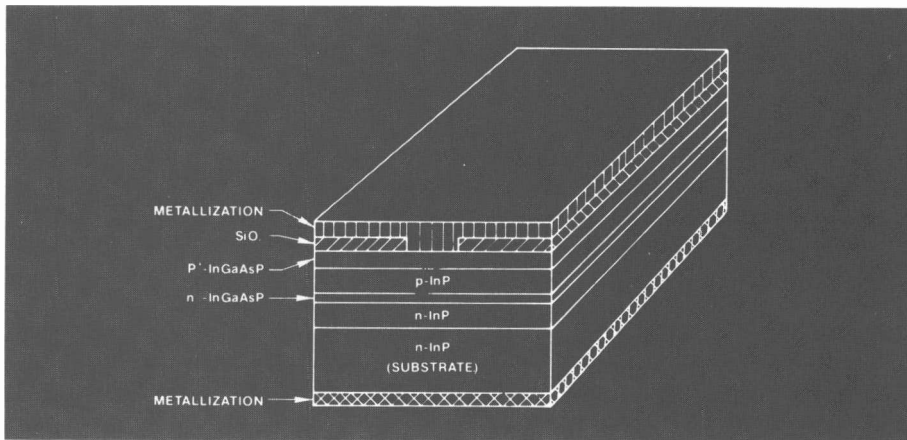


Fig. 6. Structure of InGaAsP LED pellet C86013E fabricated by NPD.

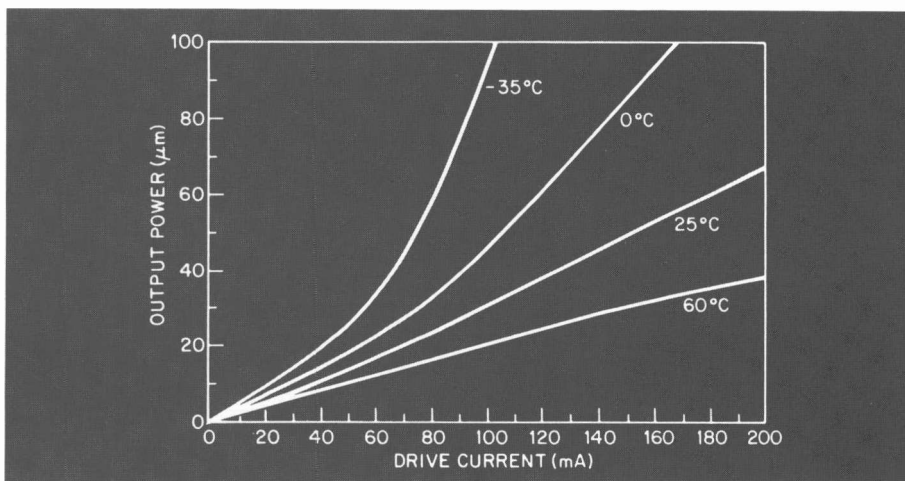


Fig. 7. Power output vs. current at several temperatures, for the LED of Fig. 6, coupled into a 50- μm core graded-index fiber.

apart into chips about 0.25×25 mm on a side. Each device will therefore have two cleaved and two sawn or scribed facets. Light is extracted from one of the cleaved facets, and the other one is usually coated with a reflecting film. A feature of the device is the presence of a dielectric layer, typically SiO_2 , between the semiconductor and the metal. This layer contains a stripe opening, which is extremely important for devices intended to be used for fiber-optic applications.

Conventional telecommunications fibers have an active core diameter of only 50 micrometers and a numerical aperture (NA) of about 0.2. Therefore, in order to maximize the amount of light launched into the optical fiber from the LED, it is essential to make the radiating spot smaller than the 50-micrometer diameter of the fiber and to direct as much of that light as possible into the 11.5° acceptance cone of the fiber. The function of the stripe is to force the current into a small region of the junction and to keep the radiating

spot smaller than 50 micrometers. The InP cladding layers form a plane waveguide that tends to focus the radiation pattern and increase the radiance of the LED so that more of its output is within the capture angle of the fiber. Even so, less than 10 percent of the total LED output is actually collected and transmitted by the fiber. For the C86013E, about 50 microwatts (-13 dBm) is available from the 50- μm core, 0.2-NA fiber pigtail. The actual usefulness of this signal in a communications system now depends upon the sensitivity of the receiver at the other end of the cable.

The RCA C30986 is an excellent example of an InGaAs p-i-n photodiode receiver that includes a GaAsFET transimpedance preamplifier. For a digital system operating at 50 Mb/s of NRZ data this receiver has a sensitivity of -46 dBm at a bit error rate (BER) of 10^{-9} . Allowing 10 dB of margin for connector losses, temperature compensation factors, etc., this would allow a loss budget of over 20 dB for fiber attenuation losses. Thus, a system

that employs cable with a loss factor of 2 dB/km should operate easily over a length of 10 km without the need for a repeater. (Somewhat longer distances are obtainable by using state-of-the-art cables with 0.7 dB/km attenuation.) A power versus current curve for the C-86013E coupled to a 50- μm core, graded-index fiber is shown in Fig. 7. LEDs can also be used for driving single-mode fibers with typically 8- μm core diameters, resulting in a 7 to 10-dB diminution in available power, but for that application there are more efficient designs, to be discussed later.

Lasers

The LED structure we have discussed so far is also capable of yielding a laser, since it already includes both optical confinement (through the index steps), and carrier confinement (through the bandgap steps). Thus, many LEDs can be driven into the lasing region merely by increasing the current applied to them. In practice, there are various design constraints that make this approach undesirable.

Before discussing laser designs, it might be useful to review the process of lasing as it applies to semiconductor lasers. The fundamental observation is that if the recombination layer consists of a semiconductor with a direct bandgap, the injection of a large number of carriers by a forward-biased p/n junction will achieve population inversion (a term meaning that more carriers are in an excited state than in a ground state). When such a state exists inside an optical cavity, i.e. a region providing optical feedback, and assuming that the recombination mechanism is radiative, an electromagnetic standing wave will develop and any additional recombination events generated by increases in current will feed this standing wave. Thus, the injected current is converted into optical power, which is emitted through the cleaved ends of the diode. When the device has just reached this state, it is said to be at lasing threshold. Experimentally this point is recognized by the sudden increase in output power as the current is increased by a small amount.

The practical differences between a laser and an LED concern linearity of output, angle of the emitted beam, spectral distribution, temperature dependence, and output efficiency. In an LED, light output increases more or less linearly with current. In a laser, light output also increases linearly up to the threshold current, at which point it increases exponentially to another linear region but with a slope much higher than

in the LED. The light beam emitted by an LED is broad, with a beam angle (FWHM) of 90° or more. A laser is capable of emitting a beam of 20° or less in both the transverse (perpendicular to the p/n junction plane) and lateral (parallel to p/n junction plane) directions. The reason the laser emits a narrower beam is that the optical mode assumes directional properties set by the internal waveguide. The spectrum of the laser usually consists of a few spectral lines, or even a single line in specially designed lasers, whereas the LED spectrum consists of a broad line (about 700 Å in half width), with sometimes a multiline spectrum superimposed on it. The output efficiency of the laser is greater than that of the LED, because the emission is in the form of a Gaussian beam with planar phase front on the axis of the beam. Thus, the emerging radiation encounters a facet reflectivity approximately equal to the reflectivity of a plane wave at normal incidence, which is about 30 percent for III-V materials with index in the neighborhood of 3.5. In contrast, the average reflectivity for an LED is very large, because the emission is the sum of components emitted over a wide range of angles, and at angles larger than 16° to the facet normal (the critical angle) the light is totally internally reflected.

Returning to the point made earlier, an LED with two cleaved facets becomes a laser when the applied current is high enough. In many cases, either by design (applying a very low reflectivity coating to the emitting facet, for example) or inadvertently, the current needed to reach lasing threshold is higher than the device can tolerate, and such devices cannot be made to lase under practical conditions. Optical gain and lasing in an edge-emitting LED occurs only in the region of current flow defined by the stripe opening. Such lasers are called "gain-guided" lasers.

Temperature dependence of lasers

In common with many semiconductor devices, lasers and LEDs are sensitive to temperature changes. While the LED output is affected by temperature due to changes in radiative recombination efficiency, the sensitivity of a laser to temperature changes is increased due to the threshold phenomenon. The usual way of describing the effect of temperature on the laser threshold is through the following formula:

$$I_{(th)} = I_0 e^{T/T_0}$$

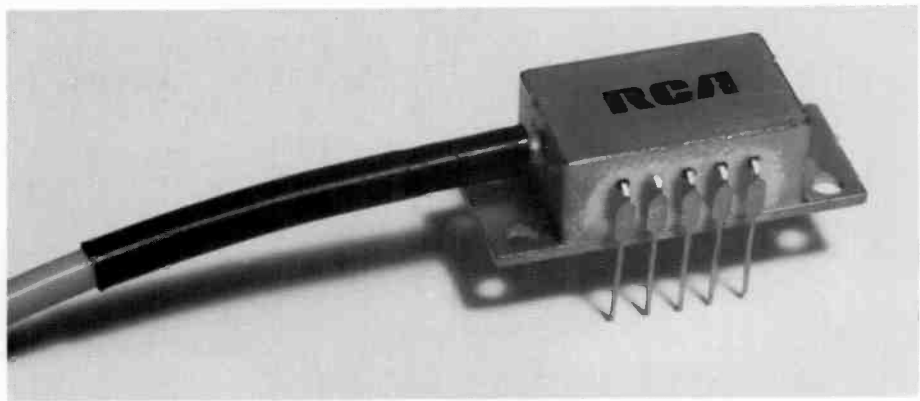


Fig. 8. Photograph of fiber-coupled emitter module, C86042E.

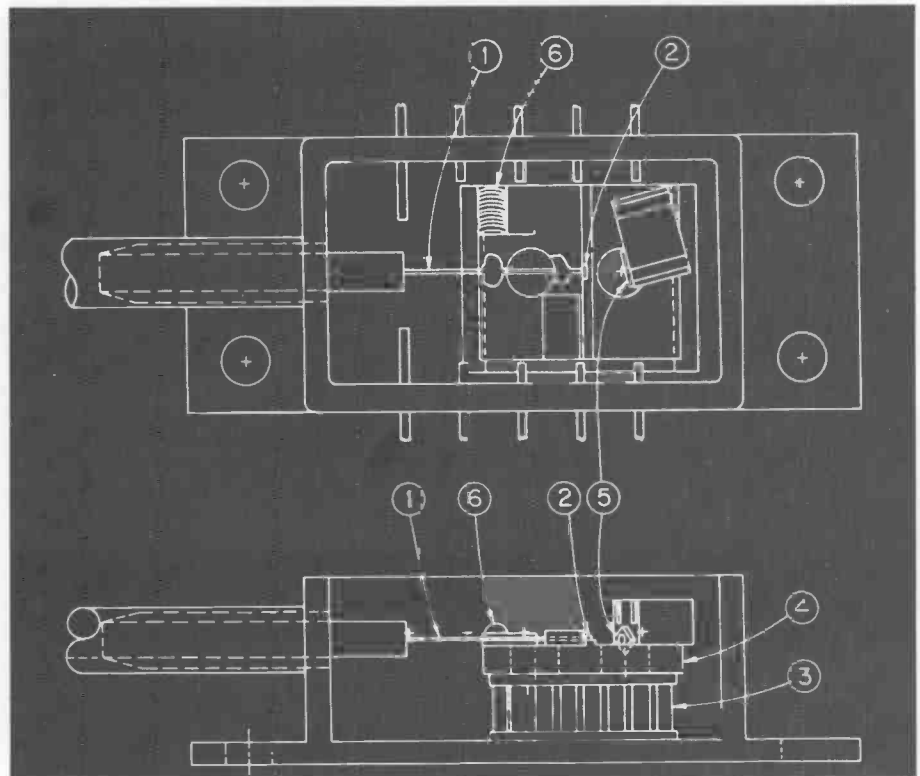


Fig. 9. Internal arrangement of C86042E.

The change in threshold current is an exponential function of temperature, the magnitude of the effect being described by the value of T_0 . AlGaAs lasers have typical T_0 values of 120 K, whereas InGaAsP lasers have T_0 values in the vicinity of 50-60 K. The reason InGaAsP lasers have so much greater temperature sensitivity has been explained on the basis of nonradiative Auger recombination, a process that becomes more likely as the bandgap is reduced. Nevertheless, properly made InGaAsP lasers do not suffer in performance in any significant way because of this effect.

Another consequence of temperature changes is a shift in the emission wave-

length. In an LED, this occurs because of the change in bandgap, but the shift is negligible compared to the wide emitted spectrum. In lasers, the bandgap shift, which occurs in steps of a few Å at a time, is accompanied by another shift, caused by the change in refractive index of the lasing cavity. Thus, there is a gradual shift of about 1 Å/°C caused by the index change, on which is superimposed a stepwise shift from one cavity mode to the next one, which averages to about 5 Å/°C.

Several methods have been used to compensate for this thermal sensitivity by means of external control elements.

These have included the use of Peltier coolers to control the junction temperature

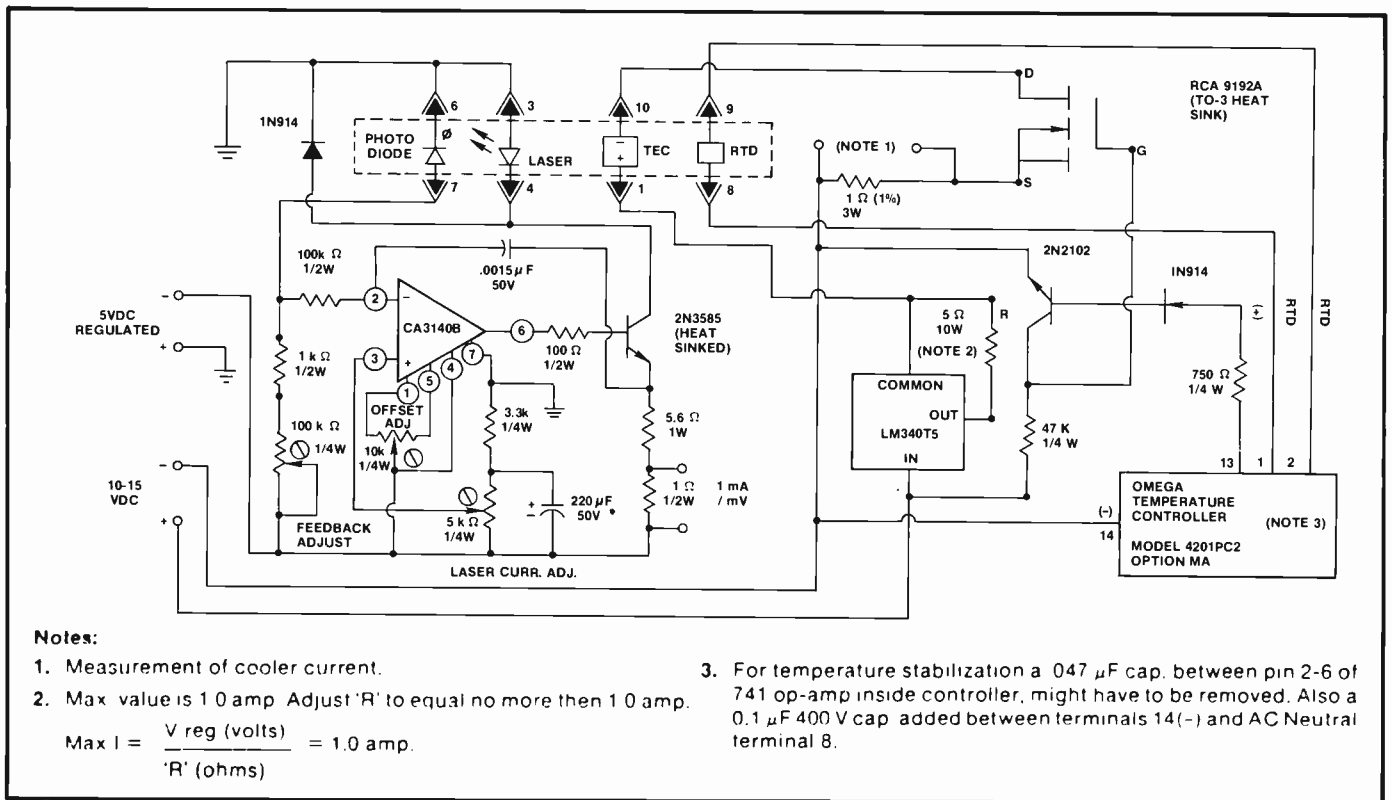


Fig. 10. Typical dc bias circuit for the C86042E module.

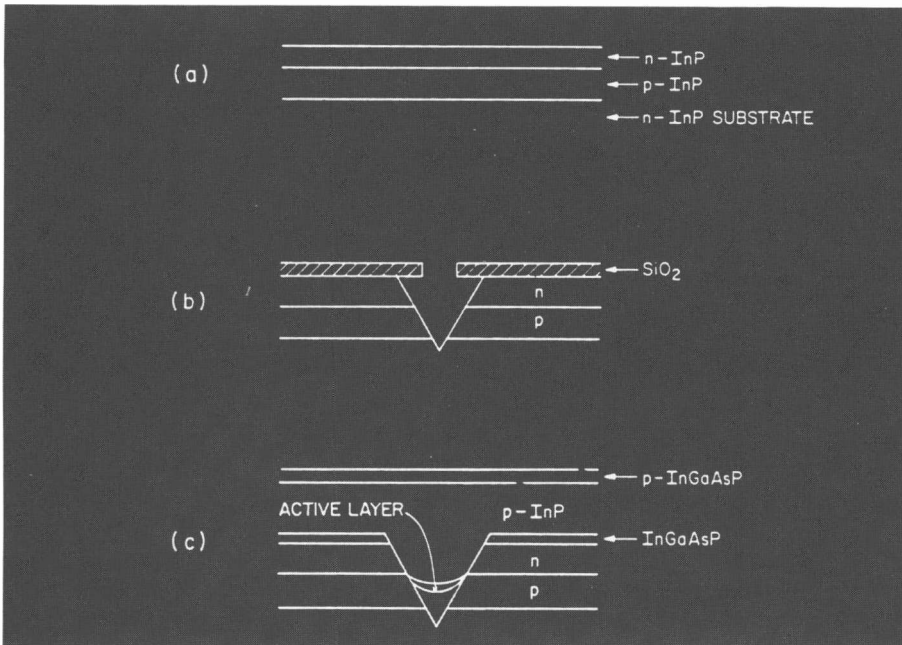


Fig. 11. Construction of the BC laser.

of the laser chip, and monitor photodiodes that can be used to control the drive current to the laser by means of a feedback circuit. A photograph of the C86042E is shown in Fig. 8, and the internal structure is shown in Fig. 9. This device employs a $1.3\text{-}\mu\text{m}$ gain-guided CW laser diode (2) that is coupled to a 50-micrometer core,

graded-index telecommunications fiber (1). The temperature of the laser chip is actively controlled using the thermistor temperature detector (6) to control the current through a multi-element cooling module (3). The action of the Peltier cooler pumps sufficient heat away from the chip mounting plate to maintain the laser at a temperature of

25°C when operating the unit at an external heat sink temperature of 70°C . Further control of the laser output is achieved by intentionally making the rear facet reflector on the laser chip slightly leaky by giving it a reflectivity of about 90 percent. The flux emitted from the rear is captured by a photodetector (5) positioned behind the laser. The photocurrent generated by the detector is supplied to the input circuit of a negative feedback op amp that controls the drive current of the laser. Any increase or decrease in the output of the laser is sensed by the photodiode and a corresponding change is made to the laser drive current to force a constant laser output. Typical examples of the circuits required to operate the device are shown in Fig. 10.

Single-spatial mode lasers

Although early lasers had the same structure as the LED described above, currently made lasers are based on more refined designs. The thrust of these methods is to provide lateral optical confinement by making that cavity dimension small enough to allow only the lowest order spatial mode to be excited. It will be remembered that the lateral confinement in an LED arose from the current constriction introduced via the stripe opening in a dielectric

film. However, the current spreads under the stripe, thereby widening the emission region. Furthermore, carriers generated in the active region are free to move sideways into unpumped regions (regions where there is not much current flow, and where they will recombine without contributing to the lasing process). Finally, it should be pointed out that the lasers discussed here are intended for driving fibers with core diameters of about $8\ \mu\text{m}$ (single-mode fibers), and thus benefit from having narrow emitting regions. For optimum coupling, the laser mode should produce a single-lobed Gaussian beam from a spot narrower than the fiber core diameter, and the beam angle should be as small as possible in both the lateral and the transverse directions.

The lateral confinement of the mode is obtained by introducing steps in the refractive index (lasers containing lateral steps in the index are called index-guided lasers). Carrier confinement is obtained from the simultaneous bandgap step, as discussed above, while efficient utilization of current is obtained by the introduction of current blocking layers, such as back-biased p/n junctions, which prevent current flow outside the cavity.

The buried crescent (BC) laser, fabricated at RCA Laboratories (and elsewhere), seems to satisfy most of the requirements discussed above (the origin of the name will be clear presently). The structure is fabricated (see Fig. 11) by first growing a series of alternating p- and n-type layers onto a substrate of InP. Next, a V groove is etched into the wafer, the V going all the way to the n-type layer. Using LPE, a series of layers consisting of an n-type cladding layer, an InGaAsP active layer, a p-type cladding layer, and an InGaAsP "cap" layer are grown into the groove. After the groove is filled, growth proceeds evenly over the wafer, resulting in a planar top surface. This growth takes advantage of the properties of LPE in achieving the peculiar shape of the active region, reminiscent of a crescent. The active region is very small, $1\text{-}2\ \mu\text{m}$ in width, and a fraction of a μm at its widest point. Some of the properties of these devices are illustrated in Fig. 12, which shows the output powers vs. current plots for a number of lasers obtained from a single wafer. Figure 13 illustrates typical far-field beam patterns, and Fig. 14 shows the emission spectrum. Coupling efficiencies between 35 and 50 percent can be obtained with such structures, both because the emitting region is small, and because

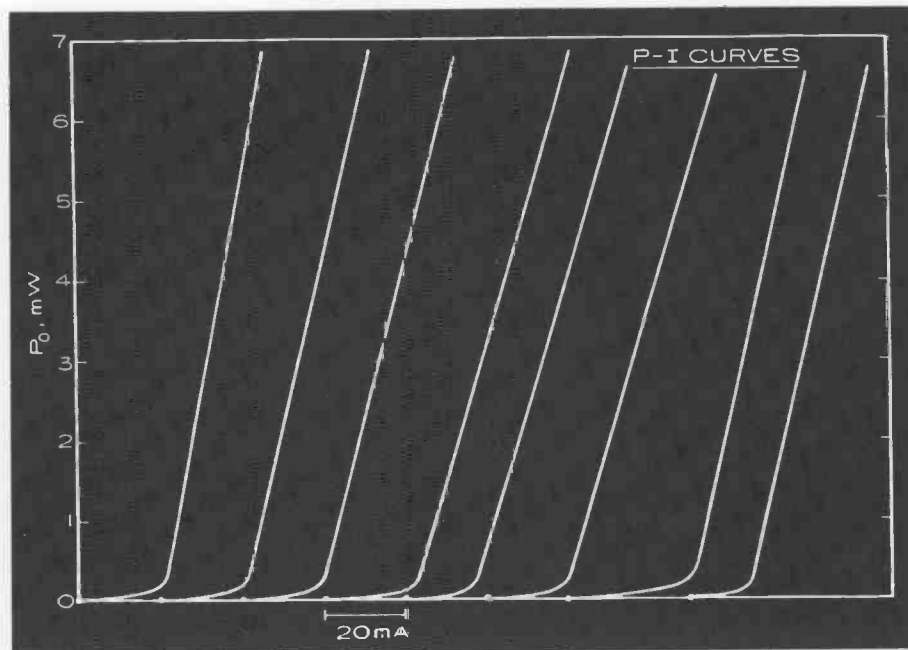


Fig. 12. *P-I characteristics for a series of BC lasers.*

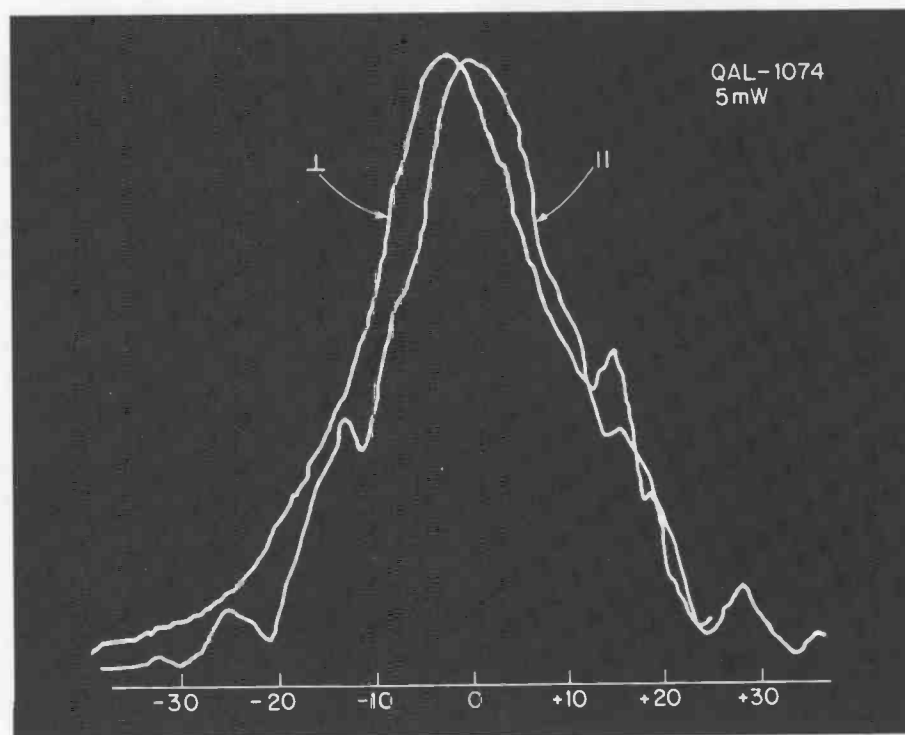


Fig. 13. *Far-field pattern in the horizontal and vertical planes for a BC laser.*

the beam is narrow. It is interesting to note that the narrow beam results because the extremely small size of the active layer forces the optical mode to spill out of the cavity, resulting in a round spot of about $3\text{-}\mu\text{m}$ diameter at the laser facet.

Dynamic single-mode lasers

Although the laser described above is capable of emitting a single line spectrum

over some range of currents or temperatures (see Fig. 14), it generally will not maintain a single-line emission under dynamic conditions. Thus, it becomes necessary to devise means for stabilizing the laser wavelength. A method that appears to be coming into general use depends on a grating built into the structure to select and hold the emission to a single line. Such lasers are called distributed feed-

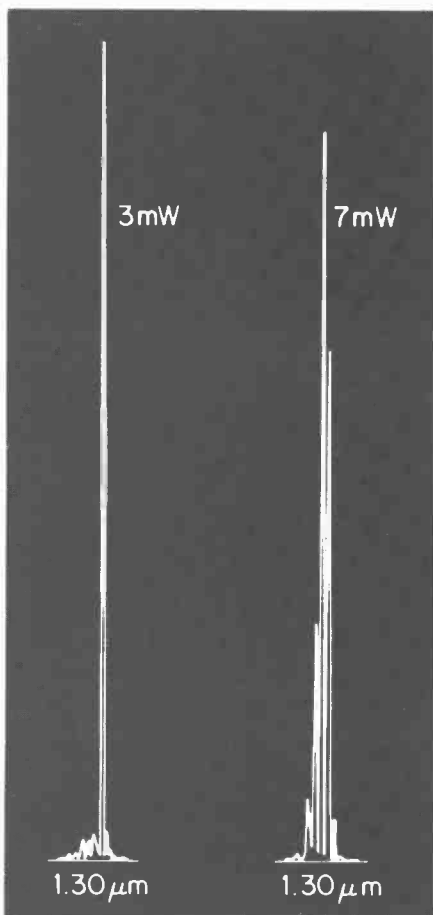


Fig. 14. Spectrum of a BC laser at two different drive currents. Note that an almost single line spectrum at 3 mW output becomes a multiline spectrum at 7 mW.

back lasers (DFB), since the grating is distributed along the cavity. This DFB action is illustrated in Fig. 15, which shows feedback as obtained by reflection from parallel mirrors (the Fabry-Perot cavity) occurring in ordinary lasers, and feedback as obtained by scattering from a grating located parallel to a traveling wave. The equation defining the connection between the grating period P and the emitted wavelength is easily obtained by looking at the scattering as an example of X-ray diffraction. Identifying the period P with the lattice spacing d , letting the angle of incidence become 90° , and letting the wavelength in the crystal equal the free space wavelength λ_0 divided by the effective waveguide index n_c , one obtains

$$2P = m(\lambda_0/n_c).$$

For most structures m is set equal to 1 or 2, i.e., first or second order gratings are used. To fabricate such a structure it is necessary to combine an index-guided single-spatial mode laser together with a

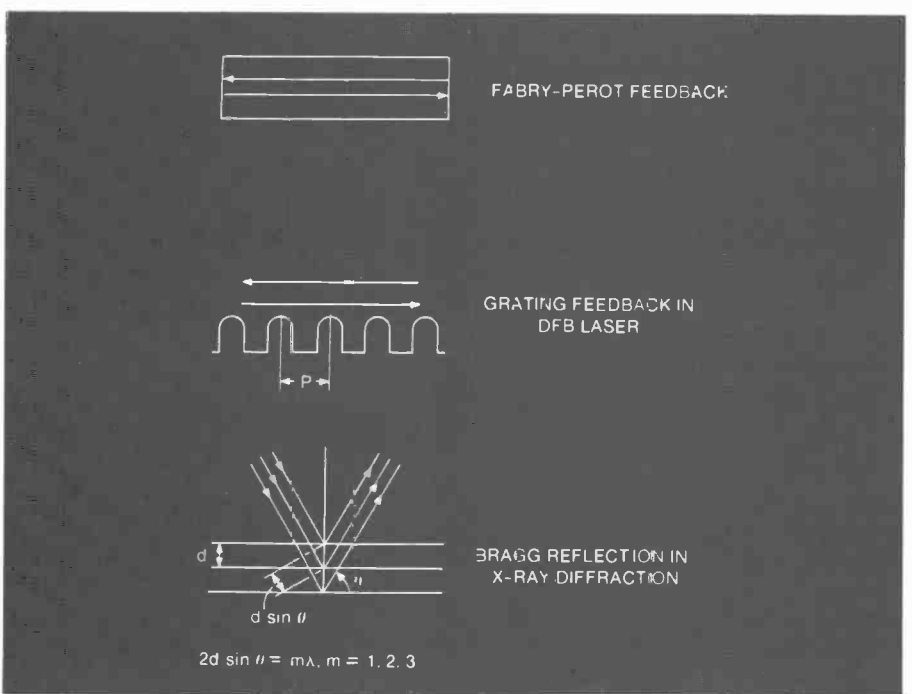
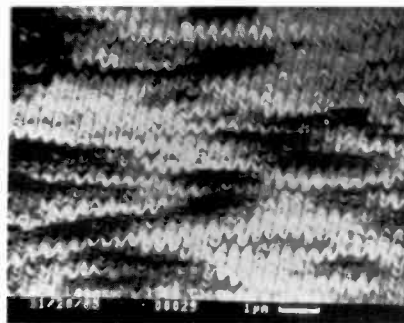


Fig. 15. A comparison of conventional laser feedback with grating feedback, and the analogy with X-ray diffraction.



GRATING IN InGaAsP BEFORE GROWTH

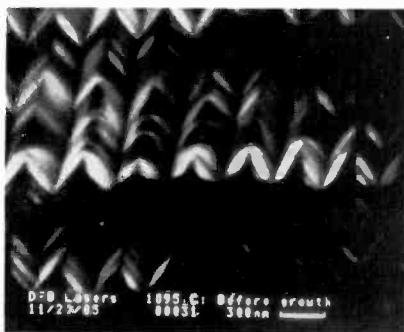
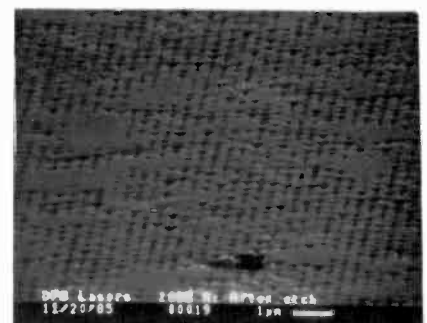


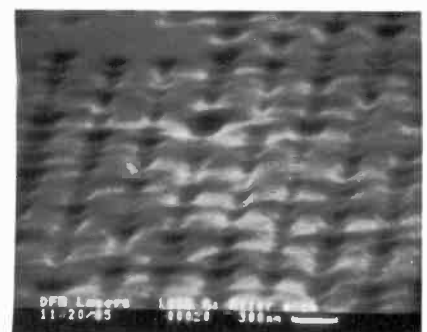
Fig. 16. LPE growth over a grating.

grating. The grating is made by exposing photoresist to the interference pattern formed by two laser beams. This produces a corrugation in the photoresist, which is next transferred into the semiconductor material through chemical etching. (Other methods for making these gratings have also been described.)

For InGaAsP emitting near $1.3 \mu\text{m}$,



AFTER GROWTH, InP REMOVED BY ETCHING



the grating period (for a second order grating) is $0.4 \mu\text{m}$. One of the problems in fabrication is to grow over the grating without destroying it. Figure 16 shows a grating as it appears after removing the overgrowth by etching in selective etches. It can be seen that the grating is largely undisturbed, even though it has been subjected to cleaning, etching, heating in a

furnace, and epitaxial overgrowth.

A DFB laser under development at RCA and several other laboratories is shown in Fig. 17. This laser obtains lateral guiding through the ridge structure, which imposes a higher effective index in the region under the ridge. A DFB laser does not stabilize the wavelength completely, but it prevents mode jumping. This is illustrated in Fig. 18, which shows a series of spectra taken on a DFB laser³ operated at different temperatures and at different drive currents. The wavelength shifts about $1 \text{ \AA}/^\circ\text{C}$ due to the temperature rise, which changes the refractive index of the grating and thus the grating period. The wavelength sidelobes present in ordinary lasers are largely suppressed.

Facet coatings

The need for facet coatings was alluded to earlier, during the discussion of LEDs. A variety of coatings are used in order to accomplish certain functions. To increase the light output of an LED and to suppress lasing, an antireflection coating is often used on the front facet, with a highly reflective coating on the rear facet. A similar arrangement is used on high-power lasers, except that the front facet is coated with a layer yielding a reflectivity of 5-10 percent, which increases the output power without at the same time making the laser threshold too high. Commonly used materials for these coatings are Al_2O_3 ⁶ or SiO_2 for the non-reflecting facet and multistack layers of Si and Al_2O_3 for the reflecting coatings.⁷ A special situation arises in the case of LEDs, since none of the above materials have the required index to obtain the lowest possible reflectivity. A typical effective index for both AlGaAs and InGaAsP double heterostructure materials is 3.35. Thus, a single layer antireflection film should have an index given by $\sqrt{3.35} = 1.83$. Two materials have been reported capable of yielding this value: specially prepared SiN_3 ⁸ and Sc_2O_3 .⁹ With these, reflectivities as low as 4×10^{-4} have been obtained. Using such films on the front facet of highly efficient index-guided lasers, one obtains a device called a superluminescent diode (SLD). This structure shares some properties of the laser and of the LED, in that it has a broad spectrum and a relatively narrow output beam, typically 35° in both directions. The laser power curve and the SLD power curve for a buried crescent structure are compared in Fig. 19.⁸ SLDs are seen to be LEDs of extremely high performance.

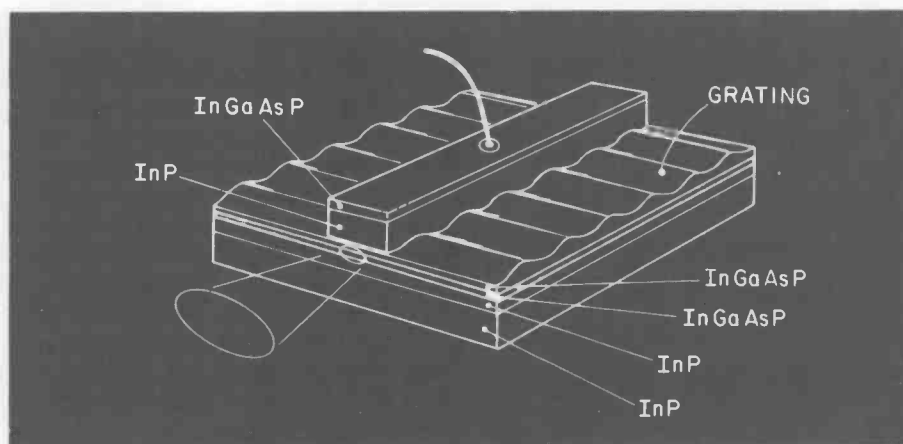


Fig. 17. Structure of a ridge-guide DFB laser.

Reliability

The components of a fiber-optic system are expected to show excellent reliability, with a period of 10 years before replacement being an often quoted goal. A great deal of work has been devoted to the study of reliability and degradation in LEDs and lasers, both under conditions simulating their use and under conditions of accelerated degradation. An example of a real-life study made at RCA consisted of a group of AlGaAs lasers operated continuously for seven years before they were removed from the test fixtures. Other tests (one of which will be described below) were made on InGaAsP devices.

The main causes of degradation seem to be the solid diffusion of gold from the contact into the active region of the device, the creep of solder or flux along the device surface, the generation of nonradiative centers along etched surfaces, the generation of intermetallic compounds at the contact-to-solder interface, and the occurrence of high electrical transients in the bias circuitry. Careful attention to these factors has resulted in the development of extremely long lived devices. The most important degradation factors in AlGaAs, namely facet damage and the generation of dislocation networks fueled by nonradiative recombination events, seem to be of much less importance in InGaAsP devices.

Telecommunication systems requirements demand that system components exhibit mean times to failure (MTTF) in the range of 10^6 – 10^8 hours. Since it is clearly not possible to test devices for such a long time period, methods have been developed to predict the MTTF by means of accelerated tests. As in the case of most other types of semiconductors, lasers and LEDs are assumed to have

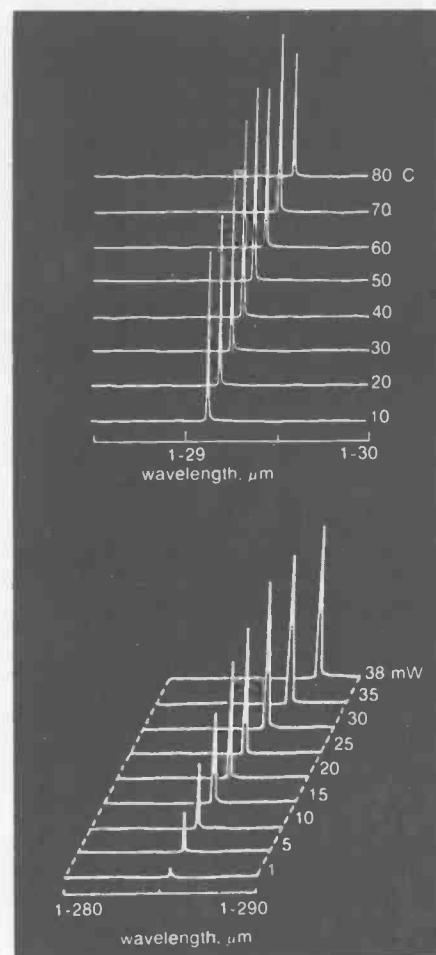


Fig. 18. Spectral shifts due to temperature and due to internal power dissipation in a DFB laser.

failure mechanisms that are based on reaction rates described by the Arrhenius relation:

$$F = Ae^{-\Delta E/kT}$$

where F is the failure rate, equivalent to the inverse of MTTF, ΔE is the activation energy of the process (usually between

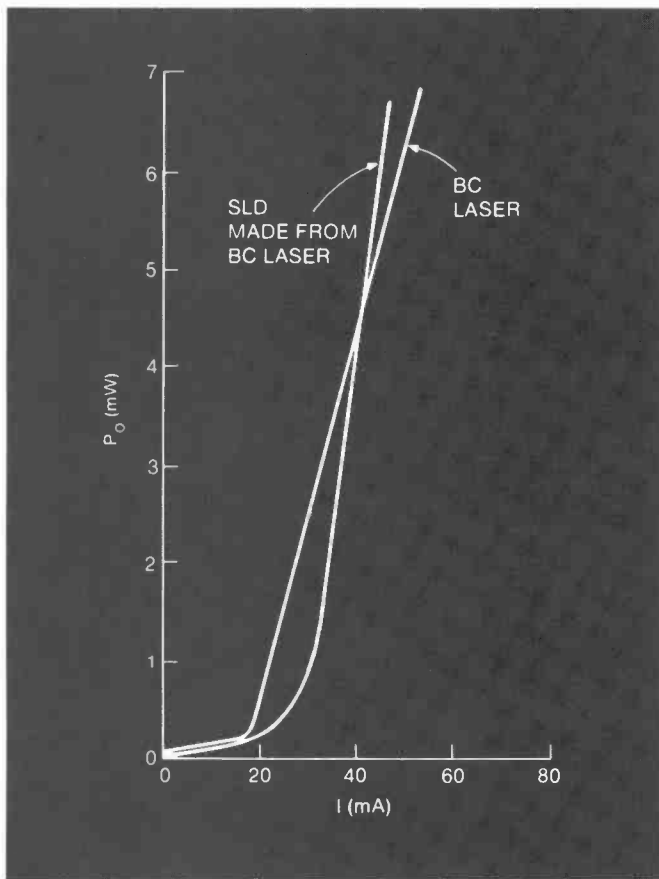


Fig. 19. Power output for a BC laser and for a superluminescent LED made from that laser.

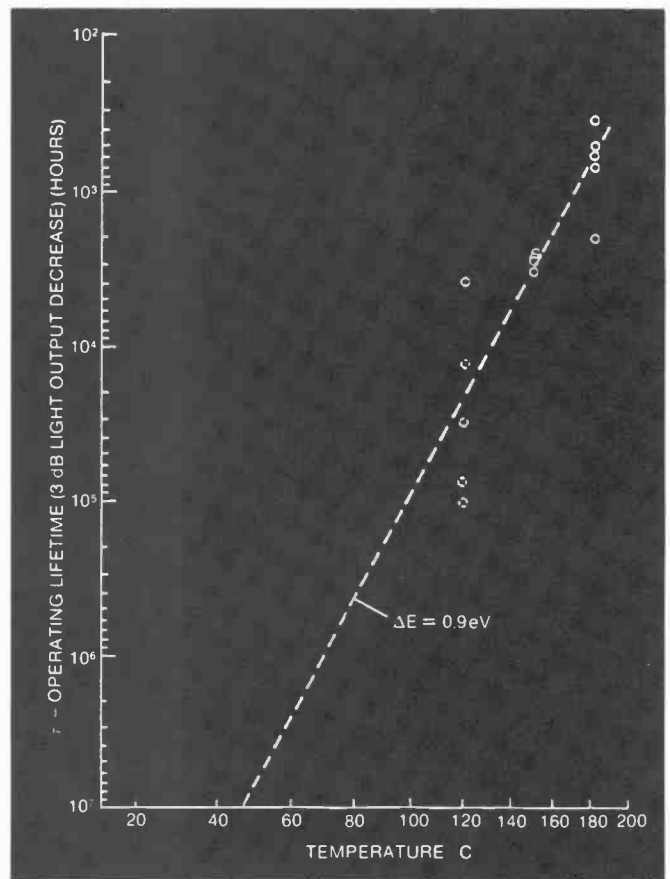


Fig. 20. Mean time to failure data for groups of InGaAsP diodes operated at three different temperatures, plotted so as to facilitate extrapolation to lower temperatures.

0.65 and 1.0 eV), and T is the absolute temperature in Kelvins.

Using the above model, it is possible to test groups of devices at various temperatures above their normal operating range in order to induce failures at an accelerated rate. Since the process is assumed to follow the Arrhenius relation, a linear curve is expected when the data are plotted as log (time) vs. $1/T$. The MTTF at other temperatures is then estimated from an extrapolation of the curve. Figure 20 shows the results of tests run on several groups of $1.3 \mu\text{m}$ IR emitters tested at 125, 150, and 180°C .¹⁰ These data project a mean operating lifetime of almost 10^7 hours at 50°C , where failure was defined as a decrease in output to 50 percent of the initial value.

Conclusion

A review has been given of some of the current fiber-optic light sources. The advances have been extremely rapid, and the amount of work done in this area, in many different countries, has been enor-

mous. Is it possible to make any statements about the future trends in this field? Advances are to be expected in DFB lasers and other novel devices, and these should become important commercially. Even lower attenuation is predicted for non-silica-based fibers at longer wavelengths, such as $2.5 \mu\text{m}$, and fibers, light sources, and detectors for this range are under active study in many laboratories. Instead of constructing systems from discrete devices, there will be monolithic drivers incorporating lasers and amplifiers on the same chip, another area currently under active development. There is no doubt whatsoever that fiber optics will continue to take over communication channels now served by other means, and that it will do it more efficiently and more cheaply than anyone could have imagined only a few years ago.

Acknowledgment

Numerous individuals at RCA, both in Princeton and in NPD-Lancaster, have contributed to the development and study

of devices mentioned in this article, and it is to them that the authors wish to express their appreciation.

References

1. T. Miya, Y. Terunuma, T. Hosaka, T. Miyashita, *Electron. Lett.*, 15, 106 (1979).
2. H. Nelson, *RCA Review*, 24, 603 (1963).
3. H. Moon, Ga.A. Antypas and L.W. James, *J. Electron. Mat.*, 3, 635 (1974).
4. The version used here is from E. Kuphal, FTZ 65TBr20, Darmstadt, Fed. Rep. Germany, Feb. 1983.
5. M. Kitamura et al., *Electron. Lett.*, 19, 840 (1983).
6. I. Ladany, M. Ettenberg, H.F. Lockwood and H. Kressel, *Appl. Phys. Lett.*, 30, 87 (1977).
7. M. Ettenberg, *Appl. Phys. Lett.*, 32, 724 (1978).
8. G. Eisenstein and L.W. Stulz, *Appl. Opt.*, 23, 161 (1984).
9. I. Ladany, P.J. Zanzucchi, J.T. Andrews, J. Kane and E. DePiano, *Appl. Opt.*, 25, 472 (1986).
10. M. Ettenberg, G.H. Olsen, F.Z. Hawrylo, *J. Light-wave Tech.*, LT-2, 1016 (1984).



Ivan Ladany received a BS in 1949 and an MS in 1952, both in Physics, from Northwestern University. He then worked at the Naval Research Laboratory from 1953 to 1966. He joined RCA Laboratories in 1966 as a Member of the Technical Staff, and since then has worked on GaP, GaAlP, InGaAsP, and GaAs electroluminescence. For his work on GaP electroluminescence, Mr. Ladany received an RCA Laboratories Outstanding Achievement Award in 1969. In 1980, he was a corecipient of an RCA Laboratories Outstanding Achievement Award for his work on InGaAsP lasers. He is the author or coauthor of a number of papers, and holds more than 15 patents, and is a member of the American Physical Society, the IEEE, and Sigma Xi.

Contact him at:
RCA Laboratories
Princeton, N.J.
Tacnet: 226-2914

James T. O'Brien has been Manager of Product Development and Applications Engineering for Solid State Emitters at New Products Division, Lancaster, Pa. He has a BS in Physics from St. Joseph's College and an MS in Engineering from Newark College of Engineering. In 1978 he received the M. Admin. degree in Business from Pennsylvania State University.

Contact him at:
New Products Division
Lancaster, Pa.
Tacnet: 227-6669

Multichannel diode laser arrays for high-data-rate optical recording

Monolithic linear arrays of individually addressable high-power diode lasers are being developed as the light sources of a new generation of extremely high-performance multichannel optical data storage systems.

One of the most successful consumer products of the decade is the Digital Audio Disk (DAD), or Compact Disk (CD), system for the playback of recorded music. A computer counterpart, the CD-ROM, has also entered the marketplace recently with products announced by a number of manufacturers. The digital data on these disks was originally recorded onto a master by focusing the modulated light of a laser to submicron spot diameters. The compact disks are fabricated from the master; they are accurate, archival duplicates. Data is retrieved in the audiophile's home, auto-

Abstract: *Semiconductor diode lasers have become the preferred light source in a wide range of consumer and commercial optical data storage systems. RCA has been a world leader in the development of both diode lasers and high-performance optical memories. Recently, multichannel optical recorders have been developed to meet the very high data rates required for the storage and retrieval of vast amounts of data in satellite imaging and supercomputer memory applications expected over the next decade. Monolithic arrays of high-power diode lasers, developed at RCA Laboratories over the past four years, will serve as the optical source in a new generation of high-performance optical data recorders under development in the Advanced Technology Laboratories and the Communications and Information Systems Division.*

©1986 RCA Corporation.
Final manuscript received February 21, 1986
Reprint RE-31-3-3

mobile, or at the computer workstation by focusing the light of an unmodulated (i.e., cw) diode laser on a spinning disk and detecting the modulated reflection of the light.

The products are so well designed and professionally manufactured that there is a strong temptation to think that optical recording technology has now developed into a mature industry. In fact, this is not the case. The products mentioned above represent the "low end" of the performance spectrum available from this technology. A strong effort is underway at RCA Laboratories, Advanced Technology Laboratories, and the Communications and Information Systems Division to meet the demands of the highest performance requirements. Applications are envisioned in which massive amounts of data (10^{11} to 10^{15} bits) must be both recorded and retrieved at data rates of many hundreds of megabits per second with fast random access to any bit of data in storage. In many of these applications, the recording medium must be erasable for repeated use.

RCA has been extremely active in the development of optical data storage media,¹ semiconductor diode laser sources,² and recording systems^{3,4} development throughout the history of the field. This paper will review a recent advance in diode laser technology that has generated a new class of extremely high-data-rate optical recording systems, which record and play back multiple channels of independent data simultaneously, allowing commensurately multiplied data rates.

Multichannel optical recording

The maximum rate at which data can be recorded on a spinning optical disk is determined by the optical power density at the spot focused on the disk, the optical sensitivity of the recording medium, the disk rotation velocity, and the response of the servomechanisms required to keep the laser focused on the moving target. For single-channel systems using an argon ion laser as the recording source, the practical continuous recording rate available to the system user is about 33 Mbits/s. Systems based on aluminum-gallium-arsenide (AlGaAs) diode laser sources will have decreased capabilities due to their longer wavelength (approximately 830 nm versus 488 nm). Despite this, the AlGaAs diode laser is supplanting other types as the preferred source in recording systems because of its compactness, high electrical-to-optical power conversion efficiency, ease of modulation, low cost, and long life. Also, media manufacturers are starting to mass produce both archival and erasable optical discs tuned for use with diode lasers. These disks typically require peak powers of 6 to 15 mW, focused to spots having full-widths at half-maximum of $0.75 \mu\text{m}$, in order to record data that arrives at the recorder with an average duty cycle of 50 percent. Many write-once diode laser optical memory systems are now on the market that operate at data rates up to 24 Mbits/s (3 Mbytes/s).

Such data rates, while impressive, will not suffice for imaging instruments and supercomputers planned for deployment and installation in the next decade. For

example, the NASA Space Station, planned for operation in 1994, will be the platform for several imagers, each transmitting enormous amounts of data (10^{13} bits/day) at 300 Mbit/s data rates.⁵ Advanced Technology Laboratories has responded to the need for large libraries of stored digital data by developing "jukeboxes" of optical disks.⁶ Two systems, delivered to NASA's Marshall Spaceflight Center and the Rome Air Development Center, each store 128 discs, totaling 10^{13} bits, with random access to any bit of data on any disk within 6 seconds. Both units use an argon ion laser source. In the NASA machine the beam is split into two channels, each externally modulated by use of acousto-optic deflectors, to double the data transfer rates. ATL has, in fact, implemented nine-channel heads in developmental argon laser recorders, attaining recording rates of 300 Mbit/s.⁶ The direction of the industry, however, demands that the next generation of high-performance optical recorders be based on solid-state diode laser technology.

Furthermore, the use of erasable media is critical for many data storage applications. Some systems, such as the Optical Disk Buffer under development at ATL,⁶ must retain data only for relatively short times. The disks must be erased frequently for this buffer memory system to perform its function. In other applications, the availability of reusable media greatly decreases the cost of operation.

The most advanced erasable media currently being manufactured is based on a magneto-optic effect in which magnetic domains of the material change the direction of their magnetization due to local heating by the laser in the presence of a magnetic bias field.⁷ In order to erase the data in a single pass of the laser, as is desired in most applications, the laser must be operated continuously at the power level required for recording. This doubles the thermal load on the laser and necessitates the use of a diode with approximately twice the output power capability as is necessary for archival recordings. Fortunately, recent advances in semiconductor diode laser technology make the development of diode laser-based erasable optical recorders possible.

Individually addressable diode laser arrays

A monolithic linear array of individually addressed diode lasers, each falling within the field of view of imaging optics, is an obviously appropriate configuration for the

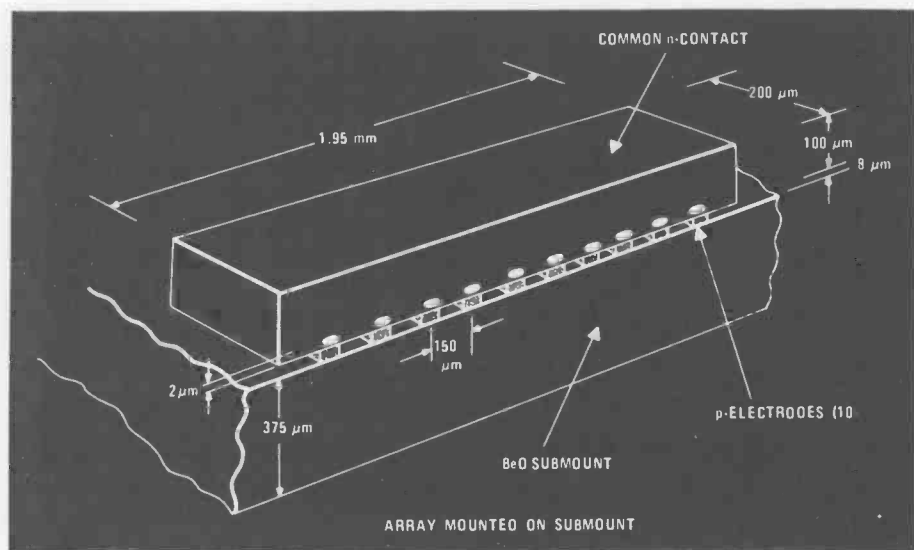


Fig. 1. Schematic view of an individually-addressed ten-element diode laser array chip mounted on a beryllia submount.

realization of compact, practical, high-performance optical recorder. A schematic drawing of a ten-element array is shown in Fig. 1. Each diode laser is independently, directly modulated by the injection current supplied to the lasers via individual contacts, and the separate data channels are simultaneously recorded on multiple, parallel tracks on a moving optical recording medium. The data transfer rate of the system is the sum of the data rates of each independent channel. Fabrication of the sources on a single semiconductor chip ensures that they will be in spatial and angular registry. All the sources lie on a straight line perpendicular to the optic axis, allowing the use of a single, wide field-of-view collimation lens to collect the light.

RCA Laboratories has been a world leader in the development of AlGaAs diode laser technology since the inception of the field. During the early 1980s, a prime motivation in the field was the need for a high-power (approximately 20 mW cw), index-guided device capable of emitting laser light in a fundamental spatial mode for optical recording applications. The light output from index-guided diode lasers is characterized by having negligible astigmatism, and can therefore be focused to a diffraction-limited spot by the use of suitable optics to produce high-quality recordings. These efforts led to the development of the CDH-LOC (constricted double heterojunction, large optical cavity)⁸ and CSP (channeled substrate planar)⁹ structures, both of which have been used successfully as optical recording sources. Historically, RCA Laboratories concentrated

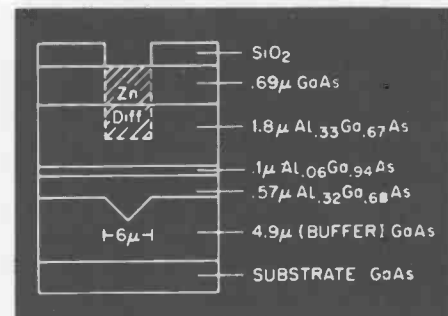


Fig. 2. Structure of the CSP (channeled-substrate-planar) AlGaAs diode laser structure showing layer compositions and dimensions.

on the development of the CDH-LOC laser first, both as single devices and as arrays of sources.¹⁰

More recently, development of the CSP structure has resulted in very-high-power, single-spatial mode lasers. The CSP is fabricated by liquid phase epitaxial growth over a single channel etched using photolithographic techniques into a GaAs substrate. The layers of the structure grow flat, as the name of the device suggests; the laser growth is, therefore, relatively easy to reproduce. The structure of this device is depicted in Fig. 2, with the compositions and thicknesses of the layers shown on the right of the figure. Light is generated in a thin (approximately 800 Å thick) active layer of undoped $\text{Al}_{0.06}\text{Ga}_{0.94}\text{As}$ sandwiched between cladding layers of p-doped and n-doped AlGaAs (top and bottom of the figure, respectively) of higher aluminum concentration. This stack of layers forms a real index guide that confines the laser light in the transverse direction

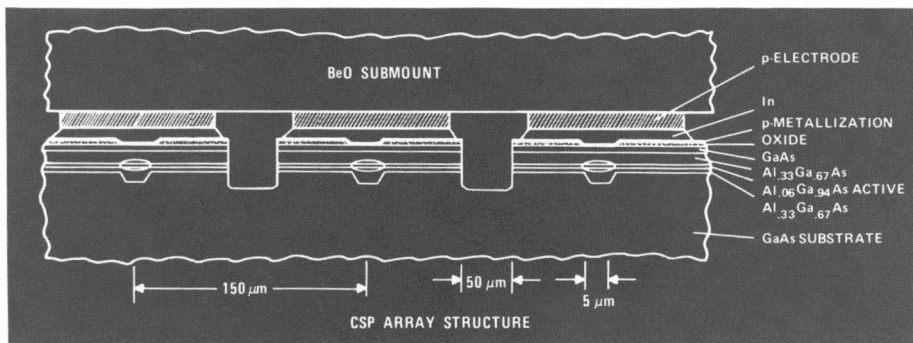


Fig. 3. Three elements of a multielement CSP diode laser array bonded to the metallized electrodes of a submount.

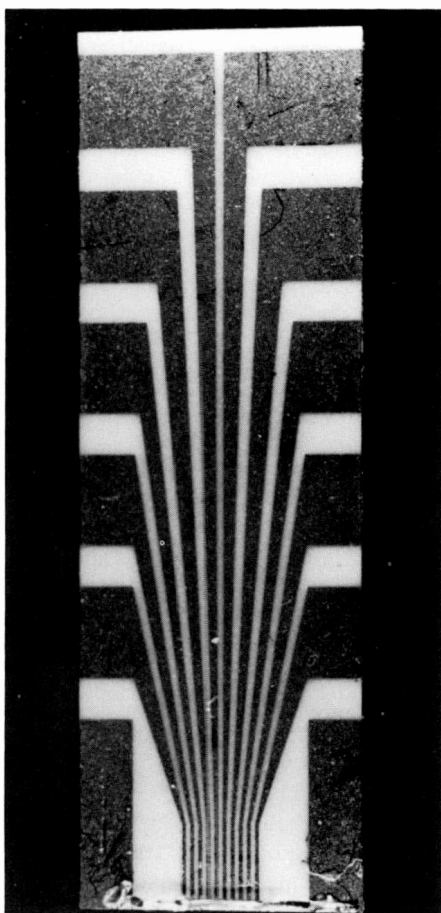


Fig. 4. Photograph of a mounted laser array. The array chip is at the bottom edge of the submount with laser emission toward the bottom of the page. The p-electrode pattern is evident. Gold ribbons connect the n-side (top) of the chip to rectangular contact pads.

(perpendicular to the heterojunction plane). The injection current is confined both by a narrow contact stripe in the p-side metallization, defined by an SiO_2 insulation film deposited on the GaAs cap layer, and by the diffusion of a zinc finger partially through the p-cladding layer. The injection current would itself confine the

lateral spatial mode (parallel to the junctions) by affecting the gain distribution, but such a gain-guided laser structure would emit an astigmatic beam of light. The lateral spatial mode is also well-confined by the shoulders of the channel. The laser light has a higher energy than the bandgap of the n-GaAs substrate material and is, therefore, heavily absorbed outside the channel region. In addition, the indices of refraction of the layers support radiation modes into the substrate, which also increase the loss outside of the channel.

Array processing, mounting, and addressing

Incorporation of such sources in optical recording systems also necessitates the development of a package that allows simultaneous addressing of each element of the laser array in an appropriate thermal and mechanical environment. For each different recorder configuration, compact multiple electrical laser drivers must be developed as well as optical systems that image the array onto the recording surface with an appropriate spacing between the recorded tracks.

Figure 3 depicts three elements of an array of CSP diode lasers. The lasers are separated by $150 \mu\text{m}$, defined by the mask pattern used to photolithographically etch the channels and contact stripes. This distance is a compromise between the desire to pack as many lasers as possible into the field-of-view of the optical system and the need to minimize crosstalk between the diode elements. Electrical crosstalk between elements is eliminated by the formation of $50\text{-}\mu\text{m}$ channels between the elements. These channels are ion-milled through the p-contact metallization (comprised of Ti-Pt-Au) and the active layer of the CSP structure. Optical interactions between laser elements is insignificant at $150 \mu\text{m}$ separations in the CSP design. In addition, the

heat generated by each diode laser (100 to 250 mW under typical operating conditions) is substantial, and could perturb the operating conditions of adjacent devices in an array. In the present array geometry, such thermal interactions have not significantly affected the output power of the laser elements.

The array is bonded to a submount, as shown in Fig. 4, which provides individual electrical contact to each of the diodes and makes handling easier. The design of the submount is dictated by these requirements as well as the need to minimize the thermal resistance between the heat sources (the diode laser junctions) and a heat sink. Beryllia (99.5-percent BeO) was the material chosen for this purpose as it has a relatively high thermal conductivity ($2.2\text{W}/\text{cm}\text{-}^\circ\text{C}$) and a coefficient of linear thermal expansion that matches that of GaAs, minimizing thermally induced stress at the array-submount interface.

The p-side of the chip is soldered to the metallized submount. The front facet of the array must be positioned to within several microns of the submount edge, to avoid obscuring the highly divergent output beam. Also, the array must be positioned laterally to a tolerance of $\pm 50 \mu\text{m}$ because of the narrow electrical isolation channels in the chip and the small separation of the electrode fingers. The n-side of the array is electrically connected to each of two submount grounding pads using large-cross-section gold ribbon to carry the combined currents necessary to operate all diodes simultaneously. The submount is attached to a thermoelectrically-cooled copper heatsink maintained at approximately 23°C to keep the laser threshold current (and light output) constant and because laser life decreases exponentially with increasing temperature.

For characterization of the diodes or use in a recording system, the array-submount-heatsink unit is installed in a driver package that has been designed specifically to individually address each of the ten laser sites on the array chip. This package was developed in collaboration with the Hybrid Development Laboratory at Missile and Surface Radar Division. One version of the driver package is shown in Fig. 5. It contains two five-driver hybrid electronic boards symmetrically positioned on either side of the array submount. Each driver circuit is capable of modulating a laser at rates of up to 70 MHz. Hybrid electronics were needed in order to pack ten driver circuits around the array with short lead lengths to minimize ringing of

the modulation current. Small phosphor-bronze leaf springs connect the driver circuits to the metallized contact pads on the submount. Mounted vertically at the rear of the driver package is an interface board that transforms the ECL input signals generated by the computer hosting the optical memory peripheral to the levels required by the differential pair drivers.

Test results

Prototype arrays of the CSP structure have recently been fabricated and tested, with extremely encouraging results. Figure 6 shows the optical output power versus input current (P-I) characteristics of one of the best devices produced to date, a ten-element array with all lasers operating to at least 30 mW cw. The curves show similar threshold currents (76 to 92 mA) and differential slope efficiencies (38 to 56 percent). Figure 7 shows the lateral far-field intensity profiles for each of these ten lasers. The full-widths at half-maximum (FWHM) of these angular distributions are also reasonably uniform, ranging from 7.8 to 9.5°. The transverse far-field profiles are even more uniform but wider, with FWHMs averaging about 30°, due to the nature of the waveguide in the direction perpendicular to the laser junctions. These output characteristics are well within the tolerances required by optical recording systems.¹¹

The output wavelength of an array with eight contiguous diodes operating at 20 mW cw is shown in Table I. For this particular device, the emission from each element was within $\pm 12 \text{ \AA}$ of the average value. Relatively tight wavelength control is important, because the optical system must be achromatized to accommodate the maximum range over which the lasers may operate. Optics are currently being designed and fabricated to allow imaging of all ten elements of an array operating within $\pm 50 \text{ \AA}$ of their average. Furthermore, the recording sensitivity of some types of media are highly dependent on the wavelength of the laser light.

Work is in progress to develop reproducible processes by which arrays having three to ten contiguous high-power, single-spatial mode laser elements can be economically manufactured. Reliable sources of this type would be applicable to a wide range of uses, including optical scanning, printing, and signal processing applications in addition to optical recording. Production of such devices requires development of a suitable commercial package for the

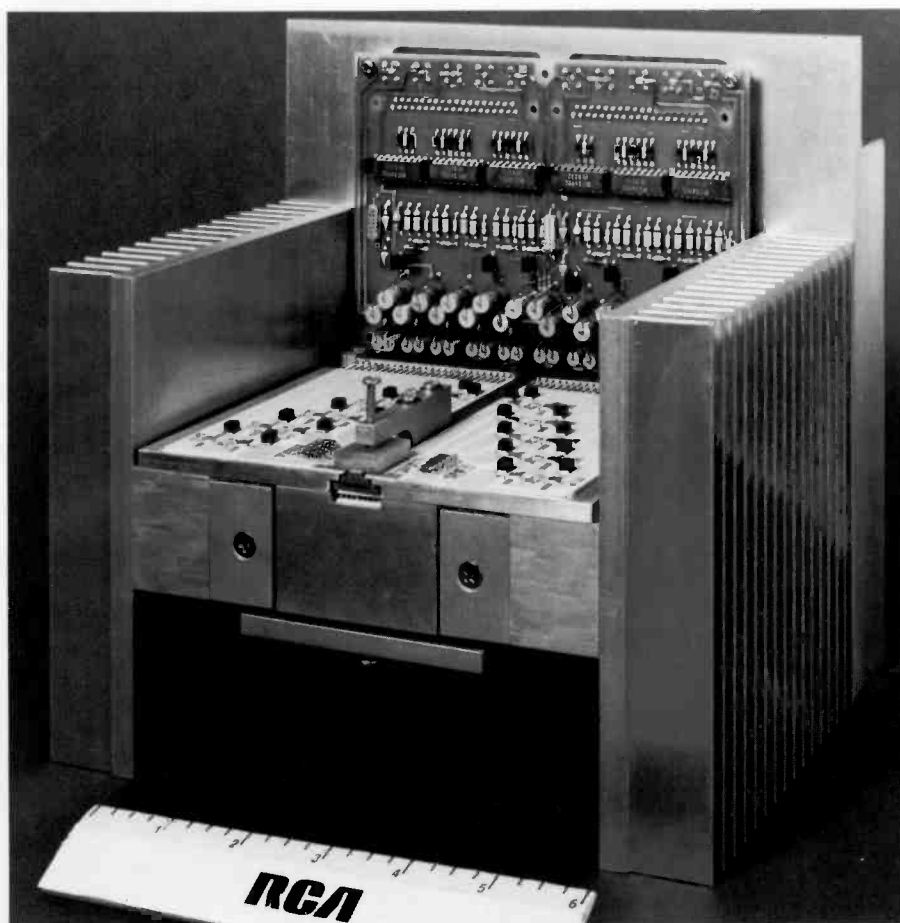


Fig. 5. Hybrid electronic ten-channel driver package.

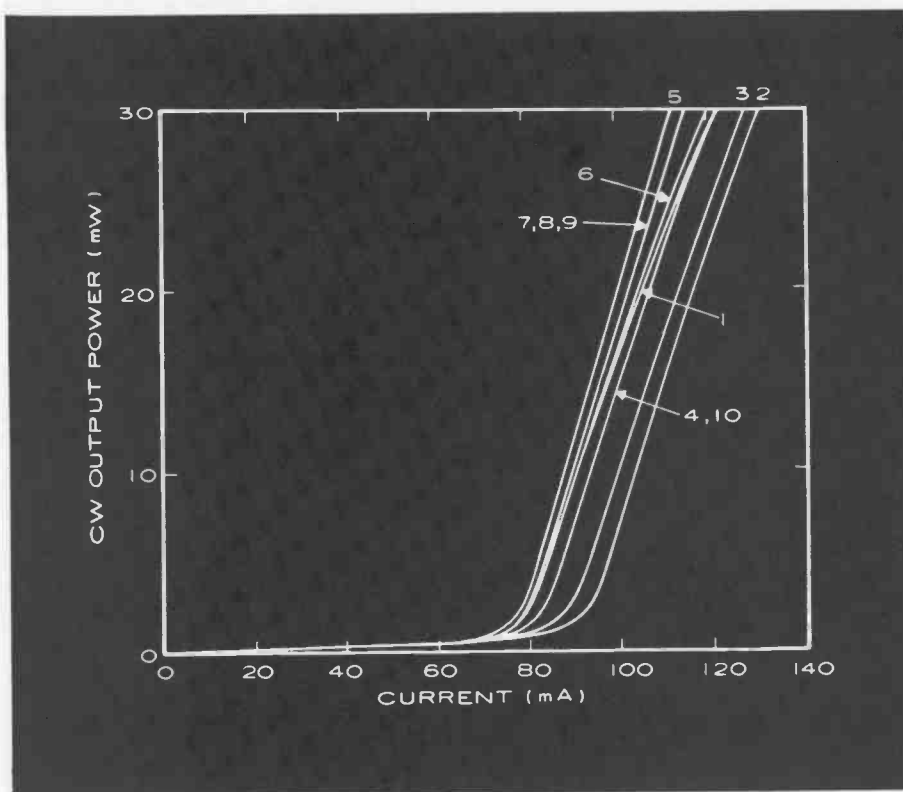


Fig. 6. Power-versus-current characteristics of the lasers in a ten-element array.

Table I. Monolithic CSP diode laser array output spectra

Array position	Output wavelength (Å) at 20 mW cw
1	8433
2	8447
3	8428
4	8439
5	8452
6	8436
7	8440
8	8430
Average wavelength	8438

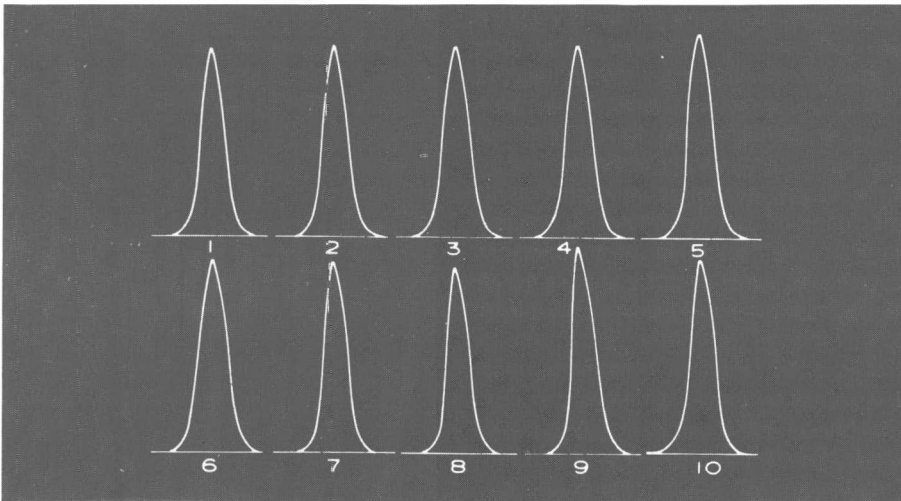


Fig. 7. Lateral far-field intensity profiles of the laser in a ten-element array.

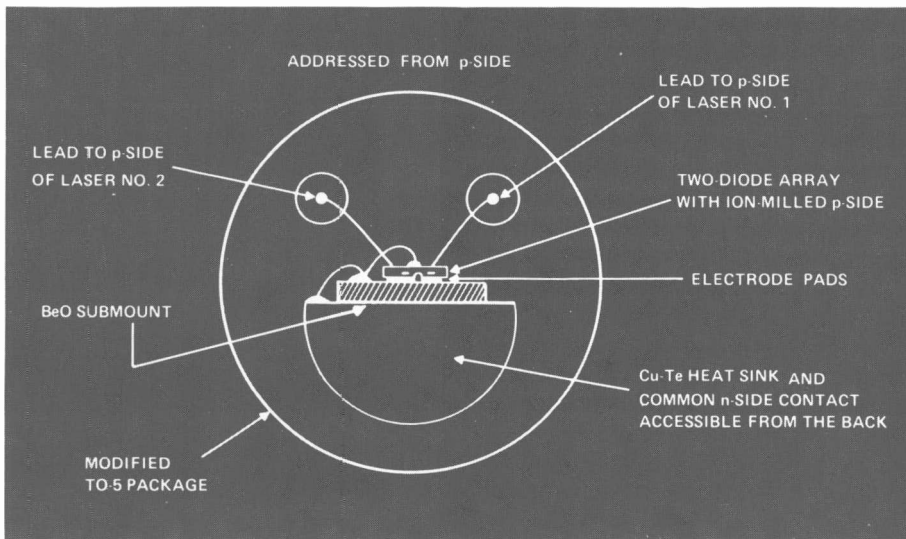


Fig. 8. Schematic view of the two-diode array package.

array and automated mounting and characterization systems.

Two-diode arrays

A ruggedized dual-channel data storage system, the Durable Disk Optical Recorder, is being developed by Communications and Information Systems Division.¹² Although the recording system itself will be subjected to extremes of environmental conditions, the packaging considerations of this array chip are simpler than for the longer multielement arrays because only two diodes must be addressed. In fact, an existing package has been adapted for the prototype sources in the Durable Disk Optical Recorder.

Shown in Fig. 8 is a schematic drawing of a two-diode array mounted in a modified TO-5 package. The two-diode array is fabricated by processes identical to those used to make the ten-diode devices. In this case, however, photolithographic definition of dual channels and dual contact stripes forms two-diode units. The array is soldered to a small metallized beryllia submount which, in turn, is bonded to the heat sink of the TO-5 package. A photograph of a packaged array chip is shown in Fig. 9. The package can be hermetically sealed, if necessary. The laser emission would then be through an optically flat window.

Two-diode arrays are also useful for different applications in optical recording. NEC has developed such a device so that one laser reads the data that the other has just written in order to detect errors in the stored data.¹³ Such errors can be corrected by rewriting entire blocks of data in archival systems, or by erasing and rewriting the data in the same physical location on reusable media.

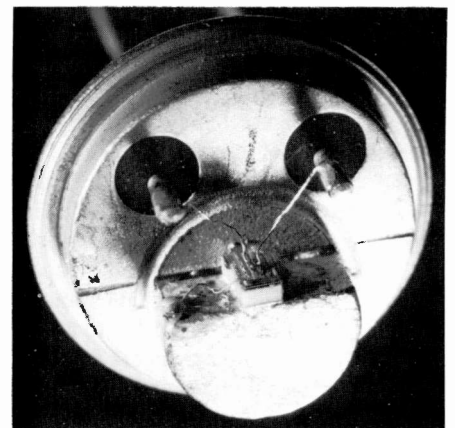


Fig. 9. Photograph of a two-diode array mounted in a modified TO-5 package.

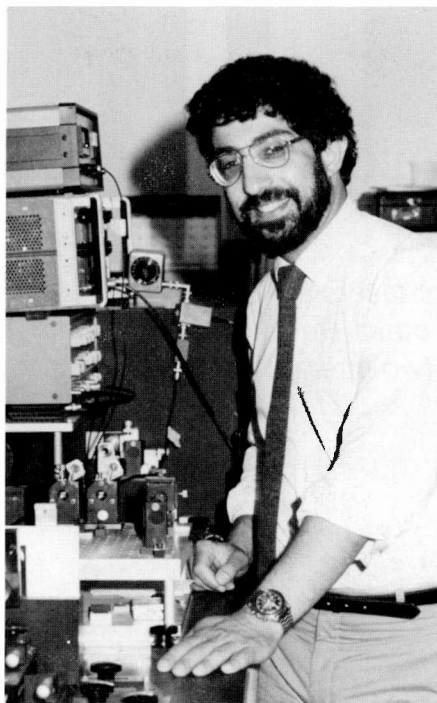
Conclusion

The initial results with monolithic arrays of AlGaAs diode lasers demonstrated the feasibility of using such sources in extremely high performance optical data memories. By using semiconductor laser sources, these data storage devices will be more compact, efficient, and reliable than the previous generation of ion laser-based systems. Also, the concurrent development of erasable optical storage media allows the use of high-data-rate multichannel recording in a wider range of applications. The requirement for single-pass erasure, however, places increased demands on laser performance.

The incorporation of the CSP structure into arrays has resulted in devices that have shown the promise of meeting the source requirements for advanced optical data recorders. Further development will result in the realization of both a product line of diode laser array emitters and new high-data-rate optical memories.

Acknowledgments

The success of this program is the result of the dedicated efforts of a large number of contributors at RCA Laboratories, Advanced Technology Laboratories, Communications and Information Systems Division, and Missile and Surface Radar Division. In particular, the author acknowledges the technical contributions of Bernie Goldstein and Nancy Dinkel for the growth of the arrays, Maria Harvey for bonding, Charlie Kaiser, Jim Bednarz, and Dave Freedman for package and electronics development, Gerry Alphonse and Dennis Truxal for array characterization, and the support and guidance of Bob Bartolini, Mike Ettenberg, and Bernie Hershenov.



Donald B. Carlin received the SB and SM degrees in Physics from MIT in 1970, and the PhD degree from Yale University in 1977. From 1977 to 1981, Dr. Carlin was a Research Associate at Harvard University's Division of Applied Sciences, investigating the thermodynamics and hydrodynamics of liquid crystals.

Since joining the technical staff of RCA Laboratories in 1981, Dr. Carlin has been concerned with the application of diode lasers to optical recording and data transmission. His work is focused on the development of monolithic arrays of individually addressable high-power, single-mode diode lasers. He led the effort that culminated (in 1984) in the first demonstration of multiple-channel high-data-rate optical recording by the use of a multiple-element array of sources.

Dr. Carlin is a member of the Optical Society of America, the IEEE, and Sigma Xi.

Contact him at:

**RCA Laboratories
Princeton, N.J.
Tacnet: 226-2985**

References

1. R.A. Bartolini, A.E. Bell, and F.W. Spong, "Diode laser optical recording using trilayer structures," *IEEE J. Quantum Electron.* QE-17, pp. 69-77, 1981.
2. D. Botez, "Single-mode diode lasers for systems-oriented applications," *RCA Engineer*, 27-3, pp. 8, May/June 1982.
3. R.A. Bartolini, "High-density optical recording using laser diodes," *RCA Engineer*, 27-3, pp. 20, May/June 1982.
4. G.J. Ammon and C.W. Reno, "Data recording on optical discs at 300 Mb/s," *RCA Engineer*, 27-3, pp. 36, May/June 1982.
5. K.R. Wallgren, "Optical discs and supercomputers," *SPIE*, Vol. 529, Optical Mass Data Storage, pp. 212, 1985.
6. W.P. Altman, G.M. Claffie, and M.L. Levene, "Optical storage for high-performance applications in the late 1980's and beyond," *RCA Engineer*, 31-1, pp. 46, Jan./Feb. 1986.
7. R.P. Freese, R.N. Gardner, T.A. Rinehart, D.W. Siltari, and L.H. Johnson, "An environmentally stable, high performance, high data rate magneto-optic media," *SPIE* Vol. 539, Optical Mass Data Storage, pp. 6, 1985.
8. D. Botez, "CW high-power single-mode operations of constricted double-heterojunction AlGaAs lasers with a large optical cavity," *Appl. Phys. Lett.* 36, pp. 190, 1 February 1980.
9. B. Goldstein, M. Ettenberg, N.A. Dinkel, and J.K. Butler, "A high-power channel-substrate-planar AlGaAs laser," *Appl. Phys. Lett.* 47, pp. 665, 1 October, 1985.
10. D.B. Carlin, J.P. Bednarz, C.J. Kaiser, J.C. Connolly, and M.G. Harvey, "Multichannel optical recording using monolithic arrays of diode lasers," *Appl. Optics*, Vol. 23, pp. 3994, 15 November, 1984.
11. D.B. Carlin, "Spot-forming efficiency of optical recording systems using high power diode lasers," *SPIE* Vol. 382, Optical Data Storage, p. 211, 1983.
12. D.B. Carlin and R.W. Johnston, "Durable optical disk system—an update," *SPIE* Vol. 529, Optical Mass Data Storage, pp. 102, 1985.
13. M. Itoh, H. Kawano, S. Shimonou, and T. Yoshiura, "Real-time error detection using a laser diode array optical head," CLEO '85, paper WM-48, Baltimore, MD, 21-24 May, 1985.

Solid-state and semiconductor lasers

Both solid-state and semiconductor lasers are directed by technologies independent of each other. However, for certain applications such as in space, the two interact to serve a single purpose.

Since the advent of the first lasers, it has been quite obvious that many practical applications of lasers would evolve because of the narrow linewidth and the high directivity of laser output. During this period of time, the laser has been suggested for or applied directly to many applications such as welding and cutting, weaponry, medical applications for surgery and diagnosis, materials analysis, spectroscopy, metrology, and communications.

RCA's interest in lasers has been continuous and has been directed toward a small number of applications, with the emphasis on two types of lasers—solid-state and semiconductor. Solid-state lasers are being applied to efforts in the near-infrared wavelength region because they operate outside the visible portion of the spectrum, making them covert, and because they can achieve high output powers. Semiconductor lasers are important because they are very small devices, thus matching the requirement for miniaturization, and have selectable output wavelengths.

Abstract: *For ATL's Electro-Optics Unit, interest is chiefly in two types of lasers—solid-state and semiconductor. Though operating under technologies independent of each other, the two lasers can interact in one system. In some cases, the solid-state laser can benefit from the high reliability (long lifetime) and high energy conversion efficiency of the semiconductor laser. Such an application is found in laser communications between a submarine and a satellite.*

©1986 RCA Corporation.
Final manuscript received February 24, 1986
Reprint RE-31-3-4

Even though solid-state and semiconductor lasers operate under different technologies, there is interaction between the two. A result of this interaction is a significant application of semiconductor lasers—they can serve as a pump source for solid-state lasers. Therefore, while differing capabilities and applications, in general, separate solid-state and semiconductor lasers, there are important applications in which the two technologies are used together.

In a more general sense, RCA is also interested in lasers for use in communications, although some of these do lie outside this narrow field. For communications applications, solid-state lasers can be used when large amounts of output power are required, while in others, such as for Light Detection and Ranging (LIDAR), lasers can be used in evaluating the state and constituents of the atmosphere, range finding, and target designation. In these cases, the lasers must have output powers up to the megawatt range and output energy up to the 1- to 10-joule range.

Semiconductor lasers

Semiconductor lasers, on the other hand, are inherently low-power devices that usually provide output powers in the 10- to 100-milliwatt range, although some have outputs as high as one watt. The most prominent communications application for these lasers is in fiber-optic communications systems where the miniature size and high reliability of these devices make them ideal. Because the laser output is guided in a low-loss wave guide, the relatively low output power does not incur a $1/r^2$ loss. These lasers can also be used for communi-

cation over atmospheric paths if the range is kept short and for space communication where the lossy air transmission path is absent. Thus, semiconductor lasers have attained a position of great value in applications such as these and owe much of their success to two characteristics—a very high reliability (lifetimes on the order of 10,000 hours are achievable) and a high energy conversion efficiency (efficiencies of 25 percent are readily obtainable).

Such characteristics make semiconductor lasers ideal for space applications where lifetime and power efficiency are of prime concern. They also become advantageous to solid-state lasers because the semiconductor lasers, as previously mentioned, can be used to pump the solid-state lasers. Therefore, when the semiconductor laser output is tailored to match the absorption bands of the solid-state laser material for a pumping application, the solid-state laser benefits too from features of reliability and efficiency.

Solid-state lasers

A typical solid-state laser consists of a rod of the lasing material, a cavity that forms a resonator for the laser, and a pumping source. The pumping source is usually a flash lamp in a linear configuration and can have various gases for different output spectra. Figure 1 presents the output spectrum of a lamp designed for pulsed operation that uses xenon. As indicated in this figure, the output spectrum is a strong function of the operating current, and for low currents the output has a significant line content.

Figure 2 illustrates the output from a

krypton-filled lamp that is designed for cw operation. In this case, the output is dominated by the line spectrum. To couple the radiation from the flash lamp into the laser rod, a reflector (Fig. 3) must be provided to ensure that the maximum amount of light is absorbed by the laser material. In one case, the rod and the flash lamp are inside a reflecting cylinder, with most of the light from the lamp passing through the laser rod. In the other case, the lamp and the laser rod are located at the foci of an elliptical reflector and again we have a good coupling efficiency between the lamp and the laser rod. The laser rod is mounted in a resonator cavity that has end mirrors to define the cavity (Fig. 4). The light absorbed in the laser from the flash lamp raises the active atoms to a higher energy state (Fig. 5). This upper energy level is actually a continuum of energy levels and provides for a more efficient absorption of the pump energy. At this point, however, we must distinguish between three-level and four-level systems.

In both systems, when the atoms are raised to the absorption continuum, they decay nonradiatively to the upper laser level. Radiative decay from the upper laser level to the lower laser level can occur either as a spontaneous emission process (i.e., fluorescence) or by stimulated emission. In the stimulated emission process, a photon of the proper wavelength can cause the emission or absorption of radiation at the same wavelength. At the beginning of the lasing process, photons that are emitted spontaneously are reflected back and forth between the resonator mirrors and cause stimulated transitions. If there are more atoms in the upper level, a net gain will occur. But, if the lower level has a greater population, a net loss will occur.

In the three-level system, when the lasing action begins, the stimulated emission process will depopulate the upper laser level in competition with the pumping process. For this reason, three-level lasers are useful only for pulsed operation. In a useful four-level system, the lower laser level has a fast nonradiative decay mode, with the lower laser level always having a very low population. Thus, four-level systems are very well suited for cw operation.

Under the proper conditions, both the three-level and four-level systems can be approximated by a two-level approach. Therefore, if the ions that are pumped to the upper levels decay very quickly to the upper laser level, if the lifetime of the upper laser level is sufficiently long, and if the lower laser level decays to the ground

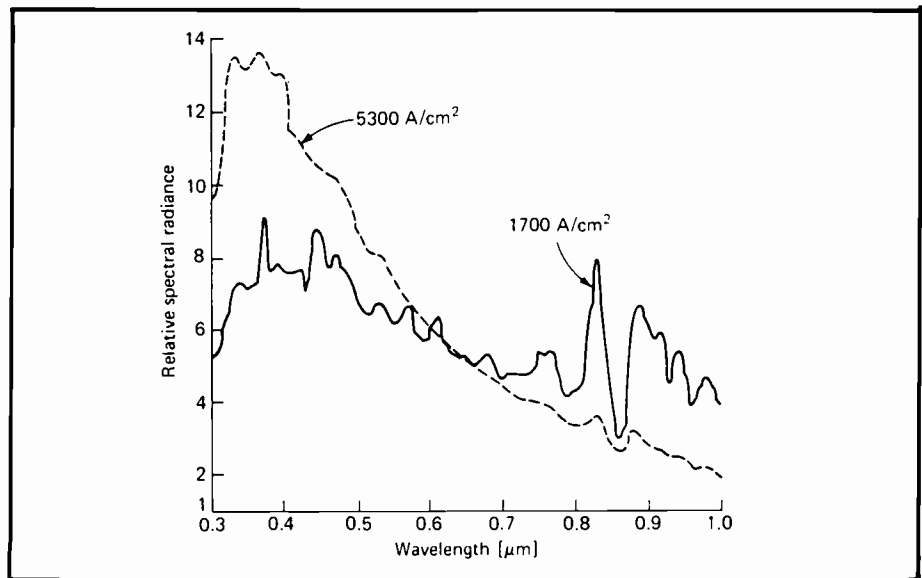


Fig. 1. Spectral emission of a xenon flash tube operated at high current densities.

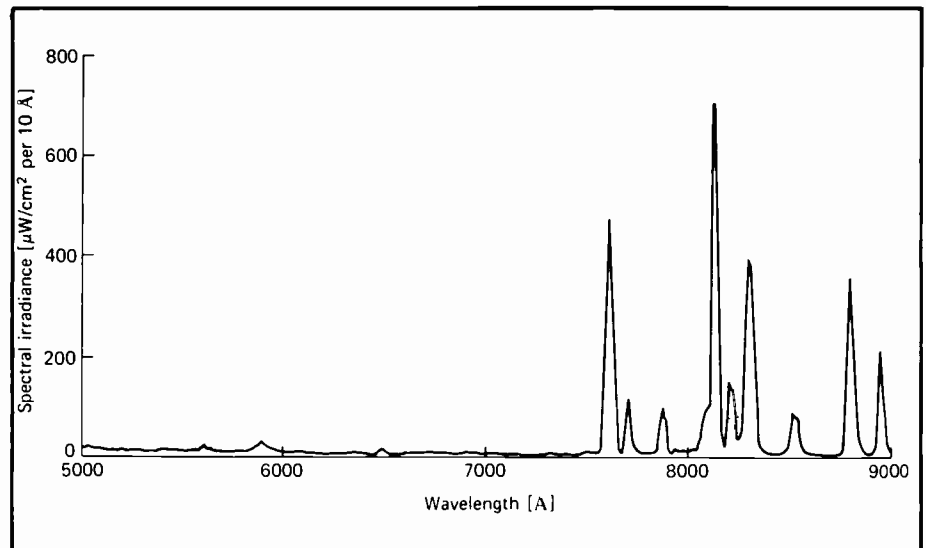


Fig. 2. Emission spectrum of a typical cw-pumped krypton arc lamp.

state quickly, the system can be modeled by a process in which pumping effectively raises the atoms from the lower laser level into the upper laser level. With this approximation, the rate process for a laser can be described through the equation:

$$\frac{\partial n}{\partial t} = -\gamma n \phi \sigma c - \frac{n + n_i(\gamma - 1)}{\tau_f} + w_p(n_i - n)$$

where n is the population inversion (i.e., $n_2 - n_1$), γ is a constant which has different values for three- and four-level systems, ϕ is the photon density, σ is the stimulated emission cross section, c is the speed of light, n_i is the total ion density, τ_f is the fluorescence decay time, and W_p is the

pumping rate. This equation provides an effective description of the lasing process and has general utility.

The lasing material itself consists of a transparent host material, which can be either a crystalline or noncrystalline medium, and has an active ion incorporated into its structure. Some of the more commonly used solid-state laser materials are listed in Table I.

Nd:YAG has the lowest lasing threshold (amount of pump power needed to initiate lasing) of the lasers listed here. In addition to the low threshold, the YAG host has very good thermal properties and can, therefore, be used both for pulsed and cw operation. Figures 6, 7, and 8 show the absorption spectrum for YAG in the vicinity

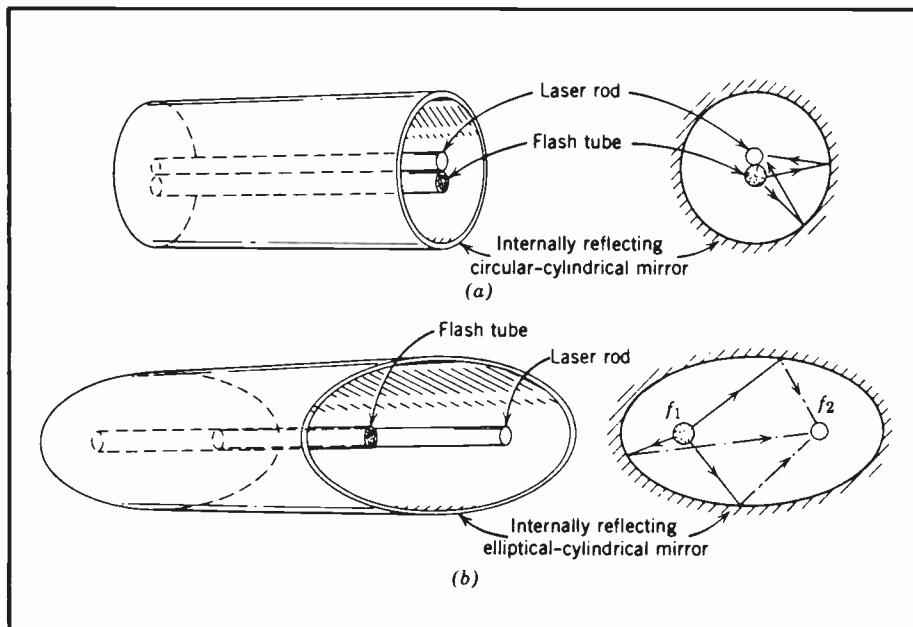


Fig. 3. Two laser cavity configurations for coupling pump-lamp radiation into the laser rod.

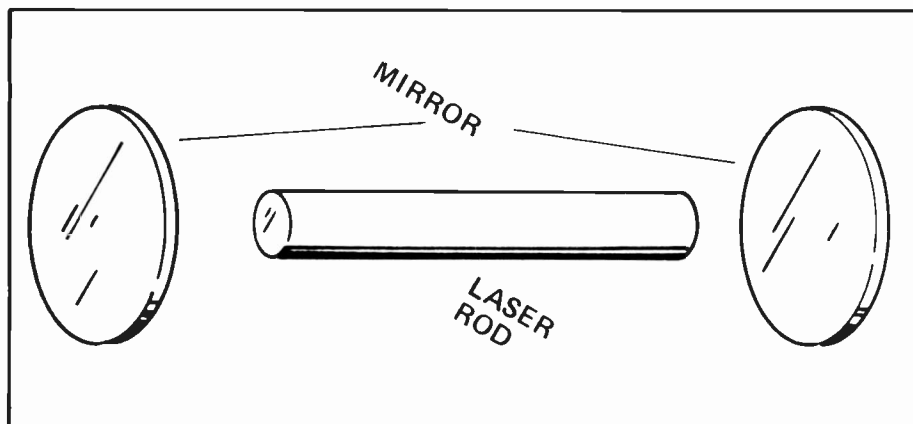


Fig. 4. Diagram of laser resonator cavity.

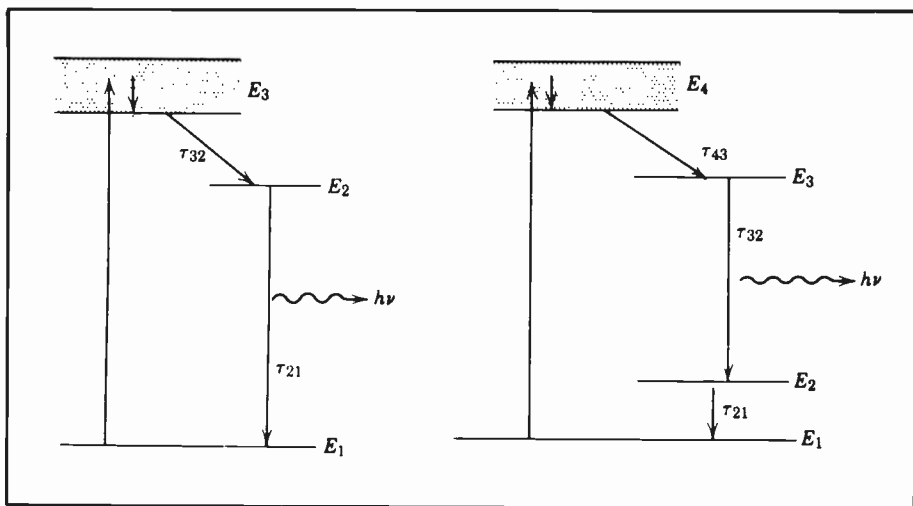


Fig. 5a. Energy level diagram for the model of a three-level laser.

Fig. 5b. Energy level diagram for the model demonstrating four-level laser operation.

of its strongest lines, the spontaneous emission curve for YAG, and a typical output versus input power curve for YAG.

As a wave propagates in the laser cavity, we have the effects of both gain, due to the stimulated emission process, and losses, due to mirror transmission and other loss mechanisms. If g is the gain and α is the loss, the lasing condition is

$$R_1 R_2 e^{(g-\alpha)2l} = 1$$

where R_1 and R_2 are the mirror reflectivities and l is the cavity length. From the rate equation, the oscillation condition can be derived by setting $n/t = 0$, which gives

$$n = n_t \left[w_p - \frac{(\gamma-1)}{\tau_f} \right] \left(\gamma c \sigma \phi + w_p + \frac{1}{\tau_f} \right)^{-1}$$

Because $g = \sigma n$, using the previous result, the gain is

$$g = g_o \left[1 + \frac{\gamma c \sigma \phi}{w_p + 1/\tau_f} \right]^{-1}$$

where g_o is the small signal gain defined for $\phi = 0$ and is given by

$$g_o = \sigma n_t [w_p \tau_f - (\gamma - 1)] (w_p \tau_f + 1)^{-1}$$

The output power from the laser can be calculated by

$$P_{out} = \sigma_s (P_{in} - P_{th})$$

where P_{th} is the electrical input power to the flash lamp for threshold, P_{in} is the input power, and σ_s is the slope efficiency. The slope efficiency itself is given by

$$\sigma_s = K I_s A^2 (1 - R_1) \times [R_1^{1/2} (L - \ln R_1)]^{-1}$$

where K and I_s are constants that are a function of the materials and the structure, A is the cross-sectional area of the laser rod, L represents the lumped-loss mechanisms, and R_2 is assumed to be 100 percent. Therefore, from this expression, for a given system there is a value of the mirror reflectivity that optimizes the output intensity. This optimized value is given by the following expression:

$$R_1 = 1 - \frac{(2K P_{in} L)^{1/2} - L}{1 + L}$$

The Nd:glass laser is similar to the Nd:YAG laser but has a somewhat wider absorption spectrum. Glass has a lower thermal conductivity than YAG and, because of thermal problems, it is not used for cw operation

but works well in pulsed operation. The Cr:sapphire (ruby) laser is a three-level device and is usable only for pulsed operation. The Ti:sapphire laser is unusual in that the Ti ion is coupled to the lattice in such a way that the fluorescence line is very wide. The fluorescence line (shown in Fig. 9) is a wide line and, because of this property, the laser is tunable over almost the entire curve and lasing has been demonstrated over the range of 650 to 950 nm. The Er:glass laser is of interest because its output wavelength is in a region where the cornea is not transparent. Thus, the laser can be operated in an "eye-safe" region and is of interest for application as a rangefinder.

In general situations, when lasers are used in a pulsed mode the pulse length will be determined by the fluorescence decay time of the upper laser level. For example, in Nd:YAG the decay time is 240 microseconds, and if short pulse operation is desired, different techniques must be used. Two such techniques are Q-switching and cavity dumping.

The Q-switching technique enables one to obtain a sharp, single laser pulse with a large peak intensity. The principle of this technique can be explained as follows. First, losses are introduced into the optical resonator of the laser during the pumping cycle so that the gain can rise to a very large value, yet not exceed the oscillation threshold condition. During this time, the atomic population of the gain medium is inverted and acts as an energy storage mechanism. Because the quality factor (Q)

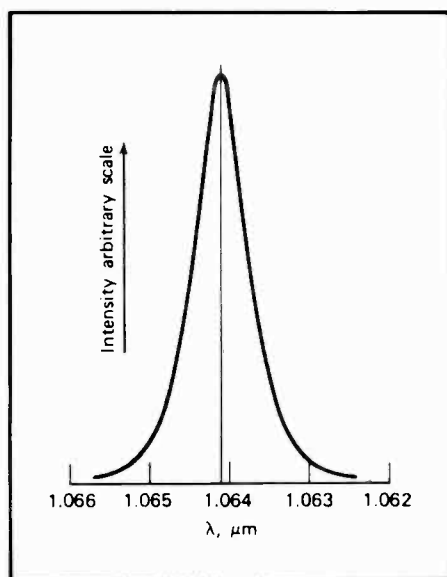


Fig. 7. Spontaneous-emission spectrum of Nd^{3+} in YAG near the laser transition at $\lambda = 1.064 \mu\text{m}$.

Table I. Solid-state lasers

Active ion	Host	No. of levels	Output (λ) (μm)
Nd	YAG	4	1.06
Nd	Glass	4	1.06
Cr	Sapphire	3	0.69
Ti	Sapphire	4	0.76
Er	Glass	3	1.54

Note: YAG—Yttrium Aluminum Garnet

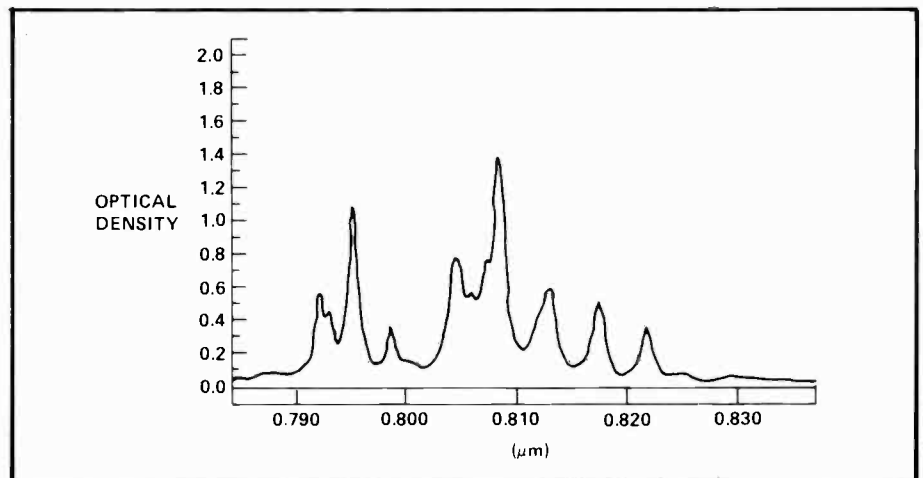


Fig. 6. Absorption in a 4-mm length of Nd:YAG with AR-coated faces.

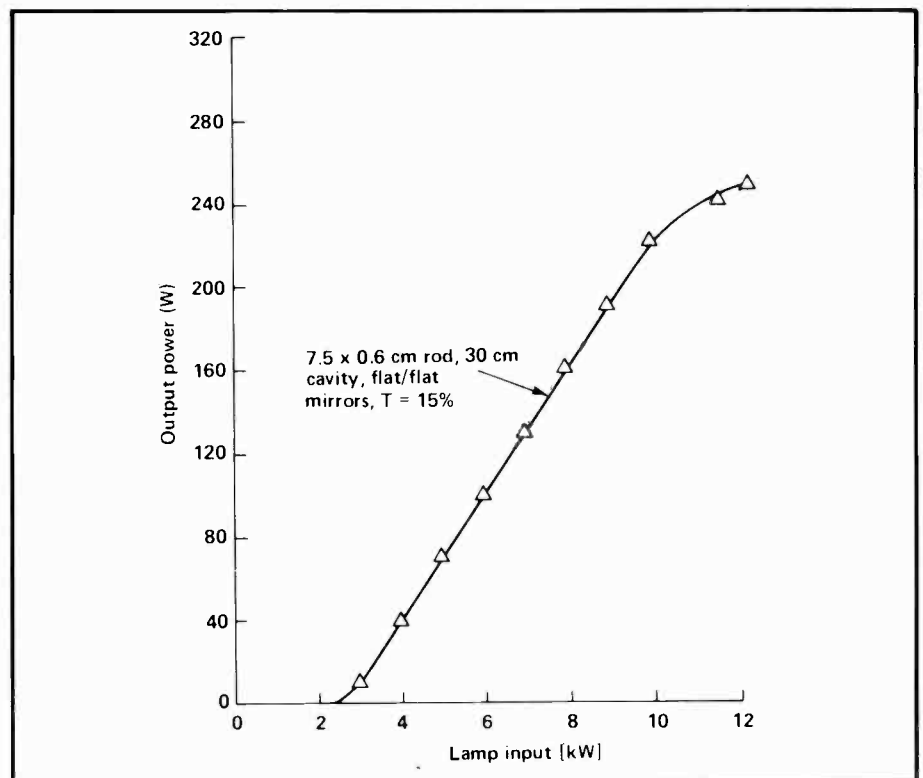


Fig. 8. Continuous output versus lamp input of a Nd:YAG laser.

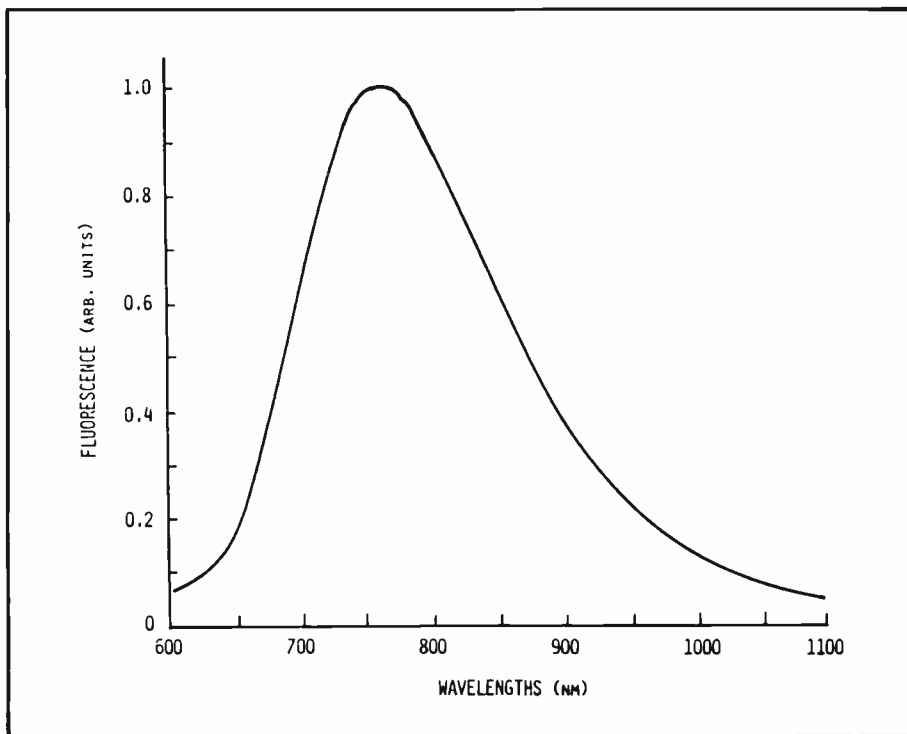


Fig. 9. Fluorescence of $Ti:A^{2}O^{3}$.

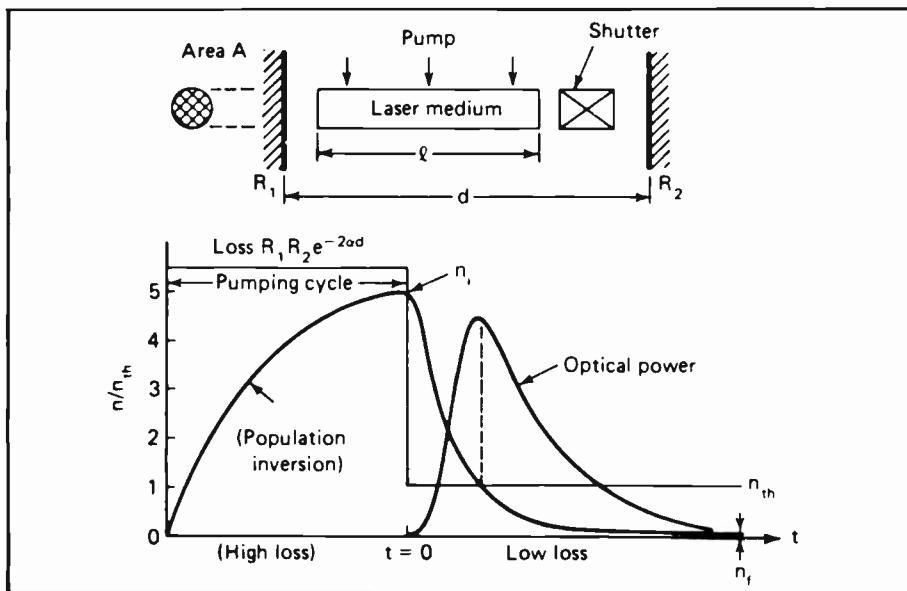


Fig. 10. Sequence of events that occur during a Q-switched pulse.

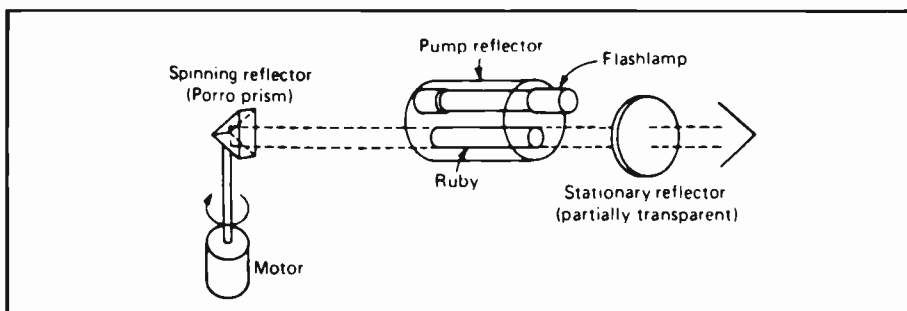


Fig. 11. Diagram of a ruby laser employing a spinning prism Q-switch.

of the cavity has been degraded, the population remains inverted during the pumping cycle. No stimulated emission takes place during this time, although spontaneous emission still occurs. When the inversion reaches its peak, the Q of the cavity is abruptly restored (i.e., the losses are removed). The laser will now have a gain much greater than the losses. The oscillation field will build up extremely rapidly and the energy stored will be released in the form of a short, intense light pulse. The concept works well provided the shutter is opened in a time that is comparatively short to that of the build-up time of the laser pulse. If the switching speed is relatively slow, multiple pulses may occur. This is because each pulse drives the gain below the instantaneous threshold, thus inhibiting further oscillation until the loss in the cavity decreases to the new lower threshold. Figure 10 illustrates the sequence of events that occur during a Q-switched pulse.

Numerous techniques are available for temporarily spoiling the Q of a laser and then restoring it at a predefined time. Some of the more common techniques are discussed in the next few paragraphs.

Mechanical shutters can be realized by a rotating mirror or porro prism. This technique, illustrated in Fig. 11, involves simply rotating one of the two resonant cavity reflectors so that parallelism of the reflectors occurs for only a brief instant of time.

Another commonly used technique for spoiling the Q of a laser cavity involves the use of a saturable dye cell located within the laser cavity. The absorption frequency of the dye must be coincident with the laser frequency and must have an initial absorption characteristic of approximately 50 percent. Laser oscillation is delayed until the population inversion has reached a level such that the gain of the active material compensates for the loss of the saturable absorber plus cavity loss. At this point, laser oscillation starts and the saturable dye is rapidly bleached. The bleaching must be sufficiently fast so that the inversion of the active material is not decreased significantly from its initial value. When the saturable dye is bleached, the original high Q of the laser is restored. The laser will, therefore, have a gain much larger than the losses, causing a giant light pulse to develop. Polymethine dyes such as Eastman 9740 and Eastman 9860 are commonly used for Nd⁺ lasers.

Utilizing the electro-optic effect in crystals or liquids is another method by which very fast optical shutters can be made. An

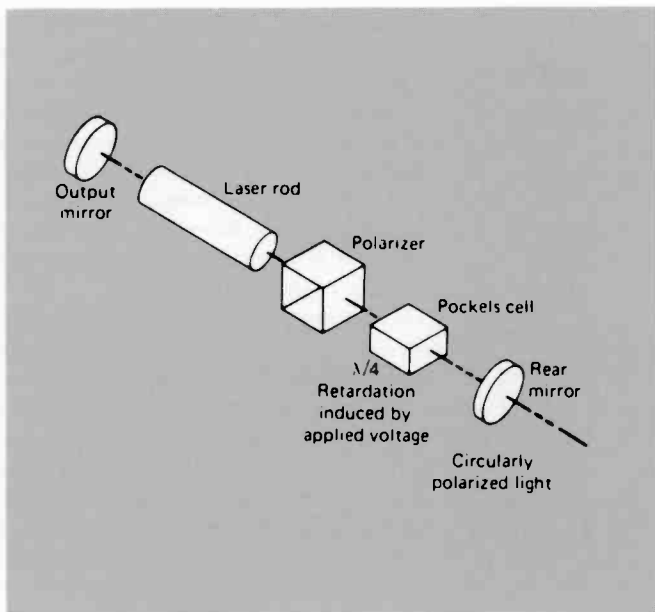


Fig. 12. Typical arrangement of components for an electro-optically Q-switched laser.

electro-optic crystal is one that becomes birefringent when an external electric field is applied. Two commonly used electro-optic crystals are KD*P (potassium dideuterium phosphate) and its isomorphs, and LiNbO (lithium niobate). Important attributes of KD*P are its resistance to laser damage and high optical quality. A disadvantage of KD*P is that the crystal is water soluble and must be enclosed in a suitable cell to prevent humidity from deteriorating the polished surfaces. LiNbO is a nonhygroscopic crystal that can be readily polished; however, this material is susceptible to optical damage induced by high-intensity visible light. Power densities must be maintained below 40 MW/cm^2 .

A typical arrangement of components for an electro-optically Q-switched laser is diagrammed in Fig. 12. The Q-switch assembly consists of a polarizer and an electro-optic crystal. During the pumping cycle, a voltage is applied to the electro-optic cell such that the linearly polarized light passing through the polarizer is one-fourth wave retarded (circularly polarized) by the Pockels cell. The radiation is then reflected by the back mirror and again passes through the electro-optic cell, undergoing another one-fourth wave retardation. The light is once again linearly polarized, but at 90 degrees to its original direction. As the light reaches the fixed polarizer, it is ejected from the laser cavity, thus preventing optical feedback. Toward the end of the pumping cycle, the voltage on the cell is switched off, permitting the polarized beam to pass through the electro-optic cell with-

out differential phase retardation. Therefore, the high-Q of the laser cavity is restored, allowing oscillation within the cavity to build up, and, after a short delay, a Q-switched pulse is emitted from the cavity.

Q-switching theory

In this section, we present the basic starting equations for the derivation and indicate the important results that can be obtained from a complete analysis. The analysis begins by describing the functional relationship between photon density (ϕ), population inversion density (n), and time (t). This relationship can be represented by the following coupled differential equations:

$$\frac{\partial \phi}{\partial t} = \phi \left(\frac{n}{n_i} - 1 \right)$$

$$\frac{\partial n}{\partial t} = -2\phi \frac{n}{n_i}$$

where n_i is the population inversion density at threshold.

Figure 13 shows the relationship between ϕ and n as a function of time for a Q-switched pulse. Upon solving the previous equations, the following expression can be derived. It describes the relationship between the initial (n_i) and the final (n_f) population inversion densities.

$$\frac{n_f}{n_i} = \exp \left(\frac{n_f - n_i}{n_i} \right)$$

Figure 14 illustrates this result graphically. Of special interest in the design of a Q-

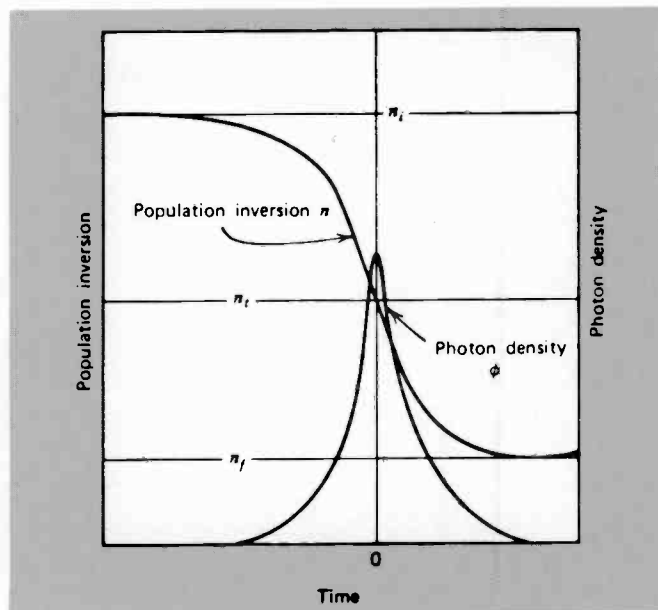


Fig. 13. Population inversion density and photon density during a Q-switched pulse.

switched laser is the peak output power (P), the total energy (E) in the pulse, and the pulse duration (Δt). These can also be obtained from the previous equations and are as follows:

$$P = \frac{h\nu}{2t_c} \left[n_i \ln \frac{n_i}{n_f} - (n_f - n_i) \right]$$

$$E \approx \frac{1}{2} h\nu (n_i - n_f)$$

$$\Delta t = t_c \frac{n_i - n_f}{n_i - n_f [1 + \ln(n_i/n_f)]}$$

where n_i , n_f , and n_t are the initial, final, and threshold population inversion densities, respectively, and t_c is the cavity lifetime. Numerical solutions of the photon density corresponding to different initial population inversions are given in Fig. 15. For initial population inversions much greater than the threshold inversion, the rise time becomes short compared to the cavity lifetime. The fall time, however, approaches a value nearly equal to the cavity lifetime.

Cavity dumping

Cavity dumping is a technique that can be used to obtain high peak powers similar to those of Q-switching, but at higher repetition rates than are available by Q-switching. The maximum repetition rate for a Q-switched Nd:YAG laser ranges from 50 to 100 kHz. By cavity dumping a continuously pumped Nd:YAG laser repetition rates from 125 kHz up to several megahertz can

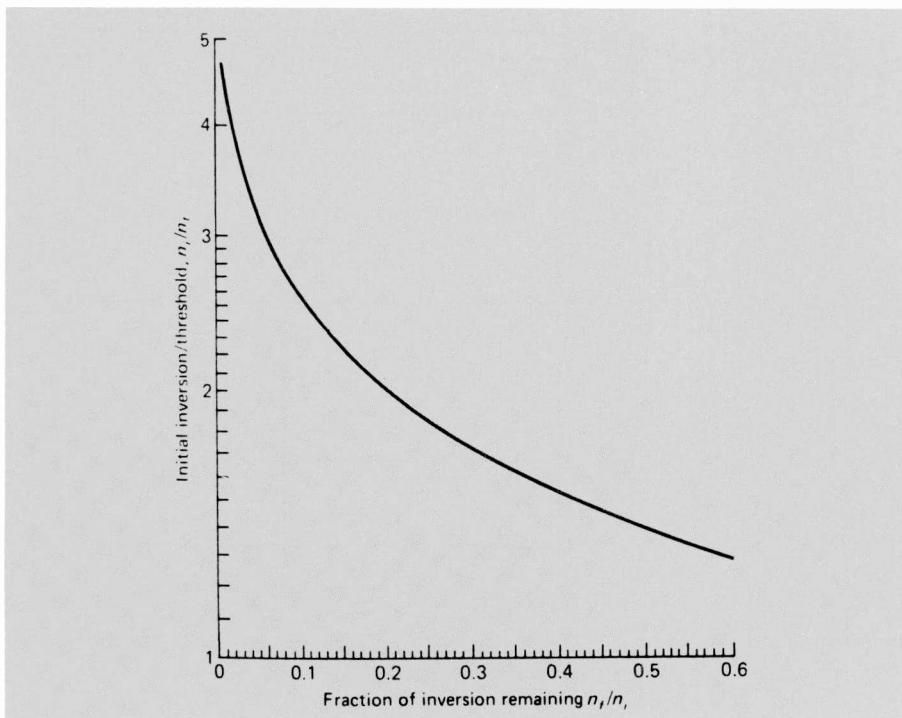


Fig. 14. Fraction of population inversion remaining in the active material, as a function of initial inversion, after emission of a Q-switched pulse.

be achieved. The primary difference between cavity dumping and Q-switching is that in the former, the energy of the pulse is stored in the optical field confined between two very highly reflecting mirrors, while in the latter the energy of the pulse is stored in the atomic population inversion. The energy from a cavity-dumped laser can be switched out by an acousto-optic cell to allow some of the optical field to escape from the cavity. Typical arrangements for a cavity-dumped laser are shown in Fig. 16.

Semiconductor lasers

Semiconductor lasers are fabricated from a variety of materials, including GaAlAs and GaInAsP. Lasers fabricated with GaAlAs materials operate with wavelengths in the 0.8- to 0.9- μm region, depending on material composition. Lasers fabricated with GaInAsP materials operate in the 1.3- to 1.5- μm region. With present technology, double heterostructure lasers are fabricated in GaAlAs compounds with a geometrical structure (shown in Fig. 17).

The laser is an oxide-stripe laser with a multilayer structure. An oxide layer on the surface has a stripe window to allow electrical contact to a portion of the surface. Light is generated in the recombination layer through the recombination of charge carriers. The oxide stripe defines the width

of the active region by delineating the current flow. The generated light travels along the stripe dimension with cleaved end facets serving as the mirrors for the optical cavity.

Figure 18 contains a detailed view of the layer structure of the laser. The recombination region has a higher index than the surrounding layers; the light that is generated is contained within the waveguide structure that is formed by the index discontinuity. In the lateral dimension, the light is confined by the index difference that is formed by the effect of the carrier density. Thus, a two-dimensional waveguide is formed, with the light traveling in this waveguide between the two cleaved facets.

The lasers are grown as a wafer. Next, the wafer is cleaved into discrete devices with typical lengths of 100 to 200 μm and stripe widths of 10 to 100 μm . Photons are created by recombination of the charge carriers across the bandgap of the semiconductor material. The bandgap can be varied by changing the composition and thickness of the layers.

Thus, although the mechanism for photon generation is different, the operation of the semiconductor laser is analogous to that of the solid-state laser. Then, the output power can be written as a function of the input current in the form

$$P = \frac{\eta h\nu}{q} (I - I_{th})$$

where η is the external quantum efficiency, $h\nu$ is the photon energy, q is the electron charge, I is the current, and I_{th} is the threshold current. Figure 19 illustrates the P versus I and V versus I curves for a typical laser. The typical output spectrum of a semiconductor laser is given in Fig. 20. As is evident, the output spectrum is a series of lines, with this line content a function of the drive current.

Using practical values for the aluminum concentration in the materials, the output wavelength can be varied over the range of 0.8 to 0.84 μm , and also in the vicinity of 0.9 μm . Because the wavelength can be varied over this wide range, the possibility exists for matching the output wavelength exactly to the absorption peak of the laser material. This capability is of special concern in the case of Nd lasers that have an absorption peak at 0.8085 μm . With diodes of the proper wavelength, it is possible to have almost 100 percent of the light emitted actually absorbed in the laser.

Because the semiconductor laser diodes emit light from only one end, they can be placed close to the laser rod and all of the diodes' emission will be coupled to the rod. Thus, with the proper wavelength match and a sufficiently long absorption path, all the emitted radiation can be absorbed. This ability to get good absorption, together with the very good power efficiency and very high reliability of the laser diodes, make the semiconductor laser diodes an invaluable replacement for flash lamps in a number of applications.

These capabilities are most important for space applications, but have significance for terrestrial applications as well. One example is found in a lightweight, handheld laser rangefinder. For such a device, weight is a critical factor; a large part of the weight is due to the batteries used for the power supply. If a pump source with greater efficiency can be provided, the weight of the device can then be reduced.

For space communications applications, a solid-state laser would be used in a pulsed mode; the "figure-of-merit" for reliability would be the number of pulses that could be emitted before system failure. A typical 10-year mission might require on the order of 10^{10} shots. Flash-lamp lifetimes in the range of 10^6 to 10^7 can be obtained, but diode lifetimes far in excess of the requirement should be realizable. Figure 21 contains lifetime data for cw laser diodes. The lower curve in the figure is measured data from earlier diodes, while the upper curve is extrapolated data from high temperature tests on recently developed

lasers. Because of the long lifetimes involved, we must resort to accelerated lifetime measurements. It is usually found that failure mechanisms show a temperature dependence of the form

$$\exp(-E_a/kT)$$

where E_a is the activation energy for the failure mechanism. Thus, if the activation energy is known, accelerated measurements can be made at elevated temperatures and the results extrapolated to operating temperatures. In Fig. 21, the upper curve is the more significant one because it represents the current capabilities, and comparison with the lower curve indicates the effects of fabrication improvements. As shown here, lifetimes in the 10^4 - to 10^5 -hour range are predicted. In evaluating diode lifetime in pulsed mode operation, it is assumed that the important factor is the total on time that the diode is exposed to. The case of 10^{10} shots corresponds to a total on time of approximately 300 hours for pulses of $100 \mu\text{s}$ in duration. Thus, we are predicting capabilities far in excess of requirements.

RCA developments

Space applications are important to future developments with emphasis on submarine laser communications from a satellite (SLCSAT) and LIDAR. In both cases, Nd:YAG or Nd:glass lasers are essential parts of the system and, because the application is for use in space, diode pumping is required. High-power, double-heterostructure, GaAlAs lasers are available and techniques for assembling these lasers into two-dimensional arrays are being developed. With these two-dimensional arrays, pumps can be fabricated that have output power densities of up to 1800 W/cm^2 . To achieve high output powers from the

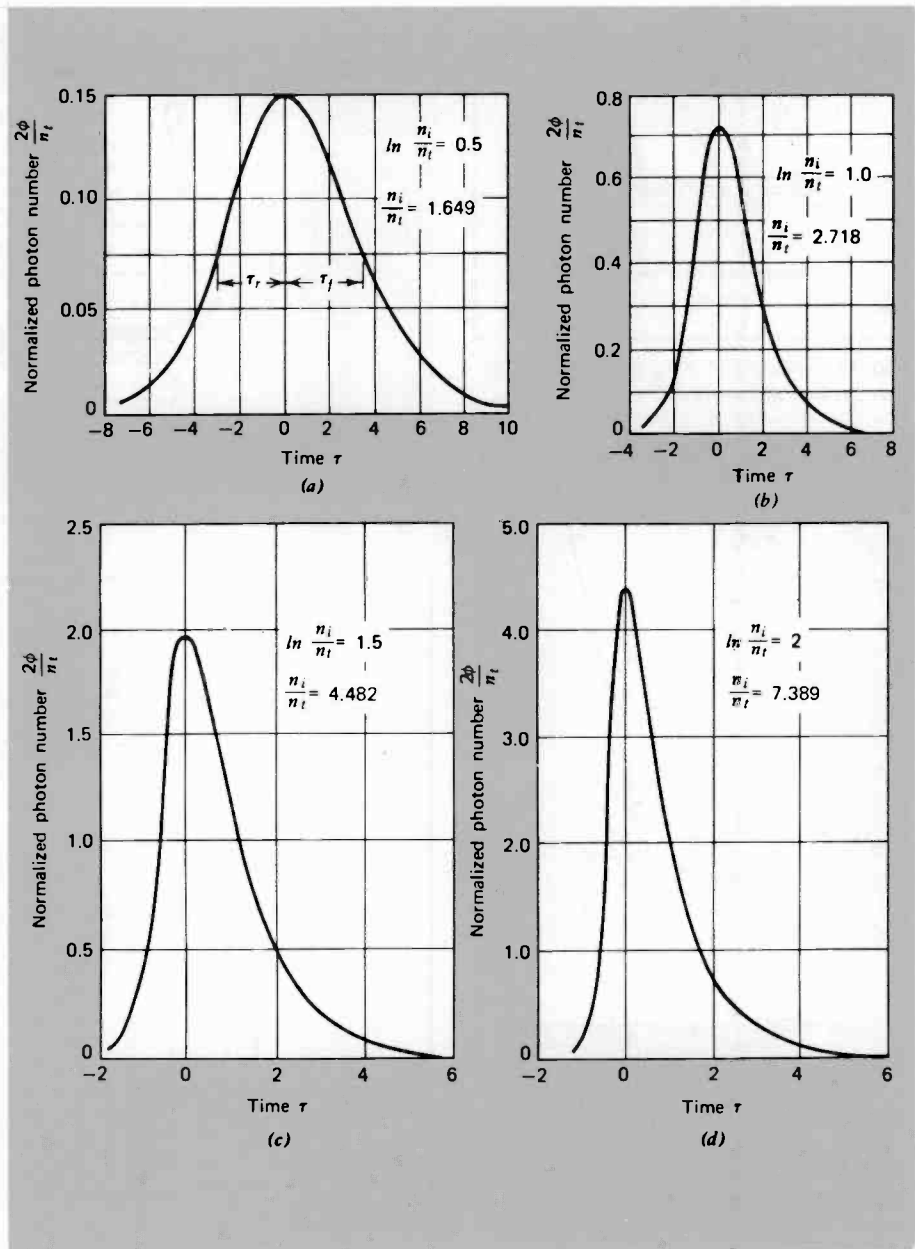


Fig. 15. Photon number versus time (measured in units of photon lifetime) in the central region of a giant pulse.

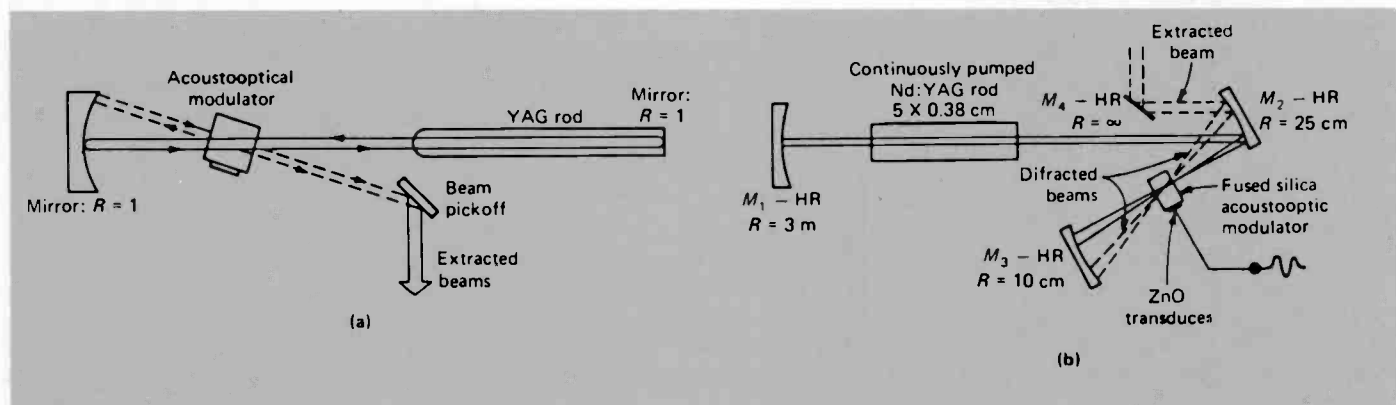


Fig. 16. Common arrangements for cavity dumping of cw-pumped solid-state lasers. The broken lines indicate the beams that are diffracted by the modulator.

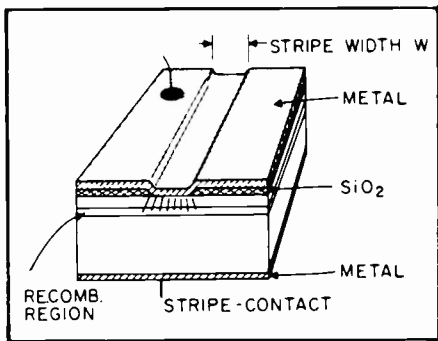


Fig. 17. Schematic diagrams of a stripe-contact diode with SiO₂ isolation.

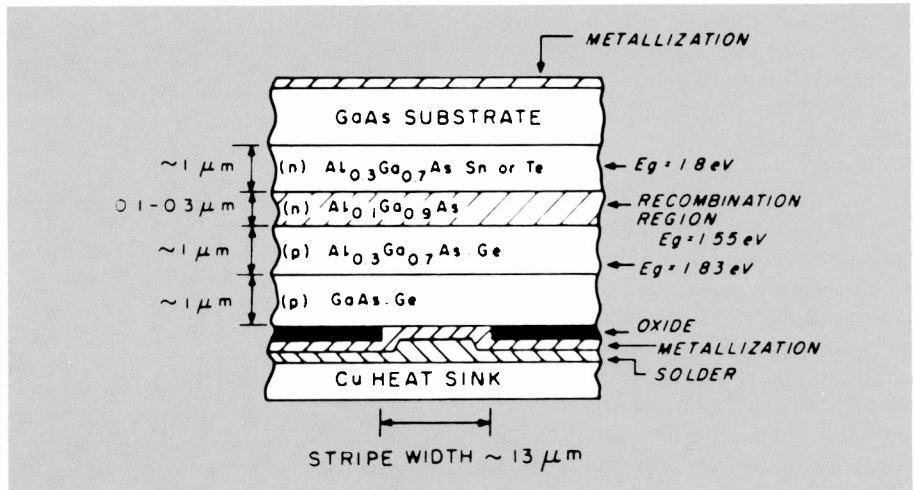


Fig. 18. Layers in a typical double-heterostructure laser.

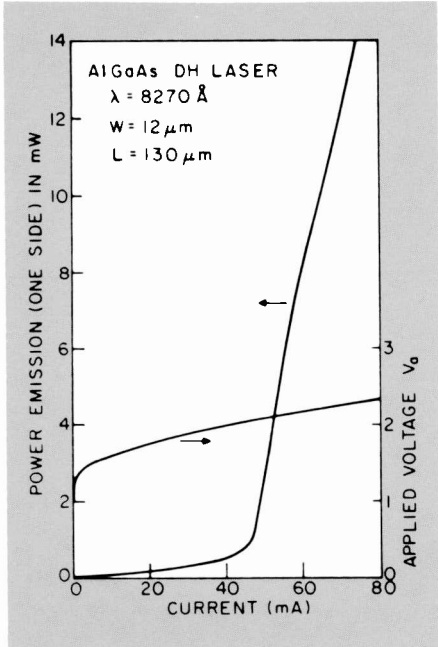


Fig. 19. Power emission from one side of a stripe contact, cw AlGaAs laser diode, and the diode voltage as a function of the diode current. The stripe width is 12 micrometers.

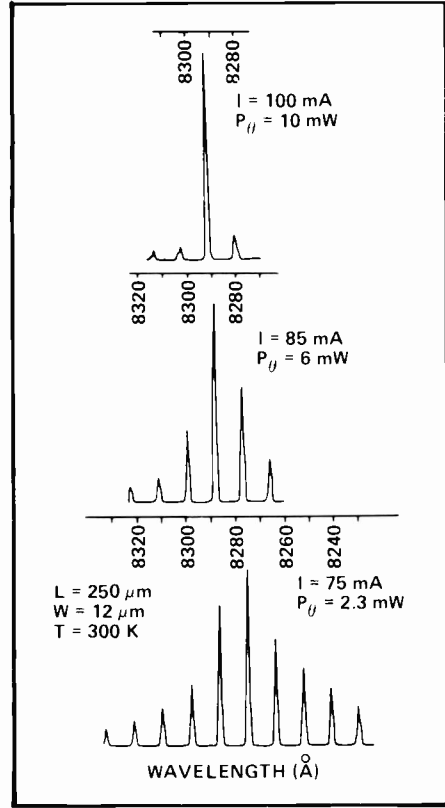


Fig. 20. Emission spectrum of a typical double-heterostructure laser as a function of current.

Nd lasers, an oscillator/power amplifier arrangement can be used with enough amplifier stages to reach the required output power. In this case, each stage would have a complete diode pump. With this sort of arrangement, very high-power pulsed operation can be achieved.

The Nd lasers have an output at 1.06 micrometers; this output can be readily converted to an output at 0.53 micrometers by passing the 1.06-micrometer radiation through a frequency-doubling crystal. This can be achieved with a better than 50-percent conversion efficiency, and thus we have a capability to produce either wavelength, in pulsed operation, with high power outputs. These two wavelengths are sufficient for many LIDAR applications, but for SLCSAT applications other frequency (wavelength)

conversion steps are required. For example, the doubled output from an Nd laser can be used to pump a Ti:sapphire laser, which would be tuned to operate at 0.911 micrometers. This radiation could then be doubled to produce the 0.4555-micrometer radiation required for SLCSAT. Other frequency conversion techniques can be used to reach the required wavelength such as Raman shifting, and these are being explored.

Hence, we see the development of diode-pumped Nd lasers as a key development issue for future applications. Lasers such as Ti:sapphire can be applied to the frequency conversion process, but also have application in the countermeasure area because the output is tunable over such a wide range. Another important diode-pumping application occurs in the area of eye-safe lasers. While SLCSAT and LIDAR require diode lasers with an output at 0.8085 micrometers, the Er:glass material has a strong absorption band at 0.9 micrometers. Laser diodes are available with outputs at 0.904 micrometers, but there is presently no array technology. Approaches using small linear arrays are being investigated.

Single laser diodes are used for fiberoptic communications and have sufficient output power and beam quality to provide a very useful capability. For other applications such as intersatellite links, higher power than can be obtained from a single diode is desired. For such applications, the means of combining the outputs from a number of diodes is needed. The simplest approach is to combine the outputs incoherently from a number of single diodes, but this approach is limited in growth capability. The best approach is to use a phased array of laser diodes with all the diodes emitting coherently. In this case, the diodes effectively function as one large diode and high brightness (power density per unit solid angle) can be achieved. At present, linear phased arrays of laser diodes are under development that have a much higher brightness than incoherent arrays. Development of two-dimensional phased arrays of diodes is under way, and will provide an increased capability and much higher brightness. These required developments are outlined in Table II.

References

1. Hellworth, R.W., *Advances in Quantum Electronics*. J.R. Singer, Ed. Columbia University Press, New York (1961).
2. Verdeyen, J.T., *Laser Electronics*, Prentice-Hall, Englewood Cliffs, N.J. (1981).
3. Koehner, W., *Solid-State Laser Engineering*. Springer Series in Optical Science. Springer-Verlag, New York (1976).
4. Yariv, A., *Quantum Electronics*. John Wiley and Sons, New York (1975).

Table II. Required laser developments

Application	Laser	Development required
SLCSAT	Diode-pumped Nd laser 0.4555- μm output 0.8085- μm pump	High-density diode arrays Frequency conversion techniques
LIDAR	Diode-pumped Nd laser	High-density diode arrays
Eye safe	Diode-pumped Er laser	High-density diode arrays
Rangefinder	0.9- μm pump	
Space communication	Laser diode array	2-D phased array

John P. Kurmer is a Senior Member of Engineering Staff in ATL's Device Technology Laboratory where he is currently conducting research in semiconductor diode-pumped Nd:YAG lasers, solid-state tunable lasers, nonlinear optical devices, and optically activated microwave switches. Recently, he successfully completed the Advanced Technology Study for Satellite Laser Communications Applications. This involved a detailed conceptual design effort for three different approaches, each of which used a laser diode-pumped Nd-laser subsystem. He also performed a technology-development and risk assessment study for each approach. While at Cornell University, his doctoral studies focused on opto-electronic devices, guided-wave optics, and thin-film technology. Dr. Kurmer received his BS in Physics and in Mathematics from Drexel University in 1977, and his MSEE and PhD in EE from Cornell University in 1983. Contact him at:

Advanced Technology Laboratories
Moorestown, N.J.
Tacnet: 253-6504

Douglas Wille is Unit Manager of the Electro-Optics Applications group in ATL's Device Technology Laboratory. His responsibilities include development of laser systems and applications. He is currently managing the PILOT unit-cell definition program, the PILOT 2-D array development, and the Diode-Pumped Laser program. He recently supervised a study of techniques for using lasers for satellite communications with submarines. Prior to joining RCA, he was a Unit Work Leader in the Avionics Laboratory at Wright-Patterson Air Force Base, engaged in development of acousto-optic and electro-optic systems. Dr. Wille received his PhD in Physics from Ohio State University. Contact him at:

Advanced Technology Laboratories
Moorestown, N.J.
Tacnet: 253-6498

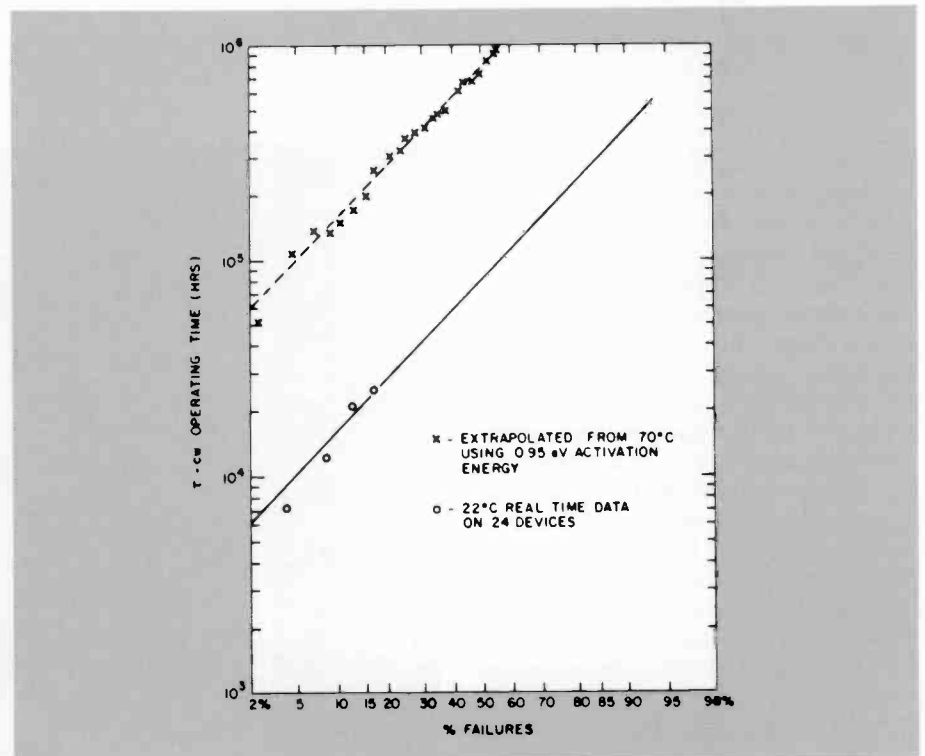


Fig. 21. Statistical distribution of laser diode failures from realtime room temperature lifetests and from accelerated 70° C lifetests.



Authors Wille (standing) and Kurmer

Optical disk recording

The laser diode array, an RCA technological breakthrough, has provided CISD with the tool it needs to design high-data-rate optical disk recorders with the capacity industry will need in the late 1980s.

Optical disk recording at RCA is aimed at addressing the growing needs produced by new computer and sensor systems being developed. The data rates for these systems range from 50 megabits per second to 500 megabits per second. Storage capacities needed range from 5×10^{10} bits to 1×10^{13} bits on line.

Two designs of recorders are being developed at RCA to meet these needs. The lower capacity and data transfer rate requirements will be met by 50-megabit-per-second rack-mountable units, such as that shown in Figs. 1 and 2, which store 5×10^{10} bits per side of a 14-inch disk. The higher capacity and data transfer rate requirements are being met by 500-megabit-per-second "jukebox" systems, such as

Abstract: *There is an ever increasing need for data storage and retrieval systems with higher density, larger capacity, lower cost per bit, longer storage life, lower bit-error rate, and faster access. At the present time magnetic tape, magnetic disks, and photographic film are the principal storage media for large database systems. As sensor and computer dynamic range and bandwidth improve, orders of magnitude more data will be stored, sorted, processed, and disseminated, making present technologies inadequate for the later 1980s, when requirements for recording in excess of 10^{14} bits per day for some of these systems are anticipated. This equates to 100,000 present-technology magnetic tapes per day.*

©1986 RCA Corporation.
Final manuscript received April 21, 1986
Reprint RE-31-3-5

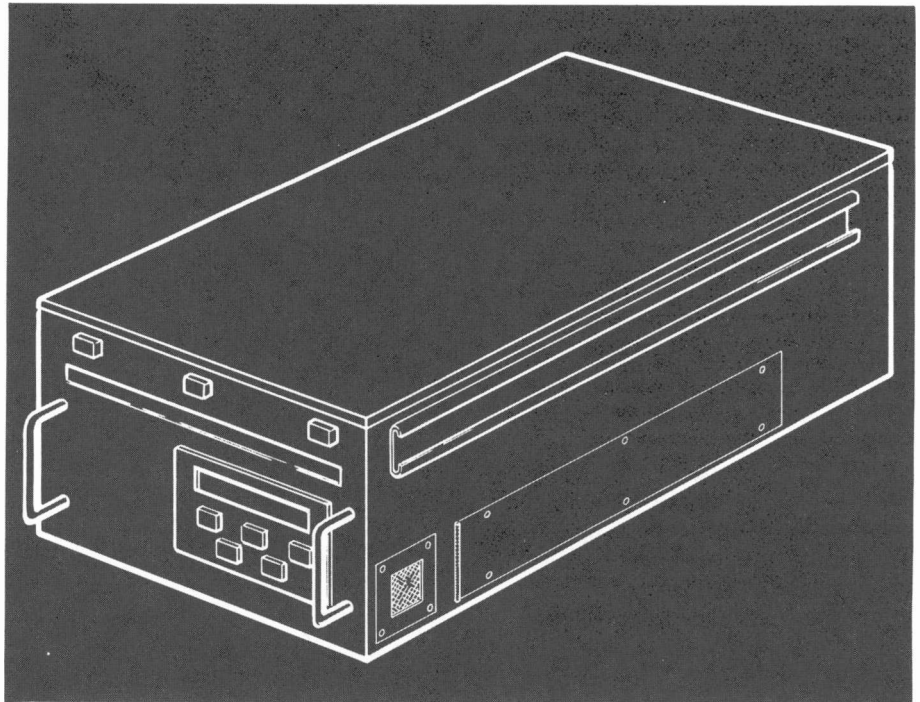


Fig. 1. Rack-mountable, 50-megabit/second optical disk recorder.

that shown in Fig. 3, which store 1×10^{11} bits per side of a 14-inch disk and contain 128 robotically handled disks.

Optical disk recording is essentially a thermal process; recording efficiency is directly related to peak irradiance (energy density per unit time) of the recording spot. To achieve data rates of 500 Mbps and data storage of 1×10^{11} bits per surface of a 14-inch disk, high-power argon lasers operating with multiple beam configurations have been employed in jukebox systems. The lower capacity rack-mount systems have used multiple diodes (for multiple tracks) to provide data rates up to 50 Mbps and data storage of 5×10^{10}

bits per surface of a 14-inch disk. The optical, mechanical, and electrical systems used by these smaller rack-mount units will be discussed in this article.

System description

The RCA concept of an optical disk system, illustrated in Fig. 4, comprises two major elements: the controller/formatter (C/F) and the disk drive unit (DDU). For purposes of description, the C/F hardware is subdivided into a data processor unit (DPU) and the control processing hardware (CPH). The DPU contains all of the user data interface and the buffer/

format electronics. The CPH consists of the microprocessors, the system software, and the magnetic disk drive used as an embedded directory unit. The DDU includes all of the high-speed serial data processing electronics, the electro-optical and optical components, the mechanisms, and the servo electronics that control the mechanisms.

Building an optical disk system that effectively meets the desired objectives required certain initial decisions at the system level to form a baseline for hardware design. The driving requirements are disk capacity, access time, and bit error rate. These are dependent upon a number of individual factors, which are described below.

Physical limitations

The optics and mechanisms have physical limitations that limit optical disk recorder system performance. Disk capacity is directly related to the minimum feature that can be recorded onto the disk. For a semiconductor laser, a $0.7\text{-}\mu\text{m}$ diameter recording spot is close to the theoretical minimum feature size. The total number of features (F) that can be recorded in a single revolution of the disk at a given radius (r) is:

$$F = \frac{2r}{s} \quad (1)$$

where F is the number of features, r is the radius (meters), and s is the feature size (meters).

It should be pointed out that a feature does not always represent a binary digit (bit) of data. Higher bit packing densities can be achieved by utilizing encoding schemes in which one recorded feature represents more than one digital bit. Optical disk recording employs a 3-phase code that effectively produces 1.33 bits per feature.

Disk capacity is most affected by the unused space between adjacent tracks. Adjacent tracks can be as close as $0.6\ \mu\text{m}$ (the resolving limit of the read beam). The effect of adjacent track spacing is given by:

$$N = \frac{(r_o - r_i)n}{\Delta} \quad (2)$$

where N is the number of tracks per disk, r_o is the outer radius (meters), r_i is the inner radius (meters), n is the number of tracks at each stage position, and Δ is the stage jump increment (meters).

The product of $F \times N$ defines the total

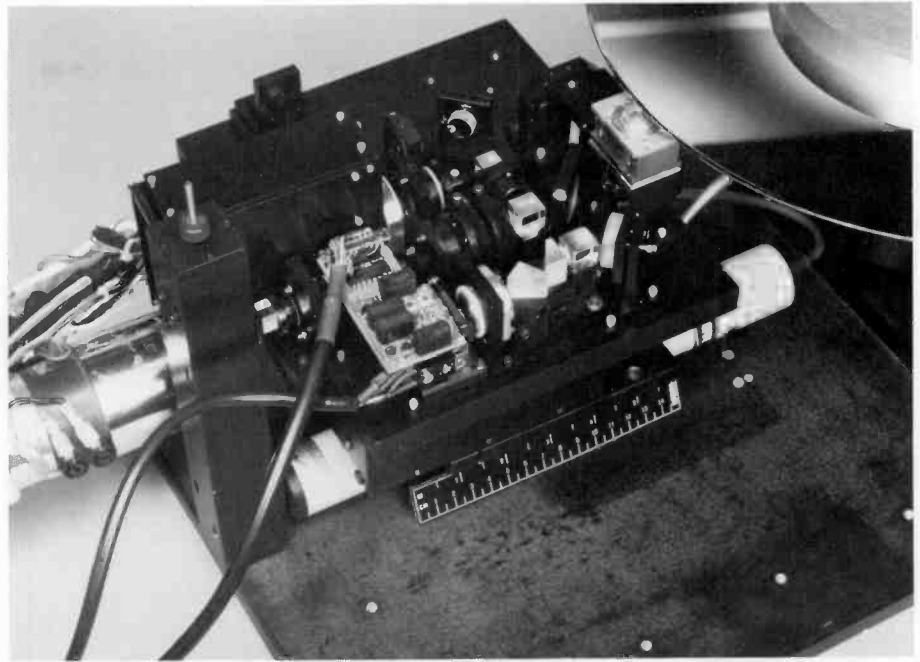


Fig. 2. Fifty-megabit/second optical disk recorder stores 5×10^5 bits per side of a 14-inch disk.

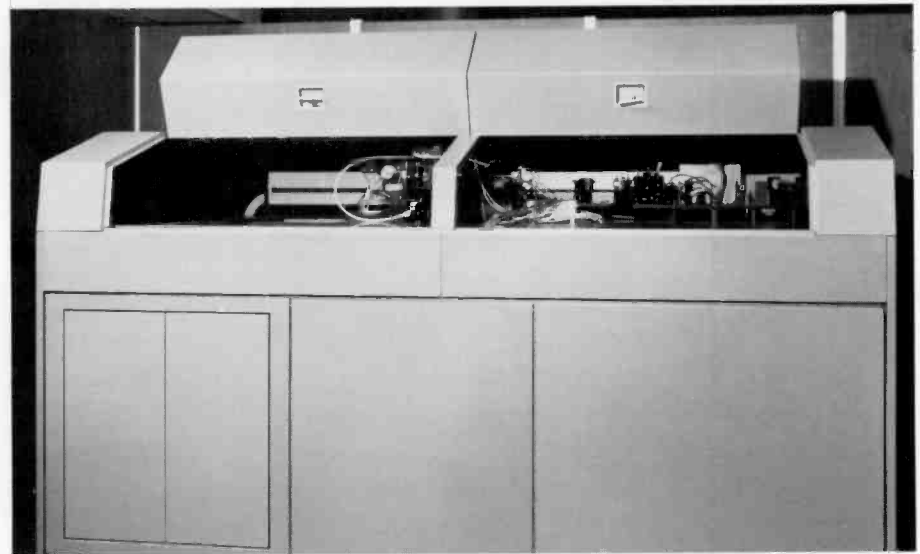


Fig. 3. High-capacity optical disk recorder with a data transfer rate of 500 megabits/second.

number of features that can be recorded on a disk surface.

Disk capacity

The useful area of typical 14-inch disks lies between 95.3 mm and 172.7 mm radii. The number of features per disk track is determined by substitution into equation 1. If a semiconductor laser is employed for the record source, the feature size will be 0.7×10^{-6} meters. This results in 1,130,624 bits per track when encoded

with 3-phase code. Also, a 33-percent format overhead must be provided, resulting in a user capacity of 851,968 bits per track. The rack-mounted optical disk recorder utilizes a dual laser diode array to produce to simultaneous, independently-modulated laser beams that write a pair of tracks at a time. The two tracks are nominally $1.25\ \mu\text{m}$ center-to-center. A guard band of $3\ \mu\text{m}$ is used between track pairs to accommodate the translation stage tolerances. This results in two tracks per $5\ \mu\text{m}$ stage movement. Substitution into

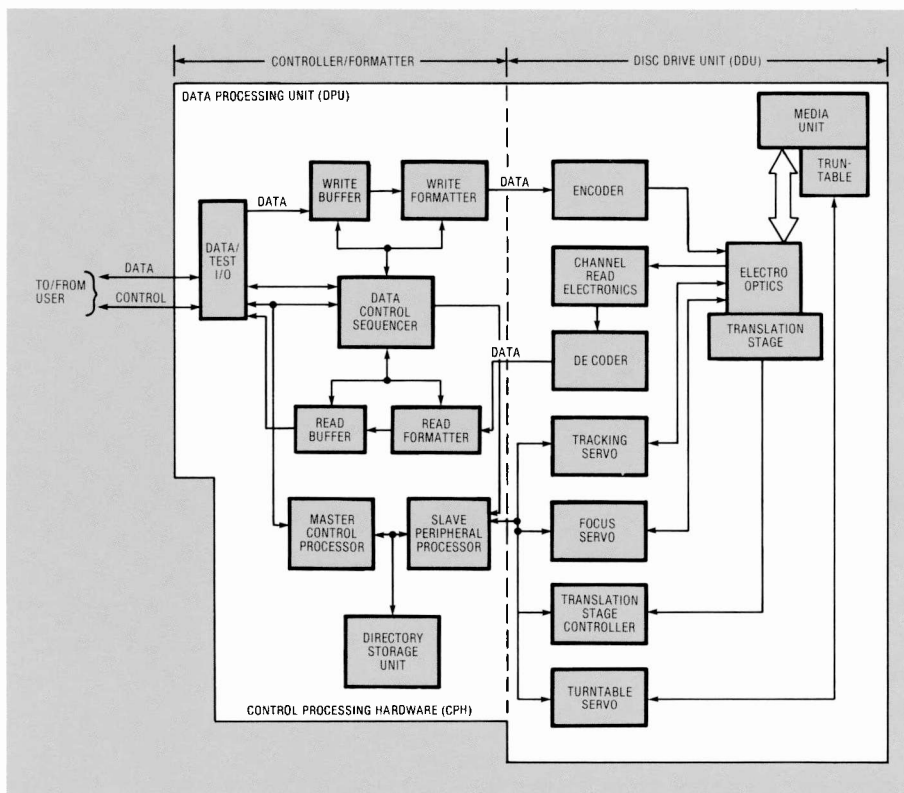


Fig. 4. RCA concept of an optical disk system, with two major elements: the controller/formatter and the disk drive unit.

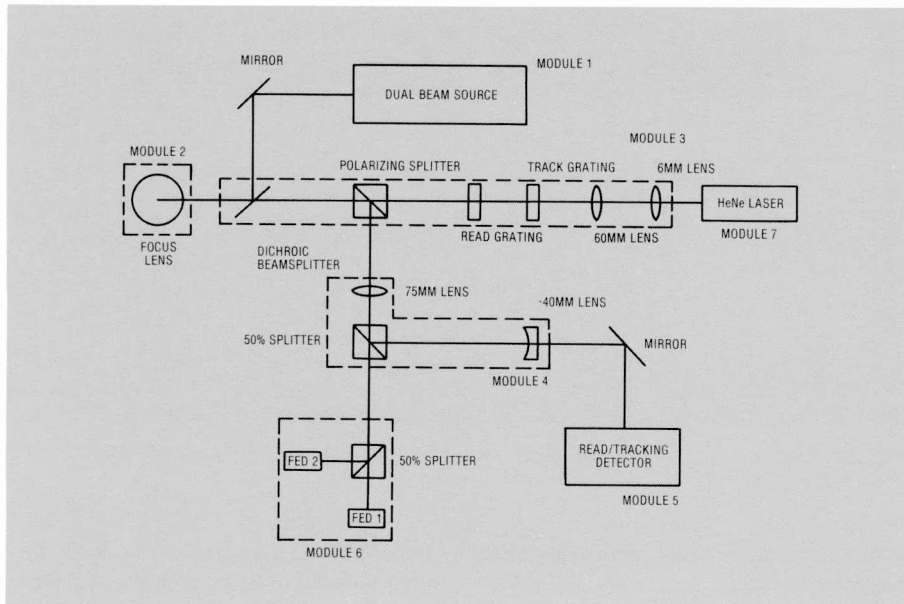


Fig. 5. Schematic of the optics system for a rack-mountable optical disk recorder.

equation 2 reveals that 30,960 track pairs can be recorded per disk side.

The total capacity for the system is therefore $(851,968) \times (30,960) = 2.6 \times 10^{10}$ user bits. Although this figure is approximately half of the desired capacity, the planned use of a better translation mechanism and a more efficient data format

will allow this system to achieve the desired capacity.

The values presented here are for a dual-diode laser array system. Other systems can be analyzed in a similar manner.

The need to transfer and store data at continuous rates of 25 Mbps or greater in compact units that could easily be trans-

ported required the development of new technologies and subsystems beyond those developed in the early jukebox units. The remainder of this article concentrates on the development of the key optical subsystems in the rack-mountable equipment. These major subsystems are laser diode arrays, modular optical mounting, and mechanical structure.

Mechanical system

The basic objectives of the mechanical design are to provide a unit that can be critically aligned optically and maintain that alignment under all operating and environmental conditions. The design configuration must also be compact and of minimum weight. The specific areas addressed in meeting these objectives are discussed below.

Vibration problems

Mechanical vibration is a most serious threat to system performance, and may be induced by either electromechanical subsystems within the equipment or from the environment. When the vibration frequencies lie in or near the servo bandwidths, the effects are particularly serious. Whereas sophisticated damping may be considered in a final mechanical design, certain fundamental steps must be taken in the early stages of development. These consist of designing all mechanical structures to have mechanical resonant frequencies much higher than the servo bandwidth. In general, this means designing all structures to have the highest possible stiffness in both bending and torsion.

The basic equipment frame or mounting base is of primary importance since it must maintain the fixed alignment of all subsystems and optical modules mounted to it. The concept of single metal plate as the sole support structure has proven less than satisfactory because of its tendency to bend under conditions of static and dynamic loading. The optical modules are mounted to a metal plate platform that attaches to the moving carriage of the electromechanical translation stage. Since the optical platform must react to the acceleration of the moving stage, its rigidity is also an important factor. Yet, minimizing its weight is of key importance to translation servo performance.

Disk drive module

The disk drive module is comprised of the disk spindle motor support structure,

disk motor stator, rotor with integral shaft, bearing suspension, disk mounting hub assembly, and the 14-inch disk itself. Minimization of the disk rotational runout is essential, and the design of each of the disk drive component parts is critical. The resonant frequencies of the rotating assembly in various modes are also of great concern, and are design drivers.

Mounting of optical components

Mirrors, lenses, electro-optic detectors, and lasers have heretofore been mounted individually on a common base, or plate, employing commercially available adjustable mounts where possible. While the individual adjustable mounts are usually adequate, this "optical bench" approach poses problems in terms of an ordered alignment procedure. A key design improvement was to modularize the optics into functional and physical entities, each providing a mounting sub-base for all its components. This enables optical pre-alignment of the individual modules and facilitates final optical alignment of the whole system.

Optical system development

The rack-mount optical disk recorder optics system utilizes two channels of write signals, two channels of direct read after write (DRAW) signals, and control signals for the radial tracking and focus servos. The complete optical system consists of seven modules. Alignment tolerances between modules are reasonable to work with, but the individual modules require critical alignment. Figure 5 shows the optics system schematic and the relationship of the various optics modules.

Dual-diode source module (module 1)

The first major development was that of a modular laser diode array for use in this equipment. The discussion of that development is covered in another article in this issue (see D.B. Carlin, page 20). The dual-diode array source module is the most sophisticated part of the optics system and represents a technological breakthrough unique to RCA. Figure 6 is a photograph of the module containing a two-diode laser array, a collection lens, two Littrow prisms, and a polarizing beam splitter. The laser array provides two record beams in the same space as a single laser diode.

The laser array was developed at RCA

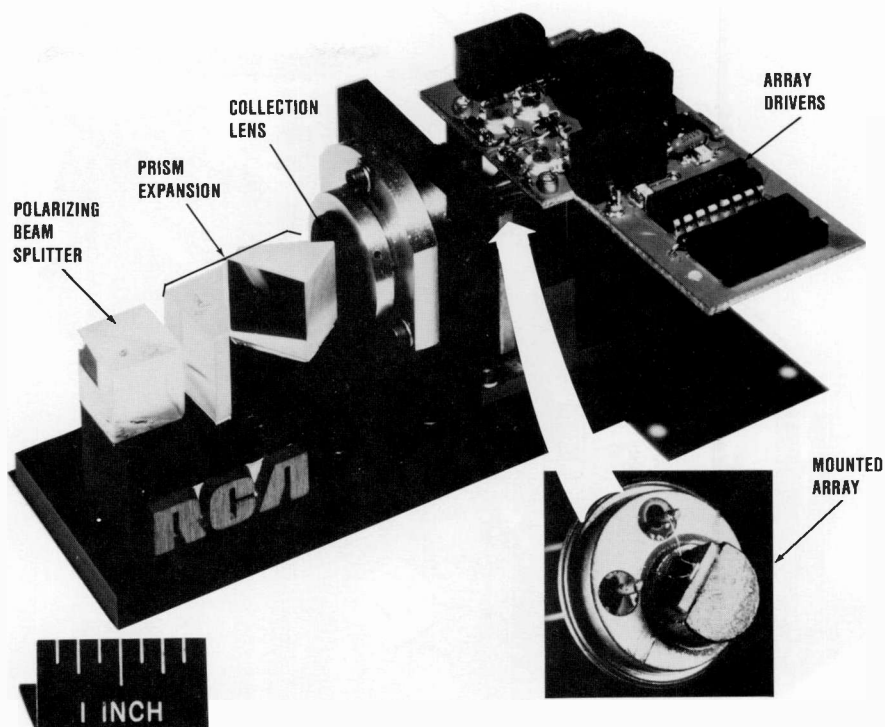


Fig. 6. The dual-diode array source module, which contains a two-diode laser array, a collection lens, two Littrow prisms, and a polarizing beam splitter.

Laboratories especially for the program. The diodes are $150\mu\text{m}$ apart on a wafer mount.

Each diode emits an elliptical, diverging, fundamental spatial-mode laser beam with a wavelength in the near infrared. Typical wavelengths are in the 780-830 nm range, and typical divergence (at 50-percent intensity points) is 30° perpendicular to the lasing junction, 10° in the parallel direction.

This array is placed in the focal plane of the collection lens, with the diodes straddling the optical axis of the lens. The lens is a 0.43 NA, 7.55 mm effective focal length lens and it exhibits minimum wavefront distortion at infinite conjugate. The lens forms the laser diode output into two collimated beams with elliptical spatial profiles. When properly aligned, the beam centroids are diverging from the optical axis within ± 1 milliradian in the direction of diode separation (parallel to the lasing junction).

Optical recording is a thermal process, and better results are achieved when the focused spots are circular. The Littrow prisms provide anamorphic 3:1 expansion of the two beams with a minimum amount of wavefront aberration in a compact design. The prisms also reduce the centroid divergence by the reciprocal of the magnification. A polarizing beam splitter is included in the dual source module to

prevent the reflected beam from feeding back into the laser diodes.

This optical subsystem, in combination with the focus lens, forms two $0.7\mu\text{m}$ spots on the surface of the disk on $1.25\mu\text{m}$ centers.

Optical subsystems

By combining the optical modules into an assembly as shown in Fig. 7, the optical subsystems are formed. Each module contributes to one or more subsystems. The three subsystems are the write subsystem, the read/track subsystem, and the focus subsystem. Each subsystem has a specific function and will be further discussed.

Write subsystem. The write subsystem consists of the dual source module (module 1) and the focus/galvo module (module 2). These modules together produce the two spots for recording on the optical disk.

Recording efficiency is directly related to the peak irradiance and energy density per unit time of the recording spot. A fundamental trade off is depth-of-field versus defocus. As the spot size decreases, the change in spot size per focus error grows. An optical system with a numerical aperture of 0.65 allows the desired packing

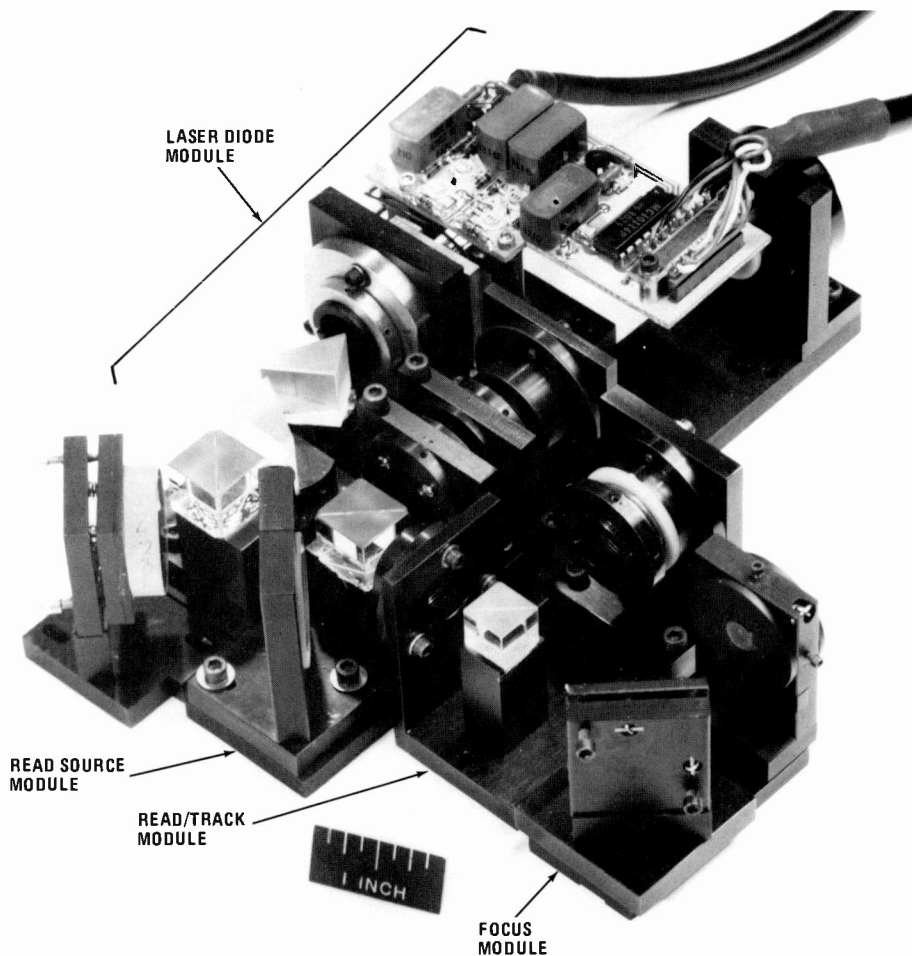


Fig. 7. The optical modules are combined to form the optical subsystem.

density and a realistic focus servo. The focus lens required by the system is a 5-mm effective focal length lens with a 3.25-mm radius aperture. This high-quality lens, whose specifications are listed in Table 1, was designed specifically to meet the demands of optical recording. With this lens a 830-nm diode laser will form a 0.7 μm full-width half-maximum spot with a beam whose fundamental mode is a gaussian intensity distribution.

Wavefront aberration due to the lens effects write performance. An ideal lens forms a perfect spherical wave, thus providing minimum spot size and maximum peak irradiance. Wavefront aberration is the measure of how the actual wavefront varies from a perfect sphere. For small aberrations, the spot size will remain constant, but the peak irradiance will drop. Such a lens (or optical system) is said to be diffraction limited. This system has less than one-quarter wavelength ($\lambda/4$) wavefront aberration. The diode collection lens

and the focus lens were designed in tandem to provide less than $\lambda/10$ aberration for a 100 μm radius field of view in the focal plane of the lens.

In addition to the focus lens, the write system performance is greatly affected by power delivered to the disk surface. Things that affect power are: diode output, clear aperture transmission, number of components, and aperturing affects. The first two must be maximized and the third minimized. The components used in write path are all anti-reflection coated in the near infrared. The coatings are the best possible and no component causes more than a few percent power loss.

To minimize the affects of aperturing as the diverging record beams leave the collection lens, the design minimizes the optical path between the collection lens and the focus lens. A relay system to overlap the two beams in the entrance pupil of the focus lens would eliminate truncation losses at that aperture, but would

be large and cumbersome, and therefore not consistent with the compact, fast design requirements.

Read/track subsystem. Five modules contribute to the read/track subsystem. The design was constrained by the focus lens (module 2) and the layout of the detector array (module 5). The diffraction grating specification and relay module (module 4) design is a result of these constraints.

The laser/injection mirror module (module 7) and playback module (module 3) generate the multiple beams for DRAW and tracking. The diffraction gratings give angular separation of ± 3 milliradians and ± 6 milliradians. The 2:1 angular separation comes from the detector array layout, where the DRAW detector spacing is twice the tracking detector spacing.

The lenses located in modules 3 and 4 must have a field of view of $\pm 100 \mu\text{m}$ for diffraction limited performance. Alignment and tracking requires the array of spots to fall within $\pm 30 \mu\text{m}$ of the center of the focus lens (module 2). The spot spacing at the disk equals the focal length of the focus lens times the centroid angle for collimated beams in the focal plane of the lens. Mathematically:

$$X_f = f\theta_c$$

$$(\theta_c)_{max} = \frac{+30 \mu\text{m}}{5 \text{ mm}} = 6 \text{ mr}$$

where θ_c is the centroid angle for collimated beams, X_f is the read spot spacing, and f is the focal length of the lens.

This relationship between spot separation and centroid angle also applies to the detector array (module 5). Maximizing the angular spacing into the focus lens (module 2) minimizes the focal length of the -40 -mm imaging lens in module 4. Even so, the required focal length is 345 mm to satisfy the spacing requirements of the detector array.

The relay module (module 4) solves this problem by positioning the relay and imaging lenses to form a 345-mm effective focal length lens. The image plane is 105 mm from the relay lens instead of 345 mm, thus saving 240 mm of optical path.

Focus subsystem. The focus technique uses geometric focus error detection, reducing the required number of optical elements by 66 percent when compared to previous techniques. The operation of the focus subsystem is as follows:

- When in focus, the 75-mm relay lens forms a waist midway between the focus error detectors, or FED (module 6). With defocus, the waist moves toward one detector while the cone angle of the beam remains constant. This generates an error signal that drives the focus coil (see Fig. 8).
- The beam used is the first-channel read beam, with no offset (angle or translation) into the objective. This minimizes field curvature impact on the focus servo. Completely truncating the focus beam becomes almost impossible. No separate focus beam must be generated.
- The focus error signal is detailed in Fig. 8. There are two zero crossings, but of opposite slopes, which allow proper lock-up.

The implemented focus system was analyzed with an optics ray trace program developed by CISD for use on an IBM PC. This improved focus error signal model successfully simulated the optical system shown in Fig. 9. Table II defines the quantities shown in Fig. 9.

Performance

The performance demonstrated (see Table III) by the present rack-mountable disk drive unit meets the needs of the late 1980s. The data rate of 50 megabits per second was made possible by the technological breakthrough of laser diode arrays. To achieve the data rate, each channel of the array supports half of the total 50 megabits per second. These arrays have allowed two or more channels of data to pass simultaneously through a common optical path, thus saving space. Although the capacity is only 2.6×10^{10} bits and not the 5×10^{10} bits desired, it is a simple matter to achieve the 5×10^{10} bits capacity. The demonstrated capacity was achieved with unformatted media and 3-phase coding. When preformatted media and 5-phase code are employed the 5×10^{10} bits capacity will be obtained. When comparing a magnetic cartridge disk unit with access time of 30 ms to the optical cartridge disk unit with access time of 190 ms the demonstrated access time appears long. Since optical recording is 40 times denser than magnetic recording per unit area, the average access to an equivalent amount of data is 4.75 ms for the optical system. This also does not include the time penalty that the magnetic systems suffer when changing cartridges to reach data that is not on the magnetic disk but which could

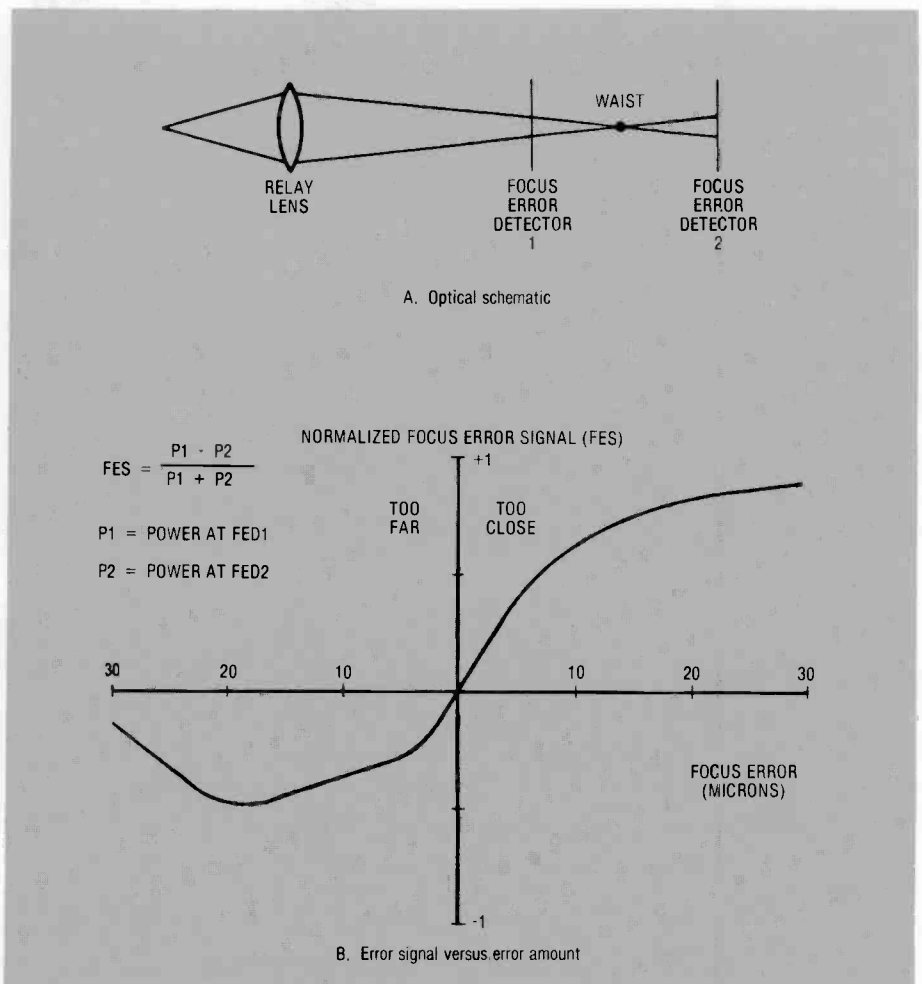


Fig. 8. With defocus, the waist moves toward one of the error detectors, generating an error signal that drives the focus coil.

Table I. Dual-wavelength micro-objective lens specifications

Effective focal length	5.0 nm
Numerical aperture	0.65
Entrance pupil diameter	6.5 mm
Wavelength	632.8 and 830.0 nm (parfocal)
Field of view	± 0.1 mm
Working distance	0.9 mm min.
Barrel diameter	0.5 mm
Barrel length	11.0 mm \pm 1.0 mm
Weight assembled	3 grams

be on the optical disk. The error rate of 1 in 10^{10} bits of data is a good measure of system reliability. The error correction and detection techniques employed were developed to provide reliable system operation with a medium that provides a raw data error rate of 1 in 10^5 bits. The error rate achieved compares favorably with current magnetic disk storage operating at

1 in 10^{10} to 1 in 10^{12} bits. As the medium matures the raw error rate is expected to improve, which will place optical disk recording on a firm footing when compared to magnetic cartridge disk applications.

The physical size of the unit at 3 cu. ft. and 150 lbs also compares favorably to magnetic cartridge disk systems and occupies an equivalent amount of rack space.

Table II. Quantities that affect focus error signal

Variable	Definition
f_{θ}	Focus lens focal length
f_r	Relay lens focal length
W_L	Beam radius at grating
θ_{G1}	Angle of 1st order, 1st grating
θ_{G2}	Angle of 1st order, 2nd grating
L_T	Axial distance
L_2	Axial distance
L_{3T}	Axial distance to FED ₁
S_{WT}	Slit width at FED ₁
L_{32}	Axial distance to FED ₂
S_{W2}	Slit width at FED ₂

Table III. Demonstrated performance

Data rate	50 megabits per second
Capacity*	2.6×10^{10} bits per surface
Access time (average)	190 ms
Error rate	1×10^{-10}
Size	3 cubic feet
Weight	≈ 150 pounds

*NOTE: Although the capacity is only 2.6×10^{10} bits and not 5×10^{10} bits desired, it is a simple matter to achieve the 5×10^{10} bits capacity by employing preformatted media and a higher order recording code such as 5-phase.

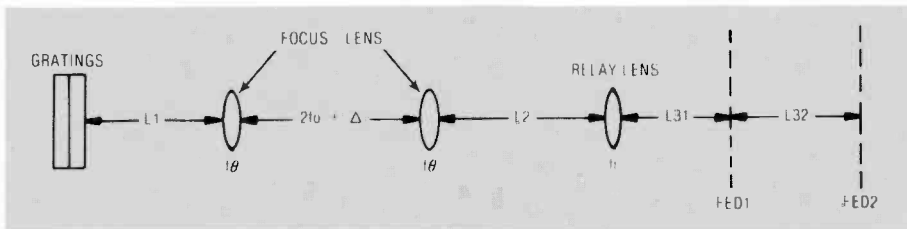


Fig. 9. The optical system simulated by the CISD-developed optics ray trace program.

Having successfully demonstrated the dual-channel recording system based upon semiconductor laser arrays described above, RCA is planning to incorporate the findings of this effort in future systems that can fully employ the performance.



Authors Ravner, left and Johnston.

Ross Johnston became a unit manager of the Recording Systems group at CISD in 1983, responsible for design and development of optical disk storage equipment. He is currently the technical director on the durable optical disk project. The durable optical disk system is a rack-mountable unit intended for airborne applications requiring 25 megabytes per second transfer rates and 5×10^{10} bytes of

storage per disk surface. The work described in this article laid the foundation for the durable project. Since 1974 he has had responsibility for high-data-rate digital recording systems.

Prior to joining RCA, Mr. Johnston was responsible for two major development programs at Control Data: a reel-to-reel tape transport and a 200-inch-per-second start/stop tape transport. Mr. Johnston

holds a BSME from the University of Pittsburgh (1969), and performed graduate study at the University of Pennsylvania.

Contact him at:

Communication and Information Systems Division

Camden, N.J.

Tacnet: 222-6294

Stephen Ravner has over 25 years of experience in program management and engineering of high-performance image and data recording systems. He has been responsible for CISD's optical disk recording program activities since 1980. This work includes IR&D of solid-state laser diode recorders, development and test of optical disk media, design and analysis of optical disk mass data storage systems, and associated proposals and business plans.

Prior to transferring to CISD in 1977, Mr. Ravner worked at Astro-Electronics, where he was responsible for the development of high-resolution laser image recorders and advanced video equipment associated with satellite programs. He received the BSEE and MSEE degrees at the Polytechnic Institute of Brooklyn, is a member of IEEE, and has authored and presented many technical papers in the areas described above.

Contact him at:

Communication and Information Systems Division

Camden, N.J.

Tacnet: 222-3889

Local-area networks employing fiber optics at very high data rates

Optoelectronics can make LANs more efficient and effective.

Over the past several years many technical articles^{1,2,3} have described the progress and application of fiber optics technology to the telecommunications industry. Previously unattainable bandwidth-distance performance has been demonstrated with state-of-the-art fiber-optic systems employing laser diodes as optical sources. Single-mode, low-loss optical fiber has allowed repeaterless point-to-point digital links spanning distances greater than 100 kilometers with rates of transmission of gigabits per second.⁴

A new application area for high-speed fiber-optic systems is in the distribution of digital data within a building or small geographical area such as a college campus. These local-area networks (LANs) had been previously limited to low data rates and modest distances because of the attenuation and limited bandwidth characteristics of coaxial or twisted-pair type of transmission media. A fiber-optic approach allows much greater distance-bandwidth performance even though the "power"

transmitted in fiber-optic systems is orders of magnitude lower than with coaxial alternatives, and the received "power" must be much higher than conventional wired or coaxial systems. What is lost in signal-level range is gained in the greatly improved bandwidth-distance performance with fiber-optic technology.⁵

As the data rates of equipment at the user level increase, the need for even higher-speed data transmission systems for multiple users also increases. The special needs of shared memory facilities, particularly for high-speed graphics, has increased with magnetic disc and optical disc bulk storage. Local data retrieval rates approaching a hundred megabits per second are projected.⁶ To provide this information on a shared basis to many users quickly requires line transmission rates of hundreds of megabits per second. Additional applications for high-resolution workstations, interactive video and audio transmissions, and mainframe computer access have stimulated local-area network development of 100 Mbit/second, 200 Mbit/second, and even greater line transmission rates.⁷

The development of these specialized high-speed fiber-optic systems has stimulated extensive study and hardware development activity at both RCA Laboratories and Communication and Information Systems Division (CISD). The specifications and operating characteristics for the fiber-optic transmitters and receivers are influenced by many factors including the physical structure of the networks and the method by which any user of the networks gains access to that network.⁸ Results of RCA's efforts over the last four years in the development of a very-high-speed, efficient, and reliable test network are described in the next sections.

Architecture

Several different physical interconnection approaches have been evaluated in very-high-speed (several hundreds of megabits per second) fiber-optic systems.⁹ Figure 1 shows several of the physical approaches broadly classified as the ring, star bus, and loop bus configurations. The ring approach places all of the terminal locations or nodes in a series path. The reliability of this type of network is poor, since it fails if the series ring is broken at any one point. It is, however, the easiest architecture to implement from the fiber-optic standpoint. All fiber links in the simple ring are of the point-to-point type, which have fewer critical requirements for laser stabilization, receiver sensitivity, and dynamic range performance but may require some coarse adjustments when first installed.

The tapped architecture in the loop bus configuration is similar to the approaches used for cable television distribution systems and digital networks such as Ethernet. The difficulty in this approach is that a suitable low insertion loss equivalent to the coaxial cable tap does not exist for fiber optics. The loop bus configuration places very severe requirements on the fiber-optic receiver sensitivity, which limits the number of taps that can be placed in a practical fiber network of this type to less than 10 (typically). The addition of repeaters to re-establish the signal level prior to additional taps introduces active elements that can reduce the reliability of the network.

The star bus configuration allows the distribution of the signal from any one node to all of the receivers on the network in a broadcast fashion over a totally passive medium. Depending upon the individual optical losses in each path, the successive

Abstract: *A new application area for high-speed fiber-optic systems is in the distribution of digital data within a building or small geographical area such as a college campus. These local-area networks (LANs) had been previously limited to low data rates and modest distances because of the attenuation and limited bandwidth characteristics of coaxial or twisted-pair type transmission media. This article describes the fiber-optic approach being developed by CISD and RCA Laboratories.*

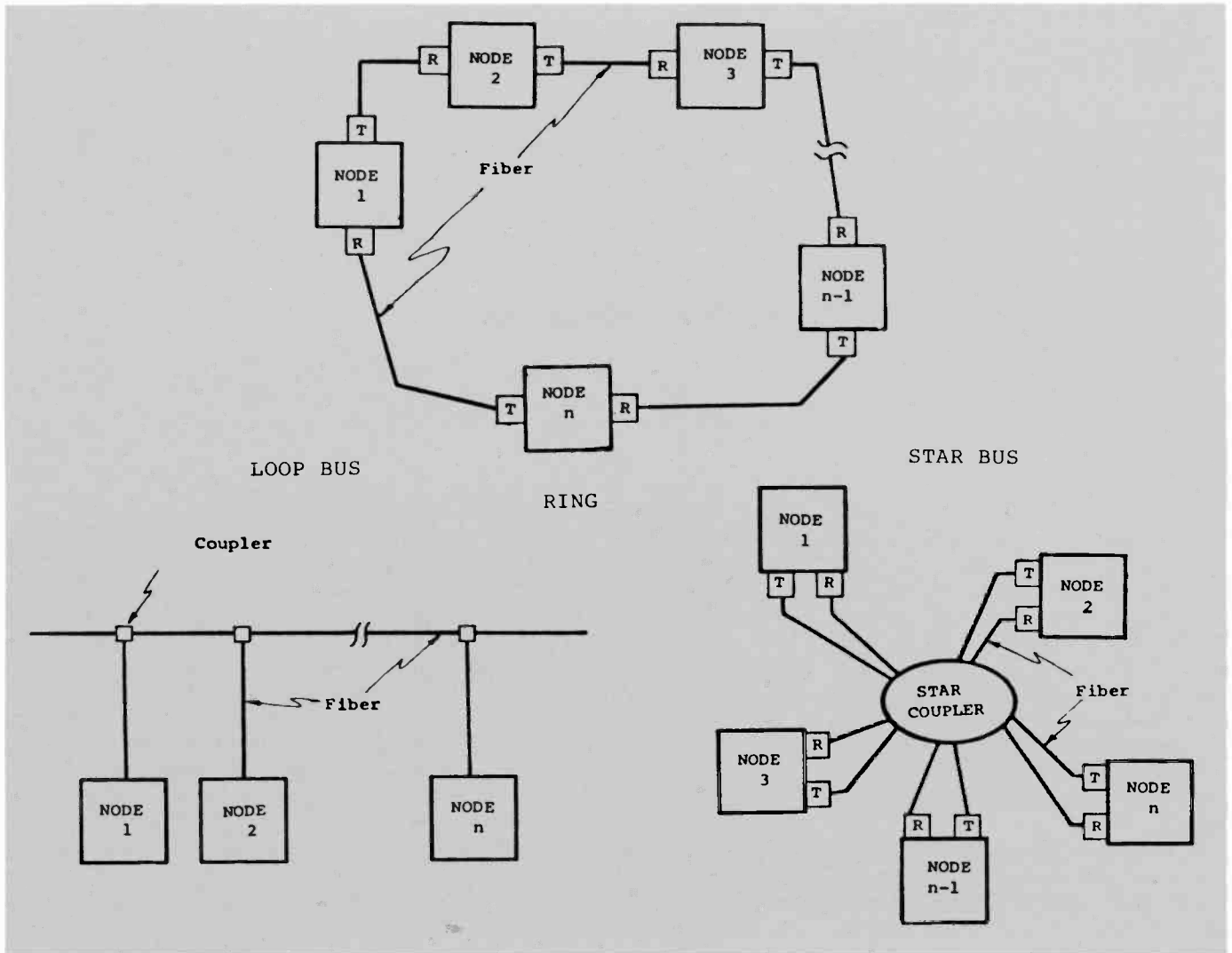


Fig. 1. Network architectures.

Table I. Fiber-optic transmitter and receiver requirements

Ring LAN	Bus LAN
Continuous data transmission	Burst or intermittent transmission
Conventional interstage designs	Performance trade-offs; sensitivity
"Average" level stabilization, and data recovery circuits	Inter-message dynamic range
Maximum sensitivity and dynamic range performance	No background light permitted
	Special clock recovery circuits
	Dynamic threshold recovery circuits
	Listen while transmitting
	Fast stabilization of light output
High-speed pulse fidelity	
Environmental and lifetime effects	
High optical power	

signals that any receiver must interpret may also differ dramatically in the optical signal level. In bus networks the reception and transmission of data is not of a continuous nature. This type of system is characterized as an intermittent or burst mode (packet data) type communications system. Digital regeneration and clock extraction under burst mode conditions also require a different system approach than with conventional point-to-point links. Although the fiber-optic transmitter and receiver requirements are more stringent than with point-to-point links, the star bus configuration has fewer requirements for dynamic range and sensitivity than the loop bus.

Thus, the physical implementation of a fiber-optic network can have a great effect on the requirements of the optoelectronic subsystem transmitters and receivers. Another factor defining the operating characteristics of the modules is the network protocol.

Network access protocol

The protocol of a local-area network defines the operating procedure by which stations or nodes may gain access to the network. One protocol widely used at lower data rates (Carrier Sense Multiple Access, CSMA) requires the receiver of any node to listen before and during transmission. Propagation delays within the network may normally result in nodes transmitting and interfering with each other. Retransmission must then take place with an adjustable delay for each station in order not to again interfere with other contending stations.¹⁰ At high data rates this process reduces the efficiency of actual message throughput as the distance between nodes increases relative to the length of the message to be transmitted.¹¹ The popular Ethernet system uses this approach efficiently at data rates of 10 megabits per second. Several vendors offer fiber-optic versions of this system.

A token-passing protocol has proven to be a practical method of access to higher speed networks with several different types of physical structures. This method requires the reception of a permission message (token) before information may be sent to another station. Several methods exist to direct the token from station to station and/or establish priority nodes that would have greater access to the token. In a token ring configuration when all stations have equal priority for the token, this network approach has been shown to have excellent results.¹¹ If, however, one or two nodes serve as a source of data for the other operating nodes, as a mass storage data source, inherent delays in the propagation of the token around a large ring

would greatly reduce the ability of the network to deliver large amounts of data efficiently. In the ring configuration these inherent delays would result from the time delays of repeating each message at every node and the accumulated delay of all the interconnecting fiber in a large ring architecture. In a token bus protocol, the network access is more flexible than with a ring at the sacrifice of only a small amount of network efficiency. Deterministic operation is supported, which permits real-time access by a broad class of users over a variety of data loading requirements. Even with these advantages and disadvantages it is not evident that one network configuration and protocol choice will meet all of the various requirements for local-area networks at very high data rates.

Special optoelectronic module requirements

Bus architectures and protocols place different requirements on the optoelectronic transmitters and receivers than would be required in more conventional telecommunications¹² and point-to-point type (ring) local-area network applications, as has been discussed. Some of these differences are summarized in Table I. The best performance in terms of receiver sensitivity and dynamic range can be achieved under point-to-point conditions because conventional, AC-coupled receiver gain stages may be employed that have been optimized for continuous data transmissions.

Lasers are threshold devices requiring a well-defined bias current for stable operation at high data rates. The laser output

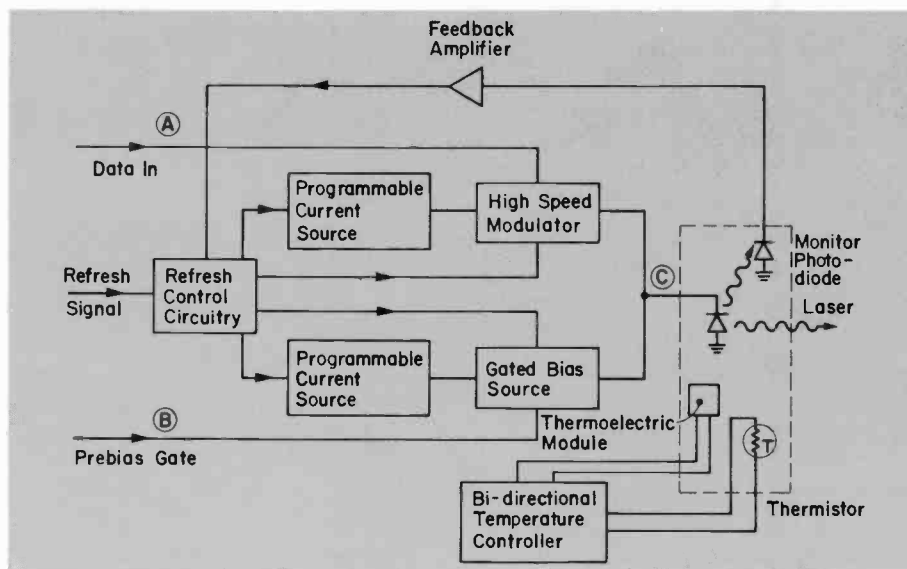


Fig. 2. Prebias laser transmitter with refresh.

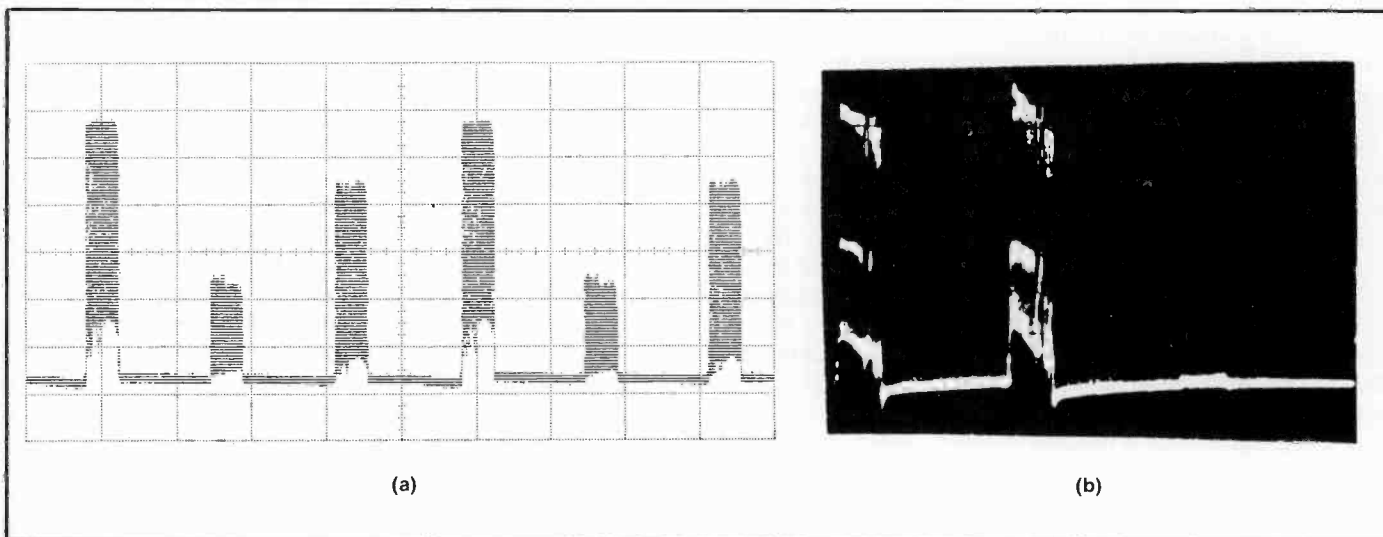


Fig. 3. Intermessage dynamic range performance.

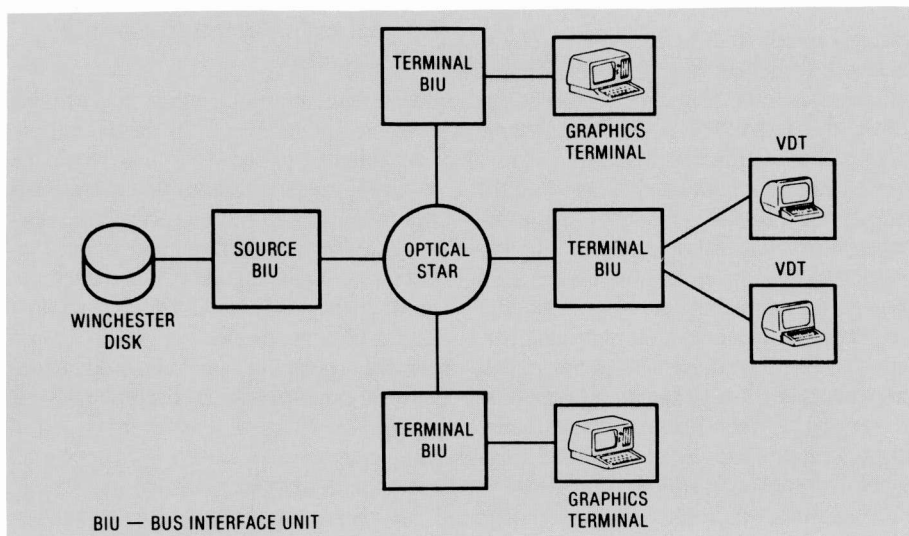


Fig. 4. 200-Mbits/second fiber-optic network testbed.

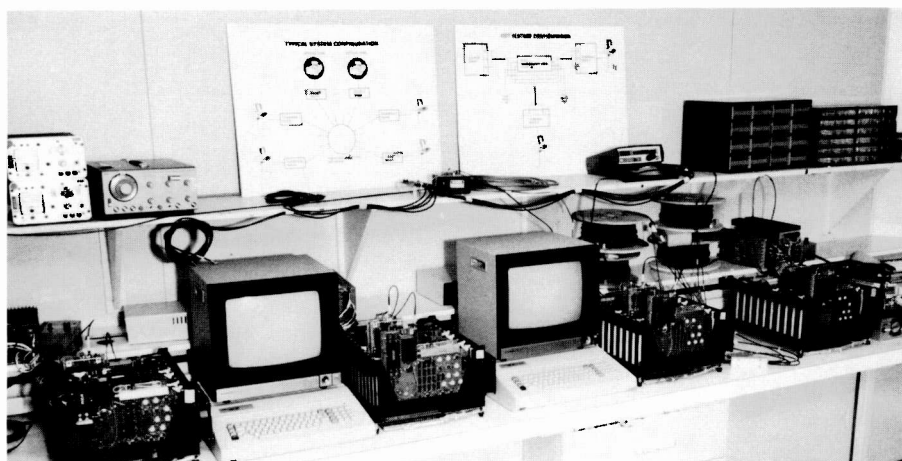


Fig. 5. Photograph of 200-Mbits/second testbed.

for off-on type digital signals has some residual or background light present even in the off condition.¹³

Bus-oriented protocols require an intermittent type transmission format (packitized data). The laser transmitters are required to rapidly stabilize, transmit a high-speed burst of data, and then completely turn off without contributing any residual background light. The receivers are also required to adjust rapidly to packet burst transmissions that may represent a relatively high optical level from one node or a very low level signal coming from a transmitter at a distance with greater losses. To keep the overall system efficiency high this process must be done all within a period equivalent to a few bits of data once a data transmission is detected. Figure 2 shows the block diagram of a high-speed local-area network transmitter that features rapid stabilization of the laser diode and very-high-speed performance.

Figure 3 shows the performance achieved with a specially designed local-area network optical receiver for different levels of optical power. Figure 3a shows an optical "line" signal of several successive node transmissions of a short message type token signal. The level differences under these conditions was on the order of 5 to 7 dB. The photograph in Fig. 3b shows a more severe case with a 20-dB signal level difference. The low-level transmission is the third signal shown as a small base line disturbance. This burst-mode optical receiver design was able to reproduce the short token transmission without distortion.

Average-feedback type laser stabilization circuits as used in conventional point-to-point fiber-optic links are also not suitable for burst-mode applications because of the very short transmission times of the data. In a specially designed burst-mode transmitter developed by RCA Laboratories,

the operating points for the laser bias and modulation currents are stored as a digital word in programmable memory elements. The burst-mode transmitter utilizes the stored values of laser bias and modulation current without waiting for a feedback signal to stabilize the laser operating points. Periodically, the stored values are reestablished to compensate for gradual changes in the laser characteristics. Stabilization of the laser operating temperature is provided continuously by a temperature controller utilizing a Peltier (thermoelectric) module within the laser package. The high-speed modulator and bias switch circuits utilize microwave transistors in an emitter-coupled configuration to supply subnanosecond current switching speeds.

RCA local-area network development

Since 1982 and under a continuing program with RCA Laboratories and CISD, fiber-optic approaches to local-area networks have been investigated and a high-performance network technology developed. The particular network requirements investigated were for a system to be used for the interconnect of multiple bulk storage devices with potentially hundreds of uses. Users and host computers could be separated by several kilometers between operating nodes or stations.

In 1984, a four-node, high-speed network was assembled based on the results of a system study phase.¹⁴ The study provided information on the physical structures, protocols, optoelectronic components, line coding methods, and the clock recovery and timing requirements. The Optical Data Transmission (ODT) Testbed consists of a source Bus Interface Unit (BIU) and three terminal BIUs on an optical star-coupled bus. Figure 4 is a block diagram of the Optical Data Transmission Testbed.

This system is capable of demonstrating the request for and transmission of data messages (graphics information) stored on a magnetic disc at the source node. The magnetic disc unit simulates an optical disc or similar bulk storage device. Messages are requested from and displayed on color graphic terminals connected to each of the two terminal node BIUs or by using multiple RS-232-type text terminals on the third node. The complete 200-Mbit-per-second, four-node network is shown in the photograph in Fig. 5. The storage disc unit is in the right corner of the photograph with the four BIUs (including the optoelectronic transmitters and receivers) and graphic terminals. Table II

summarizes the testbed characteristics as presently employed in the network testbed.

A version of the token-bus protocol is implemented in the network. The permission to transmit in the local-area network testbed is in the form of a token packet that is directed around the network in a predetermined logical ring fashion. Figure 6 shows the form in which data is transmitted within the network. The traces were made utilizing a digitizing storage oscilloscope. Shown in Fig. 6a is the Manchester encoded data packet. The minimum pulse width is 2.5 nanoseconds. In Fig. 6b an optical "line" signal shows several token transmissions from three nodes at different optical levels prior to being processed by an optical receiver. The difference in optical level is on the order of seven decibels. Figure 6c shows a data packet transmission of 16 thousand bits of data within a continuous field of smaller token packet transmissions.

Table III describes the performance characteristics of the 200 Mbit/second Manchester data (400 Mbits/second NRZ) optical transmitters and receivers. An optical sensitivity of -38 dBm for a bit error rate (BER) of 10^{-9} , at a data rate of 150 Mbit/second RZ pseudorandom data was achieved. An intermessage dynamic range of greater than 20 dB was demonstrated on the 200-Mbit/second test bed. The optical output of the transmitter is 0 dBm at a wavelength of 820 nanometers from the multimode laser device. The transmitters are fully ECL logic compatible.

Higher-data-rate LAN development

As part of RCA's continuing program in high-speed local-area networks the fiber-optic testbed is being reworked to allow operation at 500 Mbits/second. Optoelectronic modules were constructed that will allow a burst-mode Manchester coded transmission rate of 500 Mbits/second (1000 Mbits/second NRZ data).¹⁵ Recently developed GaAs digital logic is used to process and buffer this very-high-data-rate signal in the optical transmitters and receivers and the encoder and decoder modules.¹⁶ A special RCA high-speed laser package was developed with the help of the New Products Division, which manufactures RCA's laser sources and optical detectors for commercial use.

A complete 500-Mbits/second optical transmitter is shown in Fig. 7. Silicon microwave transistors in an emitter-coupled configuration are used to develop the very

Table II. Testbed characteristics

Data rate	200 Mb/s
Architecture	Optical star bus
Access protocol	Token bus
Optoelectronic transceivers	
Type	Bus compatible/burst mode
Device	Laser/APD
Coding	Manchester
Clock extraction circuit	400-MHz resonator
Fabrication technique	Multilayer/microstrip PCB
Node control processor	M68000 μ P
Message scheduling and packetization	AM29116 ECL μ CTRLR

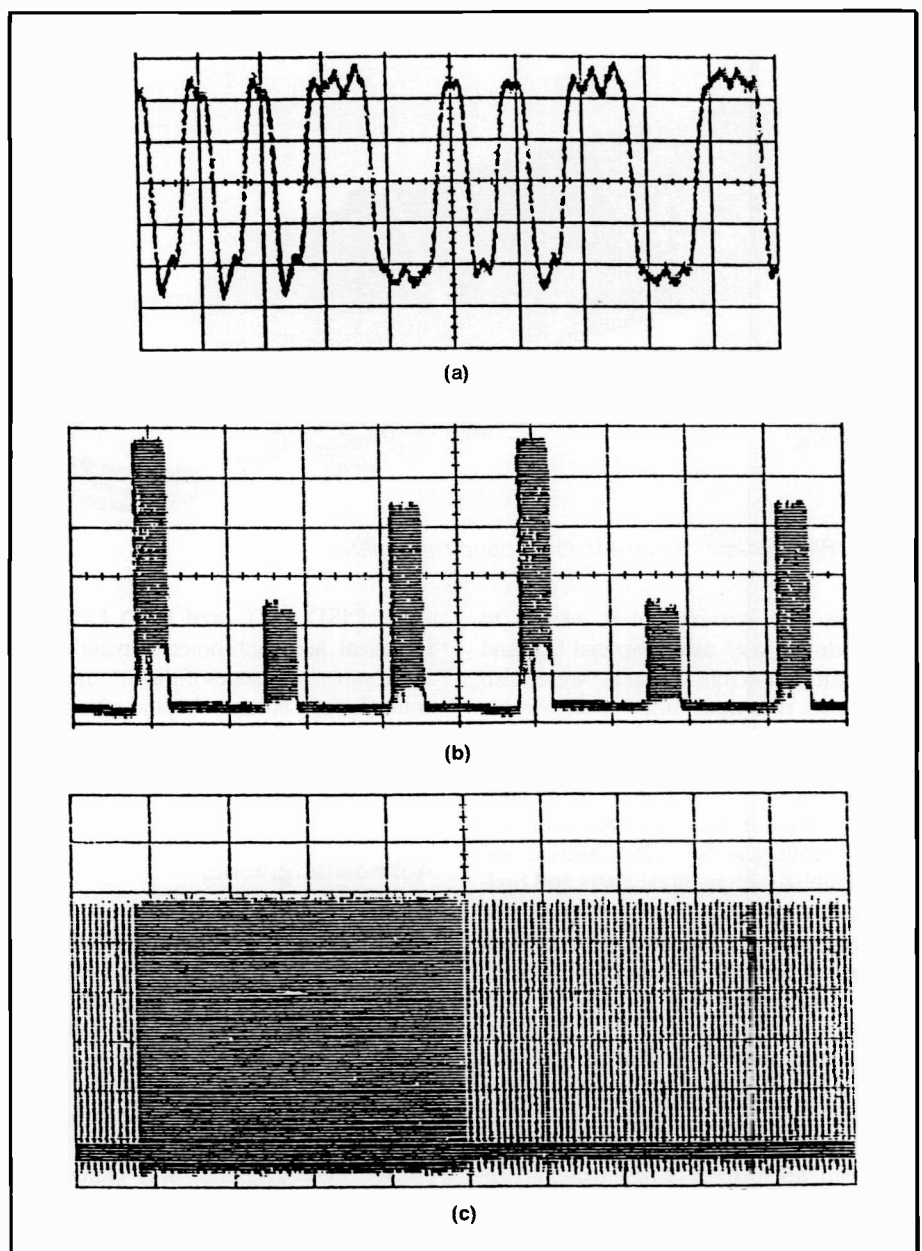


Fig. 6. Token and data transmissions at 200 Mbits/second.

Table III. Transmitter and receiver characteristics (200 Mbit/s)

Receiver	
Sensitivity	-38 dBm @ 150 Mbit/s RZ for BER 10^{-9}
Dynamic range	
Conventional	20 dB
Inter-message	20 dB
3 dB bandwidth	>500 MHz
Data output	Complementary ECL logic
Transmitter	
Output power	0 dBm
Extinction ratio	10:1 (0.2 to 20 mW)
Rise and fall times	<1.0 nanosecond
Data input	ECL logic

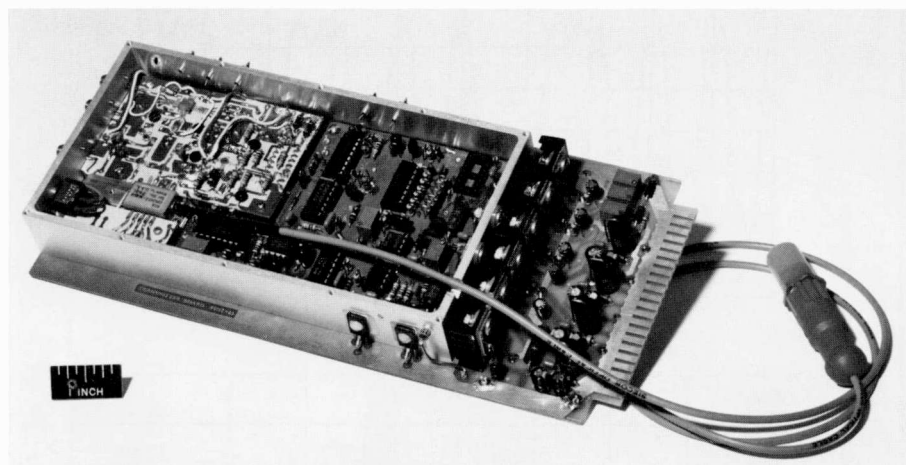


Fig. 7. Photograph of 500-Mbits/second transmitter.

fast rise time current pulses needed to modulate the laser diode. Special bias and modulation current circuits were also needed in this transmitter to allow the laser to stabilize, transmit a very-high-speed data packet, and then completely shut down until the next transmission time.

In 1986 a three-node demonstration network operating at 500 Mbits/second will be assembled. Single-mode lasers and optical devices will allow high-data-rate transmissions over several kilometers distance for the test network. Additionally, the network bus interface units will also be redesigned with GaAs integrated circuits to permit data and token packet exchange and full network operation at 500 Mbits/second.

This continuing program represents the successful application of new technologies from four operating units of RCA: Labora-

tories, CISD, ATL, and NPD Lancaster. Technical accomplishments included the development of state-of-the-art optoelectronic devices, advanced optoelectronic circuit designs, and GaAs circuit designs using both discrete and LSI devices.

Acknowledgments

We would like to acknowledge the contributions to the high-speed local-area network programs at both RCA Laboratories and CISD by Steve Siegel, Jeff Viola, Jim Baroni and Don Channin. Contributions to the high-speed packaging of the RCA laser used in the 500 Mbits/second network were made by Ted Jones, NPD Lancaster. A prototype GaAs LSI Manchester word generator was made available by R.H. Schellack and W.F. Heagerty

from ATL for initial data testing at 500 Mbits/second.

References

1. S.D. Personick, "Telecommunication Network Trends for Optical Fiber Technology," *Laser Focus/Electro-Optics*, Vol. 20, No. 9, September 1984, p. 104.
2. B. Mullinax, "Fiber Optics In The Subscriber Loop," *Photonics Spectra*, Vol. 20, No. 1, January 1986, pp. 49-56.
3. P. Fraser, "One More Look At Fiber," *Telephone Engineer & Management*, Vol. 90, No. 4, February 15, 1986, pp. 65-70.
4. R. Goodfellow et al., "Practical Demonstration of 1.3 Gb/s over 107 km of Dispersion Shifted Fiber Using a 1.55 micrometer Multimode Laser," Post-deadline Papers, Conference on Optical Fiber Communications (Optical Society of America, Washington, D.C., 1985), paper PD5.
5. S.D. Personick, "Minitutorial: Distribution and Local Networks," Conference on Optical Fiber Communications (Optical Society of America, Washington, D.C., 1984), paper WC1.
6. S. Joshi and V. Iyer, "New Standards for Local Networks Push Upper Limits for Lightwave Data," *Data Communications*, July 1984, pp. 127-138.
7. J.B. Sergi and J.P. Viola, "Very High Speed Fiber Optic Data Distribution Network," IEEE Military Communications Conference, Washington, D.C., October 1983.
8. D.J. Channin and D.R. Patterson, "Fiber-Optics for Broadband Local Area Networks," Conference on Optical Fiber Communications (Optical Society of America, Washington, D.C., 1986), paper MD1.
9. C.A. Villarruel et al., "Single Mode Data Buses for Local Area Network Applications," *IEEE Journal of Lightwave Technology*, Vol. LT-3, No. 3, June 1985, pp. 472-478.
10. S.Moustakas et al., "Passive Optical Star Bus with Collision Detection for CSMA/CD-Based Local-Area Networks," *IEEE Journal of Lightwave Technology*, Vol. LT-3, No. 1, February 1985.
11. W. Bux, "Local-Area Subnetworks: A Performance Comparison," *IEEE Transactions on Communications*, Vol. COM-29, No. 10, October 1981.
12. N.L. Rhodes, "Interaction of Network Design and Fiber Optic Component Design in Local Area Networks," *IEEE Journal on Selected Areas in Communications*, Vol. SAC-1, No. 3, April 1983.
13. D.R. Porter et al., "A High Speed Fiber Optic Data Bus for Local Area Communications," *IEEE Journal on Selected Areas in Communications*, Vol. SAC-1, No. 3, April 1983.
14. D.J. Channin et al., "Fiber Optic 200-Mbit Local Area Network," Conference on Optical Fiber Communications (Optical Society of America, Washington, D.C., 1984), paper WC2.
15. D.R. Patterson et al., "Fiber-Optic Modules for 500-Mbit/s Local Area Network Applications," Conference on Optical Fiber Communications (Optical Society of America, Washington, D.C., 1986), paper MD4.
16. J.Barresa et al., "Digital GaAs ICs Hit Gigahertz Speed Mark," *Microwaves and RF*, February 1984.



Authors Patterson, left and Sergi.

David R. Patterson graduated with honors from Drexel University, earning a BS degree in Electrical Engineering. He did additional graduate work at the Moore School of Electrical Engineering at the University of Pennsylvania.

Mr. Patterson first worked at RCA Laboratories in 1962. From 1962 to 1978 he participated in research and development programs in the areas of infrared television systems, power semiconductors, solar cells, light-emitting diodes, semiconductor lasers, and fiber-optic systems.

From 1978 to 1982, Mr. Patterson was Manager of Systems Development and Engineering at Exxon Enterprises' Optical Information Systems. There he managed the development of a product line of fiber-optic subsystems and laser subassemblies for commercial fiber-optic systems.

In 1983, Mr. Patterson returned to RCA Laboratories as a Member of the Technical Staff. As a member of the Optoelectronic Systems Research group, he is the Principal Investigator in an IR&D program to develop fiber-optic components for high-speed local-area network systems.

Mr. Patterson has written several papers on laser stabilization and on fiber-optic components and systems, and has been awarded two U.S. patents in these areas.

He is a member of the IEEE and Eta Kappa Nu.

Contact him at:
RCA Laboratories
Princeton, N.J.
Tacnet: 226-2156

Joseph Sergi is a Senior Member of the Engineering Staff at Communication and Information Systems Division. A member of the Digital Communications Equipment Engineering group since 1977, he has been involved primarily in research and development of state-of-the-art communication networks.

His most recent assignment has been as principal investigator on an internal research and development project that produced an operational 100 Mbit/s fiber-optic local-area-network testbed in 1982. Continuing in his lead role in hardware, software, and system design, he has since been working to upgrade the testbed to higher speed and greater capabilities. Having recently completed development of a fully capable 200 Mbit/s testbed, he is currently working on applying fiber-optic networks to the NASA Space Station application.

He is a member of the IEEE and has recently presented and coauthored a paper at the IEEE Military Communications Conference and coauthored a paper at the Optical Fiber Communications Conference.

He has a patent for a switched bias scheme for high speed laser transmitters.

Mr. Sergi received his BS degree in Electrical Engineering in 1977 from Lehigh University and his MS degree in Computer and Information Sciences in 1981 from the University of Pennsylvania.

Contact him at:
Communication and Information Systems
Division
Camden, N.J.
Tacnet: 222-2347

Lightweight target designator

Engineers at Automated Systems Division have designed a laser target designator with a conduction-cooled laser cavity, which reduces the weight and bulk and simplifies maintenance.

There is an increasingly large number of commercial and military applications for lasers—from supermarket scanners to the Strategic Defense Initiative. The military's primary interest is in target designators and rangefinders, with the major emphasis on small, lightweight systems. Rangefinders currently being produced, such as RCA's Mini Laser Rangefinder (2.5 lb), have already reached that goal, but most target designators are still large, heavy, expensive, and difficult to maintain.

Laser target designators now used by the military include the TADS/PNVS (Target Acquisition Designation System/Pilot Night Vision System), the MULE (Modular Universal Laser Equipment) and the G/VLLD (Ground/Vehicular Laser Location Designator). The TADS/PNVS is gimbal-mounted in a helicopter, and the MULE and G/VLLD are forward-observer-type systems.

The laser target designator (LTD) con-

cept is straightforward: a high-brightness, 1.06-micron laser, operating at a pulse-coded 10-Hz to 20-Hz rate, projects a spot onto a target such as a tank. This allows "smart" weapons such as laser homing missiles and projectiles with infrared detectors to follow the reflected beam to the target (see Figs. 1 and 2).

These military high power dissipation systems are liquid-cooled, which makes them heavy, bulky, costly, and difficult to

maintain. Size and weight are of top priority, as the forward observer is already carrying about 75 lb of survival gear.

LTD design

In response to this problem, RCA has developed a conduction-cooled laser cavity that eliminates the need for a liquid-cooled loop and is more efficient than most liquid-cooled laser cavities. This laser

Abstract: *Current military high power dissipation systems for target designation are liquid-cooled, which makes them heavy, bulky, costly, and difficult to maintain. In response to these problems, RCA has developed a conduction-cooled laser cavity that eliminates the need for a liquid-cooled loop and is more efficient than most liquid-cooled laser cavities. These two factors have resulted in a small, lightweight designator design with no cooling liquid, no pump or tubing, a smaller laser power supply, and smaller batteries.*

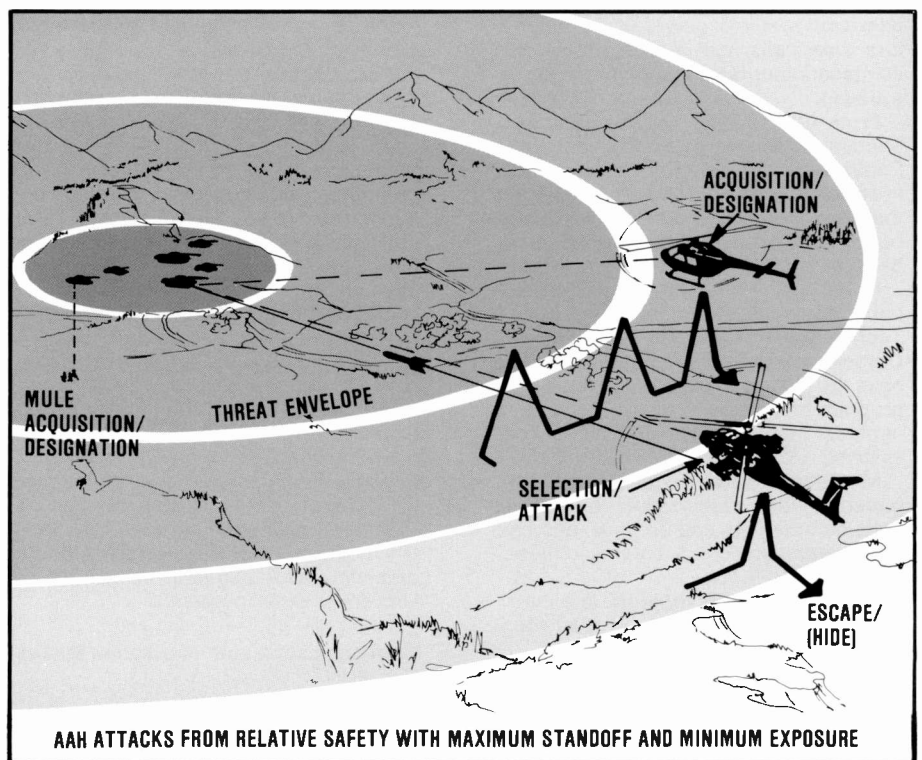


Fig. 1. *Illuminating the enemy target for the attack helicopter: left, by the forward observer using a MULE designator, and right, by a TADS/PNVS laser designator gimbal-mounted in the search helicopter.*

©1986 RCA Corporation.
Final manuscript received April 14, 1986
Reprint RE-31-3-7

cavity has small air gaps (0.001 in.) between the rod and the pump reflector, and between the flash lamp and the pump reflector, to enhance gaseous conduction cooling (Fig. 3).

A sapphire separator with a small air gap to the laser rod is interposed between the flash lamp and rod and clamped to the reflector halves for good heat transfer. Also, a thin piece of samarium-doped glass is placed between the lamp and sapphire separator to absorb 1.064-micron energy radiated off-axially by the laser rod. This reduces depletion of stored energy resulting from off-axis "super radiance." Super radiance occurs when the gain in the laser rod becomes sufficiently high that 1.064-micron radiation emanating from the flash lamp or reflected back from the pump cavity walls depletes the stored energy faster than the flash lamp is putting it in; i.e., for increased pump energy, stored energy does not increase and may even decrease. The reflecting surface is a highly polished nickel base coated with vacuum deposited silver, then overcoated with sapphire. This coating has been life-tested in the laboratory for 2×10^7 shots at 10 Hz with no measurable loss in performance. By minimizing the air gap in the cavity for enhanced heat transfer, the optical efficiency was increased, thereby reducing the heat input. Also, the sapphire separator provides a close optical coupling by producing an equivalent air space between the lamp and rod of thickness $t' = t/N$, where N for sapphire ≈ 1.8 . It also prevents the hot air at the lamp from entering the cooler air around the rod.

The flash lamp, which pumps the laser rod, is held by alumina blocks that combine good electrical insulation with reasonable thermal conductivity. Figures 4

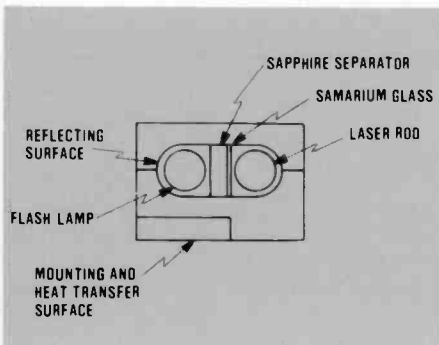


Fig. 3. Cross section of conduction-cooled cavity showing critical placement of laser rod and lamp to the metal reflecting surface. The 0.001 inch gap provides a good heat transfer path to the aluminum housing.

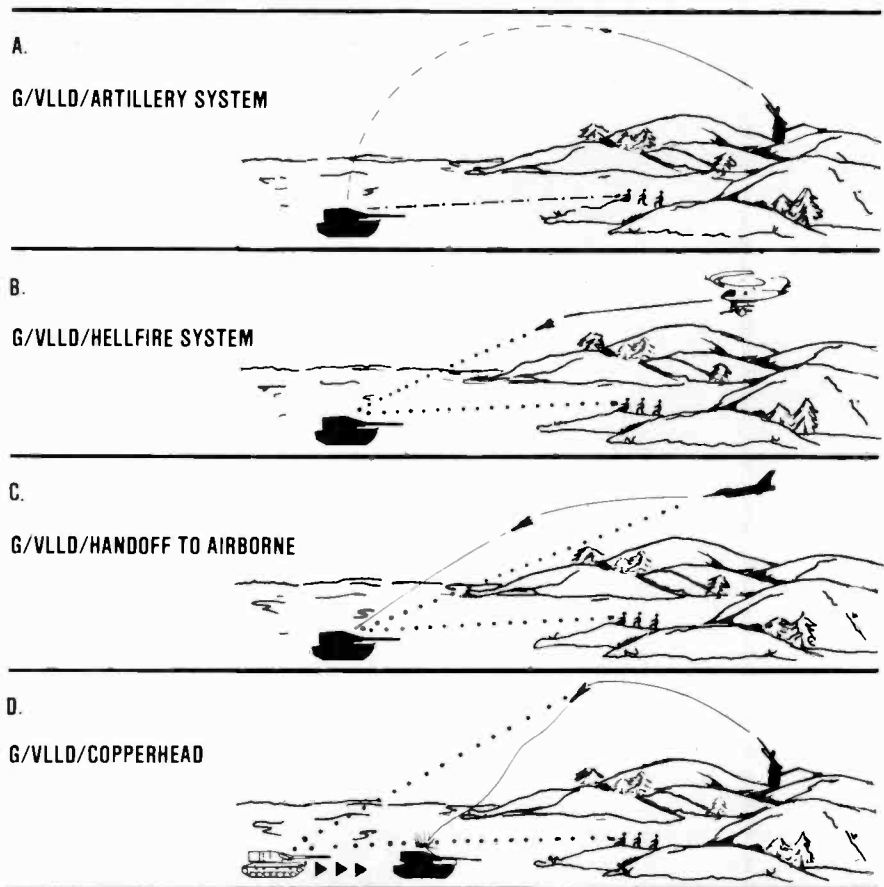


Fig. 2. Forward observer actions using the G/VLLD system: a) ranging to the enemy target and relaying distance information to artillery; b) illuminating the enemy target for helicopter-fired, laser-homing missiles; c) illuminating the enemy target with coded signals for handoff to laser sensor equipped aircraft; and d) maintaining illumination on a moving target for laser-homing, cannon-launched guided missiles.

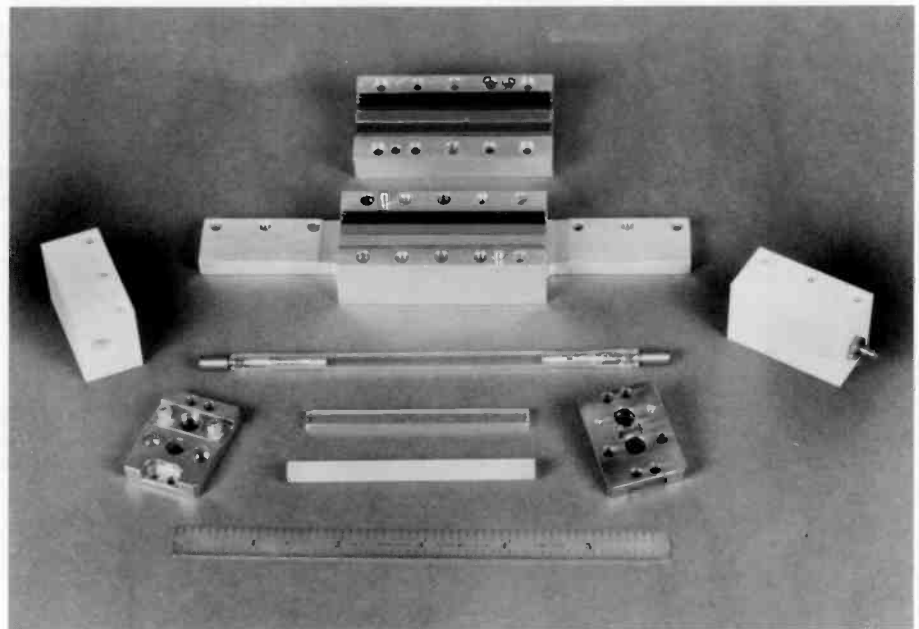


Fig. 4. Conduction-cooled cavity disassembled, showing all components: pump cavity top and bottom, BeO end caps, flash lamp, end plates (to hold laser rod and flash lamp), sapphire separator, and laser rod.

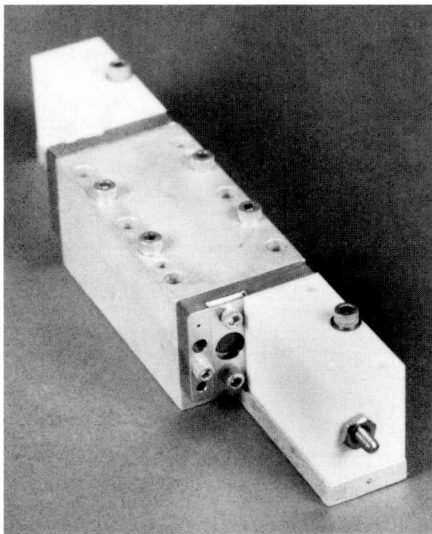


Fig. 5. RCA conduction-cooled laser pump cavity shown fully assembled.

and 5 show the cavity disassembled and assembled.

This cavity design now makes it possible to design an LTD that is smaller and lighter than its liquid-cooled counterpart, because it eliminates the requirements for liquid coolant, tubing, connectors, and pump. Also, because of this cavity's higher efficiency, the LTD has a smaller laser power supply, less heat exchange area, and a smaller battery pack.

Laser transmitter operation

The LTD laser transmitter consists of the optically pumped, neodymium-doped Yttrium Aluminum Garnet (YAG) laser with optical and electronic parts configured to form a resonant interferometer with its output coupled to the propagating medium through the transmitter collimating telescope. Figure 6 is an optical block diagram of the transmitter resonator and telescope.

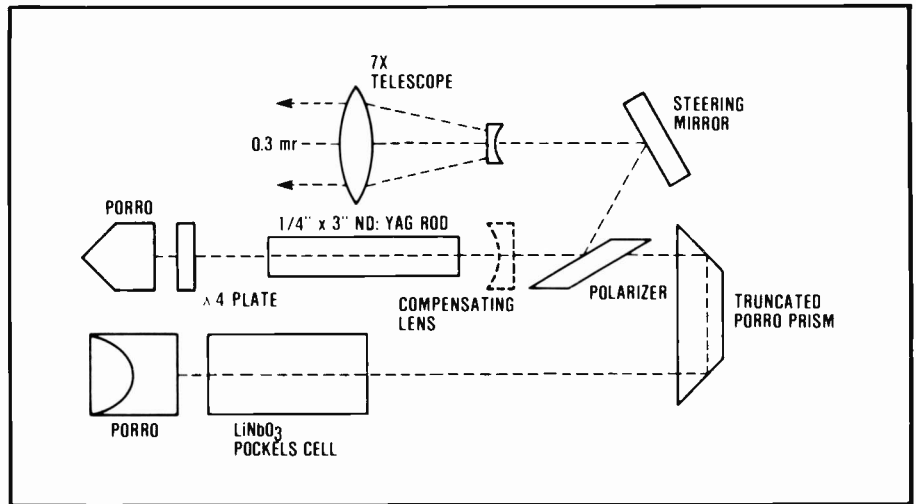


Fig. 6. Optical block diagram showing arrangement of all optical parts in a folded TVR resonator. NOTE: The compensating lens shown is used only if needed to achieve 0.3 mr beam divergence.

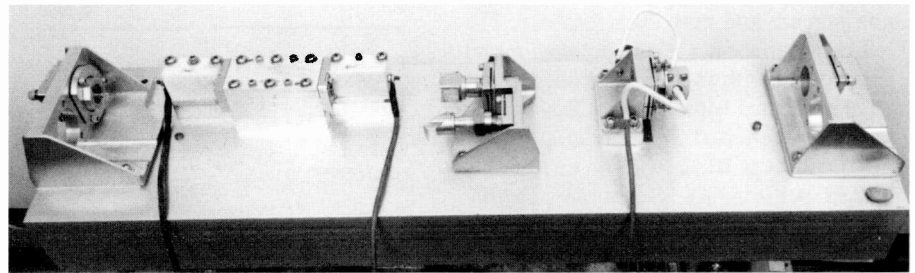


Fig. 7. TVR resonator test bed with porro prisms and RCA-developed, conduction-cooled laser pump cavity. All results obtained were performed on this lab test bed.

The gain medium is a 3-in. long by 1/4-in. diameter rod fabricated from a grown, single-crystal YAG boule doped with 1 to 1.3 atomic percent neodymium. When the laser rod is optically pumped by subjection to light principally in the spectral region of 0.6 to 0.9 microns, it stores energy in a high-energy-level band and gives up this energy as light emission at

1.064 microns by spontaneous radiative decay to a lower energy level with a decay time constant (fluorescent lifetime) of about 230 μ s. If stimulated by external feedback of its own emission, it can exhibit gain and give up its stored energy in a single, high-energy pulse of electromagnetic energy at 1.064 microns. If one of the optical devices used to provide the feed-

```

*****      ROUND TRIP NO. = 33          TIME =147.502(NSEC)          NO. CF RAYS= 1296

      ** ENERGY **
TOTAL ENERGY      0.9052E-01 JOULES
AVERAGE ENERGY DENSITY  0.4977E-02 JOULES/CMSQ
PEAK ENERGY DENSITY    0.1075E-01 JOULES/CMSQ
PEAK/AVERAGE DENSITY    2.160

      ** POWER **
TOTAL POWER        0.2387E+05 WATTS
AVERAGE POWER DENSITY  0.1313E+04 WATTS/CMSQ
PEAK POWER DENSITY    0.7664E+04 WATTS/CMSQ
PEAK/AVERAGE DENSITY    5.838

      ** DIVERGENCE ANGLE (MILLIRADIANS)**
AVERAGE X          -0.0146          AVERAGE Y          -0.0012
RMS                 0.1799          +DIFFRACTION       0.1878
90 PERCENT          0.2433          +DIFFRACTION       0.2496
  
```

Fig. 8. Computer run with same inputs as in lab test bed computes expected output of: total energy=90 millijoules; total power=2.38 megawatts; peak energy density=0.01 joules/cm²; peak power density=7.6 kilowatts/cm².

back is a partially reflective or selectively transmissive device, it can feed back an appropriate percentage of the stored energy to produce the desired oscillation and couple the balance of the radiation out of the laser into the radiating telescope.

Optical pumping of the laser rod, and switching from no feedback to high feedback (Q-switching) in the laser resonator, are synchronized by suitably timed electronic signals. This results in emission of laser pulses at a controlled repetition rate with a controlled interpulse period. The operation of the laser in general terms is as follows.

The laser rod, with polished end faces, is mounted in a resonator which has retro-reflectors on an optical axis through the rod axis and parallel to the rod faces. This forms the laser feedback mechanism, in that energy emanating axially from either rod face can be totally reflected back through the rod. Also, mounted between one rod end and one reflector are a polarizer and an electro-optic polarization rotator (Pockels cell Q-switch). Between the other rod face and other reflector is a quarter-wave ($\lambda/4$) plate, a device that can convert linearly polarized light into elliptically polarized light.

The laser rod is mounted in an optical pump cavity with a linear flashlamp parallel to the rod and close to it but separated by a double window of sapphire and samarium glass. Flashlamp and rod are contained in a silvered cylindrical reflector that reflects flashlamp light into the laser rod through the sapphire and samarium windows. The flashlamp is connected to pulse forming network (PFN) capacitors through a trigger transformer which is used to ionize the lamp, thus discharging the PFN capacitors and injecting optical energy into the laser rod. The principal energy in this optical pulse lasts about 150 μ s, less than the fluorescent lifetime of the laser rod. The flashlamp trigger is timed by the code generator, as is the power supply that charges the PFN capacitors.

The electro-optic Q-switch (a Pockels cell using a LiNO_3 crystal) in the laser resonator is normally biased so that the plane of polarization of energy passing into it, through the reflector and back out of the Q-switch, is rotated by 90 degrees (from the x to the y plane). Under this condition, energy of the proper polarization to pass through the polarizer (x plane) is rotated 90 degrees to the y plane and will not pass back through the polarizer. Thus, there is no feedback in the laser resonator,

FAR FIELD ENERGY	NEAR FIELD ENERGY	NEAR FIELD POWER
SCALE= 0.660 MRAD	SCALE= 4.812 CM	SCALE= 4.812 CM
00000000000000000000	00000000000000000000	00000000000000000000
00000000000000000000	00000000001000000000	00000000001000000000
00000000000000000000	0000000002121414000000	0000000001121424000000
00000000000000000000	0000010212012010000000	0000000202012010000000
00000000000000000000	0003103214090201100000	0003003104380101100000
00000000000000000000	0000322211000120000000	0000211100000000000000
0000000157533000000000	00101133544512134510	00001032523501024510
0000002475332200000000	0001327294229102220000	00001271940170020100
0000002467677310000000	0004044311144620120000	00030243100344101100
0000004489556610000000	0009234132213213200000	0009124022101213000000
0000013759934300000000	00013422384122303010	0000241022731113010000
0000001346982300000000	0002112146356362622000	00020010342352416210
0000000155423100000000	0003155231227321210000	00030551300042202100
0000000000000000000000	0121220433224411030000	01201104231133000300
0000000000000000000000	0001312031061321110000	0000211201006121100000
0000000000000000000000	0000000120110411000000	0000000100100311000000
0000000000000000000000	0001031130340620000000	0001020030140510000000
0000000000000000000000	0000000010010000000000	0000000000000000000000
0000000000000000000000	0000000000300000000000	0000000000300000000000
0000000000000000000000	0000000000000000000000	0000000000000000000000
FAR FIELD ENERGY	NEAR FIELD ENERGY	NEAR FIELD POWER

Fig. 9. Computer printout showing: a) laser energy distribution and beam size in the far field (on target); b) laser energy distribution and beam size in the near field (at exit aperture of 7X telescope); and c) near field power distribution.

TIME (NS)	POWER	ENERGY (J.)	DIVERG.+DIFF. (MR)
0.00000E+00	0.22846E-03	0.10212E-11	0.61105E+00
0.40000E+01	0.51996E-03	0.33453E-11	0.59893E+00
0.80000E+01	0.92099E-03	0.74618E-11	0.54431E+00
0.13000E+02	0.18313E-02	0.15647E-10	0.47354E+00
0.17000E+02	0.47718E-02	0.36976E-10	0.34629E+00
0.22000E+02	0.14470E-01	0.10165E-09	0.28682E+00
0.26000E+02	0.46282E-01	0.30852E-09	0.26328E+00
0.31000E+02	0.15226E+00	0.96908E-09	0.26641E+00
0.35000E+02	0.50673E+00	0.32540E-08	0.26115E+00
0.40000E+02	0.16925E+01	0.10821E-07	0.25572E+00
0.44000E+02	0.57678E+01	0.36601E-07	0.25209E+00
0.49000E+02	0.19458E+02	0.12357E-06	0.24982E+00
0.53000E+02	0.65276E+02	0.41534E-06	0.25157E+00
0.58000E+02	0.22063E+03	0.14015E-05	0.25819E+00
0.62000E+02	0.74564E+03	0.47343E-05	0.26671E+00
0.67000E+02	0.25139E+04	0.15971E-04	0.25494E+00
0.71000E+02	0.84765E+04	0.53859E-04	0.25001E+00
0.75000E+02	0.28326E+05	0.18047E-03	0.24855E+00
0.80000E+02	0.93693E+05	0.59925E-03	0.24627E+00
0.84000E+02	0.30086E+06	0.19440E-02	0.25044E+00
0.89000E+02	0.90551E+06	0.59914E-02	0.25507E+00
0.93000E+02	0.21779E+07	0.15726E-01	0.25236E+00
0.98000E+02	0.37105E+07	0.32311E-01	0.24366E+00
0.10200E+03	0.42016E+07	0.51091E-01	0.24333E+00
0.10700E+03	0.34818E+07	0.66654E-01	0.24570E+00
0.11100E+03	0.22823E+07	0.76856E-01	0.24718E+00
0.11600E+03	0.13292E+07	0.82797E-01	0.24813E+00
0.12000E+03	0.77304E+06	0.86252E-01	0.24898E+00
0.12500E+03	0.41744E+06	0.88118E-01	0.24927E+00
0.12900E+03	0.24228E+06	0.89201E-01	0.24937E+00
0.13400E+03	0.14409E+06	0.89845E-01	0.24947E+00
0.13800E+03	0.81044E+05	0.90207E-01	0.24952E+00
0.14300E+03	0.45324E+05	0.90410E-01	0.24959E+00
0.14700E+03	0.23874E+05	0.90517E-01	0.24963E+00

Fig. 10. Computer printout of power (watts), energy (joules), and beam divergence (milliradians) as a function of time.

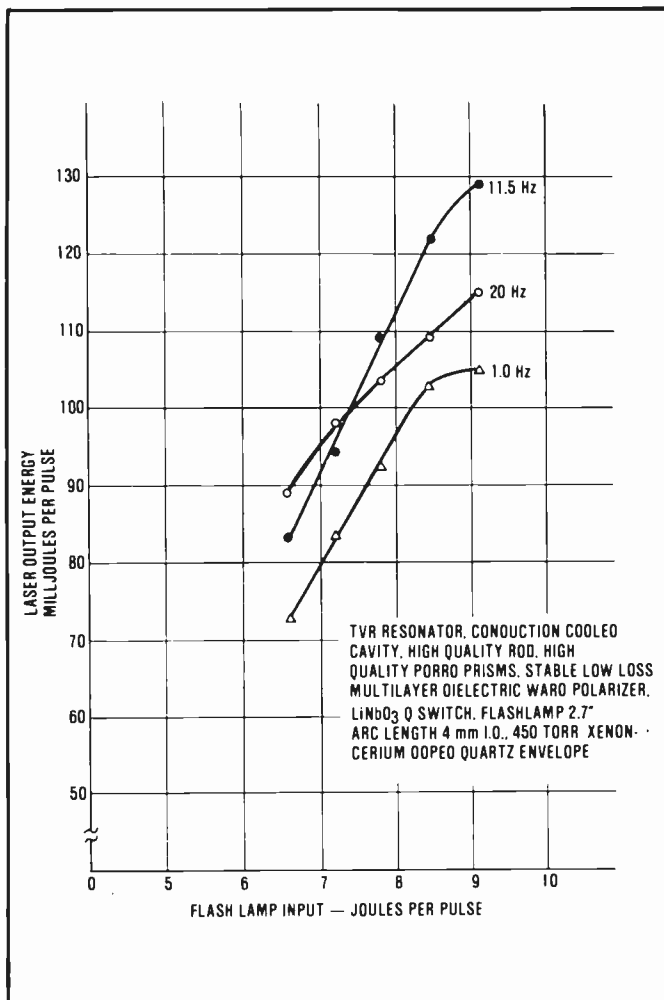


Fig. 11. Laser output energy vs. input energy plotted for 1.0, 11.5, and 20 Hz, obtained with a lab test bed.

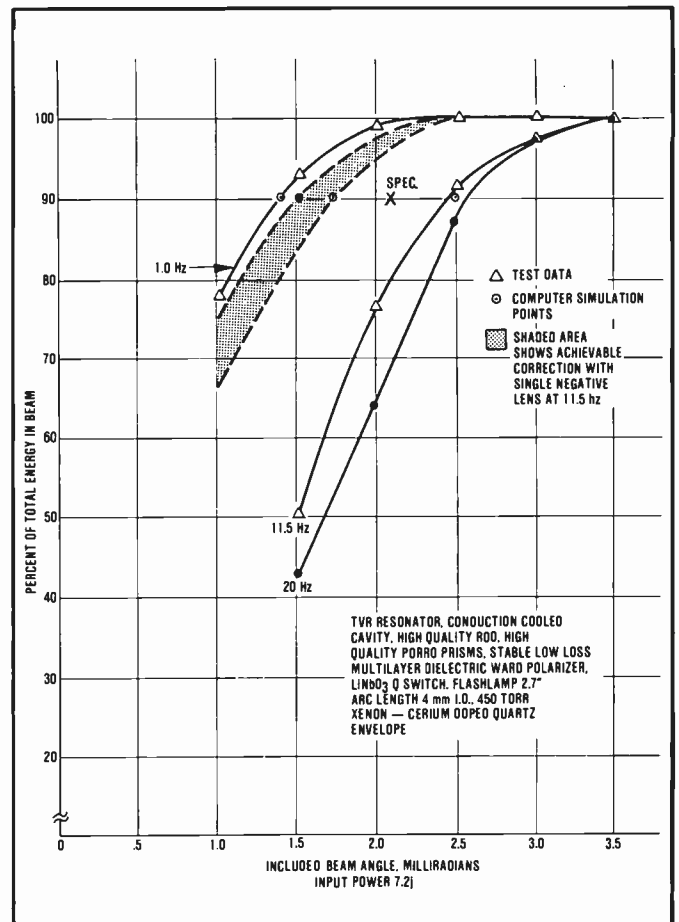


Fig. 12. Raw (uncorrected by 7X telescope) beam divergence data from lab test bed and computer simulation plotted, with shaded area showing achievable results when a single negative lens is introduced into the resonator for beam correction.

no stimulated emission, and no output. When the Q-switch is pulsed (about 140 μ s after the flashlamp trigger), its bias is changed and it does not rotate polarized light passed by the polarizer. The laser oscillation thus builds up rapidly, discharging the stored energy as a high-intensity pulse at 1.064 microns.

The quarter-wave plate is adjusted so that the linearly polarized light entering it (x plane) leaves elliptically polarized, that is, with both x and y plane components. The x plane component stays in the resonator to maintain the laser emission until the stored energy is depleted. The y polarization component is reflected out of the resonator by the polarizer and into the transmitter telescope, where it is then radiated to the sighted target. The telescope reduces the laser raw beam divergence by its magnification (7X).

Note that in the RCA LTD the retro-reflectors in the resonator are Porro prisms with their vertex planes crossed, thus form-

ing an alignment-insensitive resonator. This resonator is a time varying reflectivity (TVR) type and is a means for generating extremely short Q-switched laser pulses. The TVR technique involves Q-switching the laser with 100-percent mirrors on both ends of the cavity and then, at the peak of circulating power, rapidly switching the output mirror from 100 percent to an optimized reflectivity by changing the voltage on the Pockels cell. This leads to a rapid dumping of the optical energy from within the cavity.

Laboratory tests

A TVR resonator as described was assembled, aligned, and tested from parts that were available in the lab (Fig. 7). A second resonator was built and tested from parts that were purchased to very tight specifications to ensure that the resonator performance was not being compromised because of poor optical quality. The goal was to

achieve or exceed the following parameters:

- Energy output—80 millijoules or greater
- Beam divergence—90 percent of E_0 within 0.3 mr. dia. beam
- Pulse width— 20 ± 5 nanoseconds
- Input—8 joules nominal, 10 joules max.
- Pulse repetition frequency—8 to 11.5 pulses per second

First, the pulse forming network and Q-switch timing were optimized so that the maximum output in a single pulse could be obtained for a given input. Alignment of the resonator was done with a three-meter helium neon collimator system having a resolution of five arc-seconds. The initial test results fell significantly below our set goal. The output energy (E_0) reached only 75 millijoules with a ten-joule input, and because of the high input, the beam divergence was only 50 percent of the E_0 in the 0.3-mr beam. As a result of this poor performance it was then decided to rebuild the resonator with all

new parts of known optical quality. During the rebuild, a computer program for laser resonator design and diagnostics was obtained from Big Sky Laser Corporation. Their program, called *Lasercode*, calculates the output characteristics of complex, solid-state, Q-switched laser resonator configurations. The software is based on geometric optics using ray tracing methods. It propagates a large number of randomly chosen rays back and forth through a laser resonator whose sequence of optical elements is chosen by the user, and computes the output properties after each pass or round trip. Figures 8, 9, and 10 show typical printouts.

In order to minimize the number of hours needed in the lab to obtain data for various optical configurations and elements, the program was used to determine what parameters required manipulation in order to meet the set goals. First, all the optical properties of the elements were measured, including insertion loss, and entered into the program. The program was then run to see what the ideal resonator would yield. The new resonator was then assembled and aligned and data obtained. From the combined data we were able to determine which optical parameters were the most critical in obtaining the desired output parameters. A plot of the results is shown in Fig. 11.

The data shows that all output parameters were met except the divergence at 11.5 Hz. This was due to more thermal lensing in the laser rod than predicted. In order to meet the desired divergence, a single negative lens would have to be introduced into the resonator to compensate for this lensing. The shaded area in the plot (Fig. 12) shows achievable correction with this type of lens. The computer program also indicated that if a much higher quality laser rod could be used, correction might not be needed because the input to the system would be even lower, thereby reducing the thermal distortion and lensing. Such a rod was obtained (0.3-wave total distortion) and tested. Results for this rod are shown plotted at 11.5 Hz (Fig. 13).

From the test results it can be seen that all goals have been met. The goals versus the lab results are shown in Table I.

With all of the inputs and outputs defined, the designator package can now be designed. The block diagram in Fig. 14 shows the electrical design for the LTD with a ranging capability.

The ranging function was included in the design because the added components

Table I. Design goals and achievements

Goal	Lab test
$E_o \geq 80$ mj	$E_o = 90$ mj
Beam div. $\geq 90\%$ within 3 mr	Beam div. 96% within 0.3 mr
Pulse width 20 ± 5 ns	Pulse width 18 ns
Input 8 - 10 joules max	Input 6.6 joules

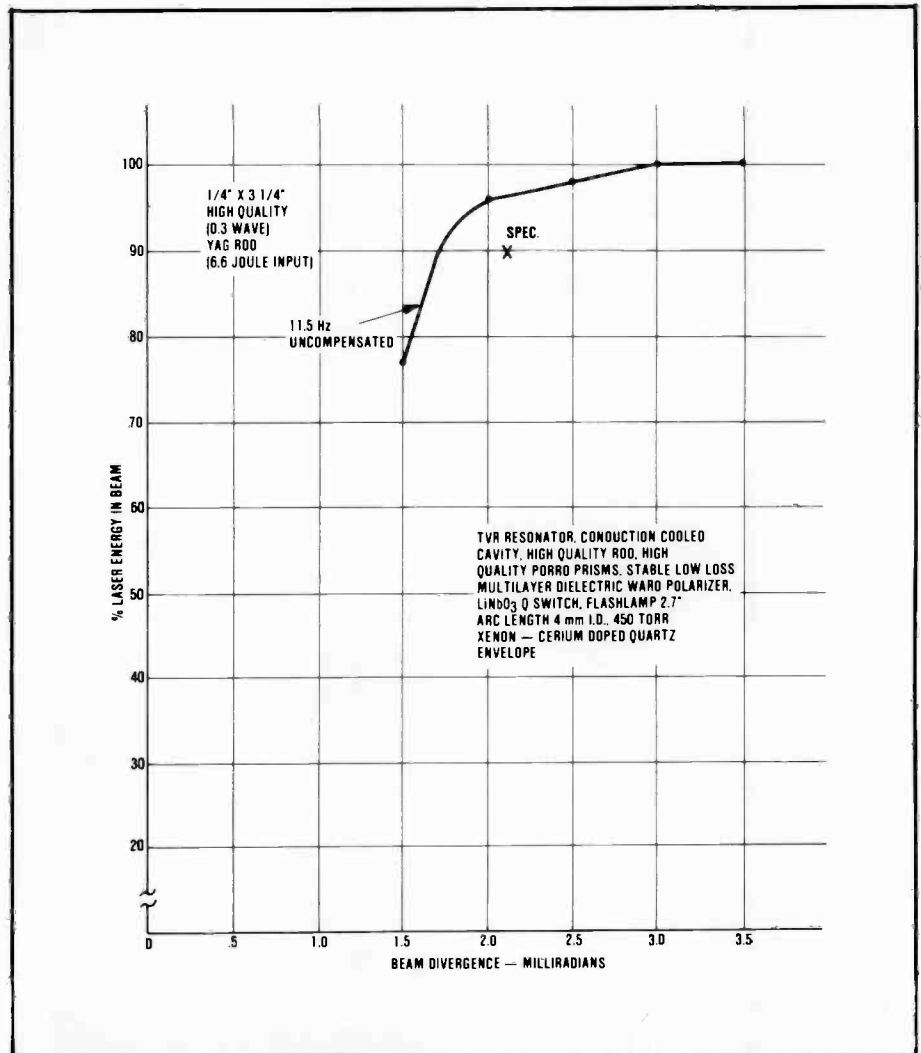


Fig. 13. Test data indicates that when a superior quality rod ($\lambda/4$ or less) is used, negative lens correction in the resonator is not needed.

(range counter, video amplifier, and detector preamplifier) are RCA-designed and developed hybrid circuits that add very little weight to the system. Figure 15 shows an artist's concept of the LTD that has an estimated weight of 11.5 lb, which is substantially less than the 21- to 52-lb liquid-cooled systems currently in use.

Conclusion

With the use of a specialized computer program and extensive laboratory tests, a very efficient conduction-cooled laser transmitter was designed, built and tested. Because of this high efficiency and non-liquid cooling, a target designator system

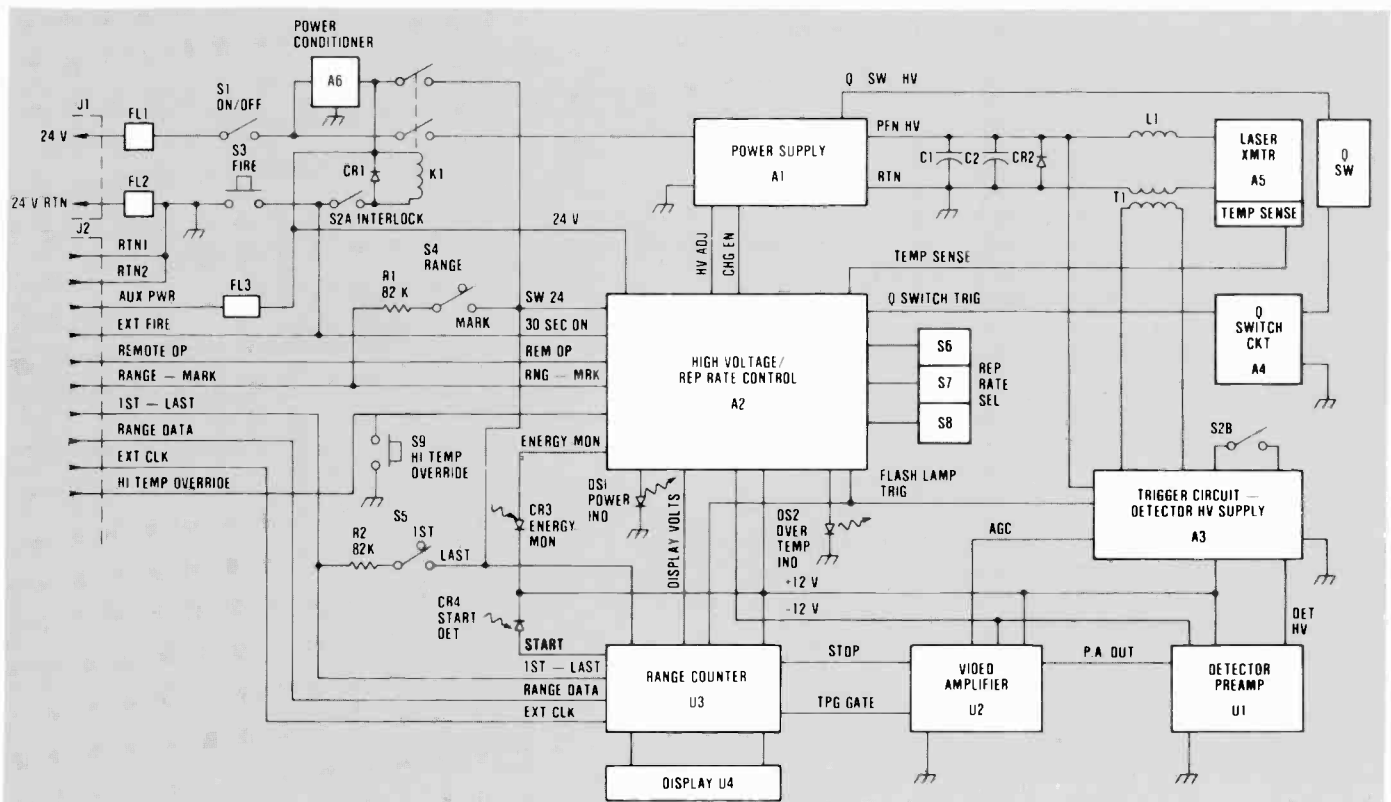


Fig. 14. Electrical block diagram for a lightweight laser designator with a range-finding function and remote operating capability.

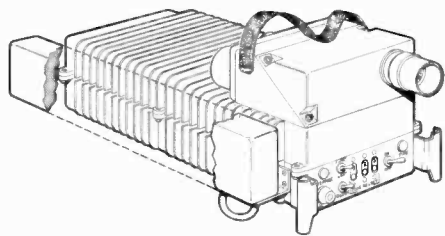


Fig. 15. Artist's concept of RCA lightweight target designator/rangefinder with carrying strap and external battery pack.

under 12 lb can be achieved. Currently there are no designator systems of this type in military inventory.

Acknowledgments

Without the contribution of the following people (Burlington's Laser Team) this work could not have been accomplished:

Norman L. Roberts and John R. Griesing, Electrical Design; Robert C. Guyer, Mechanical Optical; Bert Fitch, Design Drafting; and Robert F. Dearborn, Technician.

I would also like to thank John Carvalho, Computer Scientist, who debugged the *Lasercode* program and made it work.



Walter Radcliffe is a Senior Project Member of the Technical Staff in the C1 group at Automated Systems Division. Since joining RCA in 1965, he has been responsible for the design and development of laser systems on numerous programs including the Apollo Laser Altimeter, the Laser Range Pole, the AN/GVS-5 Laser Rangefinder, the Laser Target Designator and, most recently, the Mini Laser Rangefinder. He also coordinated the design and implementation of factory tooling for large-scale production of lasers on the AN/GVS-5 program.

Mr. Radcliffe received his BSEE from the University of New Hampshire in 1962 and did graduate work at the University of Maryland. He is a member of Sigma Xi, the Scientific Research Society.

Contact him at:
Automated Systems Division
Burlington, Mass.
Tacnet: 326-3639

CEE Video Courses on Integrated Optics

Integrated optics is a new approach to signal processing and transmission. Signals are carried by beams of light rather than by electrical current, and circuits are connected by optical waveguides instead of wires and cables.

The advantages of an integrated optic system are reduced weight, increased bandwidth or multiplexing capability, resistance to electromagnetic interference, and lower losses in signal transmission.

In support of this growing technology, Corporate Engineering Education offers two courses—*P18: Integrated Optics I*, and *P19: Integrated Optics II*—produced at the University of Delaware. There are 11 sessions to each course, and the text is *Integrated Optics: Theory and Technology*, Vol. 33, by R.G. Hunsperger (Springer-Verlag, Publishers). This is a 350-page illustrated study guide with problems and references for further reading.

The video instructor for these courses is Dr. Robert G. Hunsperger, a Professor of Electrical Engineering at the University of Delaware. He spent ten years in semiconductor microwave and optical device research as a member of the technical staff of Hughes Research Laboratories in Malibu, California. He has taught at the University of Southern California and at UCLA, and served as a consultant in the fields of semiconductor and optical devices and systems.

Organizations that have called upon Dr. Hunsperger's expertise include Hughes Aircraft Company, Martin Marietta Laboratories, E.I. DuPont Company, ISC Defense Systems, and the U.S. Army (ARDC). He has over 70 publications and holds 14 patents.

P18—Integrated Optics I

1. Introduction to Integrated Optics
2. Optical Waveguide Modes
3. Theory of Optical Waveguides
4. Waveguide Fabrication Techniques I
5. Waveguide Fabrication Techniques II
6. Scattering and Absorption Losses
7. Radiation Losses
8. Coupling Into and Out of Waveguides
9. Waveguide-to-Waveguide Couplers and Modulators
10. Electro-Optic Modulators
11. Acousto-Optic Modulators

P19—Integrated Optics II

1. Basic Principles of Light Emission in Semiconductors
2. Semiconductor Lasers
3. Integrated Heterostructure Lasers
4. Distributed Feedback Lasers
5. Modulation of Semiconductor Lasers
6. Integrated Detectors I
7. Integrated Detectors II
8. Applications of Integrated Optics
9. Trends in Integrated Optics
10. Devices and Systems for Optical-Fiber Communications
11. Optical Integrated Circuits and Devices

For technical questions:

If you have technical questions about the course content, you may wish to speak directly with Dr. Hunsperger. He can be reached at the University of Delaware (302-451-8031), or call Tony Hearn at the Technical Excellence Center, Tacnet: 226-2149.

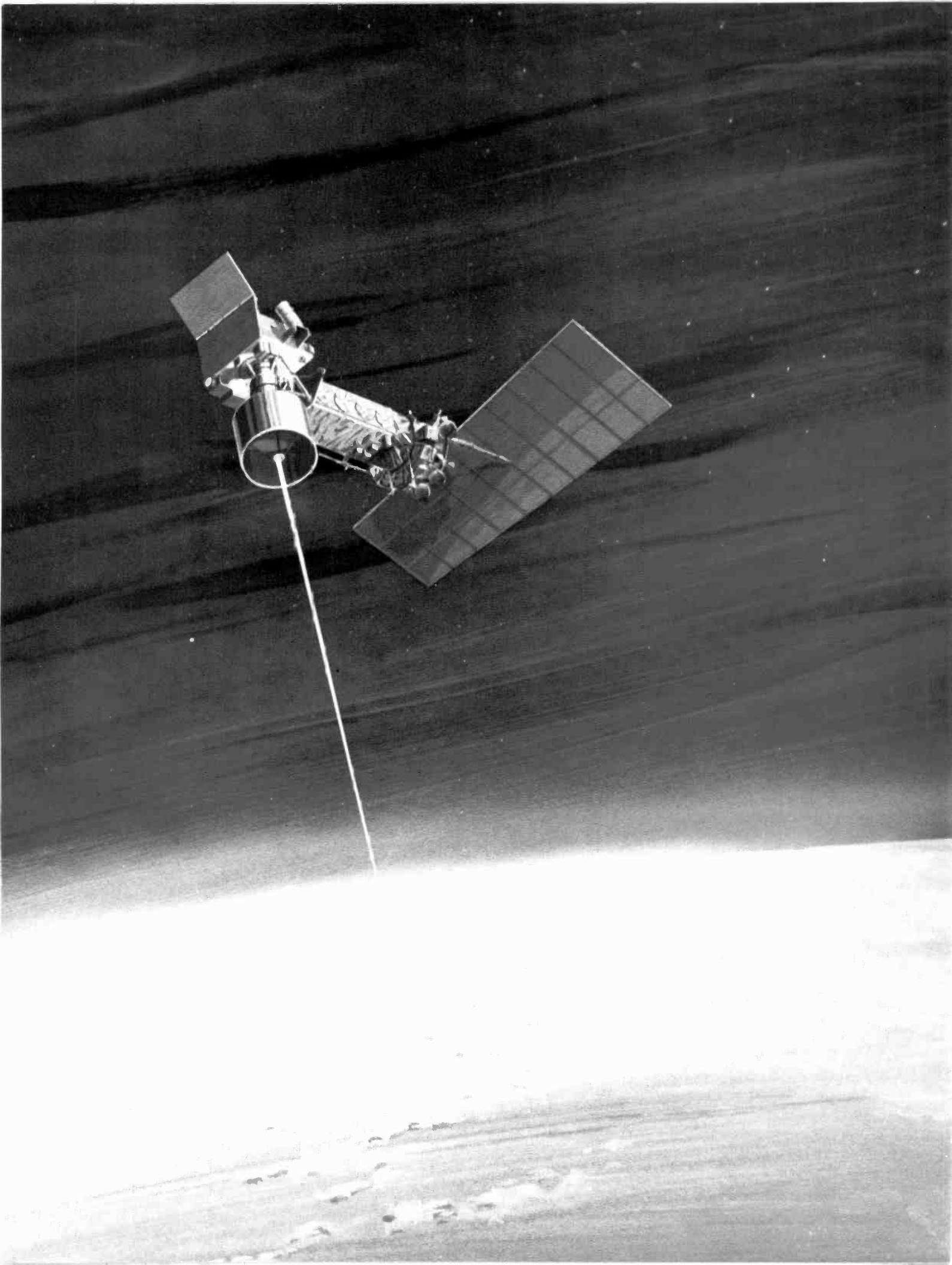
Who should take these courses?

Integrated Optics is suitable for engineers, scientists, and technical managers who are involved in the design or use of integrated-optic/fiber-optic devices, circuits, and systems.

To register:

For schedule and registration information, call Shirley Treherne, Corporate Engineering Education, Tacnet: 226-2227. Mailing address: RCA Technical Excellence Center, 13 Roszel Road, P.O. Box 432, Princeton, New Jersey 08543-0432.





Laser remote sensors for space applications

Laser-based sensors on meteorological satellites herald a new era in our knowledge of the atmosphere

The current remote sensors on operational meteorological satellites are termed passive because they do not have their own source of radiation. Rather, they measure the net natural radiation being emitted and reflected by the earth and the atmosphere in specific spectral bands or channels. The measuring device can be a radiometer that comprises a detector with a rotating filter wheel, a number of detectors with different filters, a grating or a prism spectrometer, or a Fourier transform interferometer. Such passive sensors operating in the visible, infrared and microwave regions provide useful, but not adequate, information about the state of the atmosphere. For example, a visible channel can distinguish between the solar radiation reflected from a cloud and that reflected from the earth, due to the large difference in the reflectivity. During the night, an infrared channel can differentiate between the cold radiation emitted by a cloud and the warmer radiation emitted by the earth and the atmosphere. While such channels can provide day and night cloud maps, they cannot provide direct information on cloud height. Clearly, for cloud mapping one selects channels in atmospheric windows to minimize effects of atmospheric radiation. In contrast, for temperature and moisture measurements, the sensors probe the atmosphere in spectral regions in which the molecular species emit and absorb radiation. For temperature profiling, the infrared bands of carbon dioxide and the microwave bands of oxygen are utilized, since the relative concentration or mixing ratio of these molecules is constant and well known. For humidity measurements both the infrared and microwave bands of water vapor molecules are probed. By a careful selection of channels corresponding to different atmospheric altitudes, it is possible to obtain information about the vertical distribution of temperature

Abstract: *Global and continuous measurements of the state of the atmosphere are required for the initialization of global circulation models, from which weather forecasts are produced. The observations of particular interest to the meteorological community are cloud heights and coverage, temperature profiles, moisture distribution, and wind fields. Simulation studies clearly indicate that the quality of weather forecasts is strongly correlated to the quality of initialization data.*

and water vapor. Winds cannot be obtained directly from passive remote sensors. However, one can derive winds by tracking the motion of the clouds.

Active sensors employing lasers as the source of radiation can overcome the limitations of the passive sensors, and have the potential of providing atmospheric data with the accuracy and spatial resolution required by the meteorological community. Such sensors, known as lidars (light detection and ranging) comprise a pulsed laser source(s), a telescope, and an electronic gating detection system. This enables the lidar system to measure the laser radiation reflected by the atmospheric aerosol particles and molecules as a function of time. This then allows a lidar sensor to directly measure highly resolved layers of the atmosphere.

The basic principles of lidar sensors for measuring aerosols, winds, temperature, humidity, and pressure will be discussed in this paper. Such systems are being breadboarded at RCA Astro-Electronics Division, and they will be described in some detail. The issues involved in adapting these systems for space application will be addressed briefly.

Principles of lidar

A lidar consists of a short-pulse (10 to 200 nanosecond) laser transmitter, telescope receiver, photon detector, and a data processing and storage system (see Fig. 1). The pulse of light is transmitted into the atmosphere in a direction that is in the field of view of the telescope. As the light pulse propagates through the atmosphere, a portion of it is scattered in all directions by molecules and suspended particles. The light that is scattered back in the direction of the telescope is detected. The theoretical expression relating the measured signal to the state of the atmosphere is the lidar equation:

$$E_r(\nu', R) = E_t(\nu) \tau_o(\nu') \tau_f(\nu') \tau^2(\nu, \nu', R) \cdot (A/R^2) \cdot \beta_\pi \Delta R \quad (1)$$

where ν and ν' are the transmitted and received frequencies, respectively, E_r is the transmitted energy, E_t is the energy received from a range cell of thickness ΔR centered at a distance R , τ_o and τ_f are the system parameters for optical transmission and filter transmittance, A is the receiver area, τ^2 is the two-way atmospheric transmittance, and β_π is the atmospheric backscatter coefficient. For hard target measurements, the backscatter coefficient is replaced by surface reflectivity, or

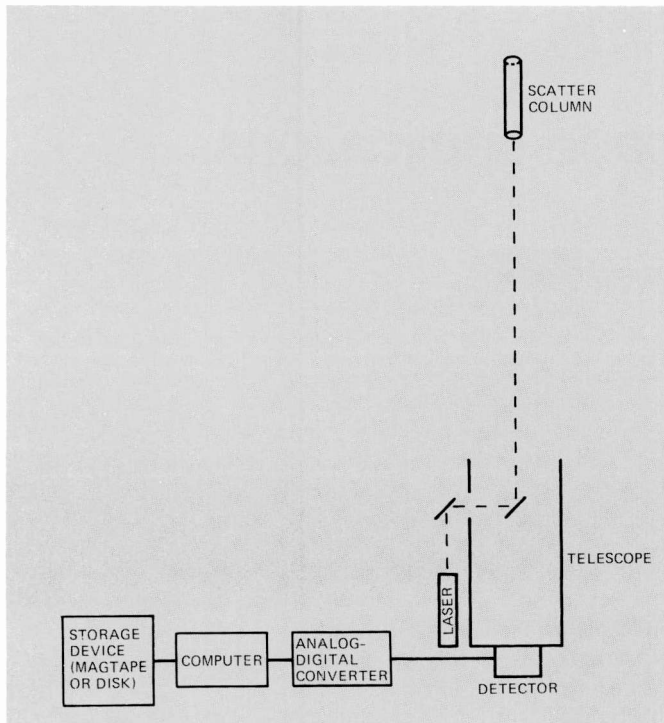


Fig. 1. Schematic of a simple backscatter lidar system.

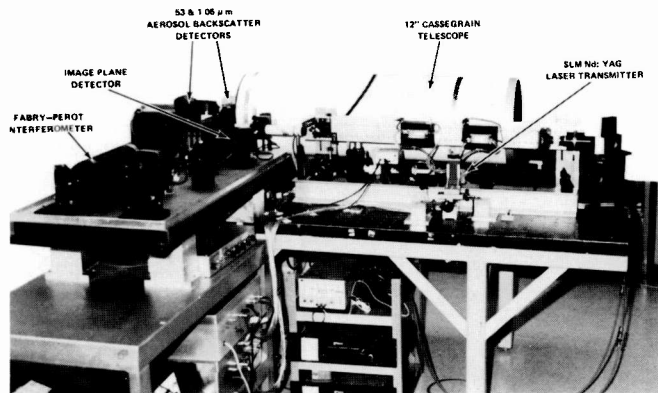


Fig. 2. Neodymium YAG laser system that can measure aerosol backscatter at two wavelengths, or winds.

albedo. With the exception of winds, information on the state of the atmosphere is contained in the terms β_{π} and τ^2 .

Since the speed of light (c) equals 3×10^8 meters/second, a 100-nanosecond laser pulse would extend 30 meters. If one fires the laser and measures the elapsed time (t) with nanosecond precision, the detector would "see up" through the tail of a column of laser radiation whose front end is at a distance $d = 1/2 ct$. The factor of 1/2 arises because t is the round trip time for the detected photon. The column is receding from the telescope 30 meters every 100 nanoseconds.

The signal received by the detector passes into a computer, where it is sampled (digitized) and stored in memory. The returned lidar signal may be analyzed in several ways to measure significant atmospheric properties. By measuring the range-resolved signal intensity, an estimate of the aerosol backscatter properties along the line of sight can be obtained. If the spectral properties of the emitted and returned radiation are known,

wind fields may be derived by measuring the Doppler shift of the backscattered signal from tracer aerosol particles. Information on molecular absorption can be obtained by comparing the relative intensity of two backscattered laser signals at slightly different wavelengths: one centered on a molecular absorption line and another just off the line. Depending upon the spectral line chosen, the amount of absorption measured may yield information on temperature or concentration of the absorbing molecular constituent.

Atmospheric aerosol backscatter

The magnitude of a lidar return signal is highly dependent on the atmospheric backscatter coefficient (β_{π}), equation (1). This coefficient describes the relative intensity of reflected to transmitted light and exhibits a large variation with atmospheric conditions. Knowledge of the magnitude of this variation is essential in designing an operational spaceborne lidar.

Currently, there is insufficient information to allow accurate characterization of β_{π} at infrared wavelengths, especially at the longer wavelengths. As a result, Astro-Electronics initiated a program in 1983 to measure the coefficient at three wavelengths; 0.53 μm , 1.06 μm and 10.6 μm . These three wavelengths were chosen because they cover most of the wavelength range of interest and employed readily available electro-optic/laser technology. Ground-based lidars have been designed and constructed at Astro-Electronics in order to assess $\beta_{\pi}(\lambda)$.

0.53/1.06 micron aerosol backscatter measurements

The lidar system used for 0.53/1.06 μm aerosol backscatter measurements is shown in Fig. 2. The transmitter is based on a neodymium-doped garnet crystal laser (Nd:YAG), which can be operated on a single frequency (or single longitudinal mode, SLM) for measuring winds, as discussed later. The laser oscillator output at 1.06 μm is amplified and a portion is frequency-doubled to 0.53 μm to achieve simultaneous operation at both wavelengths. Both beams are expanded by a $5\times$ telescope and transmitted into the atmosphere via steering optics. The backscattered light from the atmosphere is collected by a 30-cm diameter $f/16$ telescope and coupled into various detectors. The 1.06- μm backscatter is separated from the 0.53- μm by a dichroic mirror and detected by a silicon avalanche photodiode (APD). A removable mirror allows the 0.53- μm backscatter to be directed either to a time-gated photomultiplier tube (PMT) to monitor total backscatter or to the Fabry-Perot interferometric (FPI) detector system to measure winds. This arrangement allows data acquisition in three modes:

1. Simultaneous monitoring of total backscatter at both 1.06 μm and 0.53 μm ;
2. Doppler wind measurements with the FPI system;
3. Monitoring of both total backscatter (1.06 and 0.53 μm) and the backscattered spectrum (FPI system) with a beam splitter replacing the removable mirror. The signals from the detectors are digitized and stored on floppy disks for later analysis.

The data shown in Fig. 3 was taken at 0.53 μm and is an average of 94 atmospheric returns. Cloud layers are present from 9.5 to 12.5 km altitude. Figures 4 and 5 taken at a higher PMT operating voltage (to increase gain) show the single photon

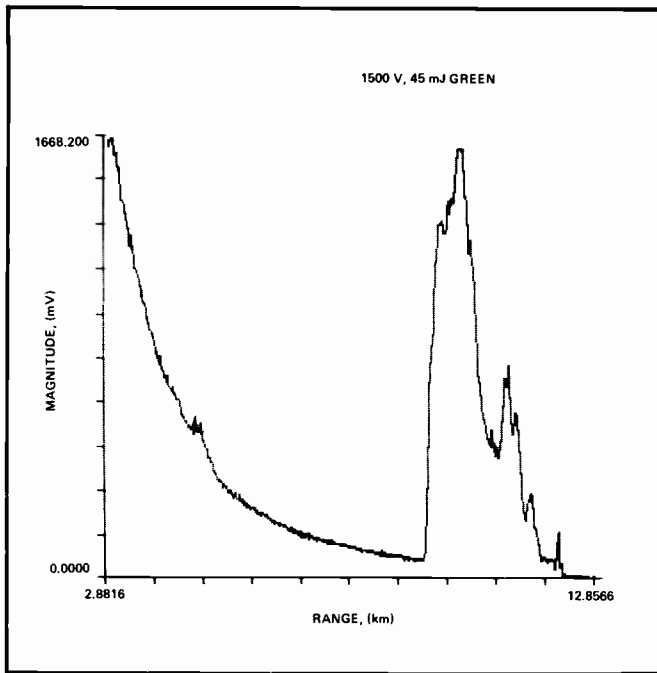


Fig. 3. Atmospheric return from 532 nm laser showing cloud layer between 9 and 12 km.

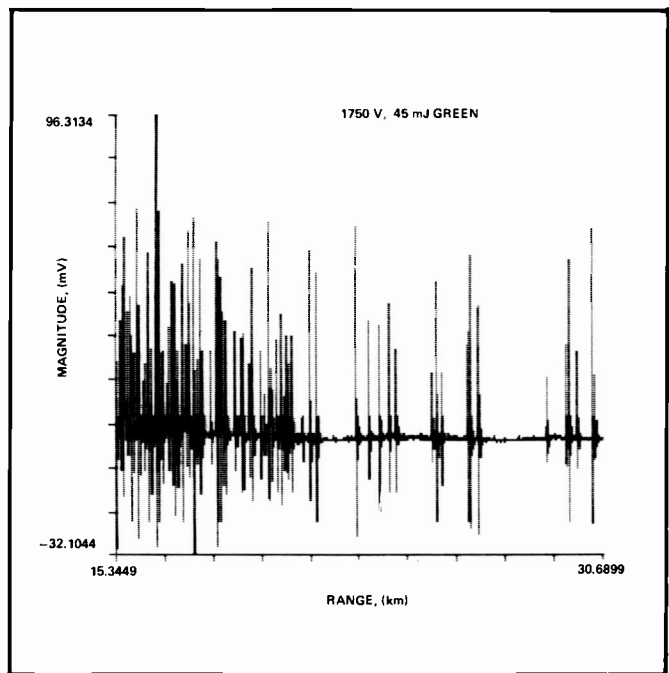


Fig. 4. Atmospheric return from 532 nm laser between 15 km and 30 km.

returns (no averaging) from 15 to 30 km, and an expansion from 20 to 25 km (the negative spikes are due to ringing in the amplifier stage following the PMT). Note that single back-scattered photons have been detected through the thin cloud layer from up to 30 km.

10.6 micron aerosol backscatter measurements

This system utilizes a 600-mJ CO₂ laser source and employs the same telescope mirror (30 cm) for the transmitter and receiver, Fig. 6. A hybrid laser (containing two lasing media) is used as the CO₂ laser source. This arrangement forces the laser to operate on a single longitudinal mode, thereby providing a spectrally pure source of radiation. The linearly "p" polarized laser beam then passes through a thin film polarizer, and is circularly polarized by a Fresnel Rhomb. It then enters a negative lens and telescope mirror, which constitute a Galilean telescope, and is transmitted to the atmosphere. The circularly polarized light reflected from the atmosphere is then collected by the telescope and redirected through the rhomb. The light is now, however, circularly polarized in the opposite direction, as a result of its reflection in the atmosphere. On leaving the rhomb it becomes linearly polarized again, but at right angles to the original transmitter laser light. This "s" polarized beam is now reflected from the thin film polarizer and is directed towards a cooled (77K) HgCdTe photovoltaic detector. In order to increase receiver sensitivity, coherent (heterodyne) optical detection is used, which is described later in this article. This approach requires the additional illumination of the detector with a local oscillator laser, whose beam path is also shown in Fig. 6. A reference detector is also provided for laser beam monitoring.

A typical atmospheric lidar return is shown in Fig. 7. The signal backscattered from the atmospheric aerosol steadily decreases with distance, as expected. The reflection from a tree covered hill at a range of ≈ 15 km is clearly visible.

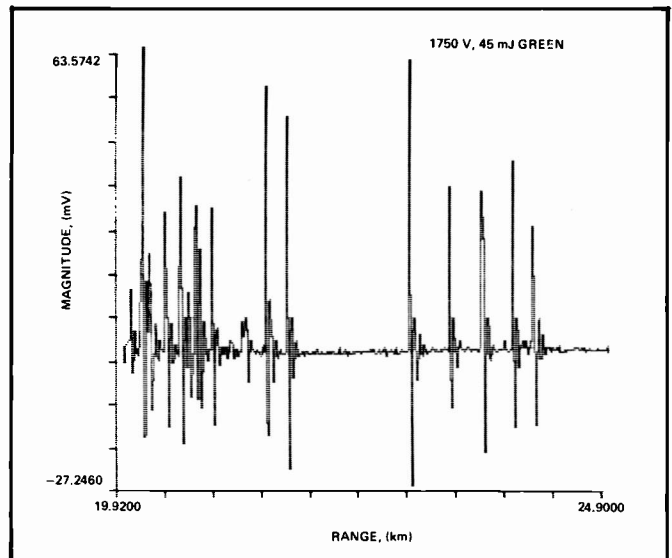


Fig. 5. Atmospheric return from 532 nm laser between 20 km and 25 km.

Wind sensors

Spaceborne lidar systems are under development to complement the current radiosonde wind measurement network by providing additional wind information on data-sparse regions over the oceans and the southern hemisphere. Simulation experiments have shown that an expanded database obtained by a combination of the radiosonde and spaceborne lidar wind measurements would improve the forecast accuracy of numerical prediction models.

Lidar measurements are based on the fact that aerosol particles suspended in the atmosphere can serve as ideal wind tracers. Photons scattered by particles moving towards the observer will experience an increase in frequency, while those scattered by

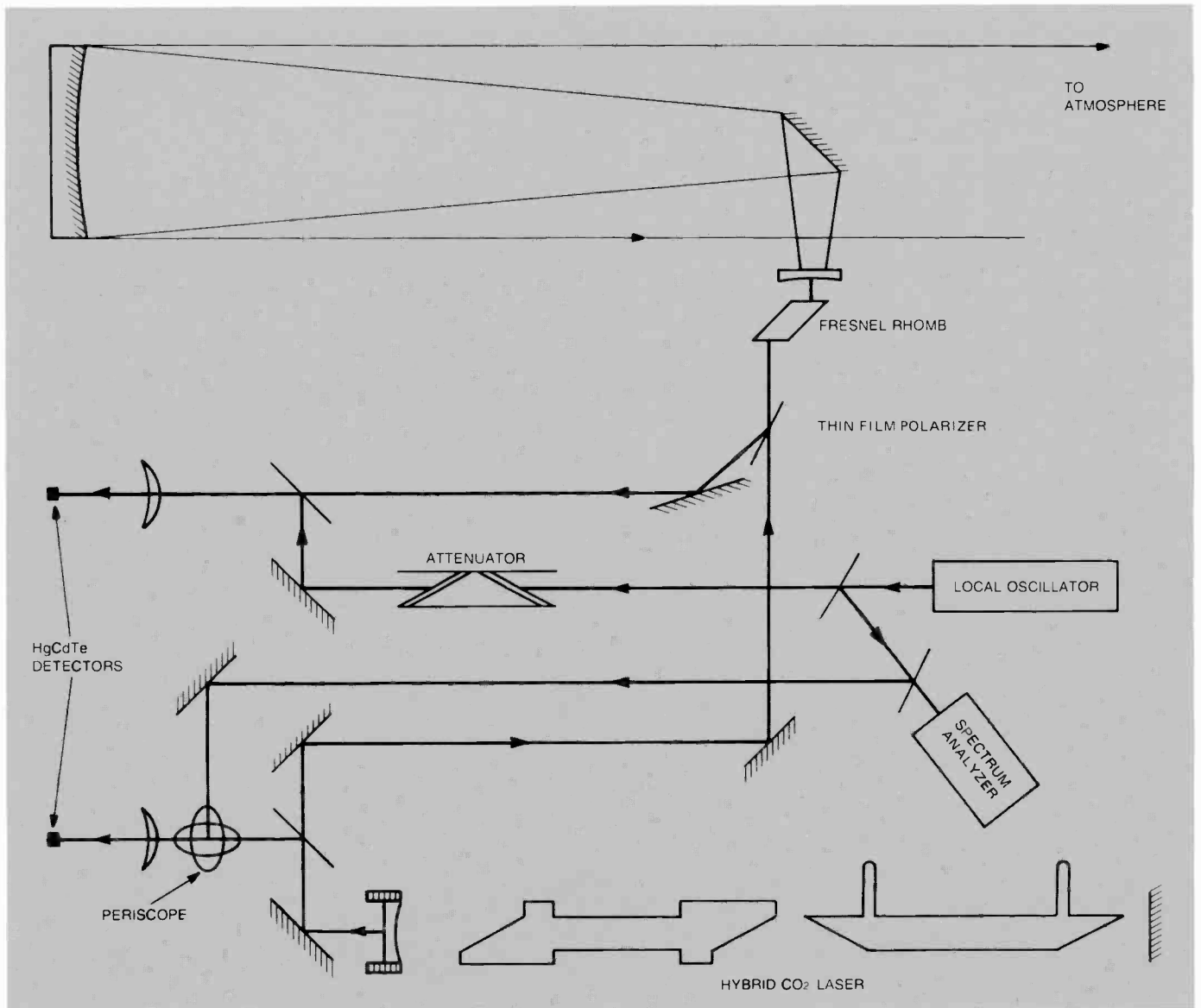


Fig. 6. CO₂ laser system that measures atmospheric backscatter at 10.6 μm.

particles receding from the observer will display a decrease in frequency. Measurements taken in a single direction can only measure the component of wind velocity along that direction. Thus, spatial scanning is required to give information in two or three dimensions.

A photon at a frequency ν backscattered by an aerosol moving at a wind velocity V_r with a line of sight component V_r , will experience a Doppler shift in frequency of:

$$\Delta\nu = \frac{2V_r}{c} \nu = \frac{2V_r}{\lambda} \quad (2)$$

The Doppler shift of a spectrally narrow laser beam can be analyzed to yield this line of sight wind velocity. The two techniques for doing this, known as coherent and incoherent detection, will be discussed in further detail below. The coherent method uses heterodyne detection, mixing the backscattered signal with a local oscillator on a detector to yield a beat frequency proportional to the Doppler shift. The incoherent technique measures spectral shifts using the FPI, which spatially

disperses the radiation, and an array-type detector. A brief comparison of our implementation of the two techniques is given in Table I.

Incoherent wind detection system

A ground-based prototype system consisting of a narrow band, single frequency, laser transmitter, an FPI to measure the Doppler shift, and a data acquisition system is currently being assembled for evaluation and testing of the incoherent Doppler lidar concept. The design of this system is based upon the technology developed for the Dynamics Explorer (DE) satellite program to measure temperature and winds in the thermosphere.

A schematic illustration of the incoherent lidar concept is shown in Fig. 8. This detection technique requires that both the spectrum of the transmitted laser pulse and the atmospheric backscatter be measured accurately to derive the relative Doppler shift velocity. The left panel of Fig. 8 shows the spectral distribution of the narrow band, single-frequency transmitted

laser pulse and the atmospheric backscatter signal consisting of a narrow aerosol "spike" superimposed upon a broader molecular return. The backscattered spectrum is shifted in wavelength depending on the relative motion of the aerosol particles to the transmitter source.

Detection of the relatively small Doppler shifts induced by normal wind velocities requires high spectral resolution. An FPI provides the spectral dispersion necessary for the small frequency shifts involved. The output of the Fabry-Perot etalon forms a circular interference fringe pattern.

A Fabry-Perot interferometer can measure the backscatter spectra by either changing the optical path between the etalon plates (refractive index or plate separation) or by measuring the spatial distribution of the transmission fringe patterns observed in the focal plane of the FPI where the change in the diameter of the central fringe is related to the Doppler shift given by equation 2. The backscattered spectrum is measured with an image plane detector (IPD), which is designed to measure equal spectral intervals by imitating the FPI fringe pattern with 12 equal-area, concentric rings. A schematic of the IPD anode is given in the central panel of Fig. 8. The photoelectron signals measured by a FPI-IPD combination are illustrated in the right panel for both the transmitted laser pulse and the atmospheric backscatter.

The broadening observed in the backscattered spectrum is due to a random molecular motion superimposed on the motion due to winds. Thus, analysis of data can give range resolved information on aerosol/molecular backscatter ratio as well as wind speed.

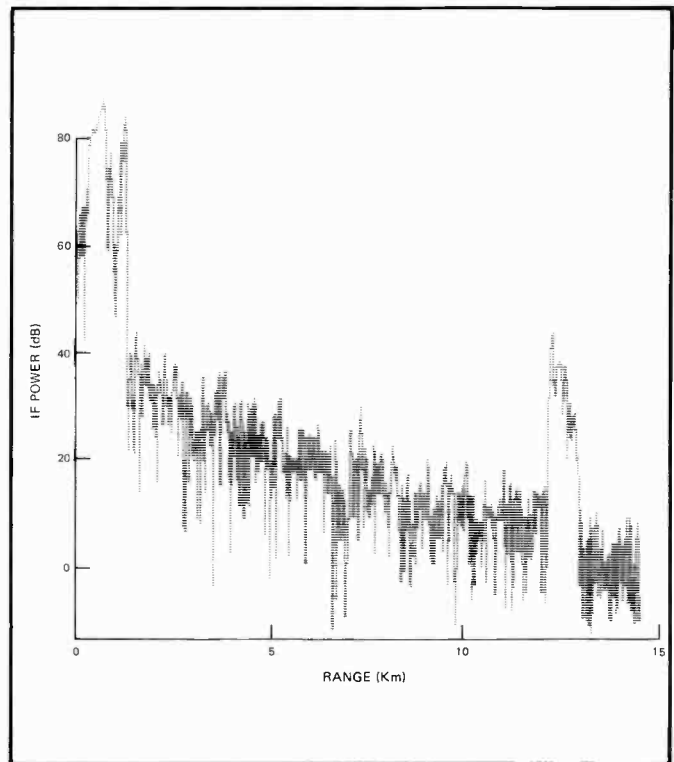


Fig. 7. Horizontal path return at 10.6 μm showing aerosol backscatter out to 10 km and a topographic target (tree-covered hill) at 14 km.

Table I. Comparison of lidar wind sensor approaches

Feature	Coherent 10 μm wind sensor	Incoherent 0.5 μm wind sensor
Overall technological development	Ground and air demonstrations	Ground-based system under development, similar FPI detection system flown in space
Laser efficiency	5-10%	0.1—1% (could increase to 5—10% with diode pumping)
Atmospheric backscatter	Low, variable, and uncertain	Higher, less variable, and better documented
Daytime operation	Same performance as at night—no special designs needed	Rejection of scattered solar light requires addition of two narrowband etalons
Eye safety	Eye safety requirements easily met	Transmit beam may have to be expanded to larger than ideal in some applications
Ancillary measurements	10 μm aerosol backscatter coefficient	0.5 μm aerosol backscatter coefficient, atmospheric density (5—15+km)

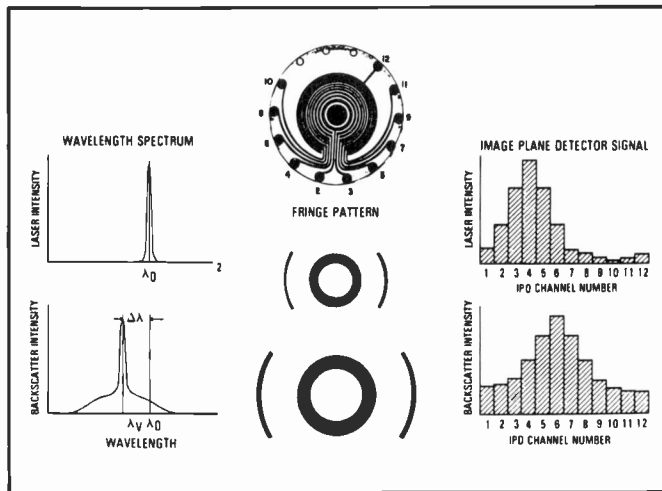


Fig. 8. Schematic of incoherent lidar for wind sensor at 0.53 μm .

Figure 9 shows an example of the atmospheric backscatter spectra measured by the Doppler lidar on June 4, 1985. The six spectra shown in this figure are presented as a histogram of the IPD signal intensity as a function of the IPD channel number for successive samples at 300-m intervals, starting at approximately 150-m altitude. The sky was overcast on this day and the total 0.532 μm backscatter measured by a photomultiplier indicated that multiple cloud levels existed between 1.0 and 2.4 km (above ground level). The height intervals labeled 4, 5 and 6 (1050, 1350, 1650 m) clearly show a narrow spectral line indicative of the strong, narrow bandwidth backscatter from clouds. The backscatter spectra sampled at height intervals labeled 1, 2, and 3 (150, 450, 750 m) are from the clear atmosphere below the cloud layers and illustrate the narrow-band aerosol signal superimposed upon the broadband molecular return. This is easily seen by noticing that the ratio of the peak to minimum signal is less for the clear air backscatter than that of the clouds.

Optical coherent detection for wind sensing

The radio-frequency technique of heterodyne detection is commonly used throughout the telecommunications industry. This technique can be extended to optical frequencies (10^{14} Hz) in the infrared region with dramatic increases in sensitivity over conventional detection techniques. In this case, a local oscillator laser and optical return signal simultaneously illuminate a detector. The detector output voltage varies linearly with input optical power (as the square of the electric field intensity associated with the optical energy). As a result of this square law dependence, a difference frequency between the local oscillator laser and the applied optical signal appears at the electrical output of the detector. This detection technique not only offers the advantage of extending photon detection into the infrared region, it also permits the measurement of line-of-site velocity, analogous to the Doppler microwave radar sets used by law enforcement agencies.

As described earlier, the suspended aerosol particles impose a Doppler shift on the optical frequency. This frequency shift, $\Delta\nu$, is directly transferred to the IF signal. For a typical laser system operating in the near to mid infrared region, this corresponds to between 200 kHz and 2 MHz per m/s of line-of-sight wind

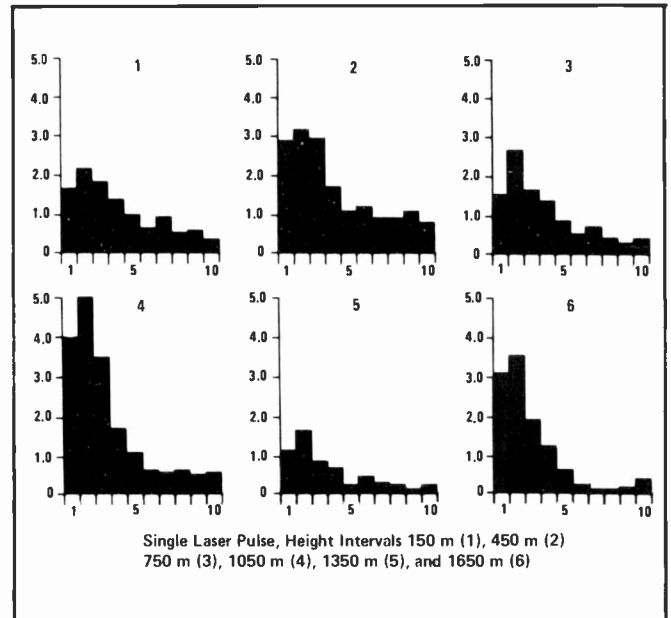


Fig. 9. Atmospheric return at 0.53 μm at six different altitude levels.

Table II. Windsat Free-Flyer mission requirements—lidar wind sounding from a free-flying satellite.

Lidar

- Aperture—1.25m
- Fixed nadir look angle—52.7°
- 10J/pulse
- 2 pps
- 3-4 μsec pulse length

Operational Modes

- (1) Continuous conical scan rotation period 19 sec.
- (2) Stop and stare
High spatial resolution intermittent observation $\geq 15^\circ$ from subtract normal

On board data processing

Real time and stored data transmission

Two-year operations goal

STS launch to Shuttle parking orbit, followed by direct or indirect ascent to operational near-polar orbit.

speed. In practical applications, both range and velocity resolution are required from the same lidar system, leading to conflicting requirements between laser pulse length and laser pulse bandwidth. These are described by the reciprocity relationship:

$$\Delta V \Delta r \geq (c\lambda)/2$$

where ΔV and Δr are the velocity and range resolution respectively. A simulation of an operational, satellite-based CO_2 ($\lambda = 10.6 \mu\text{m}$) wind sensor has been performed with a $\Delta V \sim 1$ m/s and a $\Delta r \sim 1.6$ km. The results of this study are described in the next section.

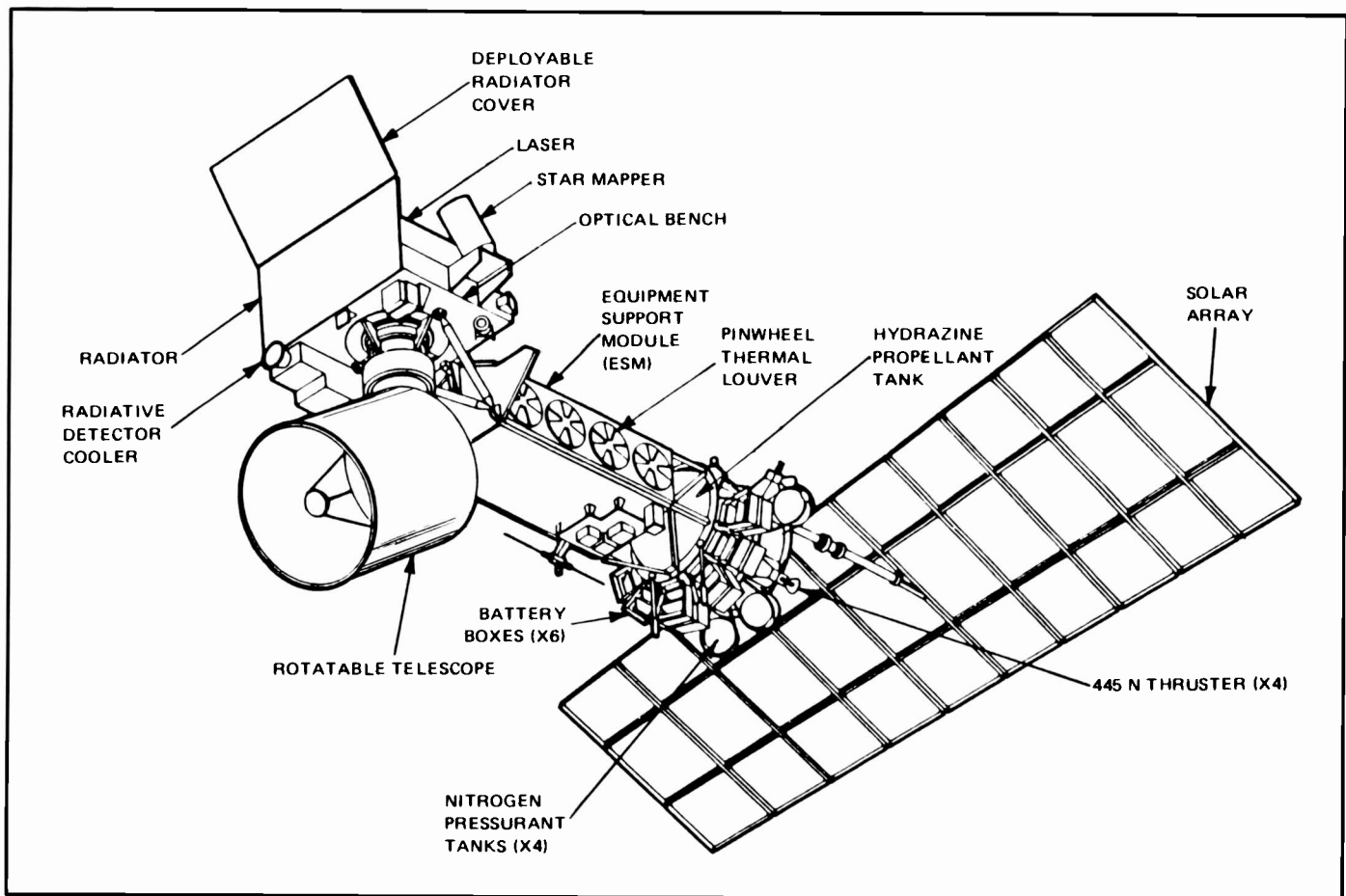


Fig. 10. 10.6 μm wind sensor mounted on Advanced TIROS-N meteorological satellite.

Feasibility of spaceborne wind sensor

In previous studies of the feasibility of an earth orbiting Doppler lidar for global wind measurement, it was found that the instrument accommodations required the Space Shuttle or some currently non-existent large satellite in low earth orbit. However, Astro-Electronics has recently completed a study that has shown that this type of instrument could now be accommodated on an Advanced Tiros-N (ATN) series spacecraft with relatively minor changes to the operation of the sensor. This concept has become known as Windsat Free-Flyer.

The mission requirements are summarized in Table II, and an artist's concept of Windsat is shown in Fig. 10. The large telescope mounted on the equipment support module (ESM) of the ATN acts as laser transmitter and receiver. Normally it will continuously scan about nadir, as the spacecraft moves in orbit, at 19 seconds per revolution. The laser fires twice per second and the return signals from the atmosphere are digitized in 15 to 20 range-gated altitude layers of interest. This mode will provide global coverage, with the data from all samples in a $300 \times 300 \times 20$ -km volume being combined on the ground to generate one vertical profile of wind data for that region. A second mode can be chosen by ground command for small regions of specific meteorological interest. In this case, the lidar scan is stopped at a specific azimuth so that it can "stare" at a small region. By fixing the azimuth, more samples are taken in the small area, and hence better resolution is obtained. Corresponding "stares" are made of the same area in the fore and aft

directions as the spacecraft moves in orbit to obtain data from two aspects for removal of any ambiguities of wind direction.

The Windsat Doppler lidar is based on the use of a 10.6- μm CO_2 laser and coherent detection, as described earlier. The overall instrument package consists of a large telescope, a detector assembly and signal processor, and a laser, integrated and aligned on an optical bench mounted at the end of the ESM.

A key result of this study is the reduction in weight of the telescope to less than 200 kg. This was achieved by removing material from the back of the 1.25-m primary mirror to produce a honeycomb structure occupying only 7.5 percent of the original volume. The study shows that the imaging properties of the mirror were unaffected by this weight reduction technique.

The laser system for the Free-Flyer lidar would consume 448 W, weigh 155 kg, and fit in a $1.5 \times 1 \times 0.5$ -m space. Laser cooling is provided by a liquid coolant pumped through a large-area passive radiator mounted on the spacecraft to face cold space. The detector on this system operates at temperatures $< 110\text{K}$ and uses a radiative cooler of the same type currently used for many spaceborne infrared radiometers.

The third major element of the lidar is the signal processor, whose primary purpose is to compress the high data rate of 242 kbps to a more manageable rate by performing real-time, on-board processing of the returned Doppler signal. The total data rate for 20 range cells per pulse at two pulses per second is 960 bps.

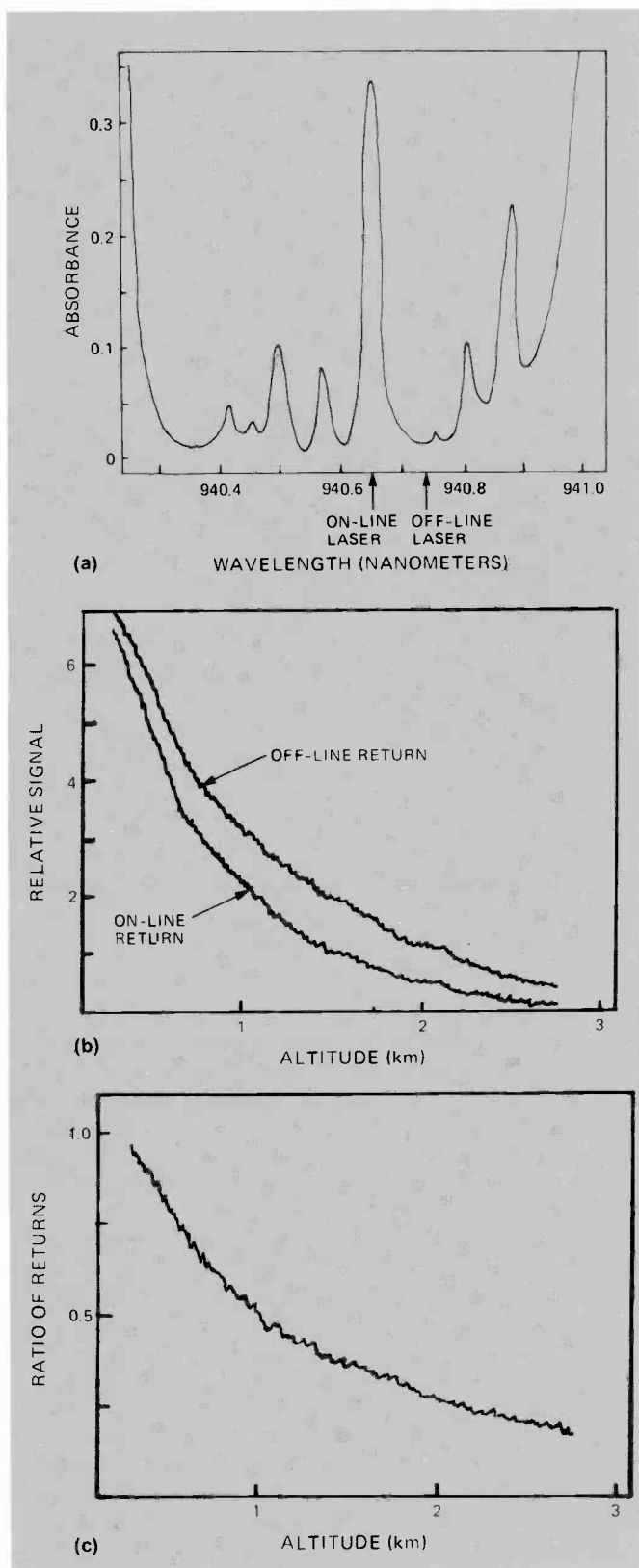


Fig. 11. Illustration of water vapor DIAL experiment. a) Small portion of 940-nm water vapor spectrum. Laser 1 is tuned on an absorption line at 940.66 nm. Laser 2 is tuned to 940.73 nm where absorption is minimum. b) Simulated DIAL returns for Laser 1 (on-line) and Laser 2 (off-line). c) Resulting ratio return (on-line/off-line), the curve from which the humidity profile is calculated.

For the lidar instrument as a whole, the power consumption is 550 W and the weight is 470 kg. The weight of the instrument is such that the total weight of the satellite is well within the capability of the on-board propulsion system for transfers to a sun-synchronous orbit at 833 km. The power consumption, however, requires limiting the range of sun angles to 5–40° and requires two more solar array panels.

DIAL system

Differential Absorption Lidar (DIAL) is being developed as a method for mapping from space the temperature, pressure, and moisture content of the Earth's atmosphere. Interest in measurements of this type arises from the significant impact that these measurements would have on weather and climate prediction. The DIAL technique takes advantage of the extreme monochromaticity of lasers and the rich spectroscopy of the molecular components of the atmosphere.

Each molecular species has its own unique absorption spectrum. The main feature of a spectrum is the wavelengths of absorption lines. The breadth, shape, and height (absorption intensity) of these lines depend on the partial pressure of the molecule producing the spectrum, and on the temperature and total pressure of the gas. It is this dependence that makes the DIAL technique a powerful tool for remote atmospheric temperature, pressure, and humidity measurements.

The differential absorption lidar differs from the simple backscatter lidar described above in that at least two narrow-band (monochromatic) laser transmitters are required. One laser is tuned to a wavelength that experiences significant absorption. The second laser is at a different wavelength and experiences negligible absorption (see Fig. 11a). The difference in these signals relates to one of the parameters being measured—temperature, pressure, or humidity.

The differential absorption lidar differs from the simple backscatter lidar described above in that at least two narrow-band (monochromatic) laser transmitters are required. One laser is tuned to a wavelength that experiences significant absorption. The second laser is at a different wavelength and experiences negligible absorption (see Fig. 11a). The difference in these signals relates to one of the parameters being measured—temperature, pressure, or humidity.

Simulated backscatter returns for these two lasers are shown in Fig. 11b. The return from the first laser is increasingly attenuated at higher altitudes due to absorption along the path from the laser transmitter to the scatter location and back down to the detector. The second laser return acts as a control; this is how the first laser return would appear if there were no absorbing molecules in the path. Fig. 11c shows the ratio that contains the information from which temperature or concentration of absorbing molecules as a function of altitude is extracted.

Humidity DIAL system

Astro-Electronics is presently building a humidity DIAL system in the laboratory to measure atmospheric water vapor. The method employed sequentially fires two lasers with a separation of 100 microseconds. As the second laser fires, the detector receives the backscatter from the first laser pulse at an altitude of 15 kilometers. The signal from this altitude will be immeasurably small, so the detector can now receive the backscatter signal from the second laser column without interference from the first. The first laser is tuned to the center of a water vapor absorption line. In general, the absorption intensity at the center of a line will depend on the concentration of absorbing molecules and on the temperature. To avoid the necessity of knowing the temperature profile in advance of the humidity measurement, an absorption line is chosen that has a negligible temperature dependence. Now, the ratio of the two signals will depend solely on the water vapor concentration at the various altitude levels.

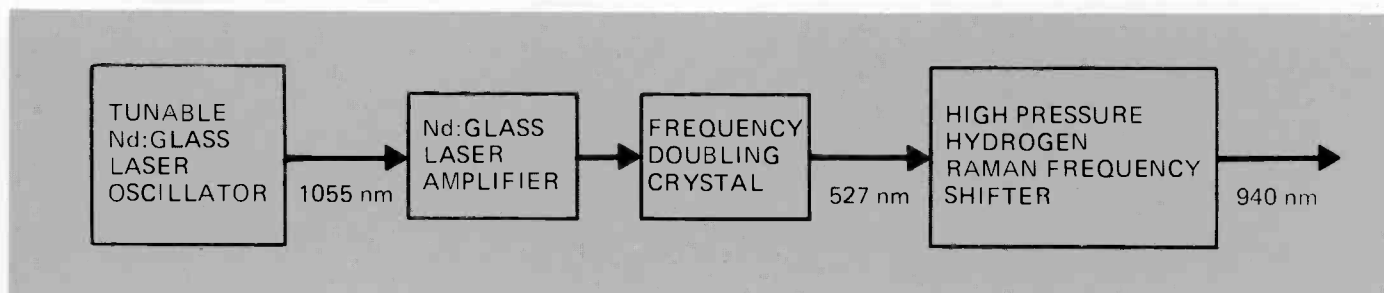


Fig. 12. Tunable ND:Glass/Raman 940-nm Laser.

For this system the water vapor absorption band (a band is a system of close-lying absorption lines) at 940 nm was chosen. A small portion of this band is shown in Fig. 11a. There is much interest in the 940 nm band because its absorption lines are very strong, and are therefore good candidates for humidity measurements in the stratosphere from space. This, however, is a spectral region that has never been observed in a lidar experiment, namely because no efficient, tunable narrow-band laser emits at these wavelengths. Our first task, therefore, was to develop a new tunable laser source at 940 nm. This we have recently achieved with the setup shown in Fig. 12. The output from a neodymium:glass laser, which can be tuned from 1045 nm to 1065 nm, is passed through a frequency-doubling crystal. The laser radiation emerging from the crystal, now ~ 530 nm, is passed through a high-pressure hydrogen cell in which the molecules induce resonant inelastic scattering in the same direction as that of the original beam. This effect is known as stimulated Raman scattering. The laser radiation emerges with a wavelength of 940 nm. By tuning the Nd:glass laser, the Raman-shifted radiation is tuned to the desired wavelength.

Fig. 13 shows a backscatter return in which the laser was tuned to a region in the 940-nm band in which there was little absorption. The sharp spikes at 2.6 and 5.3 kilometers are reflections from two cloud layers that were over the Astro-Electronics plant at the time. Measurable aerosol backscatter can be seen up to 3 kilometers. These measurements were made with laser pulses of ~ 5 mJ. The same laser presently is being modified to emit energies of ~ 100 mJ. With this, returns from 10 kilometers should be obtainable.

Meanwhile, a second laser is being developed to complete the DIAL system. This laser will exhibit the greater energy and wavelength stability necessary for "on-line" DIAL application. In addition, the laser is being packaged for use in downward-viewing airborne experiments to show its feasibility for future satellite installations.

Temperature DIAL

Temperature DIAL requires the use of absorption lines of uniformly mixed gases that are strongly temperature dependent. Temperature DIAL measurements can be made using an absorption band of a major atmospheric constituent such as the 760 nm molecular oxygen band. Molecular oxygen's atmospheric mixing ratio, 0.2095, is constant throughout the troposphere.

The temperature dependence on the absorption intensities derives from the Boltzmann distribution of the populations of the different rotational energy levels. As temperature increases, the higher rotational levels become increasingly populated. Lines that involve high-lying rotational levels are highly temperature sensitive and would make good candidates for temperature

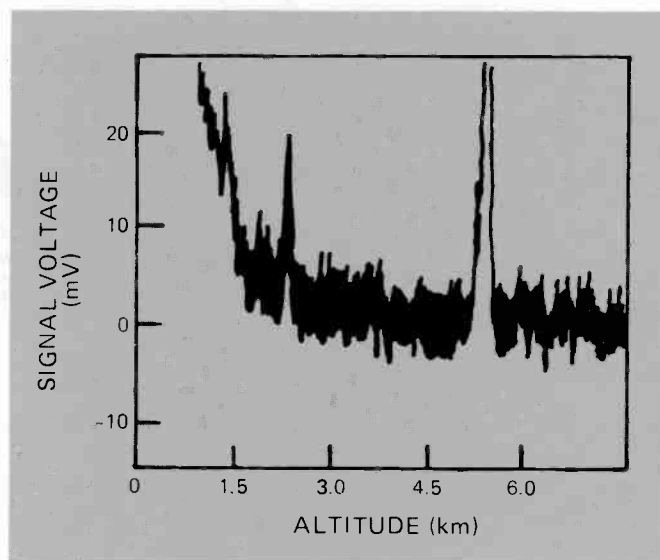


Fig. 13. Atmospheric return. The Laser was tuned to a region of low absorption within the 940-nm water vapor absorption band. Cloud layers are present at 2.3 km and 5.3 km.

DIAL measurements. The humidity DIAL system can be converted to a temperature DIAL system by changing the hydrogen gas cell to a methane gas cell.

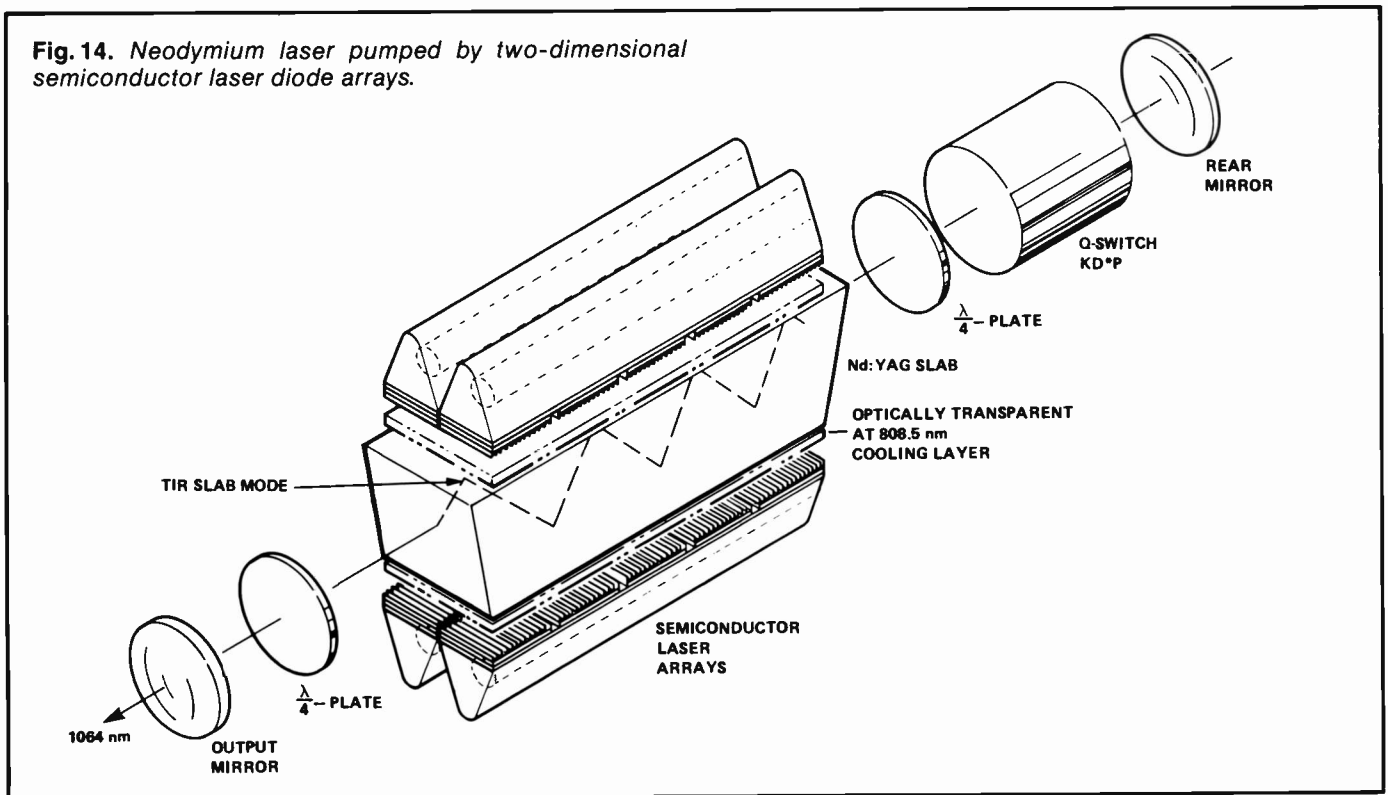
Space application issues

The main issues that arise when we consider applying laser-based technology to routine measurements of meteorological parameters from space are the large weight and power requirements, and the limited lifetime of the components.

Weight and power requirements

A key parameter in the design of a spaceborne lidar is the weight of the receiving telescope and the laser transmitter. The receiving telescope has to be large because the signal returned from the atmospheric aerosol particles is small. Furthermore, the telescope must be figured to a high precision to achieve the desired spatial resolution at the ground. The accuracy of the receiver figure is related to the wavelength. In microwave radar, where wavelengths are typically centimeters, the receiver need only be figured to an accuracy of a millimeter or so across the aperture. This degree of accuracy allows the use of lightweight resin based composites such as graphite-epoxy. In optics, the same relative precision requires an accuracy of about one-tenth of a micron, because the wavelength is ten thousand times

Fig. 14. Neodymium laser pumped by two-dimensional semiconductor laser diode arrays.



shorter. This degree of accuracy mandates the use of materials that can accept a high polish, such as glass, quartz, or beryllium and generally leads to a massive structure. For instance, Space Telescope (ST) weighs >2000 kg. Recently, however, techniques have evolved that allow for large, light-weight optical structures. Weights about one-tenth ST appear feasible. Apertures larger than about one meter may, in the future, use multiple light-weight mirrors.

The weight of the laser is related to the efficiency with which it converts electrical input to light output. An inefficient laser requires a large power supply and a large cooling system to remove the heat. Currently, efficiencies of sensor-type lasers are in the 1-percent range. A typical 1-joule laser of this type weighs approximately 150 kg. The most effective way of reducing the weight is to improve the efficiency.

Most of the lasers being considered for near-term deployment are of the optically-pumped, solid-state type. This terminology refers to the fact that the lasing medium is a solid (often a crystal such as ruby or transition-metal-doped glass) and is pumped by a flashlamp. The flashlamp emits light over a broad spectrum, only a fraction of which is absorbed by the lasing material—hence the low efficiency. A more efficient way of exciting the material would be to pump with a source that emitted most of its light directly at the absorption wavelength. Such a device is the semiconductor diode array currently under development at RCA Laboratories. Here, individual linear diode arrays are stacked in such a way that a 2-D array results. The 2-D array is then mounted against a square section of neodymium laser material, which absorbs the emitted 800 nm radiation (see Fig. 14). The neodymium laser overall efficiency is about 10 percent. Such a configuration leads to weight savings in a number of ways: (1) the device may be made physically smaller because of the compact nature of the laser diodes; (2) the power supply may be made smaller because of

the increased efficiency and lower voltages needed to drive the diodes; and, (3) the cooling unit can be made smaller because of the increased efficiency and the fact that most of the heat is removed by the diode heat sinks.

Lifetime issues

Operational sensors in earth orbit are expected to last for a minimum of two years. For a laser-based instrument operating at a nominal rate of 10 Hz this amounts to 10^9 shots. Currently available laser technology cannot achieve this kind of lifetime.

Electrically-excited gas lasers, such as CO₂/N₂/He) as they operate use up the gas mix (a mixture of CO₂/N₂/He) as they operate and need to be replenished. Carrying along large volumes of gas in space is obviously impractical, so the waste products (CO and O₂) need to be catalytically recombined into CO₂ in a continuous fashion. Such catalytic converters are currently under development, but have yet to demonstrate the required lifetime.

The lifetime of solid-state lasers is principally limited by the lifetime of the flashlamps, which is 10^7 – 10^8 shots at best. However, laser diode array pumping is expected to increase lifetimes to 10^{10} shots.

Conclusion

The meteorological community requires high quality data on the state of the atmosphere in order to improve weather forecasting. Currently, this data is provided by passive sensors that measure the natural radiation emanating from the earth's surface and atmosphere. These sensors, which have reached a high level of technical maturity do, however, possess severe limitations that affect the quality of the data. Principal among these is the lack of vertical resolution, a limitation of the measurement process itself, not of the maturity of the technology.

Active sensors, in which lasers transmit a pulse of light into the atmosphere, have the potential to overcome many of the limitations of passive sensors and permit vertical resolutions ultimately limited only by the pulse length (typically less than 15 meters). Laser technology has reached the point where ground-based measurements have been made of most of the atmospheric quantities of interest, including winds, water vapor, pressure, and aerosols. Transferring this technology to space, however, is a considerable challenge. Currently existing laser sensors are large and consume amounts of power presently beyond the capability of operational meteorological satellites. Advances need to be made not only in spacecraft payload capacity and power supply capability, but also in lidar tech-

nology. Lasers will have to become more efficient and demonstrate lifetime commensurate with a many-year life at the pulse repetition rate needed for operational sensors. While all of these challenges are formidable, the benefits that accrue from an improved knowledge of the state of the atmosphere make the effort worthwhile.

Acknowledgments

The authors would like to thank their colleagues, David Buckley and Jack McShea, for their constructive comments, and Debra Friedman for typing the manuscript.



Front row, left to right: Taylor, Rosenberg, and Sroga. Standing, left to right: Petheram, Kagann, and Bogdan.

Andrew R. Bogdan is a Senior Member of the Technical Staff at Astro-Electronics. He has responsibility for aerosol measurements at 0.53/1.06 μm and is developing capabilities in spaceborne optical communications systems. Prior to joining RCA, he performed lidar measurements on snow, fog, and rain while a Staff Scientist at Photo Metrics, Inc. He received a PhD in Applied Physics from Harvard University for his research in nonlinear optics.

Contact him at:

Astro-Electronics Division
Princeton, N.J.
Tacnet: 229-3506

Robert H. Kagann is a Principal Member of the Technical Staff at Astro-Electronics. He is currently conducting experimental research on water vapor DIAL techniques. Prior to joining RCA, he was a Senior Scientist contractor at the NASA Goddard Space Flight Center where he conducted pressure DIAL experiments and molecular oxygen spectroscopy measurements. He also performed research at the National Bureau of Standards and has published many articles in the scientific literature on molecular spectroscopy. He received his PhD in Chemical Physics at the University of Colorado.

Contact him at:

Astro-Electronics Division
Princeton, N.J.
Tacnet: 229-2080

John Petheram is a Principal Member of the Technical Staff at Astro-Electronics. Currently, he is developing a differential absorption lidar for monitoring atmospheric humidity and temperature, and is acting as system engineer on an Air Force contract for a Design Study of a Spaceborne Lidar Sounder. Mr. Petheram has 16 years of experience in lasers and laser related atmospheric studies. At the University of Hull, United Kingdom, he developed a continuously tunable CO_2 laser for backscattering effects at 10 μm . Before that, at Plessey, United Kingdom, he managed two programs—IRPROP and a NATO-funded program called OPAQUE. IRPROP compared 1 μm and 10 μm propagation under reduced visibility conditions; OPAQUE collected statistics at eight sites in Europe on light levels, instances of reduced visibility, path luminances and other photometric quantities of interest in tactical decision making. Previously, he worked on laser guidance systems for antitank missiles and the effects of atmospheric turbulence on laser beam propagation. He has a BS in Applied Physics and the Diploma in Applied Physics, both from University of Hull.

Contact him at:

Astro-Electronics Division
Princeton, N.J.
Tacnet: 229-3275

Ari Rosenberg received his BSc and MSc from the Israel Institute of Technology, Haifa, Israel, and his PhD in Physics from the Weizman Institute of Science, Rehovoth, Israel. He joined Astro-Electronics in 1980 and is currently Manager of the Advanced Earth Observing System Group. He is in charge of the development of laser remote sensors and laser communication systems for space application. Previously he performed research on atmospheric physics and molecular spectroscopy.

Contact him at:

Astro-Electronics Division
Princeton, N.J.
Tacnet: 229-2691

Jeffery Sroga is a Member of the Technical Staff at Astro-Electronics, and is responsible for the 0.53 μm Doppler Lidar Wind Sensor. He has previously worked on various lidar systems for meteorological applications. He has a BS in Physics from the University of Minnesota and an MS and PhD in Meteorology from the University of Wisconsin.

Contact him at:

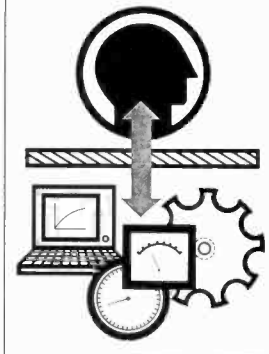
Astro-Electronics Division
Princeton, N.J.
Tacnet: 229-3387

S.E. Taylor received a BSc in Physics from the University of Nottingham, and a PhD in Physics from the University of Hull. Mr. Taylor is no longer with RCA.

How important

RCA

Man-Machine Interfaces



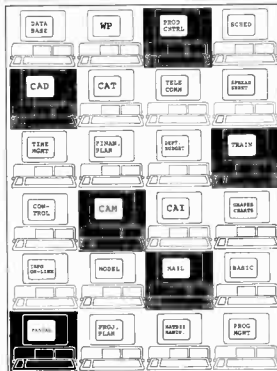
A Corporate Symposium held on September 20, 1984 at Massachusetts Institute of Technology, Cambridge, Massachusetts

Organizer and Chairman:
Dr. Peter Hahn
Government Systems Division,
Cherry Hill, New Jersey

Company Private

RCA

Personal Computers



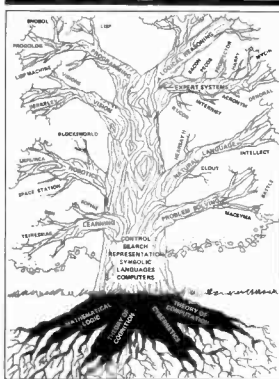
A Corporate Symposium held on September 11, 1984 at RCA Video Component and Display Division, Lancaster, Pennsylvania

Organizer and Chairman:
Dr. James C. Miller

Company Private

RCA

Artificial Intelligence



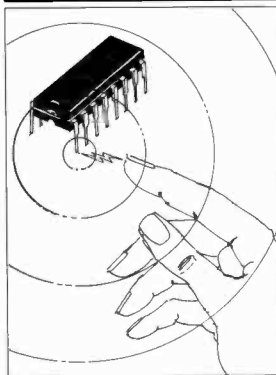
A Corporate Symposium organised by the Advanced Technology Laboratories of Aerospace and Defense and held at RCA Laboratories, Princeton, New Jersey, on October 3, 1985

Organizer and Chairman:
Dr. Eric Braude
Advanced Technology
Laboratories,
Moorestown, New Jersey

Company Private

RCA

Electrostatic Discharge



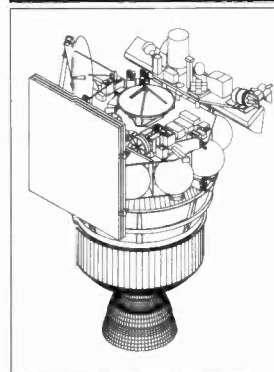
A Corporate Symposium held at RCA Laboratories, Princeton, New Jersey on December 11, 1985

Organizer and Chairman:
L.R. Avery
New Technology
Application Research,
RCA Laboratories,
Princeton, N.J.

Company Private

RCA

Special Uses of Computers in Engineering



A Corporate Symposium presented at RCA Astro-Electronics East Windsor, N.J. on March 14, 1985

Abstracts

Company Private

is keeping up to date?

Today's rapidly changing technologies and fiercely competitive markets demand that engineers have efficient access to information about their field.

We must keep informed of our company's current programs. We must know about related technical developments in our field. And we must get to know the technical experts in other divisions.

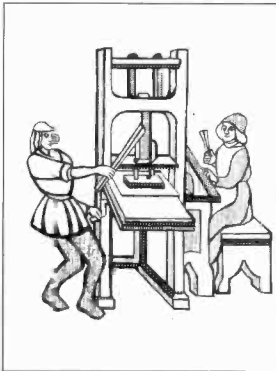
To meet these needs, RCA's Technical Excellence Center in Princeton, N.J., coordinates company-wide Technology Symposia that target state-of-the-art issues. In addition to a full day of

presentations of specific interest to RCA, symposia participants have an opportunity for face-to-face discussion with engineers who have similar interests. Three to five symposia are presented each year.

If you are interested in organizing or participating in a Technology Symposium, get in touch with Tony Bianculli at the Technical Excellence Center, c/o RCA Laboratories, Roszel Road, Princeton, N.J. Telephone: 609-734-2111 Tacnet: 226-2111.

RCA

Electronic Publishing



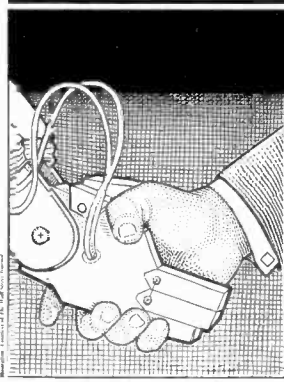
A Corporate Symposium held on May 15, 1986, RCA Missile & Surface Moorestown N.J.

Organizer and Chair: D.R. Higgs

Company Private

RCA

Robotics




A Corporate Symposium held at RCA Laboratories, Princeton, New Jersey, on April 9, 1986

Organizers and Co-Chairmen:
R. M. Correll
RCA Laboratories
J. A. D'Arcy
Aero-Electronics Division
P. B. Pierson
Advanced Technology Laboratories

Company Private

RCA

Telecommunications



A Corporate Symposium held at RCA Laboratories, Princeton, New Jersey, on June 26, 1986

Organizers and Co-Chairmen:
K. H. Powers
RCA Laboratories
A. W. Weinrich
RCA Communications and Electronic Services

Company Private

Pen and Podium

Recent RCA technical papers and presentations

To obtain copies of papers, check your library or contact the author or divisional Technical Publications Administrator (listed on back cover) for a reprint.

Advanced Technology Laboratories

G.O. Abrams | J.K. Peters | H. Rosenthal
Expansion of the RCA engineering network via personal computers—*RCA Engineer*, Vol. 31, No. 2 (March/April 1986)

G.O. Abrams | J.K. Peters
A VAX-Based Personal Computer Ethernet Network—Presented at the 1986 Spring DECUS Symposium in Dallas, Texas, April 28-May 2, 1986 and published in the *Proceedings*

G.A. Drastal | T.A. DuBois | S. Raatz | L. McAndrews | N. Straguzzi
Economy in Expert System Development: The Aegis Combat System Maintenance Advisor—Presented at the Third Annual Conference on Applications of AI in Orlando, Fla., April 1-3, 1986, and published in the *Proceedings of SPIE*

R.G. Hackenberg
An Examination of Contributions from AI Advances in Technology to the Teaching of Second Languages—Presented at the Defense Language Institute in Monterey Cal., February 6-7, 1986, and published in the *Proceedings*

V. Milutinovic | D. Fura | W. Helbig
An Introduction to GaAs Microprocessor Architecture for VLSI—*IEEE Computer Magazine*, Vol. 19 No. 3, pp. 30-42 (March 1986)

J. Pridmore | R. Niescier | G. Brucker | F. Hsueh
An SEU Hardening Approach for CMOS Static RAMS—Presented at the Symposium of Single Event Effects in Los Angeles, Cal., April 8-9, 1986

N. Straguzzi | S.P. Kennedy | T.E. Rockoff
Applying Artificial Intelligence Technology to Existing VLSI Design Tools—Presented at the 1986 IEEE Workstation Technology and Systems Conference in Atlantic City, N.J., March 18-20, 1986 and published in the *Proceedings*

Aerospace and Defense

S. Ross Chairman, Eighth DoD Science & Engineering Technology Symposium

Session, Naval Surface Weapon Center, White Oak, Md., May 6, 1986

Astro-Electronics Division

J.F. Clark
U.S. DBS Systems: The Alternatives—Presented at the AIAA Communication Satellite System Conference, San Diego, Cal., March 16-20, 1986

W. Clopp | T. Hawkes | C. Bertles | B. Pontanto | T.Kao
Geostationary Communications Platform Payload Concepts—Presented at the AIAA Communication Satellite System Conference, San Diego, Cal., March 16-20, 1986

S.M. Fox
Attitude Control Subsystem Performance of the RCA Series 3000 Satellite—Presented at the AIAA Communication Satellite System Conference, San Diego, Cal., March 16-20, 1986

P.F. Joy | L. Goliaszewski
Advanced thermal and Power Systems for the Satcom-Ku Satellite—Presented at the AIAA Communication Satellite System Conference, San Diego, Cal., March 16-20, 1986

J.E. Keigler | L. Muhlfelder
Optimum Antenna Beam Pointing for Communication Satellites—Presented at the AIAA Communication Satellite System Conference, San Diego, Cal., March 16-20, 1986

N. LaPrade | H. Zelen | P. Caporossi | L. Dolan
Ku-Band SSPA for Communications Satellites—Presented at the AIAA Communication Satellite System Conference, San Diego, Cal., March 16-20, 1986

S.V. Parekh | J. Kara | R. Kalarajah
Advanced Satcom Communication—*Microwaves and RF*, February 1986

G.C. Richardson | T.A. Cardellino
Material Selection for Satellites—SPE RETEC, Hartford, Conn., March 10-11, 1986

N. Samhammer | R. Geherty
RCA Astro Application Story—*Outlook*, March 1986

L. Slivinski | G. Clark | D. Chu
Identification of Modal Damping of Flexible Spacecraft Appendages Using Substructure Synthesis Technique—Vibration Damping Workshop II, Las Vegas, Nevada, March 5-7, 1986

Automated Systems Division

A.P. Cortizas | D.R. Haberl
A Concatenated Code and Protocol for Efficient, Reliable Data Transfer over Poor Transmission Channels—Phoenix Conference on Computers and Communications, Tempe, Arizona, March 26-28, 1986

V.E. Furno
Bus Commonality and Standardization—SAE-AE/9B High Speed Data Bus Subcommittee, Phoenix, Arizona, April 21-24, 1986

D.A. Gore | R.S. Reynolds
Techniques for the Early Detection of Gear and Bearing Failures in Helicopter Drive Trains—NAVAIR Helicopter Monitoring Workshop, Pensacola, Fla., March 1986

T.H. Huber
Integrated Electronics for Ground Combat Vehicles—Presentation to Mechanical and Automotive Design Courses at Military Academy, West Point, N.Y., March 1986

W.S. Radcliffe
Lightweight target designator—*RCA Engineer*, Vol. 31, No. 3 (May/June 1986)

M.D. Stern | V.A. Voto | V.K. Grace
Personal computers in the engineering workplace—*RCA Engineer*, Vol. 31, No. 3 (March/April 1986)

Communication and Information Systems Division

L.W. Dobbins | R.W. Johnston
Laser Specifications for Image & Optical Disk Recorder—Presented at OptoElectronics Laser Applications in Science & Engineering (O-E LASE 86), Los Angeles, Cal., January 22, 1986 and published in the *Proceedings*

D.W. Donze | S.L. Corsover
System Requirements Toward Specification of an Image Recorder—Presented at the OptoElectronics Laser Applications in Science & Engineering (O-E LASE 86), Los Angeles, Cal., January 22, 1986 and published in the *Proceedings*

E. DiRusso | S.A. Siegel | J.C. Baroni | P.R. Herczfeld
Fiber Optic Link for Space Communication Application—Presented at the OptoElectronics Laser Applications in Science & Engineering (O-E LASE 86), Los Angeles, Cal., January 22, 1986 and published in the *Proceedings*

W.T. Kelley | F.F. Lazarus
A Marriage of Strengths—*Survey of Project Management Tools*, H.A. Levine, General Electric, Schenectady, N.Y.

D.B. Wolfe | P.B. Holmes
Integrated Computer Network Facility and Application Software Development—Presented at the Automation Technology Institute (ATI '86) 76th Annual Conference on Automation Technology, CAD/CAM, and Engineering Data Handling, Monterey, Cal., February 4-6, 1986 and published in the *Proceedings*

RCA Laboratories

C.H. Anderson | P.J. Burt | G.S. van der Wal
Change Detection and Tracking—*SPIE*, Vol. 579, "Intelligent Robots and Computer Vision" (1985)

F. Aschwanden | M.T. Gale | P. Kiefer | K. Knop
Single-Chip Color Camera Using a Frame-Transfer CCD—*IEEE Transactions on Electron Devices*, Vol. ED-32, No. 8, August 1985

H. Elabd | A.D. Cope | F.V. Shallcross | W.F. Kosonocky | P.A. Levine | D.M. Hoffman
4×1024 CCD Array for Remote Sensing Applications—*Journal of Imaging Technology*, Vol. 11, No. 5, October 1985

L. Faraone
Properties of Textured Oxide/Polysilicon Interfaces—*Insulating Films on Semiconductors* (chapter author), J.J. Simonne and J. Buxo, Editors, Elsevier Science Publishers B.V. (North-Holland), 1986

L. Faraone
Endurance of 9.3-nm EEPROM Tunnel Oxide—J.J. Simonne and J. Buxo, Editors,

Elsevier Science Publishers B.V. (North-Holland), 1986

J. Fields
Model Building in Electron Optics—Phase Space in the Real World—Presented at Swarthmore College, Physics Department, April 3, 1986

A.S. Huang | Y. Arie | C.C. Neil | J.M. Hammer
Study of refractive index of GeO₂:SiO₂ mixtures using deposited-thin-film optical waveguides—*Applied Optics*, Vol. 24, No. 24, December 15, 1985

P.G. Huggett | J. Greenaway | M. L. Hitchmen
The Analysis of Silver in Germanium Selenide Photoresist by Anodic Stripping Voltammetry—*Journal of the Electrochemical Society*, Vol. 132, No. 11, November 1985

L. Jastrzebski | J.F. Corboy | R. Soydan | R. Pagliaro | C.W. Magee
New CMOS Structures for Latch-up Reduction Based on a Two Step Selective Epitaxial Process—*Journal of the Electrochemical Society*, Vol. 132, 3057 (1985)

L. Jastrzebski | J.F. Corboy | R. Soydan | R. Pagliaro, Jr. | C.W. Magee
The Fabrication of CMOS Structures with Increased Immunity to Latchup Using the Two-Step Epitaxial Process—*Journal of the Electrochemical Society*, Vol. 132, No. 12, December 1985

L. Jastrzebski | J.F. Corboy | R. Pagliaro, Jr | R. Soydan
Preparation of Thin (0.6 micron) Continuous Monocrystalline Silicon over SiO₂—*Journal of the Electrochemical Society*, Vol. 132, No. 12, December 1985

K. Knop | R. Morf
A New Class of Mosaic Color Encoding Patterns for Single-Chip Cameras—*IEEE Transactions on Electron Devices*, Vol. ED-32, No. 8, August 1985

R.A. Langley | P.M. Ryan | C.C. Tasi | M.M. Menon | E.M. Botnick | C.W. Magee
Measurement of Beam Species Mix and Beam Impurities in High-Power Neutral Beam Injectors—*J. Vac. Sci. Technol.* A3, 1085 (1985)

C.W. Magee | E.M. Botnick
On the Use of Secondary Ion Mass Spectrometry in Semiconductor Device Materials and Process Development—*Mat. Res. Soc. Symp. Proc.* Vol. 48, Materials Research Society, Pittsburgh, p. 229, 1985

J.I. Pankove
Hydrogen Neutralization of Defects in

Silicon—*Cryst. Latt. Def. and Amorph. Mat.*, Vol. 11, pp. 203-216, 1985

J.I. Pankove | P.J. Zanzucchi | C.W. Magee | G. Lucovsky
Localization of Hydrogen Near Baron in Silicon—*Applied Physics. Lett.* 46, 421, 1985

D. Raychaudhuri
High Capacity Asynchronous Random Access Using Time-of-Arrival Based Collision Resolution—Presented to the IEEE Communications Society, IEEE Global Telecommunications Conference, December 2-5, 1985

I.S.T. Tsong | U. Knipping | C.M. Loxton | C.W. Magee | G.W. Arnold
Carbon on Surfaces of Magnesium Oxide and Olivine Single Crystals—Diffusion from the Bulk or Surface Contamination?—*Phys. Chem. Minerals* 12, 261 (1985)

G.S. van der Wal | J.O. Sinniger
Real time pyramid transfer architecture—*Proceedings of SPIE*, Vol. 579

Microelectronics Center

T.B. Koss | D.R. Alessandrini
Drawsym Phase II—Symbolic Layout System Netlist Driven PCELL Placement Implemented in Calma "Custom Plus"—Presented at the Fall Ascus Meeting, Miami, Fla., September 19, 1985 and published in the *Proceedings*

W.A. Mason
Bringing up a GDSII/32 and Calmanet—Presented at the Fall Ascus Meeting, Miami, Fla., September 18, 1985 and published in the *Proceedings*

W. A. Mason
The Calma—RCA Relationship—Presented at the Calma International Sales Meeting, Berkeley, Cal., January 12, 1986

R.H. Zeien
High Density IC Ceramic Packaging for High Reliability Applications—Presented at the High Technology Ceramics Conference in Key Biscayne, Fla., March 23-25, 1986

Missile and Surface Radar Division

J.A. Adams | M. Gale | J.W. Dempsey | G.W. Kaizar | N. Straguzzi
Artificial intelligence applications—*RCA Engineer*, Vol. 31 No. 1 (Jan/Feb 1986)

J. Anders | J.A. Bauer | D.M. Jones
Production Design with Solid Modeling—

21st Industrial Associates Review, Rensselaer Polytechnic Institute Center for Interactive Computer Graphics, Troy N.Y., April 1986

J.A. Bauer
Design Considerations for Military Surface Mount Technology—Surface Mount Technology Association, New Jersey Chapter, Woodbridge, N.J., March 12, 1986

J.W. Bornholdt | V.W. Hammond | K.H. Wedge
Multiple Target Tracking Radar—New Capabilities to Satisfy Range Instrumentation Needs—Presented at the AIAA Conference, Las Vegas, Nevada, April 4, 1986 and published in the *Proceedings*

M. Davis
Surface Mount Technology Experience: Problems and Solutions—*Microelectronics Journal*, Vol. 17, No. 2, March/April 1986

R.J. DeMaria
Deposition of Aluminum Nitride Films Using RF Reactive Sputtering—Presented at the 1986 Materials Research Society Symposium on Plasma Processing, Palo Alto, Cal., April 15-18, 1986 and published in the *Proceedings*

C. Di Maria
AN/SPY-1B Window Assembly System—Presented at the Robotics Symposium, RCA Laboratories, Princeton, N.J., April 9, 1986 and published in the *Proceedings*

C. Di Maria
AN/SPY-1B Phase Shifter Automation Horn Spring to Housing Assembly—

Presented at the Robotics Symposium, RCA Laboratories, Princeton, N.J., April 9, 1986 and published in the *Proceedings*

D.J. Herman
Decision Making Processes in Combat Design—Northeastern Society of Academic Anesthesia Chairmen, Somerset, N.J., March 22, 1986

E. Langberg
Micro-CIM: An Alternate Solution—Presented at the Robotics Symposium, RCA Laboratories, Princeton, N.J., April 9, 1986 and published in the *Proceedings*

V. Mangulis
The Performance of Synchronous Direct-Sequence Spread Spectrum Signals Replicated in Several Frequency Bands—*International Journal of Satellite Communications*, Vol. 3, 1985, pp. 271-273

G. Poletti
Workstation Technology—Data Security Issues—Presented at the IEEE Workstation Technology and Systems Conference, Atlantic City, N.J., March 17-20, 1985

M. Trachtenberg
Validating Halstead's Theory—*IEEE Transactions on Software Engineering*, Vol. SE-12, No. 4, April 1986

L. H. Yorinks
The AN/SPY-1A Radar—Boston Section IEEE AES Society course on Modern Radar Technology, Boston, Mass., April 14, 1986

L. H. Yorinks
A Near-Field Antenna Range for Ultra-

Low Sidelobe Antennas—Boston Section IEEE AES Society course on Modern Radar Technology, Boston, Mass., April 14, 1986

Service Company

A.E. Hoffmann-Heyden
Tracking Radars at Flight Test Ranges—Presented at the AIAA National Flight Test Conference, April 2-4, 1986

Solid State Division

H.W. Becke | C.E. Harm | R.T. Lee | H.R. Ronan | C.F. Wheatley, Jr.
Applications of COMFETs (IGT) to 40 kHz Off-Line Switcher—Presented at the IEEE Applied Power Electronics Conference, April 1986

G.M. Dolny | C.F. Wheatley, Jr. | H.R. Ronan
Computer Aided Analysis of Gate Voltage Propagation Effects in Power MOSFETs—Presented at the High Frequency Power Conversion Conference, May 1986

H.R. Ronan | C.F. Wheatley, Jr.
Circuit Influences Upon COMFET (IGT) Dynamic Latching Current—Presented at the IEEE Power Electronics Specialists Conference, June 1986

Engineering News and Highlights

Mackin named Division Vice President

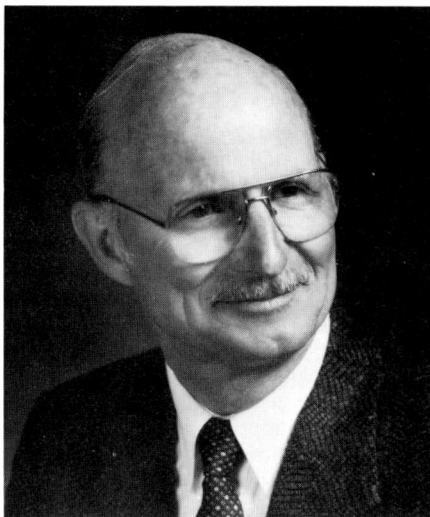


Charles A. Schmidt, Group Vice President, RCA Government Communications Systems, has announced the appointment of **Joseph L. Mackin** as Division Vice President of Government Volume Production. Mr. Mackin's operation involves more than 500 employees and specializes in high-volume production of satellite communications terminals, communications security equipment, and other electronic products for government programs.

He has been Director of Plant Operations at CISD since 1984, and for ten years prior to that he was Manager of Plant Operations for Astro-Electronics Division. His responsibilities there included all aspects of manufacturing and test operations.

Mr. Mackin holds a BS degree from St. Joseph's University, Philadelphia, and he attended the University of Pennsylvania Wharton School.

Parker is Division Vice President, CISD



Donald J. Parker has been appointed Division Vice President, Digital Communications and Recording Systems, Communication and Information Systems Division. Mr. Parker will be responsible for engineering and manufacturing of a wide range of digital systems for government and commercial customers.

Prior to this appointment, Mr. Parker was Director, and earlier Manager, of Digital Communications and Recording Systems. Before that, he was the Chief Engineer of CISD.

Mr. Parker is a Fellow of the IEEE, holds a number of patents in the field of electro-optics, and has written a several technical articles. He holds a BS degree in Optics from the University of Rochester.

as Division Vice President, Product Assurance.

James E. Carnes, Division Vice President, Engineering, announces the appointment of **John C. Peer** as Director, Engineering.

Larry J. Byers, Manager, Test Technology, announces the appointment of **James M. Keeth** as Manager, Direct Broadcast Satellite Test Systems.

Display Systems Division

Lawrence J. Schipper, Division Vice President and General Manager, announces his organization as follows: **Theodore L. Allen**, Manager, Program Management; **Larry A. Cochran**, Division Vice President, Engineering; and **Lawrence J. Schipper**, Acting Director, Product Assurance.

Lawrence J. Schipper, Division Vice President and General Manager, announces the appointment of **Edward W. Curtis** as Director, Display Systems Operations, RCA Taiwan Limited.

Lawrence J. Schipper, Acting Director, Product Assurance, announces the appointment of **James O. Early** as Manager, Product Quality.

Microelectronics Center

Ronald C. Bracken, Director, IC Design and Development, announces his organization as follows: **Albert Feller**, Manager, IC and Computer-Aided Design Development; **Carl N. Puschak**, Manager, Custom IC Design; **Thomas E. Sullivan**, Manager, Advanced Device Development; and **Michael A. Gianfagna**, Manager, Computer and Design Automation.

NBC

Michael Sherlock, Executive Vice President, Operations & Technical Services, announces his organization as follows: **David Baylor**, Vice President, Broadcast Operations; **Henry S. Kanegsberg**, Vice President, Facilities and Operations Planning; **John J.P. Weir**, Vice President, Operations and Engineering, Olympics; **Donald Brookfield**, Director, Video Tape Operations; and **Frank A. Davenport**, Project Manager, Broadcast Systems Engineering.

Staff announcements

Communication and Information Systems Division

Joseph B. Christopher has been named Director, Plant Operations, Camden.

Consumer Electronics Operations

D. Joseph Donahue, Vice President, Consumer Electronics Operations, announces the appointment of **Willard M. Workman**

RCA Laboratories

Robert D. Lohman, Staff Vice President, Solid State Research, announces the appointment of **Dr. Karl Knop** as Director, Research Laboratories, RCA Zurich Limited.

Kerns H. Powers, Staff Vice President, Government Systems and Communications Research, announces his organization as follows: **Bernard J. Lechner**, Senior Staff Scientist; **Kerns H. Powers**, Acting Director, Broadcast Satellite and NBC Research; **Edgar J. Denlinger**, Head, Signal Conversion Systems Research; **Charles B. Oakley**, Head, Video Production Technology Research; **Robert E. Flory**, Fellow of the Technical Staff; **Leonard Schiff**, Director, Communications Research Laboratory; **Paul Hashfield**, Head, Communications Technology Research; **Krishnamurthy Jonnalagadda**, Head, Communication Analysis Research; **Harvey Waldman**, Head, Video Communications Research; **Leonard Schiff**, Acting, Satellite Transmission Systems Research; **Fred Sterzer**, Director, Microwave Technology Center; **Erwin F. Belohoubek**, Head, Microwave Circuit Technology; **Raymond L. Camisa**, Head, Microwave Components Technology; **S. Yegna Narayan**, Head, Microwave Device Technology; **Markus Nowogrodzki**, Head, Subsystems and Special Projects; **Barry S. Perlman**, Head, Design Automation Technology; and **Herbert J. Wolkstein**, Head, Space and Counter Measures Program.

James C. Miller, Acting, CAD System Services, announces his organization as follows: **Rodney L. Angle**, Manager, VLSI Design System, and **William M. Cowhig**, Manager, VLSI Design Services.

Jack S. Fuhrer, Director, Television Research Laboratory, announces his organization as follows: **Lauren A. Christopher**, Head, Consumer Electronics Integrated Circuit Research; **Leopold A. Harwood**, Fellow of the Technical Staff; **Walter H. Demmer**, Head, Digital Video Research; **John G.N. Henderson**, Head, Systems Technology Research; **James J. Gibson**, Fellow of the Technical Staff; **Stanley P. Knight**, Head, Digital Signal Processing Research; **Michael D. Ross**, Head, Video Signal Processing Research; **Werner F. Wedam**, Head, Television Receiver Systems Research; **Kern K. Chang**, Fellow of the Technical Staff; and **Dalton H. Pritchard**, Fellow of the Technical Staff.

Curtis R. Carlson, Director, Information Systems Research Laboratory, announces his organization as follows: **Philip K.**

Baltzer, Staff Scientist; **Peter J. Burt**, Head, Advanced Image Processing Research; **Charles H. Anderson**, Fellow of the Technical Staff; **Jack J. Gelfand**, Head, Knowledge-Based Systems Research; **James J. Power**, Head, Home Data Systems Research; **Glenn A. Reitmeier**, Head, Home Communications Research; **Thomas M. Stiller**, Fellow of the Technical Staff; **Hugh E. White**, Fellow of the Technical Staff; and **Charles M. Wine**, Fellow of the Technical Staff.

RCA Network Services

Eugene F. Murphy, Executive Vice President, Communications and Electronic Services, announces the appointment of **Terrence P. McGarty** as Vice President, Data Transaction Services.

Solid State Division

Charles J. Nuese, Division Vice President, Manufacturing—Integrated Circuits, announces the appointment of **George W. Barclay** as Director, Manufacturing—Standard IC Products.

George W. Barclay, Director, Manufacturing—Standard IC Products, announces the appointment of **Barry A. Goldsmith** as Manager, Process Technology, and **Howard Hoskinson** as Manager, Wafer Fabrication—Bipolar Integrated Circuits.

Donald R. Carley, Manager, Applications and Product Engineering, announces his organization as follows: **Dale M. Baugher**, Manager, Applications and Product Engineering—Standard Products; **Donald R. Carley**, Acting, Technology Support; **Edward C. Crossley**, Manager, Applications and Product Engineering—ASIC; and **Michael Zanakos**, Manager, Program Management and Test Operations.

Video Component and Display Division

Charles A. Quinn, Division Vice President and General Manager, Video Component and Display Division, announces his organization as follows: **Robert K. Lorch**, Division Vice President, Strategic Planning; **Donald G. Mackey**, Division Vice President, Product Safety, Quality and Reliability; **Harlan R. May**, Director, Scranton Operations; **Thomas I. Peters**, Division Vice President, International Operations and Component Manufacturing; and **John M. Ratay**, Director, Marion Operations.

Professional activities

Princeton honors Dr. Singh

Dr. Bawa Singh, Thin Film Technology, RCA Laboratories, participated in a joint project with members of the staff of the Princeton Plasma Physics Laboratory of Princeton University under an industrial intern program. He was presented with a certificate for his contributions at a luncheon held in his honor on May 14, 1986 by the School of Engineering and Applied Sciences and the Plasma Physics Laboratory.

Dixon advances in IEEE

Douglas F. Dixon, Digital Products Research Laboratory, RCA Laboratories, has been elected a Senior Member of the Institute of Electrical and Electronics Engineers.

STC honors Dukes



Eva Dukes, RCA Laboratories, has been elected an Associate Fellow by the Society for Technical Communication "for notable contributions to the technical communication profession as editor, author, lecturer, and translator, and for continuing service to the Society for Technical Communication." The announcement was made at the 33rd International Technical Communications Conference, Detroit, Michigan.

Professional engineers

Sheng M. Huang, RCA Laboratories, New Jersey Professional Engineer's License no. GE31202.

Bruce J. Schafhauser, Missile and Surface Radar Division, New Jersey Professional Engineer's License no. 35029.

Schmidt is Fellow of AIAA

Charles A. Schmidt, Group Vice President, RCA Government Communications Systems, has been elected a Fellow of the American Institute of Aeronautics and Astronautics (AIAA). He was cited for "his widely acknowledged industrial leadership in high-performance, cost-effective communications, environmental, navigational, and scientific satellites, and for his contributions toward the potential commercialization of space."

Geshner chairs symposium

R.A. Geshner, Microelectronics Center, recently chaired the fifth international IGC Symposium on Electron Beam Photolithography. Mr. Geshner has chaired this symposium for five years in a row.

Sheffield wins academic award

Berthold Sheffield has received the Distinguished Adjunct Professor Award at Trenton State College, Trenton, N.J. The new award was announced at the Awards Convocation held on May 4, 1986 at the TSC School of Technology. Mr. Sheffield was cited for his performance and his efforts beyond the call of duty on behalf of his students.

Mr. Sheffield retired from RCA after 36 years of service.

Degrees conferred

Ronald Benton—Master of Science in Engineering, Purdue University

Arthur Baranoff—Master of Science in Electrical Engineering, Purdue University

Deborah J. Cassidy—Master of Science in Electrical Engineering, Worcester Polytechnic Institute

Edward C. Compton—Master of Science in Electrical Engineering, Northeastern University

George Economou—Master of Science in Electrical Engineering, Tufts University

Daniel J. Fabiano—Master of Science in Electrical Engineering, Northeastern University

George V. Luongo—Master of Science in Electrical Engineering, Northeastern University

John C. Marshall—Master of Science in Manufacturing Engineering, University of Massachusetts at Amherst

Terry A. Nuzzolo—Master of Science in Electrical Engineering, Tufts University

Robert J. Peters—Master of Science in Electrical Engineering, Northeastern University

Wesley W. Philbrook—Master of Science in Electrical Engineering, Northeastern University

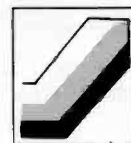
Douglas W. Smith—Master of Science in Electrical Engineering/Computer Science Engineering, University of Massachusetts

Anne P. Tjiong—Master of Science in Manufacturing Engineering, University of Massachusetts at Amherst

Chester S. Williams—Master of Science in Manufacturing Engineering, Northeastern University

Leslie G. Woodard—Master of Science in Electrical Engineering, Northeastern University

Technical excellence



First Quarter 1986 MSRD Awards



Costello



DeLuca



Friel



Parish

There are four winners of the Missile and Surface Radar Division's First Quarter 1986 Technical Excellence Awards. The citations are summarized below.

David O. Costello—For major advances in the display and evaluation of multiple radar

targets in real time. His scrolling color Range-Time Indicator, now implemented and incorporated in the TRADEX radar, displays actual range-time target paths of a multitarget complex on a color video monitor, allowing simultaneous evaluation

of radar cross section, position, and relative motion, and signature of all targets within the radar beam.

Amedeo DeLuca—For extraordinary proficiency and innovation in the successful design of a complex Standard Cell semicustom VLSI device for the Multiple Object Tracking Radar program. His concept, detailed design, simulation effort, and laboratory verification of this Standard Cell device provide practical implementation of a new, significantly improved beam steering control architecture concept for the MOTR antenna, with a large attendant reduction in hardware requirements.

Patricia A. Friel—For outstanding technical leadership and personal dedication in the

successful integration of the AN/SPY-1B radar into the AEGIS EDM-4 Combat System in preparation for formal operations performance evaluation. Her Multi-Element Integration Team, staffed with 20 systems engineering specialists, successfully tested, corrected, and released the Combat System for formal testing in spite of heavy contention for integration time and a severely limited schedule for development and operational testing.

Melvin J. Parish—For special systems engineering and team leadership achievements in the successful portrayal of DDG 51 Anti-Submarine Warfare sensor effectiveness. Undertaken as part of the overall DDG 51 ASW Combat System Effectiveness study, the translation of sonar performance characteristics into meaningful inputs to the Navy-approved RAYMODE program. The success of this effort has significantly enhanced RCA's credentials as a viable ASW systems contractor.

Three cited at Mountaintop



From left to right: Don Burke, Director of Engineering, Power Products, Pete Jones, Manager, Design Engineering, Wayne Ordille, Don Burton, Joe Yedinak, and Bob Jones, Division Vice President, New Products.

Three SSD design engineers, **Joe Yedinak**, **Don Burton**, and **Wayne Ordille**, have received Mountaintop Technical Excellence Awards for their roles in the design and production implementation of a program for the planar conversion of all epi-base and high-speed transistor product lines. These types were previously mesa non-passivated

or mesa sogo passivated. Planar conversion achieved annual cost savings of over one million dollars and provided improved electrical performance in the finished product. Over 30 transistor and Darlington types in various packages were designed and converted to planar technology.

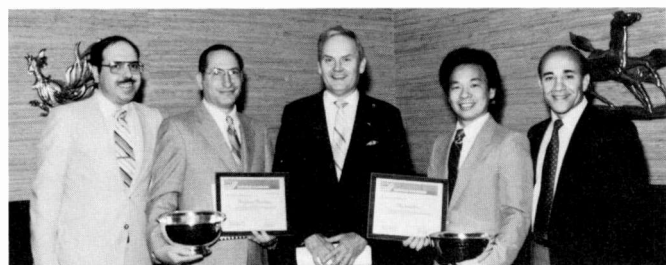
Somerville TEC Awards



Left to right: Carmine Salerno, James Magos, Carl R. Turner, James O'Keefe, Heshmat Khajezadeh, and William Allen.



Left to right: Carmine Salerno, David S. Jacobson, Frank Kuyan, Carl R. Turner, Thomas Pampalone, A. Leo Fisk, and Peter Idell.



Left to right: Carmine Salerno, Raymond Giordano, Carl R. Turner, Michael Low, and Heshmat Khajezadeh.



Left to right: Carmine Salerno, Richard Funk, Robert Isham, Carl R. Turner, Irving Martin, and Heshmat Khajezadeh.

Robert Isham and **Irving Martin** each received individual Fourth Quarter 1985 Technical Excellence Awards at the Annual Solid State Division Technical Excellence luncheon. As a result of his persistence, Bob developed a unique test to measure the upper frequency capabilities of high-speed A/D conversion. Irv's creativity contributed to the establishment of a library of model parameters for the 3-micron RAD-hard CMOS/SOS process.

Ray Giordano, **Michael Low**, and **Melvin**

Hagge received a Fourth Quarter Award as well as a Solid State Division Annual Technical Excellence Award for their design of a large custom AIU chip in a record time of five months. This achievement was further heightened by the chip working on the first cut.

A team award was presented to **Frank Kuyan** and **Tom Pampalone** for their development of a new photoresist system that minimizes dimensional variations over steps for the 1.25-micron SOS process. Both

individuals received a Somerville Quarterly Award, and they also received the Solid State Division Annual Technical Excellence Award.

The Somerville Fourth Quarter and Solid State Division Annual Technical Excellence Award was given to **James O'Keefe**. Jim, a technician in the Government and High Reliability IC Operations area, developed a software called "Autogate" that enhances the design of standard cells and gate arrays.

CE Annual TEC Awards



Left to right: W. Bishop, J. Furrey, M. Owens, J. Sosniak, J. Milnes, D. Wilson, W. Benson, and J. Hart (L. Avery and B. Whipple not pictured).

There are ten recipients of the Consumer Electronics Operations 1985 Annual Technical Excellence Awards. They are:

Jack B. Hart—For the development of a new method to deflash unfired round and oval ferrite cores for S/T yokes. The equipment produced significant gains in product quality and savings in labor and material. The system for the COTY core automatically deflashed up to three different surfaces. The previous method required maintenance every fifteen minutes for each operation. The new method has deflashed over two million cores and has required very little maintenance. Jack was the initiator, designer, and primary driving force for this project.

Will Bishop and Mark Owens—For the mechanical design of the CRK-39 and CRK-40 remote transmitters. Both employed design creativity, technical innovation, and attention to detail in the production design

cycle. Their thoroughness led to the best remote transmitter startup in recent CE history.

Jim Milnes, Bruce A. Whipple and Dan Wilson—For the successful implementation of the first CAD/CAM (drawingless) fast track tool procurement program for the #68 mask mold. Extensive and thorough analysis of the mold design was done using new computer mold analysis software. This resulted in the evaluation of several mold designs before the mold was fabricated and tested. The development cycle was shortened by 27 weeks. This was accomplished by overlapping tasks that were previously performed sequentially. The mold tool was made directly from computer-generated tapes without the aid of paper prints. The fast track design cycle enables CE to be much more responsive to changing consumer tastes and will be used on more projects in the future.

1985 RCA Laboratories Outstanding Achievement Awards

The following individuals have received the 1985 RCA Laboratories Outstanding Achievement Awards:

Lorenzo Faraone—For contributions to the science and technology of silicon-oxide growth and characterization.

Jacob M. Hammer—For the conception and design of a novel two-dimensional array of diode lasers.

Jer-shen Maa—For modeling of conductive residues formed during anisotropic plasma etching in high-density integrated circuit fabrication, model fabrication, and prediction of future process directions.

Arthur Miller—For practical computer modeling of permeable pieces on magnetic deflection yokes.

Richard W. Nosker—For basic understanding leading to development of a high-

efficiency, wide-viewing-angle illumination system for liquid crystal television displays.

Ashok N. Prabhu—For developing and introducing new processes and materials to improve the cost effectiveness of manufacturing printed circuit boards at the Consumer Electronics Operations.

David L. Rhodes—For contributions to the design and implementation of innovative software for computer-aided microwave engineering.

Robert M. Wilson—For design and development of a high-performance feedhorn for DBS antennas.

Liston Abbott, Kevin M. Kelly, Richard J. Klensch, Michael J. Shumila, and James M. Walter—For important contributions to a major hardware system enabling direct comparison of composite and component video formats for DBS transmission.

Jacob Sosniak and Leslie Avery—For the development of structures on integrated circuits that protect the device from damage due to electrostatic discharges (ESD). Mr. Avery designed and developed structures for both bipolar and analog integrated circuits that protect each pad and the internal circuits from ESD damage. Mr. Sosniak designed and developed laboratory apparatus and techniques to evaluate and quantify the performance of ESD protection structures. He also coordinated the implementation of Mr. Avery's structures in several IC designs at CE. The structures, which provide protection to discharge levels of 4 kV, offer ESD immunity levels two to three times greater than the competition.

Walter Benson—For coordinating the funding, design, and development of a 14-station in-line hot stamp system for Plastics Finishing Operations on TV cabinet fronts. The system is the first in the industry, and the project required extensive interaction between vendor and plant personnel. Mr. Benson organized appropriate training programs for both manufacturing and maintenance personnel. He has demonstrated a high degree of thoroughness and professionalism in every detail of the project, and has been responsible for the successful completion of the program.

John Furrey—For the initiation and design of a module (PWCPA) to provide cost-effective stereo in a leader model television receiver. The module combines a volume/tone control and stereo power amp. Mr. Furrey worked to minimize the parts count and power requirements to design a system that resulted in a net savings of nearly \$8.00 at the instrument level. Although the design was started at GR-1, it was completed in time to meet the original instrument introduction date.

Charles H. Anderson, Gooitzen S. van der Wal, and Joseph O. Sinniger—For the conception and construction of a pyramid-based image preprocessor and its application to automated surveillance.

Brian Astle and Stuart J. Golin—For development of an image-encoding algorithm that permits low-bandwidth transmission and very-high-speed, low-cost decoding.

Dennis J. Bechis, Stanley Bloom, and Eric F. Hockings—For the design and development of astigmatism correction in electron guns.

Chen-Chien Chen, Sheng M. Huang, Kalipada Palit, and Bruce A. Whipple—For innovation and dedication in the development and application of CAE/CAD systems for plastic molding and processing.

Doris W. Flatley and Sheng T. Hsu—For

the innovative development and effective transfer of advanced short-channel CMOS technology.

Harvey O. Hook, James R. Matey, and Aurelian Mavrodin—For the development of a device to accurately and conveniently measure at the factory the register between mask and panel in a color picture tube.

Lewis L. Stetz, Jr. and Joseph A. Zenel—For experimental measurements and characterization of the RCA Americom SSB system leading to the ability to handle high-speed voice-band modems.

Circleville TEC Award

Walter Jinks has received a Circleville Technical Excellence Award for the installation of system software, coordination and debugging of computer hardware, and the writing and implementation of user programs for a computer and process gauge system for the inspection of funnel and panel glass.

CISD team wins TEC Award

Don Bussard, Joe Everhart, Russ Haskell, Dick Dahl, George Hubbard, and Tom

Knapp have received the CISD Technical Excellence Team Award for designing a compact lightweight military three-phase power converter that provides 10.5-kW, 60-Hz output from a 400-Hz input. The unit features a unique, low-cost cooling arrangement for switching transistors, harmonic distortion of less than three percent, digitally controlled frequency, overload sensing at 10 kHz, high-speed fault detection and circuit protection, and efficiency greater than 85 percent. The weight of this converter is only about 20 percent of the weight of an equivalent motor generator set, and is not subject to the mechanical breakdowns encountered in rotating machinery.

CISD Engineer of the Month

Bill Acherman has been selected Engineer of the Month for CISD Design Engineering. This award is made in recognition of Bill's outstanding performance on the Built-in Test Equipment (BITE) development of the Low Rate Multiplexer. Working from the proposal defined concept, Bill specified hardware interfaces and developed the software structure to implement an extremely effective built-in test.

Astro Employees of the Quarter

Four employees at RCA Astro-Electronics Division have been named "Employee of the Quarter" for their high level of personal commitment, performance and leadership on the job. Honored were **Gordon Crater**, Lead Technician; **William Schulte**, Principal Member, Technical Staff; **Lawrence Trerotola**, Test Engineer; and **Harvey Mertz**, Senior Member, Technical Staff.

MEC Employee of the Month

The Microelectronics Center December Employee of the Month was **Ken Goen**. This award is in recognition of Ken's technical strength and for consistently representing RCA MEC as a professional and enthusiastic winner to customers, visitors and on college and high school campuses. Ken's high energy level and willingness to take on additional assignments single him out as our employee of the month for December.

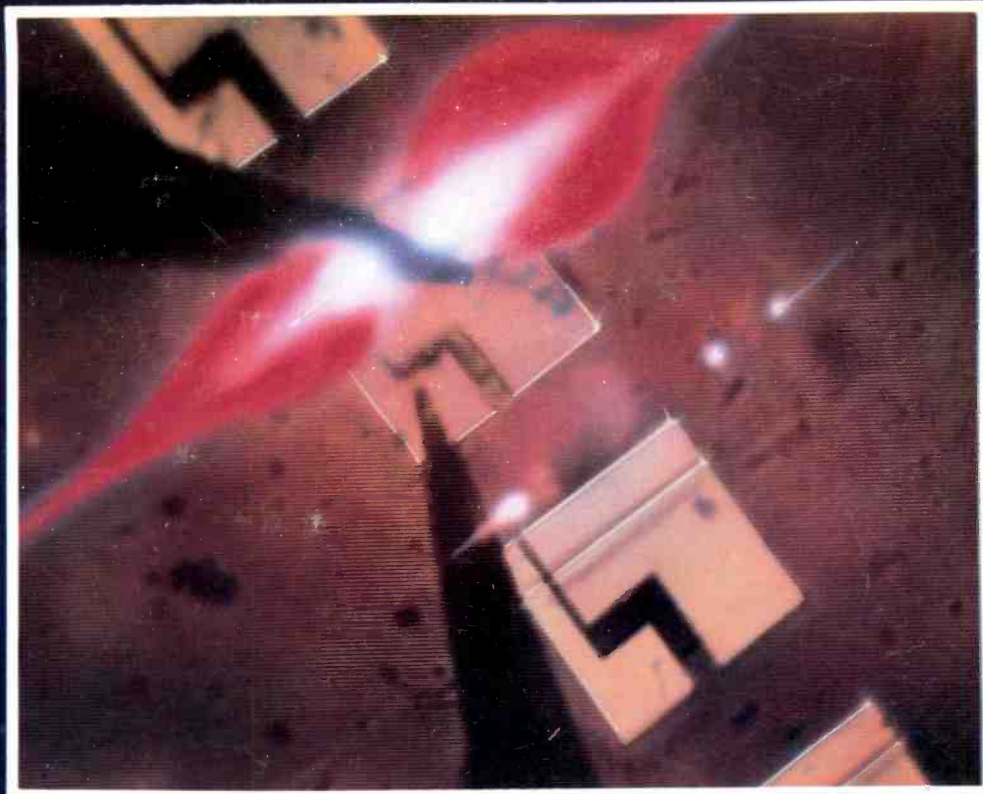
Editorial Representatives and Technical Publications Administrators

Contact your Editorial Representative at the Tacnet numbers listed below to plan your *RCA Engineer* article and to announce your professional activities.

*Technical Publications Administrators, responsible for review and approval of papers and presentations, are indicated here with asterisks before their names.

Advanced Technology Laboratories	Tacnet	National Broadcasting Company	Tacnet
*Merle Pietz Ed Master	Moorestown, New Jersey Moorestown, New Jersey	253-6429 253-6436	*Bob Mausler New York, New York
Aerospace & Defense Staff			324-4869
*Theresa Law (Approvals only)	Cherry Hill, New Jersey	222-5833	Network Services
American Communications			*Richard Spencer Princeton, New Jersey
*Anita Labib (Approvals only) Carolyn Powell	Princeton, New Jersey Princeton, New Jersey	258-4346 272-4194	New Products Division
Astro-Electronics Division			*Pete Bedrosian Bob McIntyre
*Frank Yannotti Carol Coleman	Princeton, New Jersey Princeton, New Jersey	229-2544 229-2919	Lancaster, Pennsylvania Ste Anne de Bellevue
Automated Systems Division			227-6880 514-457-9000
*Gene Galton Linda Kriesman	Burlington, Massachusetts Burlington, Massachusetts	326-3775 326-3001	RCA Laboratories
Communication and Information Systems Division			*Julie Dann (Approvals only) Eva Dukes
*Dan Tannenbaum Harry Green Bruce White	Camden, New Jersey Camden, New Jersey Camden, New Jersey	222-3081 222-2423 222-3908	Princeton, New Jersey Princeton, New Jersey
Consumer Electronics Operations			226-2061 226-2882
*Eugene Janson John Hopkins Larry Olson	Indianapolis, Indiana Indianapolis, Indiana Indianapolis, Indiana	422-5208 422-5217 422-5117	RCA Records Division
Corporate Information Systems & Services			*Greg Bogantz Indianapolis, Indiana
*Sue Handman	Cherry Hill, New Jersey	222-6242	424-6141
Global Communications			RCA Service Company
*Dorothy Unger *Paul Dixon	Piscataway, New Jersey Memphis, Tenn.	335-4358 739-0214	*Murray Kaminsky Dick Dombrosky Ray MacWilliams
Microelectronics Center			Cherry Hill, New Jersey Cherry Hill, New Jersey Cherry Hill, New Jersey
*Susan Suchy	Somerville, New Jersey	325-7492	269-5418 269-5618 269-5005
Missile and Surface Radar Division			RCA Technical Excellence Center
*Don Higgs Graham Boose Jack Friedman	Moorestown, New Jersey Moorestown, New Jersey Moorestown, New Jersey	224-2836 253-6062 224-2112	*Tony Bianculli (For corporate approvals)
			Princeton, New Jersey
			226-2111
			Solid State Division
			*John Schoen Sy Silverstein Virginia Pate Harold Ronan
			Somerville, New Jersey Somerville, New Jersey Somerville, New Jersey Mountaintop, Pennsylvania
			325-6467 325-6168 325-6704 327-1473 or 327-1264
			Dick Morey John Young
			Palm Beach Gardens, Florida Findlay, Ohio
			722-1262 425-1307
			Video Component and Display Division
			*Ed Madenford Lou DiMattio Nick Meena J.R. Reece
			Lancaster, Pennsylvania Scranton, Pennsylvania Circleville, Ohio Marion, Indiana
			227-6444 329-1435 432-1228 427-5566

Laser light coupled out of the surface of a diode laser developed at RCA Laboratories. The light gain mechanism occurs when the electrodes are driven with current as in conventional diode lasers. Light generated under the electrodes is carried to and under a diffraction grating by an optical waveguide. The grating reflects some of the light back under the electrodes to provide the feedback required for laser oscillation to occur. The grating also couples light out of the surface of the laser wafer. The bright part of the picture is due to this light emitted out of the surface.



This method gives laser beams with much smaller divergence angles and higher spectral purity than conventional laser diodes that use cleaved facets for

edge emission and feedback. The size and divergence of the beam of the surface-emitting semiconductor laser in one

dimension is now approaching that of conventional solid-state or gas-tube lasers.

RCA Engineer

A technical journal published by the RCA Technical Excellence Center "by and for the RCA engineer"

13 Roszel Road, P.O. Box 432, Princeton, NJ 08543-0432
Address correction requested

BULK RATE
US Postage
PAID
Phila., Pa.
Permit No. 2906

EJ NOSSEN
203 ELKINS RD
CHERRY HILL
NJ 08034

GSDGC